Detection and analysis of spin trapped radical adducts by using α-phenyl-*tert*-butyl nitrone (PBN) derivatives and GC/MS

Sanatkumar S. Mishra

School of Environment & Life Sciences
University of Salford, Salford, UK

Submitted in partial fulfilment of the requirements of the Degree of Doctor of Philosophy, June 2016.

Contents

List of Figures

List of Tables

Acknowledgements

I would like to show my gratitude to Dr Ian Podmore for all the guidance and encouragement he had provided me throughout the course of my Doctoral degree.

I would especially like to thank Dr Laurie Cunliffe for her support and technical advice for teaching on gc/ms.

I would like thank you Dr Steven Rossington and Patrick Killoran for their help in organic chemistry.

I would like to give a special mention to Kamran for being a very good supportive lab colleague during the course of my PhD.

I would also like to thank you Kamila for her support and sharing knowledge.

Thank you to my wonderful wife and my lovely son Abhay for their unconditional support. Many thanks to all my family and friends who belived in me I would achieve my goal.

Above all I Thanks the Almighty for the blessing.

Declaration

Except where acknowledged in the customary manner, the material presented in this thesis is, to the best of my knowledge, original and has not been submitted in whole or part for a degree in any university.

_____

Sanatkumar S. Mishra

Abstract

Free radicals are atoms or molecules with one or more unpaired electrons. They are generally unstable and short lived making them difficult to detect. Certain free radicals are constantly produced in cells by cellular metabolism and by exogenous agents. These free radicals react with various biomolecules in cells, which can lead to diseases like cardiovascular, cancer, neurological disorders and diabetes. Various methods are used to detect and characterise free radicals. Spin traps are often used as a method of trapping radicals for further analysis, as they make the trapped radicals more stable. Electron Paramagnetic Resonance (EPR) spectroscopy is the most popular method used to detect these trapped radical adducts, however, identification of the radical is still a concern owing to the limited amount of information obtained regarding the radical that is actually trapped.

In this study, hydroxyl radicals generated by Fenton chemistry have been used to generate radicals from methanol, DMSO, acetaldehyde and propionaldehyde to produce $^{\bullet}CH_2OH$, $^{\bullet}CH_3$, $^{\bullet}CH_3$, $^{\bullet}C_2H_5$ and $^{\bullet}CH_3CO$ radicals respectively. These radicals were trapped by α-phenyl-*tert*-butylnitrone (PBN) and its derivatives to form stable adducts which were then sampled by different extraction techniques like liquid-liquid extraction with chloroform as solvent, Headspace Single Drop Microextraction (HS-SDME) with decane as the solvent and Headspace Solid Phase Microextraction (HS-SPME). The extracted samples were subjected to GC/MS for detection and identification of the PBN adducts. PBN radical adducts were successfully identified by all the three extraction techniques. HS-SPME and HS-SDME are novel approaches to the detection and identification of free radical adducts. HS-SPME, in particular, is a solvent free, one step method, that only extracts the volatile compounds present in the headspace of the sample and, as the fibre can be retracted, the radical adduct may be easily stored and transported.

The trapping of $^{\bullet}CH_2OH$ radicals by PBN and its derivatives was demonstrated by the use of mixtures of methanol and DMSO. This approach for the identification of trapped free radicals is novel and coupled with headspace extraction techniques is potentially a very powerful method for free radical detection and quantification.

Chapter 1

Introduction

1.1 Introduction

The first organic free radical identified was triphenylmethyl radical by Moses Gomberg (Gomberg 1900) more than a century ago. Due to their high reactivity and short half life free radicals were not considered to be present in biological systems. However, in 1939 Leonor Michaelis (Michaelis 1939) proposed that all oxidation reactions involving organic molecules could be mediated by free radicals which stimulated interest in the role of free radicals in biological systems. In 1954, Commoner and his team found free radicals in biological systems (Commoner et al. 1954) and supposed them to be involved in various pathological processes (Gerschman et al. 1954) and ageing (Harman 1956). Since then, knowledge of involvement of free radicals in living processes has increased and they are mainly considered to play deleterious roles as damaging species which may account for cellular damage, mutagenesis, cancer and also to play a part in the degenerative process of biological ageing (Droge 2002, Harman 1956).

McCord and Fridovich's discovery of superoxide dismutase (SOD), the first protective enzyme to combat the deleterious effects of free radicals (McCord & Fridovich 1969), strengthened the supposition that free radicals are widely produced by living organisms. Free radicals were considered as deleterious to biological species and this inspired researchers to investigate oxidative damage inflicted by such species upon DNA, proteins, lipids and other components of the cell.

The deleterious role was substantially challenged when the first advantageous biological effects of free radicals was reported, that hydroxyl radicals stimulate the activation of gunaylate cyclase and formation of the "second messenger" cyclic guanosine monophosphate (cGMP) (White et al. 1976, Mittal & Murad 1977). However, later it was found $NO^{\bullet}$ was responsible for converting guanosine 5'-triphosphate (GTP) into cGMP by activating the sGC (Denninger & Marletta 1999). Studies in the 1970s suggested $O_2^{\bullet -}$ to be

responsible for combating infective agents by immune system (Babior et al. 1973, 1975, Rossi et al. 1985). In 1980, vascular endothelial release of nitric oxide from L-arginine was found to be responsible for the biological activity of the endothelium-derived relaxing factor (EDRF), which led researchers to an initial understanding of the role of nitric oxide and other reactive species in signaling function (Furchgott & Vanhoutte 1989, Palmer et al. 1988). It was also found that hormones like insulin regulate the level of free radicals (Spagnoli et al. 1995) and they were suggested to be regulators of core metabolic pathways (Shaikhali et al. 2008). Therefore, these studies have shown free radicals are active participants in diverse processes and they not only act as damaging agents but are also essential for normal functioning of living organisms. Such discoveries have led to an enormous expansion in free radical research aimed at understanding their source, their identification and their role.

1.2 What are free radicals and how they are formed?

A "Free Radical" is a molecule or ion that has one or more unpaired electron in the outer shell and is capable of independent existence (Halliwell & Gutteridge 2007). An unpaired electron is one that occupies an atomic or molecular orbital on its own. A free radical is denoted by a superscript dot, usually placed upon the element which is believed to contain the unpaired electron. The simplest free radical is atomic hydrogen, $H^{\bullet}$, with one unpaired electron. Due to the presence of unpaired electrons free radicals are slightly attracted towards a magnetic field (i.e., paramagnetic) and are generally highly reactive acting as carrier chains in chemical reactions. However, the degree of reactivity varies widely. A free radical can have a positive charge, negative charge or be neutral. Examples include: the hydroxyl radical ($HO^{\bullet}$) oxidising the sedative drug promethazine (PR) to a promethazine radical cation (1), oxygen being reduced to superoxide radical anion by addition of one electron (2) and CCl_4 undergoing dissociative electron capture to form the trichloromethyl radical (neutral) (3) (Slater 1984, Halliwell & Gutteridge 2007).

$$PR + OH^{\bullet} \rightarrow PR^{\bullet+} + OH^{-} \quad \text{——————} \quad (1)$$
$$O_2 + e^{-} \rightarrow O_2^{\bullet-} \quad \text{——————————} \quad (2)$$
$$CCl_4 + e^{-} \rightarrow {}^{\bullet}CCl_3 + Cl^{-} \quad \text{——————} \quad (3)$$

Radicals may be formed by losing a single electron from a non-radical, to give a radical cation (4) or by the gain of one electron forming a radical anion (5). Radicals are also formed by breaking of a covalent bond involving either homolytic fission or by heterolytic fission (6) and (7) respectively. In heterolytic fission Y receives both electrons, this gives Y negative charge and B is left with positive charge and neither species is a free radical.

$X + e^- \rightarrow X^{\bullet +}$ (radical cation) ——————— (4)
$Y + e^- \rightarrow Y^{\bullet -}$ (radical anion) ——————— (5)
$X{:}Y \rightarrow X^{\bullet} + Y^{\bullet}$ (homolytic fission)——————— (6)
$X{:}Y \rightarrow X^{+} + Y{:}^{-}$ ——————————— (7)

Free radicals are perpetually generated in the cells as a consequence of both enzymatic and non-enzymatic reactions. Enzymatic reactions which serve as a source of free radicals include those involved in respiratory chain, in prostaglandin synthesis, and in the cytochrome P-450 system, whereas non-enzymatic reactions involves the reaction of oxygen free radicals (Lobo et al. 2010). Other sources of free radicals include the absorption of ionising radiation such as gamma, UV, visible or thermal (Slater 1984, Halliwell & Gutteridge 2007). The effect of ionizing radiation on biological material is to produce a variety of free radicals, mainly $H^{\bullet}$ and $OH^{\bullet}$, which may react with the neighbouring biomolecules. Initiation of free radical formation can be also be undertaken in photosensitized reactions, in which the photosensitizer absorbs light of appropriate wavelengths leading to development of singlet oxygen. Singlet oxygen is not a free radical, but can interact with polyunsaturated fatty acids to initiate lipid peroxidation (Slater 1984, Min & Boff 2002).

Some endogenous generated sources of free radicals are: mitochondria, xanthine oxidase, peroxisomes, inflammation, phagocytosis, arachidonate pathways, exercise, ischemia/reperfusion injury and some exogenous generated sources of free radicals are: cigarette smoke, environmental pollutants, radiation certain drugs, pesticides, industrial solvents and ozone.

1.3 Major types of free radicals and metal induced free radicals

There are various type of free radicals generated in biological systems such as oxygen free radicals (part of a group known as “Reactive oxygen species” or ROS); nitrogen free radicals (part of a group known as “Reactive nitrogen species” or RNS), reactive halogen species and reactive sulfur species. In this section will focus on ROS and RNS. In most cases, the term “free radicals” and “ROS” are used interchangeably which can be correct, but in some cases it can be wrong. The easiest way to clarify and discriminate between these two terms can be based on analysis of ROS generation, interconversion and its elimination. These processes are schematically presented in Figure 1.1. In living organisms under aerobic conditions 90% of consumed oxygen is directly reduced to water by cytochrome oxidase in the electron transport chain (ETC) without release of any ROS (Ott et al. 2007). Of the remaining 10% most of the consumed oxygen is reduced

via one electron pathways resulting in conversion of molecular oxygen to superoxide anion radicals ($O_2^{\bullet-}$) which is further reduced to hydrogen peroxide (H_2O_2) by one electron and two protons (H^+). H_2O_2 is not a free radical but is more chemically reactive than molecular oxygen and due to this fact it is included in ROS group. Hydrogen peroxide accepts one electron to form a hydroxyl radical ($HO^\bullet$) and hydroxyl anion (HO^-). The hydroxyl radical accepts a further electron and proton to form water molecule. Summarizing the above processes: $O_2^{\bullet-}$, $HO^\bullet$ and H_2O_2 are called reactive oxygen species, but only $O_2^{\bullet-}$and $HO^\bullet$ can be called free radicals. *Hence all oxygen radicals are ROS, but not all ROS are oxygen radicals* (Halliwell & Gutteridge 2007). ROS are well known for their dual roles as being both deleterious and beneficial species within biological systems (Valko et al. 2006); when present at low or moderate concentration they act as regulatory mediators in signalling processes (Droge 2002). When there is overproduction of ROS/RNS on one side and a deficiency of enzymatic/non-enzymatic anti-oxidants on the other side, this can cause oxidative stress and nitrosative stress, for ROS and RNS respectively, which can cause damage to cell structure (lipids, cell membranes, proteins and nucleic acids) (Poli et al. 2004, Valko et al. 2007). This fine balance between the beneficial and harmful effects is a very important aspect in living organism and is achieved by mechanism known as "redox regulation". The process of "redox regulation" protects living organisms from various oxidative stresses and maintains "redox homeostasis" by controlling the redox status in living organism (Valko et al. 2007, Droge 2002). During a life cycle a cell's antioxidant defence system is involved in counteracting the oxidative damage caused by ROS, but still the oxidative damage accumulates. Moreover, radical related damage to DNA, to proteins and to lipids has been put forward as playing a key role in the development of age related diseases like cancer, arteriosclerosis, arthritis and neurodegenerative disorders (Halliwell & Gutteridge 2007).

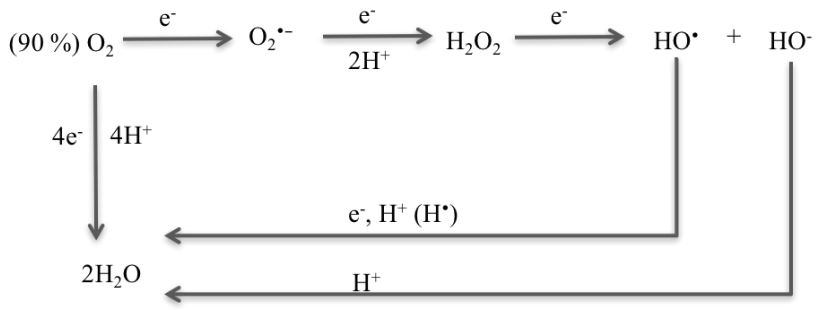

Figure 1.1: Reduction of molecular oxygen via four electron and one electron schemes (Lushchak 2014).

In past four decades numerous laboratories have confirmed that, of all the cell organelles, the mitochondria are the most actively involved in the production of $O_2^{\bullet-}$ rad-

icals. The formation of superoxide takes place on the outer mitochondrial membrane in the matrix and on both sides of the inner mitochondrial membrane (Turrens 2003). While $O_2^{\bullet-}$ is generated in the matrix, the mitochondrion has several antioxidant defences intended to eliminate both $O_2^{\bullet-}$ and H_2O_2. This, therefore leads to a steady concentration of $O_2^{\bullet-}$ and H_2O_2 which have been estimated to be around 10^{-10} M and 5×10^{-9} M respectively (Turrens 2003).

1.3.1 Reactive Oxygen Species (ROS)

Radicals derived from oxygen represent the most important class of radical species generated in living systems (Miller et al. 1990). ROS can be produced from exogenous and endogenous sources both contributing to the intracellular ROS level. The exogenous sources, like pollutants, tobacco, smoke, drugs, exposure to xenobiotics (such as chlorinated compounds), metal (redox and non-redox) ions, ionizing radiation and environmental agents (such as non-genotoxic carcinogens) can directly or indirectly induce ROS in cells (Miller et al. 1990, Klaunig et al. 1997). The endogenous source includes mitochondria, cytochrome P450 metabolism, peroxisomes and inflammatory cell activation (Inoue et al. 2003). Oxygen easily accepts unpaired electrons to give rise to species such as superoxide anion ($O_2^{\bullet-}$), hydrogen peroxide (H_2O_2), the hydroxyl radical ($HO^{\bullet}$), peroxyl ($ROO^{\bullet}$) and alkoxyl ($RO^{\bullet}$) radicals which may be involved in the initiation and propagation of free radical chain reactions and which are potentially damaging to cells (Riley 1994).

Molecular oxygen (dioxygen) has a unique electronic configuration and qualifies as free radical: it has two unpaired electrons, each in a different π^* (anti-bonding) orbital. With the addition of one electron to the ground state O_2 molecule, it enters a π^* (anti-bonding) orbital to form the superoxide anion radical ($O_2^{\bullet-}$) (Halliwell & Gutteridge 2007). A superoxide anion radical has a short half-life and serves as intermediate during the reduction of molecular oxygen to hydrogen peroxide. Hydrogen peroxide is the most abundant stable ROS with the longest half-life. It can pass easily through cellular membranes and is responsible for the production of the hydroxyl radical which is a highly reactive ROS due to a very short half-life; it reacts with other biomolecules at the site of production (Dalle-Donne et al. 2006) Figure 1.2.

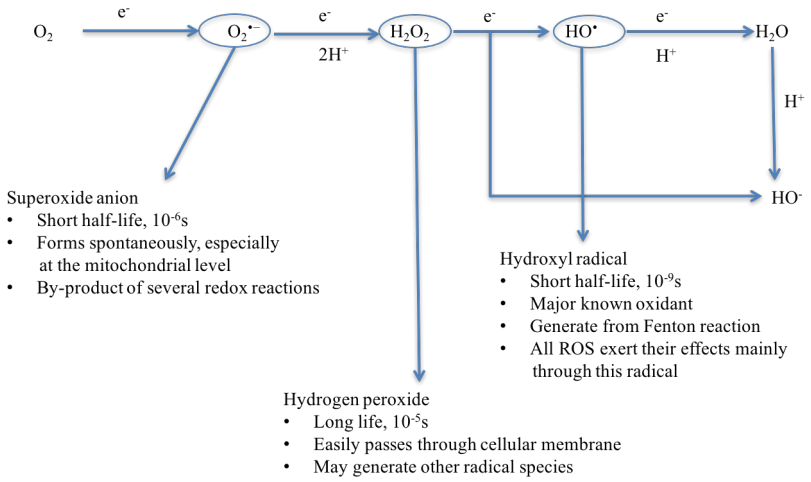

Figure 1.2: General features of reactive oxygen species (ROS) (Dalle-Donne et al. 2006).

The superoxide anion radical can arise through metabolic processes or following oxygen activation by physical irradiation; this is considered as "primary" ROS. It can react with other molecules either directly or through enzyme or metal catalysed processes to form "secondary" ROS (Valko et al. 2005). Production of superoxide occurs mostly within the mitochondria of a cell. In mammalian cells, the mitochondrial electron transport chain is the main source of adenosine triphosphate (ATP), which is essential for life. Under normal conditions it has been found that about 1% of the mitochondrial electron flow primarily leads to the formation of a superoxide anion that is generated from the univalent reduction of molecular oxygen. This process is mediated by enzymes such NAD(P)H oxidase and xanthine oxidase or non-enzymically by redox-reactive compounds such as the semi-ubiquinone compound on the mitochondrial electron transport chain (Droge 2002). At the ultra structural level, mitochondrial complex I and complex III are responsible for production of superoxide anion radical during the ETC and can easily cross the inner mitochondrial membrane. Superoxide is produced in complex I during reverse electron transport, where an electron enters complex I through coenzyme Q binding (Murphy 2009). It has been found that superoxide from Complex I is released into the matrix, as it has been shown that Complex III releases superoxide especially when mitochondrial respiration is suppressed by antimycin A to both sides of the inner mitochondrial membrane, however measurement of hydrogen peroxide suggests that this contributes to only 50 % of the total electron leakage even in mitochondria lacking Cu, Zn-SOD. The remaining 50% could be due the superoxide release to the matrix (Muller et al. 2004, Brand 2010).

Endoplasmic reticulum (ER) also produces superoxide during oxidative stress. ER is a very well-orchestrated protein folding machine containing protein chaperons, proteins

that catalyse protein folding and sensors that detect the misfolded and unfolded proteins. A very sophisticated and sensitive mechanism exists that prevents misfolded proteins from entering the secretory pathways and ensuring the misfolded proteins are directed toward the degradative pathways; during this process superoxide is generated as a by-product (Malhotra & Kaufman 2007). There are two enzymes responsible for the correct protein folding protein disulfide isomerase (PDI) and ER oxidoreductin 1 (Ero1). Ero1 is a conserved flavin adenine dinucleotide (FAD)-dependent enzyme, which can be oxidized by molecular oxygen and, in turn, can act as a specific oxidant of PDI, which can directly oxidize disulfide bonds (Tu et al. 2000). The disulfide bond formation mechanism can account for 25% of the cellular ROS produced during protein synthesis, a principle drain on cellular energy resources. PDI facilitates the correct folding of proteins by rearranging the incorrectly formed disulfide bonds and by oxidase activity that introduces disulfides into proteins. PDI is converted into a reduced form by accepting an electron, which then transfers to Ero1, thereby recycling itself. Based on flavin dependent redox chemistry, superoxide is generated when molecular oxygen accepts an electron from Ero1. Similar to the ER mediated process, a superoxide anion is also generated when glutathione (GSH) is reduces an unstable disulfide bond and is thereby depleted (Malhotra & Kaufman 2007). Reduced GSH is the most abundant antioxidant preventing thiol groups from oxidising either directly by reducing reactive species or indirectly through catalytic process such as glutathione peroxidase (GPx). GSH acts as a major thio-disulfide redox buffer in cells and the ratio of GSH and GSSG (oxidised form) is used as an index in the redox state. This ratio is normally 1:1 or 3:1 in the ER lumen. Change in the ratio of GSH (lower) to GSSG results in ER stress which can lead to the unfolded protein response (UPR) eliciting calcium leakage from ER into cytosol which triggers the production of superoxide in the mitochondria (Csordas & Hajnoczky 2009). The mechanism of protein folding and refolding is an ATP dependent process and decreases in ATP result in ER stress which can stimulate mitochondrial oxidative phosphorylation to increase the generation of ATP resulting in more formation of ROS (Malhotra & Kaufman 2007).

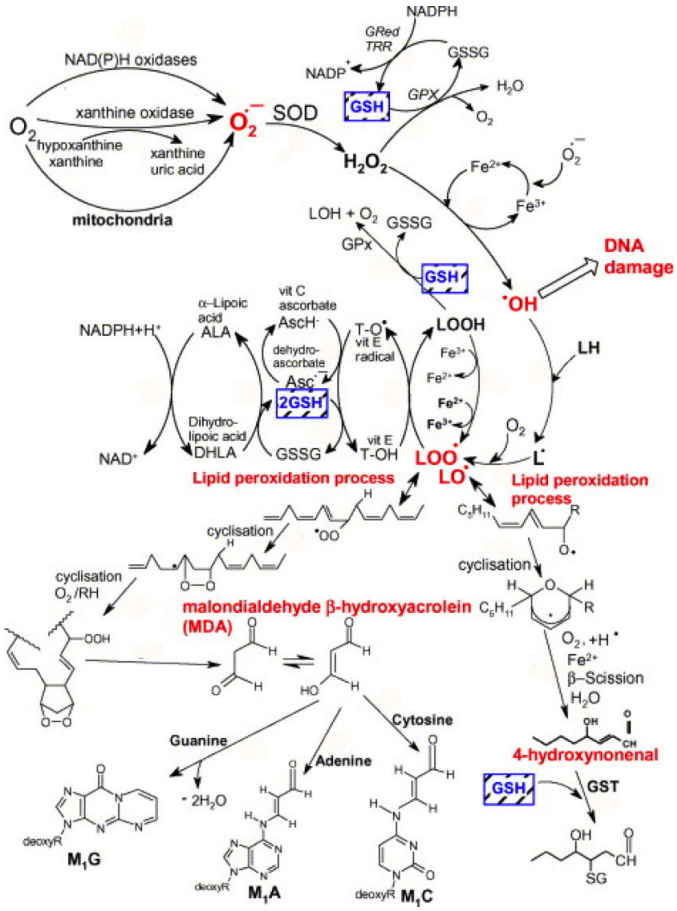

Figure 1.3: Generation of ROS (Valko et al. 2007).

SODs convert superoxide enzymatically into hydrogen peroxide, as shown in Figure 1.3 (Valko et al. 2007). In biological tissues superoxide can also be converted non-enzymatically into the non-radical species by hydrogen peroxide and singlet oxygen ($^1O_2$). In the presence of reduced transition metals (e.g. ferrous or cuprous ions), hydrogen peroxide may be converted into highly reactive hydroxyl radicals ($HO^\bullet$). Alternatively, hydrogen peroxide may be converted into water by the enzyme catalase or glutathione peroxidase (Figure 1.3). In the glutathione peroxidase reaction glutathione is oxidised to glutathione disulfide, which can be converted back to glutathione by glutathione reductase in an NADPH-consuming process (Ye et al. 2015, Droge 2002) (Figure 1.3).

The hydroxyl radical ($HO^\bullet$) is the neutral form of the hydroxide ion and is the most reactive ROS with very short *in vivo* half-life of 10^{-9}s. Thus, when generated *in vivo*, $HO^\bullet$ reacts close to its site of formation (Dalle-Donne et al. 2006). Hydroxyl radicals have the ability to oxidize the neighbouring functional group of chemical compounds; as an example, dimethyl sulfoxide (DMSO) may be oxidised to a methyl radical by a hydroxyl radical. Transition metals like iron and copper are largely linked to the redox state of the

cell, which is maintained within strict physiological limits. It has been demonstrated that iron regulation ensures that there is no free intracellular iron, however, under stress conditions, there is an over-production of superoxide anions which release "free iron" from iron containing molecules. The release of iron by superoxide has been shown for [4F-4S] clusters containing enzymes of the dehydratase-lyase family (Liochev & Fridovich 1994). The release Fe^{2+} can participate in the Fenton reaction, resulting in the production of hydroxyl radicals ($Fe^{2+} + H_2O_2 \rightarrow Fe^{3+} + HO^{\bullet} + HO^{-}$). Thus, during stress conditions, superoxide acts as an oxidant of [4Fe-4S] and facilitates $HO^{\bullet}$ production from H_2O_2 by making Fe^{2+} available for Fenton reaction (Valko et al. 2005, Leonard et al. 2004). The superoxide radical also participates in the Haber-Weiss reaction ($O_2^{\bullet-} + H_2O_2 \rightarrow O_2 + HO^{\bullet} + HO^{-}$), which combines the Fenton reaction and the reduction of Fe^{3+} by superoxide producing Fe^{2+} and oxygen ($Fe^{3+} + O_2^{\bullet-} \rightarrow Fe^{2+} + O_2$) (Liochev & Fridovich 1994, Valko et al. 2007). The Fe-S cluster contains iron responsive elements (IRE)-binding protein (IRE-BP). This Fe-S is responsible for sensing the intracellular iron level, and accordingly, modifies the ability of the IRE-BP to interact with iron-responsive elements. The cellular iron sensing mechanism for iron status is activated when the Fe-S cluster in aconitase is disassembled including the inactivation of aconitase and the subsequent activation of cytosolic IRE/IRP-1 (Iron regulatory protein-1). In mammalian cells, during oxidative stress, aconitase is inactivated or, under conditions of iron deprivation, oxidants are able to convert cytosolic aconitase into active IRE-BP which increases the "the free iron" concentration by decreasing the biosynthesis of ferritin and increasing biosynthesis of transferrin receptors (Han et al. 2005, Kotamraju et al. 2004, Mena et al. 2011).

Other reactive ROS radicals that can be formed in living system are the peroxyl radical ($ROO^{\bullet}$) (Figure 1.3), where the simplest peroxyl radical is $HOO^{\bullet}$ which is a protonated form of superoxide ($O_2^{\bullet-}$) and which is known as the hydroperoxyl radical or perhydroxyl radical. In normal cells the pKa value of $HOO^{\bullet}$ is 4.8 (approx.) and, therefore, only approximately 0.3% of any superoxide present in the cytosol is in the protonated form (De Grey 2002). It has been found that the hydroperoxyl radical initiates fatty acid peroxidation by two parallel pathways: fatty acid hydroperoxide (LOOH) dependent and LOOH independent (Aikens & Dix 1993). The LOOH dependent pathway of $HOO^{\bullet}$ initiated fatty acid peroxidation may be relevant to mechanisms of lipid peroxidation initiation *in vivo*. The addition of O_2 to the fatty acid radicals form peroxyl radicals ($LOO^{\bullet}$), which are the chain propagating species of lipid peroxidation. They can occur either chemically (K_2O_2) or enzymatically (xanthine oxidase) (Aikens & Dix 1991). The xanthine oxidoreductase (XOR) enzyme can easily be interconverted to xanthine oxidase (XO) and xanthine dehydrogenase (XD) (Borges & Fernandes 2002). In purine catabolism, XOR catalyzes the oxidative hydroxylation of hypoxanthine to xanthine and, subsequently, to uric acid. Uric acid acts as an antioxidant and free radical scavenger and, therefore, as a

cellular defence enzyme against oxidative stress. Both XO and XD, especially XO, form numerous ROS and RNS (Vorbach et al. 2003). Hence, XOR is an important protective regulator of the cellular redox as it can synthesize both the antioxidant uric acid and various free radicals (ROS and RNS). Hydroxyl radicals may react with any biomolecules either by hydrogen abstraction, addition or electron transfer. There are many examples of molecular oxygen yielding peroxyl free radicals which then readily remove hydrogen from other biomolecules, producing hydroperoxide and a free radical and thus starting the cycle again in the chain propagation process. Chain propagation is one of the reasons why ROS may cause more damage (Floyd 1990).

Hydrogen peroxide is produced in peroxisomes. Peroxisomes are known as the major sites of oxygen consumption in a cell and participate in numerous metabolic functions that use oxygen. Hence, oxygen consumption in the peroxisomes leads to the production of H_2O_2, which can oxidize a variety of molecules. The organelle also contains the enzyme catalase which decomposes hydrogen peroxide and prevents accumulation of this toxic compound. Thus, the peroxisome maintains a delicate balance of the concentration or the activities of these enzymes to make sure no ROS are produced. However, when peroxisome is damaged H_2O_2 consuming enzymes are down regulated and H_2O_2 is released into the cytosol which significantly contributes to oxidative stress (Valko et al. 2004, 2007).

1.3.2 Reactive Nitrogen Species (RNS)

The other major class of reactive species are "Reactive Nitrogen Species" (RNS) which includes nitric oxide ($^{\bullet}$NO). Nitric oxide has an unpaired electron in an anti-bonding orbital and is therefore a free radical. $^{\bullet}$NO is generated in biological tissue by nitric oxide synthases (NOSs); there are several known NOSs including neuronal NOS (nNOS), endothelial NOS (eNOS) and inducible NOS (iNOS). NOSs metabolise L-arginine to L-citrulline with the formation of $^{\bullet}$NO via a five electron oxidation reaction (Ghafourifar & Cadenas 2005). $^{\bullet}$NO has a half-life of only few seconds in an aqueous environment, however it has greater stability in a relatively lower oxygen concentrated environment (half-life > 15s). Depending upon the microenvironment, $^{\bullet}$NO can be converted to various other RNS species such as nitrosonium cation (NO^+), a nitroxyl anion (NO^-) or peroxynitrite ($ONOO^-$) (Stamler et al. 1992). $^{\bullet}$NO is an abundant radical that acts as an important oxidative biological molecule in a large variety of diverse physiological processes (such as neurotransmission, cellular defence, smooth muscle relaxation and immune regulation). Following the discovery of many of its extraordinary biological properties, $^{\bullet}$NO was given the title of "molecule of the year" in 1992 by Science Magazine (Koshlan 1992).

$^{\bullet}$NO can easily diffuse through the cytoplasm and plasma membrane as it is soluble in both aqueous and lipid media (Chiueh 1999). In the extracellular environment $^{\bullet}$NO can react with oxygen and water to form nitrate and nitrite anions. Overproduction of

RNS is called “nitrosative stress”, due to a shift in balance towards the RNS which may occur when the system’s ability to neutralise or eliminate the RNS decreases. Nitrosative stress may lead to nitrosylation reactions that can alter the structure of proteins and so inhibit their normal function (Valko et al. 2007). The effect of $^{\bullet}NO$ on cells depends on various complex parameters such as rate of production of $^{\bullet}NO$, its rate of diffusion, the levels of enzymes (e.g. catalase and SOD), the levels of antioxidants (such as GSH) and the distance between the site of production and the target cells (Chen et al. 1998). During inflammatory processes there is an oxidative burst which results in the production of both the superoxide anion and nitric oxide in the immune system cells. Under these conditions, nitric oxide reacts with the superoxide anion to produce significant amounts of a much more oxidatively active molecule (peroxynitrite). The reaction of $^{\bullet}NO$ and $O_2^{\cdot-}$ has one of the highest rate constants ($7.0x10^{-9}s^{-1}$) known for reactions, thus $^{\bullet}NO$ can predominantly be linked to its ability to combine with superoxide anions. The peroxynitrite anion ($ONOO^-$) can oxidize and nitrate DNA (and may potentially cause strand breaks by attacking on the sugar-phosphate backbone) and can also cause lipid oxidation (Carr et al. 2000). N_2O_3 is able to directly nitrosate the primary amine function of the DNA base and deaminate it.$^{\bullet}NO$ derived species can also form DNA-DNA and DNA-protein cross links (Dedon & Tannenbaum 2004).

Nitric oxide also binds with certain transition metal ions such as Fe. In fact, many physiological effects of $^{\bullet}NO$ are due to its initial binding to Fe^{2+}-Haem groups in the enzyme soluble guanylate cyclase (sGC), shown in equation (8). The product represented in equation 8 is $\{Fe^{2+}\text{-}^{\bullet}NO\}$ along with $\{Fe^{3+}\text{-}NO^-\}$. The convention $\{FeNO\}^7$, whereby the superscript is the sum of the d electrons on the metal (here 6 or 5) and the occupancy of relevant NO π^* orbital (here 1 or 2), is often employed to avoid the specific assignment of an oxidation state (Valko et al. 2004).

$$Fe^{2+}\{sGC\} + {}^{\bullet}NO \rightarrow Fe^{2+}\{sGC\} - NO \quad \text{———(8)}$$

1.3.3 Metal induced free radicals

Most of the transition metals contain unpaired electrons in their atoms/ions which makes them able to accept or donate single electrons and thus qualify as free radicals, the only exception is Zinc. Iron, manganese and copper can be grouped together as three d-block transition metals which cofactor most of dioxygen (O_2) manipulating proteins. This is due to their similar chemical and physical properties especially their characteristic of sharing their unpaired d-shell valence electron with those of O_2 (Paulette & Archibald 1987). It has also been shown that non-enzyme forms of Fe, Cu and Mn play an important role in generation of oxygen free radicals. The ability of non-enzyme Fe and Cu to catalyze hydroxyl radical production is through a “Fenton” or “Haber-Weiss” type reaction and is

dependent on $O_2^{\bullet-}$ and H_2O_2.

1.3.3.1 Iron

The most common forms of iron that are present are ferrous (Fe(II)) and ferric (Fe(III)) ions. In aqueous solution in presence of air, Fe^{3+} has the most stable oxidation state, whereas Fe^{2+} is weakly reducing and thus ferryl compounds are powerful oxidizing agents. Fe^{2+} undergoes one electron oxidation reacting with oxygen dissolved in a solution to yield $O_2^{\bullet-}$ as shown in equation 9.

$$Fe^{2+} + O_2 \rightarrow [Fe^{2+}\text{-}O_2 \leftrightarrow Fe(III)\text{-}O_2^{\bullet-}] \leftrightarrow Fe(III) + O_2^{\bullet-} \text{————————-(9)}$$

Iron has four unpaired electrons and a high spin state. When Fe^{2+} binds with a ligand the energy levels of 3d orbitals are altered; if the energy differences between different 3d orbitals are sufficient, the electron can pair up with the lower energy orbitals. These make the Fe^{2+} exist in a low spin state; with no unpaired electrons it will be more stable and difficult to oxidize e.g., oxyhaemoglobin and oxymyoglobin (Halliwell & Gutteridge 2007).

1.3.3.2 Copper

Copper has two common oxidation states, copper (I) and copper (II) as shown in equation 10. The one electron difference between Cu^+ and Cu^{2+} allows copper to promote radical reactions. Under appropriate conditions, copper ions react with two $O_2^{\bullet-}$ radicals and two H^+ ions to form H_2O_2 and O_2 i.e., catalysing the dismutation of $O_2^{\bullet-}$.

$$Cu^{2+} + O_2^{\bullet-} \rightarrow Cu^+ + O_2$$
$$H^+ + Cu^+ + HO_2^{\bullet} \rightarrow Cu^{2+} + H_2O_2$$
$$O_2^{\bullet-} + Cu^+ + H_2O \rightarrow Cu^{2+} + OH^- + HO_2^-$$
$$\text{Net: } O_2^{\bullet-} + O_2^{\bullet-} + 2H^+ \rightarrow H_2O_2 + O_2 \text{ ————————-(10)}$$

It has been shown that copper has a high affinity for and can bind to some cellular biomolecules which catalyze the formation of $HO^{\bullet}$ causing damage to cellular biomolecules (Samuni et al. 1984). In presence of hydrogen peroxide and ascorbate (vitamin C) copper can be reduced from the divalent (Cu^{2+}) to the monovalent state (Cu^+); then via a Fenton-like reaction copper catalyzes the production of hydroxyl radicals, which are probably responsible for the damage to biomolecules (Makrigiorgos et al. 1995).

1.3.3.3 Manganese

Manganese is most stable in aqueous solution as Mn^{2+}. Other oxidizing forms of manganese include Mn(III), Mn(IV) and Mn(VII). Mn^{2+} can interact with $O_2^{\bullet-}$ shown in equation 11.

$$Mn^{2+} + O_2^{\bullet-} \rightarrow Mn(O_2)^{+}$$
$$Mn(O_2)^{+} + O_2^{\bullet-} + 2H^{+} \rightarrow Mn^{2+} + H_2O_2$$
$$Mn(O_2)^{+} + 2H^{+} \rightarrow H_2O_2 + Mn^{3+} \quad \text{——————(11)}$$

Like copper, Mn^{2+} is also capable of catalysing the dismutation of $O_2^{\bullet-}$ to H_2O_2. However, like Fe^{2+} and Cu^{2+}, unchelated Mn^{2+} does not react with H_2O_2 to form $HO^{\bullet}$ at a measurable rate.

1.4 Antioxidants

Excessive or uncontrolled production of ROS can cause damage to DNA, proteins and lipids and these are closely related to many pathological conditions. However, ROS need not be harmful to normal cellular functions as long as redox homeostasis is regulated; as ROS/RNS are important signalling messengers for proliferation, differentiation, apoptosis and other critical events during development. Therefore, growth in multicellular organisms depends on maintaining the proper balance between the cell division and differentiation. Under normal conditions cells have developed enzyme and non-enzymatic antioxidant mechanisms to balance the effects of any free radicals produced (Cadenas 1997). Such antioxidant defences are extremely important as they directly remove the free radicals, thus providing maximum protection for biological sites. The antioxidant mechanisms are versatile; they not only differ between organisms and tissues but between the different cellular components of the cells as well. The defence mechanism against free radicals involves (Figure 1.4): (1) superoxide dismutase (SOD), which is a radical scavenger which accelerates the dismutation of $O_2^{\bullet-}$ to O_2 to less reactive H_2O_2, and glutathione peroxidase (GPx) and catalase (CAT) which convert H_2O_2 to water. (2) non-enzymatic hydrophilic radical scavengers including ascorbic acid (which reacts with superoxide in the aqueous phase) and glutathione (GSH), (3) non enzymatic lipophilic radicals such as alpha-tocopherol (vitamin E) and which react with superoxide in the lipophilic phase, flavonoids, carotenoids, and ubiquinol, (4) enzymes such as GSH reductase and dehydroascorbate reductase which reduce the oxidized forms of molecular antioxidants while thioredoxin reductase is responsible for the maintenance of protein thiols, and (5) glucose-6-phosphate dehydrogenase which maintains the reducing environment in the cells by generating NADPH (Beckam and Ames, 1998). Some antioxidants are able

to generate other antioxidants restoring the original antioxidants. This process is called an "antioxidant network" e.g., the redox cycles of vitamins E and C (Sies et al. 2005). The capacity to regenerate one antioxidant by another is driven by the redox potentials of a redox couple.

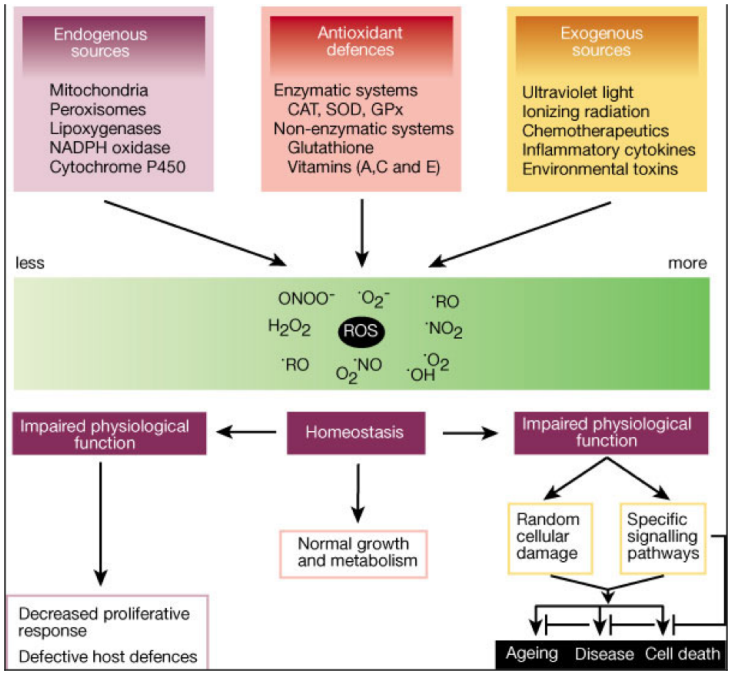

Figure 1.4: Sources and cell-based responses to ROS (Finkel & Holbrook 2000).

1.4.1 Superoxide dismutases (SOD)

SOD acts as the front line of enzymatic defence and catalyzes the conversion or dismutation of superoxide radicals ($O_2^{\bullet -}$) to H_2O_2 and molecular oxygen (O_2) (as shown in equations 12 and 13). SOD is found in both animal and plant cells with sub-cellular fractionation studies showing that Cu/Zn-SOD is located primarily in the cytosol and that Mn-SOD is located in the mitochondria for both animals and plants (Halliwell & Gutteridge 2007). Fe-SODs are yet to be found in animal tissues, but some algae, yeasts and higher plants do have Fe-SOD located in the chloroplast (Halliwell & Gutteridge 2007).

$$Cu^{2+}\text{-SOD} + O_2^{-} \rightarrow Cu^{+}\text{-SOD} + O_2 \quad (12)$$

$$Cu^{+}\text{-SOD} + O_2^{-} \rightarrow Cu^{2+}\text{-SOD} + H_2\,O_2 \quad (13)$$

The relative amount of Cu/Zn-SOD and Mn-SOD in animals depends on the tissue and species, therefore, mammalian erythrocytes (with no mitochondria) do not have Mn-SOD. For bacteria and fungi (and possibly green plants) the growth conditions can certainly

make a difference in the presence of relative amounts of different SOD, for example, fungus *Dactylium dendroides* shows 80% of its SOD activity as Cu/Zn-SOD and 20% as MnSOD in normal growth media. However, when there is a shortage of copper supply more Mn-SOD is synthesized to maintain the total cellular SOD activity (Halliwell & Gutteridge 2007).

Colombrita et al. reported the presence of the SOD in the brain and deregulation or mutation of SODs are associated with several degenerative neurological disorders including amyotrophic lateral sclerosis (ALS), Parkinson's disease (PD), Alzheimer's disease (AD) and Down's syndrome (Colombrita et al. 2003, Noor et al. 2002).

1.4.2 Glutathione

Glutathione (GSH) is a water soluble tripeptide with structure L-γ-glutamyl-l-cysteinyl-glycine. The basic function of glutathione is its antioxidant role and is present in plants, mammals, fungi and some prokaryotic organisms (Townsend et al. 2003). When present in appropriate concentrations it can postpone or prevent auto-oxidation of free radicals. Therefore, GSH provides a first line of defence against reactive species. The presence of GSH both intracellularly or extracellularly is vital for cell survival (Baskin & Salem 1997). Cells have relatively high concentration of GSH, however the level of GSH can be increased by its synthesis. There are different pathways for the synthesis of GSH which are increasing the ability to reduce glutathione disulfide (GSSG) to GSH by GSSG reductase or by *de novo* GSH synthesis through induction of glutamate cysteine ligase (GCL) (Forman 2016).

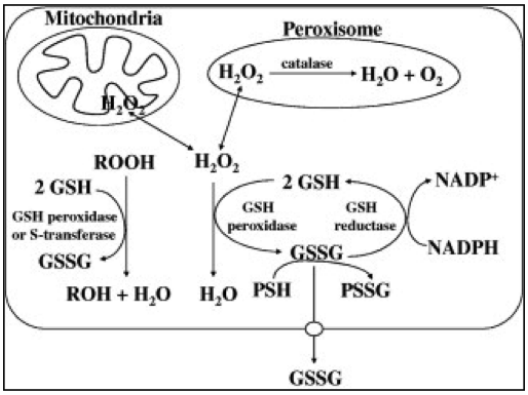

Figure 1.5: GSH's antioxidant properties (Lu 2009).

In Figure 1.5 GSH's antioxidant properties are shown which helps in regulating and maintaining the cell regulation. Under severe oxidative stress conditions the ability of a cell to reduce GSSG to GSH decreases leading to the accumulation of GSSG in cell.

Therefore, in order to prevent this, GSSG can be actively exported out of the cell or react with the protein sulfhydryl group leading to the formation of a mixed disulfide (Lu 2009). Thus, severe oxidative stress depletes cellular GSH.

1.4.3 Ascorbic acid (vitamin C)

Ascorbic acid occurs naturally and has antioxidant properties. It is a white crystalline solid which can easily dissolve in water. In 1928 Szent-Gyorgyi first isolated ascorbic acid from oranges as an acidic carbohydrate (Halliwell & Gutteridge 2007). The ascorbic acid structure (Figure 1.6) has two ionizable -OH groups with pK_a value of 4.25 and 11.5; at physiological pH (7.4) the monoanion is favoured and the compound is known as "ascorbate". Plants and most animals can synthesize ascorbate, however, for humans the enzymes required for the terminal step (gulonolactone oxidase) is absent and so an external supply of ascorbate is required in the diet. In collagen biosynthesis it plays an important role as a cofactor for at least eight enzymes such as proline and lysine hydroxylases for the hydroxylation of proline and lysine to form hydroxyproline and hydroxylysine. Hydroxyproline is essential for stabilizing the triple helical structure of collagen and hydroxylysine is important for collagen crosslink formation. Therefore, deficiency of ascorbate would produce defect in connective tissues giving rise to poor wound healing and fragility of the blood vessels because these tissues cannot stabilize the structure of collagen (Kishimoto et al. 2013). It is also an essential requirement for the dopamine-β-hydroxylase enzyme (a copper containing enzyme), for the conversion of dopamine to noradrenalin. Ascorbate deficiency leads to the disease of scurvy which can be cured by consuming oranges and other vitamin C rich fruits and vegetables (Halliwell & Gutteridge 2007).

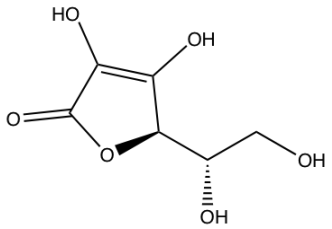

Figure 1.6: Structure of ascorbic acid.

In vitro, ascorbate can also exert pro-oxidant properties which can be used in the laboratory for the generation of hydroxyl radicals in the presence of Fe^{2+}, EDTA and H_2O_2. Ascorbate reduces Fe^{3+} to Fe^{2+} which then reacts with hydrogen peroxide to form hydroxyl radicals, as shown previously. Hence, ascorbate/Cu^{2+} mixtures inactivate many enzymes by forming hydroxyl radicals or oxo-copper species, and an Fe-salt/ascorbate

combination has been used in laboratories for lipid peroxidation and other oxidative damage (Halliwell & Gutteridge 2007).

1.5 Diseases associated with ROS

The literature supports the fact that the accumulation of free radicals can cause several degenerative diseases. The most common free radical associated diseases include: atherosclerosis, cancer, inflammatory joint disease, asthma, diabetes, senile dementia and degenerative eye disease. As mentioned previously, ROS are capable of damaging genetic material, causing lipid peroxidation in cell membranes and inactivating membrane-bound enzymes. Therefore, intervention via an external source of antioxidants is supportive in dealing with oxidative stress. The imbalance between ROS and the antioxidant defence systems are involved in the pathogenesis of several diseases and most commonly in cancer.

Also the imbalance in the concentration of $O_2^{\bullet-}$ and H_2O_2 leads to mitochondrial oxidative stress. Therefore, the diseases caused by free radicals are grouped under mitochondrial oxidative stress or an inflammatory oxidative response: (i) the mitochondrial oxidative stress group relates to diseases denoted by pro-oxidants moving the thiol/disulphide redox state and impairing glucose tolerance; (ii) the inflammatory oxidative response relates to diseases characterised the improved action of either NAD(P)H oxidase or xanthine oxidase. The damaging mechanisms of free radical such as lipid peroxidation, DNA damage, and protein oxidation are largely involved in the process of ageing (DeBalsi et al. 2016, Mandavilli et al. 2002). Oxidative/and nitrosative stress are considered as biomarkers of oxidative stress in acute and chronic diseases. These biomarkers are measured and evaluated in healthy and unhealthy subjects for long periods (Valko et al. 2007). Free radicals may be detected, directly or indirectly, using various analytical techniques, e.g. fluorimetry, spectrophotometry, chemiluminescence and electron paramagnetic resonance (EPR) spectroscopy. The methods employed to detect free radicals are often based on their redox properties. The drawback of these methods is their susceptibility to artefacts produced by species of similar reactivity or by reactive intermediates produced by the probe itself (Turrens 2003).

1.5.1 ROS and Cancer

Cancer is a multi-stage process involving unregulated cell growth. It can be categorized in at least three stages: initiation, promotion and progression. Oxidative stress plays a major role in all the three stages. ROS causes DNA damage by introducing gene mutations and structural modifications in DNA, reacting with sulphydryl groups in proteins and

enhancing the cross-linking/fragmentation of ribonucleoproteins during cancer initiation. Abnormal gene expression, obstruction of cell-to-cell communication, and alteration of second-messenger systems can all be attributes of ROS in the promotion stage. They cause a rise in cell proliferation or reduced apoptosis. Oxidative stress can further add DNA alterations to the initiated cell population participating in the progression stage of the cancer (Waris & Ahsan 2006).

In patients with diseases related to a risk of cancer there is an increased rate of oxidative DNA damage. Also, in cases such as Fanconi anaemia, chronic hepatitis, cystic fibrosis and various autoimmune diseases the patients demonstrate deficient repair mechanisms against oxidative stress. Several human-based studies experimentally demonstrate oxidative DNA damage to be the main mutagenic, and apparently carcinogenic, factor (Lee et al. 2012). The DNA damage caused by ROS during cell division is not repaired and this further leads to irreversible mutations. The most prominent mutation caused by ROS is the modification of guanine, producing G→T transversions. These transversions, if they occur in genes such as oncogenes or tumour suppressor genes (p53), result in cancer initiation and progression (Higinbotham et al. 1992, Soliman et al. 2007).

Oxidative DNA damage causes a range of mutations (such as the oxidation of the purines and pyrimidines, alkalilable sites and single stranded DNA breaks) and instability in the DNA backbone caused directly by, or during, the DNA repair mechanism. The multi-faceted DNA modifications due to ROS lead to permanent mutations that can cause carcinogenicity. Previous studies have demonstrated that ROS is capable of modifying all the four bases in DNA. The most common mutations are related to the modifications of the GC base pairs, although the AT base pairs are rarely mutated. Inducing a mutation in a single stranded DNA by treating it with oxygen free radicals introduces tandem double CC→TT substitution. The resulting raised levels of base pair modification in a tumorous tissue is due to the production of a large amount of H_2O_2 which is typical of a human cancerous tissue. Initiation of cancer in humans by ROS is further aggravated by the presence of oxidative DNA modifications in the cancer tissue. 8-hydroxy-2' -deoxyguanosine (8-OHdG) is one of the principal forms of free radical-induced oxidative lesions in nuclear and mitochondrial DNA. 8-OHdG is considered as a critical biomarker of oxidative stress and carcinogenesis (Valavanidis et al. 2009).

The accumulation of the mutated DNA bases together with increased attacks of $^{\bullet}OH$ are reported in inflammatory breast disease which can further lead to malignant breast cancer. There are reports that raised levels of 8-oxo-dG adducts in DNA are the key players in breast tumour occurrence and progression to the metastatic state (Malins et al. 1996). Chronic viral infections, like the hepatitis B or C viruses, induce oxidative damage and can cause cancerous conditions like carcinoma of the hepatic cells. The transition of G→T is also among the common types of mutation that is caused by aflatoxin lesion and

oxidative DNA damage that can lead to hepatocellular carcinoma. There are reports of the accumulation of 8-OHdG in the liver and the measurement of DNA damage in the liver function test can predict the initiation of liver cancer (Albano & Parola 2015). In the cases of chronic prostate hypertrophy the diagnosis occurs only after the age of 40 years. The delayed diagnosis is suggestive of an intricate pathway that leads to the tumorigenesis in the prostate. The prolonged accumulation of free radicals, along with endogenous cellular processes, may give rise to prostatic cancer (Sainz et al. 2012).

Comparing the typically mutated DNA bases in various tumour tissues to the respective normal tissues may help to understand the underlying mechanism of ROS involvement in carcinogenesis. Measuring the purine- and pyrimidine-derived DNA damage in tissues can provide insights into determining a link between free radical creating agents and the risk of cancer.

1.5.2 ROS and Ageing

A progressive decline in the ability of a physiological process after the reproductive phase of life can be defined as ageing. There are two theories of ageing namely: the genetic theory or intrinsic (programmed) theory and the free radical damage or extrinsic (error) theory. The genetic theory claims that the ageing process is genetically determined. It is controlled by genetic pathways. On the other hand, the free radical damage or extrinsic (error) theory leads to ageing under the influence of environmental forces and the prolonged accumulation of free radical caused damage. Certain evidence indicates that the start of senescence appears to be genetically determined, but there is an equivalent influence by the metabolic rate in the ageing process. A higher metabolic rate, the shorter the life span, as increased metabolic rates produce high ROS which cause more damage and reduce life expectancy (Simm & Bromme 2005).

Mitochondria (the cells' power house) are a major source of ROS, to which the mitochondrial free radical theory of ageing (MFRTA) has drawn attention. The literature is rich with evidence concerning mitochondrial ROS generation, toxicity and also the detoxification of ROS, as well as about how these parameters change with the physiological state of cells and organisms, and with chronological age. The theory suggests that ageing is a result of toxicity caused by ROS which is a part of a cycle wherein ROS produced in the mitochondria can damage the constituents of mitochondria leading to the generation of more ROS and so on (Balaban et al. 2005). Several observations support MFRTA, such as the fact there is a strong association between age, the extent of ROS generated and the oxidative damage caused. It has also been observed that, over the duration of ageing, the mitochondrial function is steadily lost. Evidence shows that inhibiting mitochondrial function can boost ROS generation. Nonetheless, various ageing disorders and diseases are linked with severe increases in oxidative stress. These observations provide robust

evidence that ageing is closely and strongly linked with the production of ROS and ROS-related cell damage (Balaban et al. 2005).

1.5.3 Aldehyde related disease

Aldehydes are strong electrophilic compounds with terminal carbonyl groups making them highly reactive and α,β-unsaturated aldehydes (such as 4-hydroxy-2-nonenal (4-HNE) and acrolein), also contain a second electrophile at the β-carbon (Yokoyama et al. 2001). Aldehydes are much more stable with a long life (unlike free radicals) and can react with cellular components in the vicinity of their formation and can also diffuse or be transported from the site of their origin (i.e. a membrane) and reach and attack targets intracellularly or extracellularly. Some aldehydes play a vital role in normal physiological processes, such as in vision, embryonic development and neurotransmission. However, many aldehydes are cytotoxic and carcinogenic. Aldehydes form adducts with various cellular targets like glutathione (GSH), nucleic acids and protein amino acids leading to impaired cellular homeostasis, enzyme inactivation, DNA damage and cell death (Brooks & Theruvathu 2005, Deans & West 2011).

Aldehydes that are generated can be exogenous and endogenous, and can act as precursors during numerous physiological processes (including the biotransformation of endogenous compounds such as amino acids, neurotransmitters, carbohydrates, lipids and metabolism of alcohol). A major source of endogenously produced aldehyde is lipid peroxidation (LPO). Amino acid catabolism generates several aldehydes intermediates, including glutamate γ-semialdehyde, while neurotransmitters (such as γ-aminobutyric acid (GABA), serotonin, noradrenaline, adrenaline and dopamine) also give rise to aldehyde metabolites. Xenobiotics and drugs - including ethanol - generate aldehydes and the anticancer drugs cyclophosphamide (CP) and ifosfamide generate acrolein which is an important aldehyde precursor. Various aldehydes like formaldehyde, acetaldehyde and acrolein are also ubiquitous in the environment and are present in cigarette smoke and motor vehicle exhaust fumes. Aldehydes are also used or generated in industrial applications like production of resins, polyurethane and polyester plastics. Along with these, numerous dietary aldehydes (which include citral and benzaldehyde) are naturally present or are approved additives in various foods where they impart flavour and odour (O'Brien et al. 2005).

1.5.3.1 The lipid peroxidation process

More than 200 aldehydes species are generated from the oxidative degradation of cellular membrane lipids, also known as lipid peroxidation (LPO). During LPO a variety of ROS/RNS oxidize lipids leading to free radical chain reactions and subsequent formation

of bioproducts (such as lipid radicals, hydrocarbons and aldehydes). These by-products further react and modify both proteins and DNA resulting in toxicity and mutagenesis and are, therefore, associated with ageing, neurological disorders and cancer (Dmitriev & Titov 2010). During oxidative stress ROS and RNS are released which can cause injuries to biomolecules such as nucleic acids, proteins and lipids (Sies & Cadenas 1985). Among these, lipids are the most damaging targets as the formation of lipid peroxidation products leads to a spread of free radicals. The steps involved in lipid peroxidation are initiation, propagation and termination. The initiation phase of lipid peroxidation involves hydrogen atom abstraction by ROS and RNS species. The membranes contain unsaturated lipids which are susceptible to peroxidation because of hydrogen abstraction from methylene groups (-CH_2-), leaving an unpaired electron on the carbon (-$^{\bullet}$CH-). The hydrogen abstraction is facilitated due to the presence of double bounds in the fatty acids which weaken the C-H bonds on the neighbouring carbon atom. The initial reaction of $HO^{\bullet}$ with polyunsaturated fatty acids produces a lipid radical ($L^{\bullet}$), which reacts with molecular oxygen to form a lipid peroxyl radical ($LOO^{\bullet}$). The $LOO^{\bullet}$can abstract hydrogen from adjacent fatty acids to produce a lipid hydroperoxide (LOOH) and a second lipid radical (Catala 2006). The LOOH formed can undergo reduction by reduced metals, such as Fe^{2+} producing lipid alkoxyl radical ($LO^{\bullet}$), which can stimulate the chain reaction of lipid peroxidation by abstracting additional hydrogen atoms (Buettner 1993, Winterbourn 2008). Lipid peroxidation disturbs the assembly of the membrane causing changes in fluidity and permeability, alterations of ion transport and inhibition of the metabolic processes (Nigam & Schewe 2000). Lipid peroxidation causes damage to mitochondria which result in further ROS generation. In addition, LOOH breaks down in presence of reduced metals or ascorbate, into reactive aldehyde products, including malondialdehyde (MDA), 4-HNE, 4-hydroxy-2-hexenal (4-HHE) and acrolein (Esterbauer et al. 1991, Uchida 1999). Spiteller et al. identified a series of hydroxyl-alkenals generated from low-density lipoprotein through copper ion oxidation, which was identified by GC/MS (Spiteller & Spiteller 2000, Catala 2009). The other and most common mechanism for formation of aldehyde during LPO is the reaction of singlet oxygen with unsaturated lipids which releases hydrogen peroxide. Hydrogen peroxide reacts with the protein myleperoxidase and leads to the formation of hypochlorous and hypobromous acid in presence of chlorine and bromine, respectively. The interaction of the acids with amines produces chloroamines and bromoamines and eventually aldehydes. The major aldehyde products of LPO are MDA, 4-HNE, acrolein and crotonaldehyde (Cr). These are highly reactive molecules that can damage DNA by formation of exocyclic adducts and are anticipated to be highly mutagenic. MDA is considered to be most mutagenic and 4-HNE the most toxic product of LPO (Esterbauer et al. 1991). These aldehydes can damage DNA either directly by reacting with DNA bases, by generating more reactive bifunctional intermedi-

ates which form exocyclic DNA adducts or by the formation of etheno bases initiated by addition of an exocyclic amino group of a DNA base. The ability of these reactive aldehydes to modify DNA bases, yielding promutagenic lesions, is considered to contribute to the mutagenic and carcinogenic effects associated with the elevated levels of endogenously produced reactive aldehydes under stress conditions (Voulgaridou et al. 2011).

1.5.3.2 Acetaldehyde(AA)

Consumption of alcoholic beverage is considered the chief source of acetaldehyde, which increases the risk of cancer in the upper gastrointestinal (GI) tract and is, therefore, classified as a human carcinogen by the International Agency for Research on Cancer (IARC). Alcohol on metabolism releases acetaldehyde, a primary oxidative metabolite which elevates the risk of cancer in the oral cavity (pharynx, larynx, and oesophagus), further inadequate enzymatic capacity towards AA detoxification (e.g., ALDH2 polymorphisms, ALDH2 deficient individual); there is a high risk of oesophageal cancer formation in a patient who consumes alcohol and smokes cigarettes. Hence, acetaldehyde is defined as a tumour initiator and can cause cancer. The binding of DNA and the formation of DNA adducts represent one mechanism by which acetaldehyde could trigger the initiation of a replication error or mutations in oncogenes or tumour suppressor genes.

Aldehydes are detoxified primarily through reductive and oxidative phase I enzyme-catalyzed reactions which include non-P450 aldehyde reduction enzyme systems alcohol dehydrogenase (ADH), aldo-keto reductase (AKR) and aldehyde oxidation enzyme systems xanthine oxidase (XO), aldehyde oxidase (AOX) and aldehyde dehydrogenase (ALDH). The ALDH superfamily catalyzes the oxidation of numerous aldehyde substrates while other enzymes metabolize aldehydes. Therefore, these enzymes play a critical role in the cellular protection against these toxic species, as supported by the fact that mutations and polymorphisms in ALDH genes (leading to perturbations in aldehyde metabolism) are the molecular basis of several disease states and metabolic anomalies (Marchitti et al. 2008). Ingested ethanol is mainly oxidized by alcohol dehydrogenase (ADH), CYP2E1 and catalase to form acetaldehyde which is, subsequently, oxidized to acetate by homotetrameric enzyme aldehyde dehydrogenase 2 (ALDH2) or cytochome P450 2E1 (Toh et al. 2010). The ALDH superfamily contains $NAD(P)^+$ dependent enzyme which take part in the irreversible oxidation of aliphatic/aromatic aldehydes and acts as an “aldehyde scavengers”. The human genome contains 19 protein coding ALDH genes. The ALDH proteins are found to be present in all sub-cellular compartments, such as in cytosol, mitochondria, ER and nucleus, as well as in plastids in plants. ALDH are known as the detoxification enzymes as ALDH serve to protect cells from the cytotoxic effects of aldehydes by converting them to respective carboxylic acids. However, some of the carboxylic acids generated by ALDH are important for cellular physiology e.g.,

retonic acid (RA: essential for development), betaine (osmolyte) and GABA (neurotransmitters) (Vasiliou et al. 2013).

AA is considered as genotoxic and mutagenic due to its ability to react with DNA (dA, dC, but, mainly dG) producing N^2-ethylidenedeoxyguanosine (N^2- ethylidene-dG) and its reduced form N^2-ethyldeoxyguanosine (N^2-ethyl-dG) (Figure1.7) as the primary adduct which has been detected at higher levels in animal models exposed to dosages of alcohol and in white blood cells (WBC) of alcoholic human subjects. Furthermore, it has also been shown that there is a higher rate of N^2- ethylidene-dG in presence of $Aldh2^{-/-}$, in comparison to $Aldh2^{+/+}$mice after treatment with ethanol or AA. Studies have also found several other adducts like; α-S/α-R-methyl-γ-hydroxyl-1, N^2-propano-2'-deoxyguanosine (α-S/α-R-Me-γ-OH-PdG) and the N^2-(2,6-Dimethyl-1,3-dioxan-4-yl)-deoxyguanosine (N^2-DiodG) (Figure 1.7). Recent studies showed that presence ALDH2*1/2*2 genotype showed elevated level of three acetaldehyde-derived DNA adducts, N^2-Et-dG, α-S-Me- γ-OH-PdG, and α-R-Me-γ-OH-PdG, when compared to ALDH2*1/2*1 genotype. AA also reacts with deoxyguanosine in DNA in the presence of basic molecules and histones to form 1,N^2-propano-2 -deoxyguanosine (PdG) adduct. This adduct has been shown to be a mutagenic DNA lesion in mammalian cells *in vivo* when AA is present in range of 40-1000 μM. The AA adducts formation induces the production of inter-strand DNA cross-links from the reaction of two AA molecules which blocks DNA recombination and replication, base substitutions (G→A and A→T), splice mutations and base-shifts. However, the AA-induced DNA cross-link can be repaired by the homologous recombination repair (HRR) and nucleotide excision repair (NER) pathways. AA also reacts with RNA, proteins and phospholipids and is capable of inducing DNA-protein adduct formation and can cause sister chromatid exchange in mammalian cells. AA adducts act as biomarkers of atherosclerosis (Tuma et al. 1996).

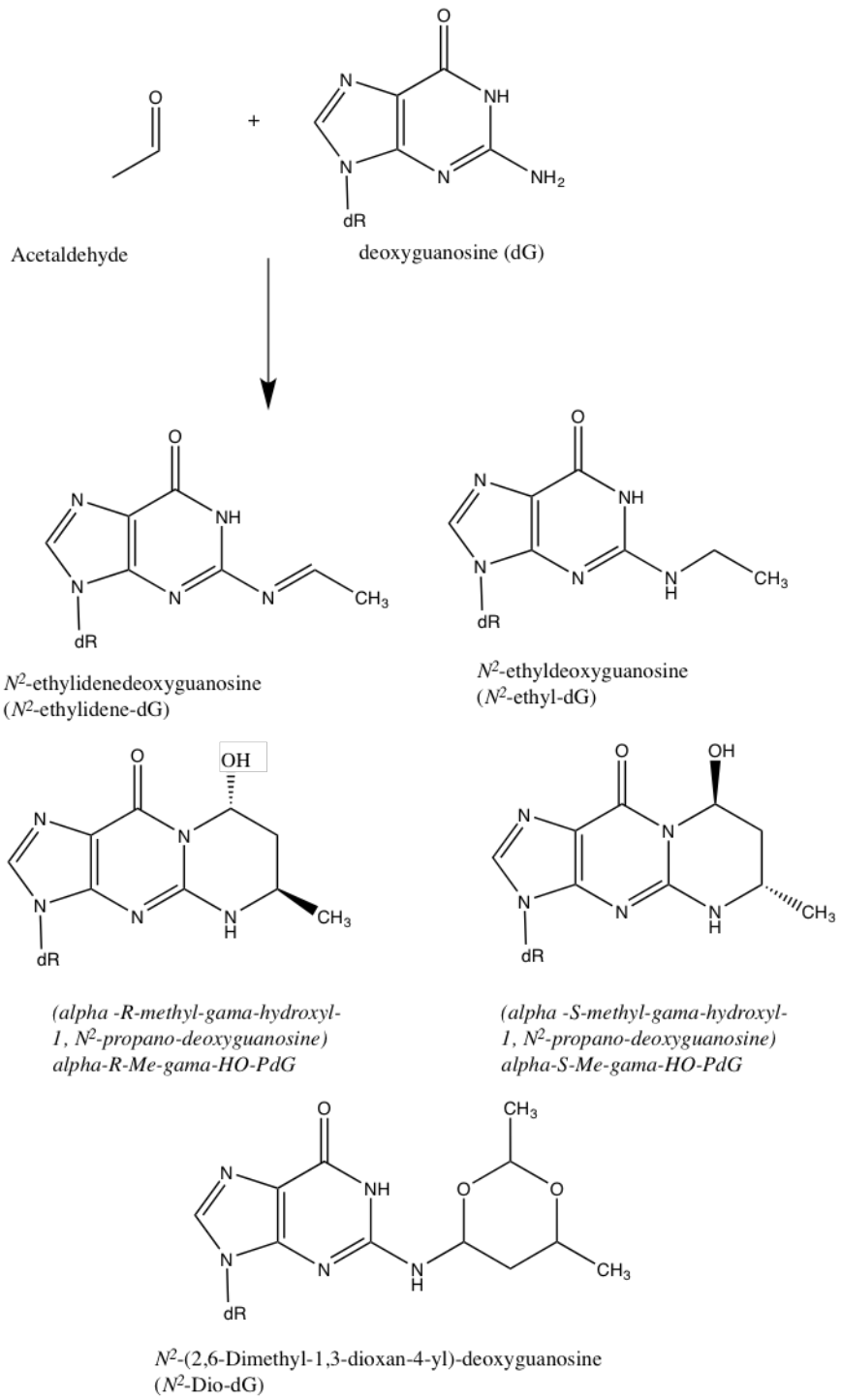

Figure 1.7: Structure of DNA adducts induced by acetaldehyde (AA) (Voulgaridou et al. 2011).

Further studies identified acetaldehyde (via metabolism of ethanol by alcohol dehy-

drogenase) and malondialdehyde (via oxidative stress) react to form hybrid malondialdehyde-acetaldehyde adducts (MAA) (Thiele et al. 2001). This adduct formation is supported because MDA in presence of monofunctional aldehyde (acetaldehyde) increases the reactivity towards amines *in vitro* (Tuma et al. 1996). These MAA adducts are unique compared to other aldehyde-protein adducts in terms of stability, potent immunogenicity, ability to alter protein regulatory elements, and dose dependent direct cellular toxicity. Interestingly, MAA adducts are identified as one of the major antigenic targets for human natural antibodies before the time of birth and MAA specific natural antibodies which are suggested to regulate apoptotic cells have been detected in the serum of preterm and full term human infants, possibly implying a role for MAA-induced apoptosis in normal development (Wang et al. 2013). MAA modification of proteins has also been shown to induce apoptosis and necrosis in a dose-dependent fashion. The suggested pathways involve the binding of MAA-modified proteins by scavenger receptors, internalization and shuttling to lysosomes (which includes lysosomal damage and cellular leakage). Macrophages when exposed to necrotic cells shows up a regulated level of CD40 and secretes proinflammatory cytokines in response to released heat shock proteins, thus stimulating T-cell proliferation (Willis et al. 2004). This stimulatory environment will lead to further migration and the activation of antigen-presenting cells (APCs). Thus, MAA induction of apoptosis and necrosis may not only be the process of normal development and physiological cellular homeostasis but, when present in excess, may induce an immune response that may be functional, dysfunctional or pathogenic (Antoniak et al. 2015). Alongside this, the MAA modification of proteins has been recognized as a pathogenic link between atherosclerosis and the classical cardiovascular risk factors that are associated with oxidative stress: hypertension (HTN), hyperlipidemia, diabetes mellitus (DM), tobacco use, and heavy ethanol consumption. These risk factors along with a potential mechanism are shown in (Figure 1.8).

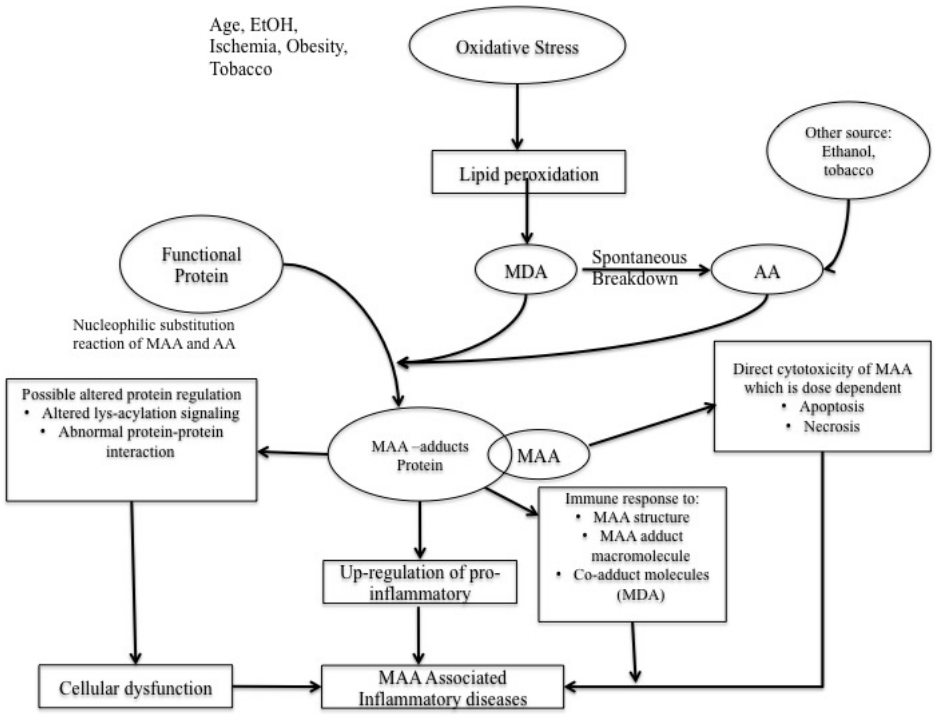

Figure 1.8: Implications of diseases related to oxidative stress and MAA adduction, which promote inflammation via various pathways, adapted from Antoniak et al. (2015)

In addition to atherosclerosis, the MAA adduction of proteins has been related to number of other disease processes. MAA adducts have been found in the liver of ethanol-consuming rats and circulating antibodies to these adducts have been detected. This finding is similar to findings from human studies in which the IgG anti-MAA level is correlated to the severity of liver injury and cirrhosis. Researchers have also demonstrated that the exposure of airway epithelial cells to MAA adducted protein has been shown to cause lung inflammation which also results in a decrease in the migration of epithelial cells into injured lung tissue and affects tissue repair and modelling (Wyatt et al. 2005). MAA adducts have also been seen in head and neck squamous cell carcinoma which is another condition associated with ethanol and tobacco exposure. All of these conditions are associated with alcohol; however, ethanol is not solely responsible for MAA, as MAA-modified proteins have been detected in neurodegenerative disorders, including Alzheimer's disease, Parkinson's disease and Huntington's disease as well as the connective tissue disease, Sjogren's syndrome, and systemic lupus erythematous (Pizzimenti et al. 2013).

1.5.3.3 Acetaldehyde and cardiovascular function

Acetaldehyde, the first metabolite of ethanol is ten times more toxic than ethanol as per its 50% lethal dose (LD_{50}) value (Brien & Loomis 1983, Eriksson 2001). There is enough evidence to prove acetaldehyde plays an important role in the pathogenesis of alcoholic cardiomyopathy (Soffritti et al. 2002). Elevated concentrations of acetaldehyde are detected within hearts in human beings who consume excessive alcohol compared to non-alcoholic consuming human beings. The main reason for this elevated blood acetaldehyde concentration in individuals who are chronically dependent on alcohol is due to the impaired ALDH enzymatic capacity to metabolize aldehyde. Individuals with defective mitochondrial class 2 aldehyde dehydrogenase (ALDH2) showed approximately tenfold higher blood acetaldehyde concentrations than healthy individuals (Nishimura et al. 2002). The direct action of acute (5-10 min) acetaldehyde exposure on cardiac and vascular tissue have been studied extensively (Brown & Savage 1996, Ren & Wold 2008). *In vitro,* acetaldehyde (< 3mM) is mediated indirectly by norepinehrine release from intramural sympathetic nerve terminals and is blocked by appropriate adrenoceptor antagonists producing vasoconstriction, as well as positive inotropic and chronotropic responses. Higher concentrations (> 3mM) produce cardiac depression, vasodilation and hypertension *in vitro*, which cannot be neutralized by reserpine pre-treatment or adrenoceptor antagonists (Ren & Wold 2008). It has been found, from *in vitro* studies of papillary muscle, acetaldehyde (> 1mM) induces a concentration dependent negative inotropic effect in cardiac and vascular preparations that may be related to reduced intracelleular Ca^{2+} release from sarcoplasmic reticulum (Doser et al. 2009). This negative inotropic effect may also be related to its inhibitory effect on voltage-dependent Ca^{2+} channels, although such effect needs to be confirmed in cardiac mycocytes (Zhang et al. 2004). Due to high volatility of acetaldehyde, when present in low (micro molar range) concentrations, it will not show any cardiac contractile effect (Zhang et al. 2004). In addition to this, acetaldehyde may also interfere with gene expression and protein synthesis in the heart. In isolated heart preparation, the addition of acetaldehyde reduces the rate of protein synthesis and a more pronounced reduction in translation rates occurs when cardiac muscles are treated with ethanol and the ALDH inhibitor calcium carbimide concurrently, indicating the role of acetaldehyde as a potent inhibitor for protein synthesis (Zhang et al. 2004, Siddiq et al. 1993). An elevated mRNA expression of atrial natriuretic peptide (ANP), often used as a marker for cardiac hypertrophy, stress and apoptosis, was found in a rat's left ventricle treated with ethanol and calcium carbimide. Interestingly, there was no significant change of ANP mRNA levels in the left ventricles of rats treated with ethanol alone, supporting the role of acetaldehyde in the up-regulation of gene coding for ANP. Investigators also found an increase in p21 gene expression and Bax:Bcl-2mRNA ratio after two day treatment with ethanol and calcium carbimide. However, after an 8-days treatment the mRNA

concentration of p21 was decreased, whereas that of p53 and Bcl-2 was increased (Zhang et al. 2004). These results support the role of acetaldehyde in regulating the expression of apoptosis-related genes in a time dependent manner, which may play a role in cardiomyopathy.

In addition to the direct organ damage, acetaldehyde may also be responsible for certain behavioural and physiological effects, for instance when acetaldehyde was administrated to lab animals it resulted in incoordination, memory impairment and sleepiness which are factors that are also associated with alcohol ingestion (Quertemont & Didone 2006). Moreover, acetaldehyde-DNA binding has been considered to promote carcinogenesis in an alcohol-dependent individual (Nakamura et al. 2003). The formation of crotonaldehyde from aldehyde is a potential carcinogenic pollutant (Ryu et al. 2013). However, acetaldehydes not only have harmful effect but also contribute to the beneficial effect following a moderate alcohol intake. It has been reported that acetaldehyde attached to a model Amadori compounds produces a chemically stable adduct that cannnot rearrange and progress to the formation of glycation end products (Al-Abed et al. 1999, Guo & Ren 2010). Amadori compounds typically arise from the nonenzymatic addition of sugar to protein amino groups and are precursor to the irreversibly bound, crosslink moieties of AGE's, which are detrimental to health. Therefore, acetaldehyde-induced protein adducts may contribute to the beneficial effect of light to moderate alcohol intake, so called "French paradox", by inhibiting advanced glycation (Guo & Ren 2010).

1.5.3.4 Malondialdehyde (MDA)

MDA is a dialdehyde with the formula $CH_2(CHO)_2$. It is generated in sufficient quantities to make it one of the most prevalent oxidative stress related aldehydes and it is one of the most commonly used markers of oxidative stress (Balasubramanian et al. 1992). It is often found as a dimer or a trimer due to its ability to act as both as an electrophile and nucleophile, while at a neutral pH level it exists as an enolate anion (a form characterized by low reactivity). Finally, MDA mutagenicity and carcinogenicity have been confirmed both in mammalian cells and in animals (Marnett 2002). Under stress condition, MDA is mainly produced when molecular oxygen reacts with polyunsaturated fatty acids, which lead to the production of peroxyl radicals; a further reduction of peroxyl radicals gives hydroperoxide through the cyclization of internal peroxyl radicals. When a second cyclization occurs, bicyclic peroxide is produced which, after reaction with molecular oxygen, produces an intermediate that subsequently delivers MDA (Marnett 1999). Alternatively, MDA can also be derived from pathways that produce acrolein in which, after the tandem production of hydroperoxide and β-cleavages of the unsaturated fatty acid, the acrolein radical is produced which reacts with the hydroxyl radical leading to the formation of MDA (Del et al. 2005). In liver mitochondria, MDA is metabolised

by mitochondrial aldehyde dehydrogenase oxidase leading to the formation of malonate which, on decarboxylation, produces acetate and CO_2 (Agadjanyan et al. 2005). On the other sites, such as on cytoplasm, the metabolism of MDA involves MDA being converted into methylglyoxal (MG) by phosphoglucose isomerase and, subsequently, MG is enzymatically (enzymes glyoxalase I and II, and with GSH as a co-factor) converted to the neutral D-lactate (Agadjanyan et al. 2005, Dmitriev & Dugin 2007).

MDA reacts with dG to form a fairly fluorescent molecule N^2-deoxyguanosine pyrimidopurinone M1dG (Figure 1.3) and with dA and dC to form the non-cyclic oxopropenyl derivatives M1dA and M1dC, respectively (Maddukuri et al. 2010). The order of formation is M1dG > M1dA > M1dC, with M1dG (detected in liver, pancreas, breast and leukocytes) representing around 1-4 per 108 nucleotides in healthy individual (Maddukuri et al. 2010). MDA-DNA adducts are formed in higher percentage in mitochondrial rather than in nuclear DNA, due to the absence of the nucleotide excision repair (NER) mechanism which is responsible for the repair of M1dG in mitochondria (Cline et al. 2010). This MDA-DNA adducts are able to induce mutations in mammalian cells mainly by G→A-T base pair substitution (Maddukuri et al. 2010).

MDA is chemically unstable and can diffuse into a cell and react spontaneously with DNA and/or proteins, in particularly to ε-amino lysine residue of protein nonenzymatically (Sayre et al. 2006). This ability to modify self-proteins makes these aldehydes prime candidates for potential autoimmune disease, carcinogenesis and ageing in humans. For example, the MDA-dA and MDA-dG adducts have been detected to be two-three times higher in a breast cancer individual compared to healthy individuals (Voss & Siems 2006). Increased level of M1dG adducts were observed in breast cancer patients and a similar result has been reported for cancerous lung tissues compared to healthy lung tissues (Munnia et al. 2006). The MDA modification of protein is considered to be a mediator or marker of inflammation as it is found in several inflammatory disease conditions. MDA is also considered as a marker for atherosclerosis/cardiovascular disease; however, the predictive value of MDA is not consistently related to cardiovascular risk (Amir et al. 2012, Kikugawa & Beppu 1987, Sayre et al. 2006), which could be due to the unstable nature of MDA adducts, large variation in MDA adducts and MDA epitopes, as well as the variable number of MDA immune response was evaluated. The interpretation and comparisons of these above studies have been supported by the lack of specificity of anti-MDA reagents whereby commercially available "MDA" antibodies cross-react with MDA and MAA (Amir et al. 2012).

1.5.3.5 4-Hydroxynonenal (4-HNE)

4-HNE, a major lipid peroxidation product of polyunsaturated fatty acids (n=6) such as arachidonic acid and linoleic acid. 4-HNE is highly chemical reactive and one of the ma-

jor generators of oxidative stress; it is often used as a bioactive marker for oxidative stress and LPO in a variety of biological systems. Production of 4-HNE during LPO can be enzymatic or non-enzymatic. The enzymatic pathway involves the enzymes lipoxygenase and hydroperoxide lyase which cleave linoleic acid to 3Z-noenal, which subsequently oxygenates to 4-HPNE in a non-enzymatic way. 4-HPNE subsequently decomposes to 4-HNE or 4-oxononenal (4-ONE). Cells have developed different defence mechanisms to remove 4-HNE, the most important being tripeptide glutathione (GSH). GSH react with 4-HNE to form a conjugate which can be a target for further enzymatic deactivation or cellular export by specific transporter like MRP2. The mitochondrial ALDH2, using NAD as a co-factor, can oxidizes 4-HNE to 4-hydroxynonenal-2 enoic acid (4-HNA) (Voulgaridou et al. 2011). Aldehyde reductase like aldose reductase and aldo-keto reductase uses 4-HNE to form 1,4-dihydroxy-2-nonene (DHN) in an NADH-dependent manner (Petersen & Doorn 2004).

4-HNE, being highly reactive, can interact with proteins through Cys, His, and Lys residue to form protein adducts that can lead to mitochondrial dysfunction and the inhibition of cell signalling. These could be one of the reasons for the elevated levels of HNE in various diseases like Alzheimer's, Parkinson's and arteriosclerosis (Petersen & Doorn 2004, Huang et al. 2010, Jomova et al. 2010). 4-HNE also has the potential to form DNA adducts which can lead to mutations. Like other enals, 4-HNE reacts with DNA nucleobases deoxyguanosine (dG) involving the Michael addition of the N^2-amine to give N^2-(3-oxopropyl)-dG adducts, which yields the exocyclic adducts, 1,N^2-dG products after cyclization of $N^1$with the aldehyde (Huang et al. 2010, Nair, Bartsch & Nair 2007). These 4-HNE-DNA adducts have been used as an indicator of oxidative DNA damage and also as a biological marker for certain human diseases (Nair, Bartsch & Nair 2007). Reports have shown that lesions that have occurred due to 4-HNE and similar aldehyde adducts are found at a frequency of 0.6-2000 per 10^9 guanines (Nair, Bartsch & Nair 2007). Not all 4-HNE adducts are capable of forming interstrand DNA cross-links, only the stereoisomer (6S, 8R, 11S)-HNE adducts (possessing stereochemistry) are able to form stable interstand DNA cross-links and have the ability to lead to mutation (Wang et al. 2003). The (6S, 8R, 11S)-HNE adduct has been found to give 3.2% G→T transversions, 0.6% G→A transitions and 0.3% G→C transversions (Minko et al. 2009).The mutagenic activity of 4-HNE adducts have been confirmed in studies using liver specimens taken from patients with Wilson's disease and hemochromatosis (Minko et al. 2009), G→T transversion at codon 249 of p53 gene was found in lymphoblastic cells (Huang et al. 2010) and also in COS-7 cells; 4-HNE led to base substitution (0.5–5% frequency) with the G→T (Minko et al. 2009, Nair, Bartsch & Nair 2007). Elevated levels of 4-HNE derived DNA adducts were found in human atherosclerotic lesions (Nair, De, Izzotti & Bartsch 2007). Lipid peroxidation related miscoding etheno-DNA adducts increased with time in chronically

inflamed target organs in both humans and in experimental animal models (Bartsch & Nair 2004). The high content of DNA-etheno adducts has been associated with Crohn's disease, ulcerative colitis, chronic pancreatitis and inflammatory cancer-prone liver diseases (Nair et al. 2010).

1.5.4 Alcohol related diseases

The alcohol family comprises three different members namely methyl alcohol (methanol, CH_3OH), ethyl alcohol (ethanol, EtOH, C_2H_5OH) and isopropyl alcohol. Among these only "ethanol" also called "alcohol" is an intoxicating ingredient in beer, wine and other forms of liquor. Drinking alcohol beverage is a common feature within social gathering. Light-to-moderate alcohol consumption protects against cardiovascular diseases by reducing artery-related issues and provides a better longevity for cardiovascular health compared to heavy drinker or non-alcoholic individual (Gitto et al. 2016). High alcohol consumption can result in life-threatening health hazards both physically and mentally (Yang et al. 2016). High alcohol ingestion may cause the development of certain devastating chronic diseases such as heart disease, Alzheimer's disease, stroke, liver disease, cancer, chronic respiratory disease, diabetes mellitus and bone disease (Wyre & Thrasher 2016, Savvidou et al. 2016).

1.5.4.1 Alcohol and heart disease

Alcoholism is one of the major causes of non-ischemic heart damage. Almost one in every three individuals who are chronically dependent on alcohol exhibit cardiac dysfunction, characterized as a unique type of dilated cardiomyopathy termed "*alcoholic cardiomyopathy*" (Liang et al. 1999), which accounts for 33% of all dilated cardiomyopathies. Alcoholic cardiomyopathy (also known as alcoholic heart muscle disease) is detectable by cardiomegaly, disruptions in myofibrillary architecture, reduced myocardial contractility, decreased ejection fraction and stroke volume, as well as by an enhanced risk of stroke and hypertension (Schoppet & Maisch 2001). These cardiac morphologic and functional alterations may ultimately lead to cardiac failure which is considered as the end point of alcoholic cardiac toxicity, as is the case with other toxins, such as doxorubicin, (Mallikarjuna et al. 2008) acetaldehyde, monocrotaline and azide. These cardiac toxins can play direct role in cardiac dysfunction and hypertrophy by enhancing the level of prooxidants, such as catecholamines and ROS. Cardiac failure associated with alcoholic cardiomyopathy is due to the direct result of the toxic effects of ethanol and its metabolites or to an indirect action such as neurohumoral, hormonal or nutritional factors (Schoppet & Maisch 2001, Badger et al. 2003). Oxidative stress, protein-aldehyde adducts, accumulation of fatty acid ethyl esters and the modification of lipoprotein and apolipoprotein particles are

also responsible for the pathogenesis of alcoholic cardiomyopathy. Additionally, several hypotheses suggest that the primary role of ethanol toxicity is an inflammatory response in cardiac tissue or organ damage such as in the liver. However, none of these hypotheses have received clinical and experimental support that validates them, e.g., direct ethanol toxicity may require for development of oxidative stress, whereas ethanol-induced oxidative stress may require the metabolism of ethanol into more reactive compounds such as acetaldehyde (Zhang et al. 2004). Furthermore, no strong correlation has been found between the onset of alcoholic cardiomyopathy and damage to organs such as liver, making the theory of cardiac toxicity as being secondary to other organ damage rather weak. It might also be possible that some of these pathways may share certain common cellular mechanisms such as enhanced oxidative stress en-route to the development of alcoholic cardiomyopathy, although convincing evidence is lacking.

1.5.4.2 Mechanisms of alcohol diseases

There have been various suggested mechanisms for the pathogenesis of alcoholic injuries and diseases, including the toxicity of ethanol and its metabolite acetaldehyde. Alcohol exposure is associated with multiple toxic effects on various organs through different mechanisms, although there are two main categories: acetaldehyde-related and non-acetaldehyde-related mechanisms.

Much of ethanol is metabolized in the cytoplasm of the liver by alcohol dehydrogenase (ADH) enzymes to form acetaldehyde (ethanal). Acetaldehyde is more toxic than ethanol and must be rapidly metabolized by aldehyde dehydrogenase in the mitochondria (Guo & Ren 2010). Acetaldehyde is further metabolized to a less reactive by-product, acetate, by ALDH. The two-enzymatic steps (Figure1.9), both require NAD as the hydrogen acceptor. High consumption of alcohol shifts cellular NAD^+/NADH ratios towards the reduced state in both cytosol and the mitochondria which may promote abnormal fat accumulation in the liver (Halliwell & Gutteridge 2007). The enzyme cytochrome P450 2E1 (CYP2E1), the ethanol-inducible cytochrome 450, in hepatocytes and kupffer cells, along with catalase, also break down alcohol to acetaldehyde. Under normal conditions, smaller amounts of alcohol can be oxidized by the peroxidatic action of catalase in the peroxisomes and by CYP2E1. All these ways of metabolizing ethanol results in acetaldehyde which is a key generator of free radicals and a known carcinogen. An increase in the level of free radicals reduces the antioxidant defence mechanism, leading to tissue damage (Guo & Ren 2010). In addition, ethanol may induce a 10-fold up-regulation of CYP2E1 in the liver which may be responsible for alcoholism-triggered oxidative damage. Cytochrome P4502E1 is also elevated in diabetes and obesity, and its synthesis can be increased by several solvents other than ethanol, including acetone, benzene, $CHCl_3$ and DMSO. Moreover, high levels of NADH in mitochondria can cause an increase in

superoxide ($O_2^{\bullet-}$) free radicals leading to the formation of hydroxyl radicals ($HO^{\bullet}$), lipid peroxidation and damage to mitochondria DNA (Mallikarjuna et al. 2008).

Alcohol related diseases can occur through acetaldehyde which is an active metabolite that induces a range of toxic, pharmacological and behavioural responses. Acetaldehyde is only short-lived before it breaks down into acetate, even though it possesses the ability to induce damage in cells and tissues. Liver is the primary site of oxidation, although other organs including the heart, pancreas, gastrointestinal tract and the brain may also participate in the metabolism of ethanol to acetaldehyde (Zakhari 2006). Acetaldehyde plays a key role in the pathogenesis of alcoholic cardiomyopathy (Liang et al. 1999), in particular to cardiac hypertrophy or dilated cardiomyopathy associated with significant increases in the hypertrophic marker skeletal actin and atrial natriuretic factor (ANF) (Agarwal & Srivastava 2001). There is enough evidence to suggest that acetaldehyde compromises myocardial excitation-contraction coupling, EPR Ca^{2+} release and cardiac contractile function (Zhang et al. 2004). The mechanism for this could be due to reduced Ca^{2+} entry through voltage-dependent Ca^{2+} channels and/or depression of sarcoplasmic reticulum Ca^{2+} release (Ren et al. 1997). Studies have shown that alcohol consumption significantly decreases the expression of intracellular Ca^{2+} cycling proteins SERCA2a, Na-Ca^{2+} exchanger and phospholamban in cardiomyocytes without much change in the SERCA2a-to-phospholamban ratio (Carruthers et al. 1999). Although, the exact mechanism is not fully clear, acetaldehyde is believed to play a role. Acetaldehyde also functions as a ryanodine receptor activator leading to disturbed cardiac contractile function (Oba et al. 2008) and an increase in intracellular Ca^{2+} levels (Carruthers et al. 1999). Acetaldehyde stimulates the release of signalling molecules (such as epinephrine, norepinephrine etc.) which lead to the cardiovascular symptoms of alcohol sensitivity reactions (such as vasodilation) and is also associated with abnormal heart rate and blood pressure (Quertemont & Didone 2006, Guo & Ren 2010). Acetaldehyde from alcohol results in the production of free radicals through aldehyde oxidase and xanthine oxidase associated oxidation which indirectly decreases the antioxidant defence (GSH levels) resulting in oxidative stress (Zhang et al. 2004). Acetaldehyde can also activate stress signalling (such as c-Jun phosphorylation) and induce apoptosis (Lee et al. 2002).

Alcoholic diseases can also occur due to acetaldehyde-independent mechanisms, whereby alcohol may induce direct toxic effects on the cardiovascular system or alter the neurohormonal and/or hormonal regulation of cardiac function. Certain metabolic products of ethanol such as fatty acid ethyl esters (FAEEs) may also alter the physiological function of the heart independently of acetaldehyde. FAEEs result from the non-oxidative metabolism of alcohol and may be the first link between the ingestion of alcohol and the development of alcohol-induced heart muscle disease. Under normal condition FAEEs

in heart are small in number, however with high alcohol consumption the FAEE concentration in the human myocardium can be 115,000-fold higher than in a normal heart muscle (Lange & Sobel 1983*b*, Yoerger et al. 2006). Accumulation of FAEEs reduces the respiratory control index that couples oxidative phosphorylation and the maximal rate of oxygen consumption which can cause improper mitochondrial function and the inefficient energy production associated with the toxic effects of ethanol on the heart (Lange & Sobel 1983*a*, Guo & Ren 2010, Yoerger et al. 2006). Additionally, ethanol metabolism can also produce stable and non-stable protein adducts, for example, AA binds to some proteins and becomes a Schiff base, thus forming protein-AA adducts. Multiple adducts like MDA adducts and 4HNE adducts can have an adverse effect on the body's immune system and are involved in the development of alcoholic organ disease including in the liver, heart and brain (Nakamura et al. 2003).

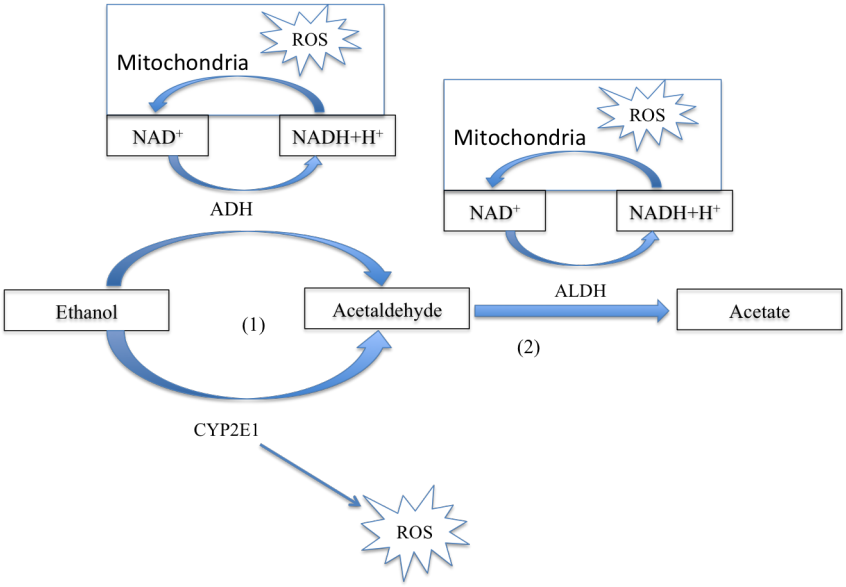

Figure 1.9: Metabolism of Ethanol. (1) Ethanol is converted to acetaldehyde (AA) by the enzyme alcohol dehydrogenase (ADH)/cytocrhomeP450 2E1(CYP2E1)/ catalase, (2) acetaldehyde is oxidized to acetate by the enzyme acetaldehyde dehydrogenase (ALDH). Metabolism of ethanol through ADH result in generation of acetaldehyde and NADH, whereas oxidation of ethanol by CYP2E1 leads to production of AA along with ROS. NADH is reoxidized to NAD^+ in the mitochondria, which leads to generation of more ROS (Brocardo et al. 2011).

1.5.4.3 Alcohol and oxidative stress

Ethanol per se, hyperlactacidemia and elevated NADH increases xanthine oxidase activity which results in the production of superoxide radicals (Das & Vasudevan 2007). The

induction of CYP2E1 in the microsomes aggravates the generation of reactive oxygen species such hydroxyethyl radicals (HER), and is another major route by which ethanol induces free radical formation in the liver. Generated HER radicals are probably involved in the alkylation of hepatic protein (Zima et al. 2001). Additionally, ethanol can also induce free radical formation via the reaction of aldehyde oxidase to generate oxyradicals. Elevated efflux from mitochondria which leads to altered mitochondrial oxidative metabolism is another manner of free radical production (Mantle & Preedy 1999, Das & Vasudevan 2007). The metabolism of ethanol is closely linked with the stimulation of Kupffer cells, the activation of NF-kB, the production of TNF-α, free radical generation, and oxidative stress. Almost all biological structures can be modified by the reactive oxygen species (Das & Vasudevan 2007).

Alcohol, when consumed in excess, generates oxygen free radicals, inhibits glutathione synthesis and impairs antioxidant mechanisms in humans. As a result there is an increase in the malondialdehyde level, a biomarker for lipid peroxidation. In addition, acetaldehyde, as an intermediate in alcohol metabolism, can impair the functions of several enzymes by reacting with sulfhydryl groups at the active sites. Acetaldehyde and aldehydic products can enhance lipid peroxidation which causes damage to hepatocytes along with other tissues. An elevated level of autoantibodies towards distinct types of adducts have been detected in patients with severe alcohol induced liver disease. A study on alcoholic patients has shown significantly higher concentration of malondialdehyde compared to non-alcoholic patients (Peng et al. 2005). In addition, the activities of antioxidant enzymes (such as superoxide dismutase and glutathione peroxidase) were low in alcohol-dependent patients compared to non-alcoholic individuals (Peng et al. 2005). However, when these patients practised abstinence, a low level of serum malondialdehyde was recorded suggesting that alcohol was responsible for the increased oxidative stress. Alcohol aggravates systemic and local oxidative stress, leading to lung injury ranging from mild pulmonary dysfunction to severe lung injury. Additionally, ROS generated in the presence of excess alcohol may also damage lipid membranes, enzymes carrying the sulfhydryl group and DNA; such oxidative damage may be involved in the aetiology of diverse human diseases caused by alcohol abuse including coronary heart disease, acute ischemia, infection, neurodegenerative diseases and cancer (Aytacoglu et al. 2006, Dasgupta & Klein 2014). Therefore alcohol drinking is not recommended for pregnant women and women who want to become pregnant as it can cause foetal abnormalities (foetal alcohol syndrome), premature delivery, and even foetal death as alcohol consumption can lead to the generation of ROS that can produce an imbalance in the intracellular redox state, leading to an overall increase in oxidative stress which may cause damage to the central nervous system (CNS) of the foetus, causing foetal alcohol syndrome (Brocardo et al. 2011). 8-Hydroxy-2'-deoxyguanosine, a marker of oxidative damage to DNA,

has been found at a higher level in alcohol-dependent patients compared to controls, and oxidative damage of DNA persisted after a week of detoxification (Chen et al. 2011).

1.6 Spin traps

A free radical, by definition, contains an unpaired electron which can be observed via electron paramagnetic resonance (EPR) spectrometry. However, due to short half-life of free radicals, only those free radical species with relatively long half-lives are measurable. However, with the development of spin-trapping reagents, it has become possible to detect a broad variety of radical species using analytical instruments such as EPR, GC/MS and LC/MS (Janzen 1970). Spin trapping is a technique in which a nitrone (like PBN) or nitroso compound (like POBN) is allowed to react with a free radical to produce a nitroxide whose stability is considerably greater than the parent free radical and which can be detected by various analytical instruments like EPR. Consequently, spin trapping permits the detection and identification of a number of various free radicals generated during the process. However, there are numerous factors that need to be considered prior to undertaking spin trapping studies. These include (Britigan et al. 1987):

1. The rate of primary as well as secondary free radical production
2. The rate of spin trapping the various free radicals generated
3. The rate of spin trapped adduct decomposition

Under optimal conditions, spin trapped adducts will accumulate with time, making the technique more sensitive compared to techniques which directly measure instantaneous or steady-state free radical concentration (Britigan et al. 1987). Spin trapping has been widely used in various fields of chemistry, such as, polymerization, radiation chemistry, biochemistry, organic chemistry and solution chemistry.

Some of the most commonly used spin trapping compound are mentioned here.

1.6.1 Nitrones

Nitrones were first recognized as spin traps in late nineteen-sixties by Iwamura and Inamoto. Since then nitrones have been extensively used for the detection and identification of various free radical species in chemistry (Halliwell & Gutteridge 2007). They have also been used in biological systems for *in vivo* detection and the identification of free radical species formed during or after the administration of drugs and xenobiotics. In nitrone spin trapping the free radical is added to the adjacent carbon thus the spectrum represents the original trapped radical. The advantage of using nitrone

is that the rate constants for the addition of the radicals to the nitrones are extremely rapid and are independent of the structure of nitrones, and also the EPR spectrum is unique ((Kotake & Janzen 1991)). There are many nitrone compounds available such as *tert*-nitrosobutane (tNB), α-phenyl-*tert*-butyl nitrone (PBN), 5,5-dimethyl-pyrroline-1-oxide (DMPO), 5-Diethoxyphosphoryl-5-methyl-1-pyrroline N-oxide (DEPMPO), α-(4-Pyridyl-1-oxide)-N-*tert*-butylnitrone (POBN) etc.

1.6.1.1 α-Phenyl-*tert*-butyl nitrone (PBN)

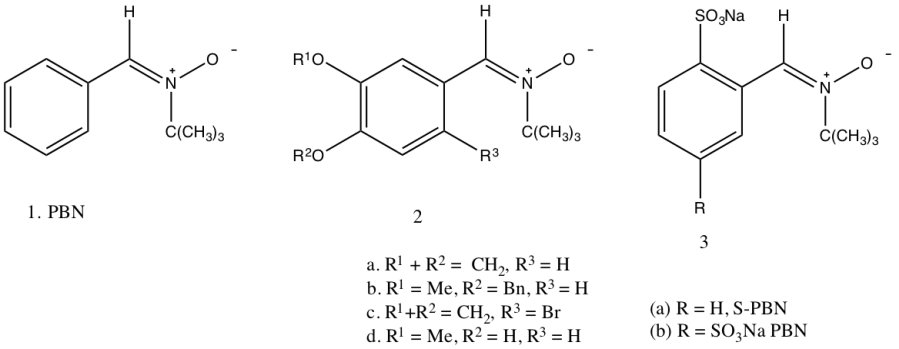

Figure 1.10: Structure of PBN (1) and PBN like nitrones (Kim et al. 2007).

PBN (Figure 1.10) is one of the most common spin trapping compounds used in free radical studies. PBN acts as an effective trapping agent by reacting with, and stabilizing, free radical species. This stabilizing property may also reduce the reactivity of the free radical species, hence, it can also act as antioxidant. However, PBN is less useful for detecting oxygen centered radicals due to the instability of the corresponding spin adducts (Kotake & Janzen 1991). However, 4-hydroxy PBN is formed by an attack of $^{\bullet}$OH radicals at the phenyl ring. The same has been found in this laboratory when the Fenton reaction (involving the phosphate buffer (pH=7.4), PBN, EDTA, ascorbate, H_2O_2 and Fe^{2+}) was extracted in chloroform and was analysed by GC/MS. The chromatogram shows a strong peak at retention (11.0 minutes) and the mass spectrum shows a molecular ion at m/z 193 corresponding to the hydroxy PBN (MW=193). The identification of this reaction product has been used as evidence for the occurrence of these radicals. The potential therapeutic value of PBN has been examined in other free radical mediated diseases such as ischemia-reperfusion damage and ageing (Floyd & Carney 1992). The life time of spin adducts was studied formed by reaction of $^{\bullet}$OH with PBN and their derivatives was studied (Kotake & Janzen 1991). In addition to these examples nitrones have also been used to reduce the damage caused by radicals in biological systems, hence acting as antioxidants to some extent. It has been reported that PBN inhibits the oxidation of lipoproteins

(Kalyanaraman et al. 1991), prevents liver injury originated from the administration of a mixture of CCl_4 and ethanol to rats, and reduces oxidative damage erythrocytes and the peroxidation of lipids caused by phenyl hydrazine (Hill & Thornalley 1983). PBN also possesses neuroprotective activity as shown in studies by Novelli and co-workers (Novelli et al. 1986). This activity is due to good blood-brain barrier penetration. PBN protects gerbils from lethality induced by global brain stroke and protects mice against MPTP toxicity for Parkinson's disease model (Floyd et al. 2002, Ferger et al. 2000). PBN also has been shown to extend life spans in mouse and rat models (Floyd et al. 2002).

In an effort to optimize the biological activity of PBN, a wide range of PBN derivatives was designed and synthesized. S-PBN (Figure 1.10) provided substantial neuroprotective properties in ischemia/reperfusion nerve injury in post-ischemic administrated rats (Gray & O'Connell 2003). NXY-059 is an effective neuroprotective agent in rat models of transient and permanent focal ischemia (Green et al. 2003). This compound showed enhanced neurological function and reduced infarct volume in a primate model of permanent focal ischemia. Nitrone 2 was patented for the treatment of neurodegenerative, autoimmune, and inflammatory diseases, and as an analytical reagent for the detection of free radicals (Kim et al. 2007). New PBN derivatives have been synthesized in order to optimize bioavailability and to reduce hypothermia, a side effect associated with PBN (Nakae et al. 1998). The inhibition of early phase carcinogenesis in the liver of rats and providing protection against myelotoxicity and adriamycin-induced cardiotoxicity has also been reported for nitrones (Nakae et al. 1998, Paracchini et al. 1993) have shown the protective effect of PBN and 2b-d (1.10) against microvascular damages induced by ischemia/reperfusion in the 'hamster cheek pouch' assay (Kim et al. 2007).

In my research experiment different PBN derivatives (4-FPBN, 4-ClPBN etc.) were synthesised to study the mechanism of trapping of aldehydes and alcohol radicals.

1.6.1.2 5,5-Dimethyl-l-pyrroline N-oxide (DMPO)

DMPO was the first cyclic nitrone spin trap used for decades to trap oxygen centered radicals such as $HO^{\bullet}$ and $O_2^{\bullet-}$ to form DMPO/OH and DMPO/OOH adducts (Figure 1.11). DMPO were used first time to detect ROS in chloroplasts (Harbour & Bolton 1975) and then on intact cells, i.e., neutrophils and macrophages during a respiratory burst (Bannister & Bannister 1985). However, there are certain limitations for the usage of DMPO as a spin trap (a) its low trapping ability for the superoxide radical, due to this, high concentration (50-100mM) is mandatory to compete with superoxide disproportionation, (b) the short half-life of the superoxide adduct (DMPO-OOH, $t_{1/2}$< 1 minute) which can easily decompose to hydroxy adduct (DMPO-OH adducts, $t_{1/2}$<2.9 min). Moreover, in metabolic processes the decomposition is so rapid making its detection difficult (Samuni et al. 1989), and (c) impurities are usually found in the commercailly available DMPO

which may react with ROS to give unwanted byproducts, hence, further purification is required which can shorten its shelf-life (Bacic et al. 2008).

To overcome these drawbacks derivatives of DMPO with different electron-withdrawing groups at position 5 such as in DEPMPO (5-diethoxyphosphoryl-5-methyl-1-pyrroline N-oxide), BMPO (5-*tert*-butoxycarbonyl-5-methyl-1-pyrroline N-oxide), EMPO (5-ethoxycarbonyl-5-methyl-1-pyrroline N-oxide) etc was synthesised which enhanced the stability of the spin adduct.

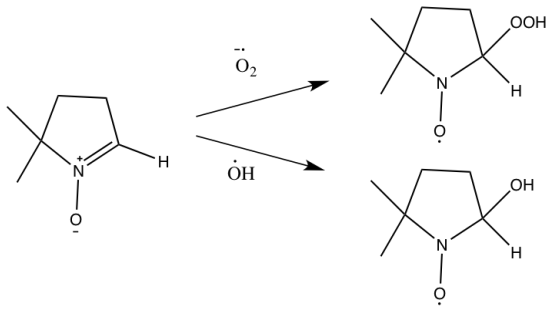

Figure 1.11: Structure of spin trap DMPO, its hydroxyl adduct and superoxide adduct (Bacic et al. 2008).

1.6.1.3 DEPMPO

In 1995, Frejaville et al. first synthesized 5-(diethoxyphosphoryl)-5-methyl-1-pyrroline-*N*-oxide (DEPMPO) which have greater affinity for trapping superoxide and peroxyl radicals. The superoxide spin adduct showed significantly increased half-life (15 times at pH 7) than the DMPO-superoxide spin adduct. The half-life of DEPMPO/ $^{\bullet}$OH is about 10 times longer (22.3 minutes) compared to the respective DMPO-$^{\bullet}$OH adduct due to the presence of β-ethoxyphosphoryl group which shields the unpaired electron of the NO (Freeman et al. 1995). The stability of the adduct result in better and distinct EPR signal for the superoxide and hydroxyl radical adduct. The presence of phosphorus (^{31}P) in DEPMPO (Figure 1.12) give choice of using NMR technique to detect the free radicals.

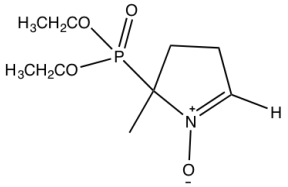

Figure 1.12: Structure of DEPMPO.

1.6.1.4 α(4-Pyridyl-1-oxide)-*N-tert*-butylnitrone (4-POBN)

Structure of 4-POBN is shown in Figure 1.13. 4-POBN is one of the most frequently used spin traps for detection of carbon centered radicals and hydroxyl radicals. 4-POBN is not suitable for detection of superoxide radicals as the adduct are not stable making it virtually undetectable. However, its affinity for trapping the hydroxyl radical makes it first choice compared to DMPO. The limitation associated with POBN is when used in relatively high concentration (50 mM) the formation of a 4-POBN radical during the reaction of the peroxidases, H_2O_2, and 4-POBN may occur, resulting in the formation of a 4-POBN$^{\bullet}$/4-POBN spin-adduct (McCormick et al. 1995). Despite this limitation 4-POBN has been successfully used in many ESR spin trapping studies of lipid peroxidation in chemical models, cellular models and *in vivo* systems to detect a variety of lipid derived carbon centered radicals and its identification not only by EPR but GC/MS (Mistry et al. 2008) and Matrix-assisted laser desorption/ionization time-of-flight (MALDI-TOF mass spectrometry) (Podmore et al. 2013).

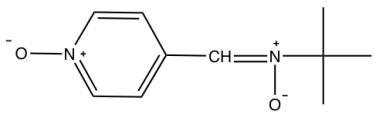

Figure 1.13: Structure of spin trap 4-POBN.

1.7 Detection of spin trap adduct

1.7.1 Spin Trapping-Electron paramagnetic resonance (ST-EPR)

EPR is a spectroscopy technique that detects unpaired electrons and so can be specifically used to detect free radicals. As an unpaired electron can have a spin of +1/2 or -1/2 and behaves as a small magnet, when exposed to an external magnetic field, it can align either parallel (towards) or antiparallel (opposite) to that field and thus creates two energy levels. If an electromagnetic radiation of correct energy is applied, it will be absorbed and used to move the electron from low energy to high energy. Thus an absorption spectrum is obtained, usually in the microwave region of the electromagnetic spectrum, for example, in the $^{\bullet}CH_3$ radical, the unpaired electron on carbon is close to three hydrogens. The field of each hydrogen can align with, or against, the applied magnetic field and, therefore, the EPR signal will consist of four lines with an intensity ratio 1:3:3:1. Hence, a radical can be identified from its EPR spectrum by looking at the g value ($\triangle E = h\gamma = g\beta H$, where $\triangle E$: energy absorbed, h:Planck's constant, γ: frequency of applied electromagnetic radiation, H: applied field strength and β: Bohr magneton), the hyperfine structure and the line shape. The EPR is sensitive enough to detect species such as ascorbyl and

alpha-tocopheryl radicals in biological material, along with radicals produced during the mechanical disruption of fingernails, bone, cartilage and tooth enamel (Halliwell & Gutteridge 2007). However, due to high reactivity and short half-lives, direct EPR detection of many free radicals (such as the superoxide radical and the hydroxyl radical) is virtually impossible. Hence, a different approach such as "rapid freezing" was used to detect superoxide radicals by EPR. However, the spectra of immobilized radicals are often difficult to identify in biological material, and so freeze-quenching techniques are not often used.

Technology in this field has developed over time and now includes a variety of methods such as chemical reaction product identification. However, none of these techniques are as direct and specific as electron spin resonance (ESR) which, when coupled with spin trapping methods, becomes a "gold standard" technique for the detection and identification of free radical species. In these techniques, a short lived free radical reacts with spin trapping compounds like PBN, DMPO and POBN to produce a long-lived nitroxide radical due to electron delocalization between the nitrogen and oxygen atoms. The EPR spectra of nitroxides have a main triplet (1:1:1) due to the interaction of the unpaired electron with the nitrogen of the nitroxide group. Secondary splitting can be due to the magnetic nuclei in the trapped radical and sometimes from other magnetic nuclei in the spin trap (Halliwell & Gutteridge 2007). Therefore, with nitroso traps, the trapped radicals thus more easily influence the EPR spectrum and usually generate hyperfine splitting, whereas, with nitrone traps, the spectra represent the trapped radicals. Hence, nitrones are more commonly used with DMPO and PBN and DEPMPO usage is also increasingly popular.

Spin trapping methods combined with ESR spectroscopy have been used to study oxidative stress. Ethanol is converted to a free radical metabolite, the 1-hydroxyl ethyl radical, in a chemical reaction that generates free radicals. Reinke et al. showed POBN as a superior trapping agent for the detection of the 1-hydroxyl ethyl radical in liver microsomes(Reinke 2002). Awasthi et al. also detected trapped free radicals by POBN after traumatic brain injury and showed, through ESR, that a brain ascorbic free radical signal was visible 60 minutes after traumatic brain injury (Awasthi et al. 1997). An ESR spectroscopy coupled with a 5,5-dimethyl-pyrroline-1-oxide (DMPO) was used to detect lipid derived radicals ($Ld^{\bullet}$) during peroxidation of polyunsaturated fatty acids (PUFA), low-density lipoprotein (LDL) and cells (K-562 and MCF-7) (Qian et al. 2000). Buettner et al. have successfully trapped carbon-centred radicals from intact cells during lipid peroxidation using EPR spin trapping (α-[4-pyridyl 1-oxide]-N-*tert*-butyl nitrone (POBN)) (Wagner et al. 1994). POBN adduct formation during cellular lipid peroxidation was confirmed with cell membrane damage as measured by the TBARS assay and the Trypan blue dye exclusion (Wagner et al. 1998). Using EPR with DMPO spin trapping, Chamulitrat et al. and Davies et al. detected oxygen-centred lipids radicals in enzyme-dependent

hydroperoxide reactions (Chamulitrat et al. 1991, Davies 1988).

ESR measurement in living organisms can provide an important new insight into the physiological and pathophysiology of clinical entities. Kazaki et al. used an *in vivo* ESR to detect ROS in rats with NH_4OH-induced gastric lesions. The rats were given a nitroxyl probe intragastrically or intravenously and the ESR result showed direct evidence of the generation of hydroxyl radicals produced from superoxide radicals derived from neutrophils causing a gastric lesion formation (Kasazaki et al. 2003). Hence, ESR with spin trapping has been very useful for in vivo measurements in real time.

Although it is possible to detect various free radicals, complete structure prediction is still not easy. It is also very difficult to perform radical detection and quantification in complex systems consisting of very different radical species of varying lifetimes at different temperatures and over a range of times. Additionally, the *in vivo* measurement of free radicals is limited due to the low concentration of free radical species *in vivo*, to the dielectric loss in water occurring in the investigated body, to low penetration depth and to the toxicity of spin trapping agents on tissues (Kopani et al. 2006). EPR spectroscopy cannot be applied easily or reliably in these cases, hence other techniques or combinations of different techniques are used such as mass-spectrometry-based species characterization and a NMR-based spin trapping compound (Khramtsov & Clanton 2011).

1.7.2 Spin Trapping Nuclear Magnetic Resonance Spectroscopy (ST-NMR)

^{31}P NMR spin trapping techniques have been shown to be very effective tools for the detection and absolute quantification of many oxygen and carbon centered free radical species (Zoia & Argyropoulos 2009). This technique was first used in 1999 by Khramtsov et al. and was termed as "NMR spin trapping" (Khramtsov et al. 1999). In this method, nitroxide phosphorus spin trap reagents, such as 5-diisopropoxy-phosphoryl-5-methyl-1-pyrroline-N-oxide (DIPPMPO), are used to which free radicals react to form stable radical adducts Figure 1.14, which can be used for both qualitative and quantitative analyses by ^{31}P-NMR in the presence of phosphorus containing internal standards (Zoia & Argyropoulos 2009). The advantage of using phosphorus containing spin trap allows for the detection of diamagnetic products by ^{31}P-NMR without the complexity of multiple signal overlap spectra usually seen during the proton or carbon nuclei examination (Crestini et al. 2015). This technique is suitable to be adapted for the detection of phenoxyl radicals, as an alternative to traditional EPR techniques. The drawback of this technique can be the reduced sensitivity of NMR compared to that of EPR. However, this can be partly overcome by the acquisition of more NMR signals with time (Zoia et al. 2011).

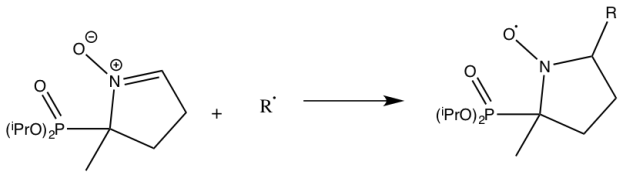

Figure 1.14: General chemical reaction between DIPPMPO and different radical species (Zoia & Argyropoulos 2009).

Argyropoulos et. al. detected and quantified oxygen centered radicals ($^{\bullet}OH$ and $O_2^{\bullet-}$) generated by ultraviolet photolysis of hydrogen peroxide solutions and their trapping by spin trap DIPPMPO to form DIPPMPO/$^{\bullet}OH$ adducts. During this processes hydroxyl radicals can react with hydrogen peroxide to form hydroperoxyl radicals which when react with spin trap to form DIPPMPO/$^{\bullet}OOH$ adducts. As the radical adducts generated are diamagnetic, they can be observed by ^{31}P NMR as distinct sharp signals Figure 1.15. The ^{31}P NMR signal shows presence of hydroxyl radicals and hydroperoxyl radicals reaction products at 25.3 ppm and 17.1 ppm. The chemical shift difference between the hydroxyl adduct signal and DIPPMPO resonance is 3.1 ppm upfield which is in accordance with Khramstov for DEPMPO and the DEPMPO/adduct reduction product that arises upon the trapping of hydroxyl radicals (3.4 ppm) (Argyropoulos et al. 2006, Khramtsov et al. 1999).

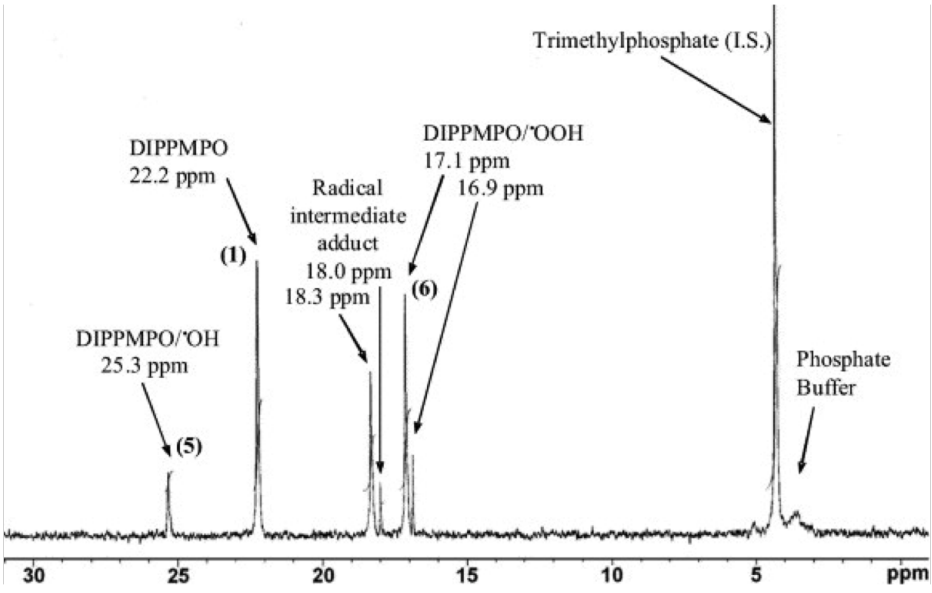

Figure 1.15: ^{31}P-NMR spectrum of spinning trapping experiment showing the species trapped in system from UV photolysis of hydrogen peroxide (Crestini et al. 2015).

The ^{31}P NMR-spectroscopy-based spin trap technique involving 5-diisopropoxy-phosphoryl-

5-methyl-1-pyrroline-N-oxide (DIPPMPO) was successfully used for quantitative analyses of the radical species that are generated in different bleaching solutions and its effect on hair. One of these system was NH_4OH (30%)/H_2O_2 (35%) at pH 10 system in the presence of trimethyl phosphate as an internal standard . The results clearly shows the difference (Figure1.16) in both the nature and amount of radical species generated in bleaching solutions when compared to the control in which only a small amount of hydroxyl-based spin adducts could be detected. When the same system was used in the presence of hair more radical species were trapped as shown in Figure 1.16. The main species involves in the oxidation processes were superoxide and amino radicals; however, their amount varied depending upon the kind of bleaching system and nature of the hair (virgin hair or dyed hair) (Crestini et al. 2015). The formation of hydroxyl radicals was confirmed when the Fenton system was used and only hydroxyl radicals were generated and detected by ^{31}P-NMR.

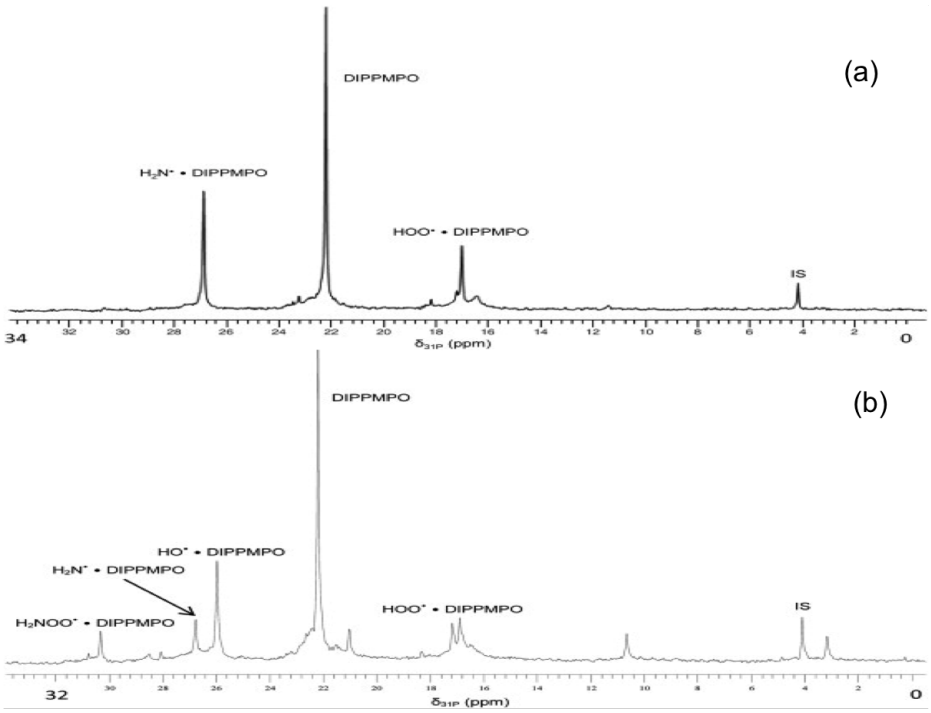

Figure 1.16: ^{31}P-NMR spectrum of a spinning trapping experiment showing the species trapped in system (a) NH_4OH/H_2O_2system without hair and (b) AB69-7 (virgin hair, copper content: < 10 ppm) treated with NH_4OH/H_2O_2. DIPPMPO = 5-diisopropoxy-phosphoryl-5-methyl-1-pyrroline-N-oxide; IS = internal standard trimethyl phosphate (Crestini et al. 2015).

This work demonstrates that free radicals react with a spin trap (DIPPMPO). This reaction forms stable diamagnetic products which, when coupled with the uniqueness of

the quantitative ^{31}P-NMR, can be exploited further to perform quantitative research work because of the following advantage of using ^{31}P-NMR :

(i) At high radical concentrations, the NMR-detected diamagnetic product is larger than the ESR detected by approximately 2 orders of magnitude (Khramtsov et al. 1999).

(ii) The NMR signal is not affected by the reducing agent by which means the ESR methods are severely limited, especially for radical adducts with short half-lives (Khramtsov et al. 1999).

(iii) The^{31}P NMR signal is specific to each trapped free radical.

1.7.3 Gas Chromatography-Mass Spectrometry (GC/MS)

ESR provides structural information about the spin adducts, however, identification of spin trapping adducts generated in the spin trapping reaction by ESR is not easy because the ESR spectra are often insensitive to the nature of the trapped radicals. Thus, there is need for another techniques for accurate identification of the spin adducts confidently. Gas chromatography mass spectrometry (GC/MS) was used by Abe and co-workers for the identification of the spin adducts. However, it was not possible to identify all the spin adducts because they were unstable under the conditions for electron impact mass spectrometry and their molecular ion cannot be observed. Some of them tend to decompose even under the GC conditions. However, this problem was overcome with the help of derivatization techniques which use a derivatization chemical (such as trimethylsilyl) to form more stable spin adducts (Abe et al. 1984). With the help of these techniques Abe et al. detected and identified hydroxyl and aryl free radicals. Even in the presence of different kinds of spin adducts, they could easily be separated by GC and identified by mass spectra.

Furthermore, Podmore et al. have developed techniques for indirect detection of the hydroxyl radicals by trapping the methyl radicals (generated from DMSO) by 4-POBN to form a POBN methyl adduct which was detected and identified by GC/MS (Mistry et al. 2008). Ortiz also demonstrated that unstable spin adducts of PBN and 4-POBN can be derivatized by silylation to produce more stable and less volatile compounds for GC/MS (Ortiz de montellano et al. 1983). Jansen et al. detected a series of alkyl spin adducts of PBN produced by the Grignard addition to the nitrone followed by oxidation of the hydroxyl amine (Janzen et al. 1985).

GC/MS was also used to identify the damage to DNA by oxygen derived species. For GC/MS, the DNA or DNA-protein complexes (such as chromatin) are hydrolysed (by formic acid) and the products converted to volatile derivatives which are separated by GC and identified by the structural evidence provided by MS. Higher sensitivity and selectivity can be achieved by operating MS in the selected ion monitoring (SIM) mode. The GC/MS-SIM technique can be used to study the precise mechanism by which DNA

is damaged in cells from oxidative stress. For example damage to DNA by the hydroxyl radical will produce a variety of base products characteristic of hydroxyl attacks should be detected (such as 5-Hydroxy-6- hydrothymine, 5-Hydroxy-6 hydrouracil etc.). These compounds have been observed in chromatin isolated from γ-irradiated human cells in culture by Nackerdien et al. (Nackerdien et al. 1992) and from murine hybridoma cells after treatment with H_2O_2. In cases where singlet oxygen is involved in DNA damage then a much more limited range of products should be measurable such as 8-hydroxyguanine (8-OHGua) and 2,6-diamino-4-hydroxy-5-formamidopyrimidine (FapyGua) (Boiteux et al. 1992). Hence, the GC/MS technique can be applied to detect, identify and study the mechanism of radical adduct formation as it is simple and fast can be useful for analysing minute amounts of unstable free radical eg. $^{\bullet}$OH. Due to these advantages, the GC/MS technique has been applied for the detection of various radicals generated from methanol, acetaldehyde, propanal and DMSO.

1.7.3.1 Solid-Phase Microextraction (SPME)

Present advances in analytical and separation methods can resolve all kinds of complex mixtures, from gases to biological macromolecules, with detection limits down to the femtogram range. Common analytical methods involve processes such as sampling (collection of samples), sample preparation (separation from the matrix, concentration, fractionation and, if necessary, derivatization), separation, detection and analysis. Among these processes, sampling and sample preparation are the most time consuming processes (about 80% of total analysis processes) because, in most cases, analytical instruments cannot handle the sample's matrices directly (Vas et al. 2004). The whole analytical method process can be wasted if an unsuitable sample preparation method has been employed before the sample reaches the chromatograph and the analyser (Pawliszyn 2003).

Current sample preparation techniques using solvents (liquid-liquid extraction (LLE)) are laborious, time consuming and incorporate a multi-stage process. Each step (especially concentration) can introduce errors and sample losses especially when analysing volatile compounds. Additionally, waste disposal of solvents in an environmentally-friendly manner is a problem, adding extra cost to the analytical procedure. Using solid-phase extraction (SPE) cartridges or discs and micro-well plates have overcome the problems of LLE to some extent. SPE needs less solvent but is time consuming, following a multi-step processes, and often requires a concentration step which may result in a loss of volatile compounds. Adsorption of analytes on the walls of extraction devices can occur which can introduce impurities in the extraction and the solvent can simultaneously become concentrated. Evaporation of the eluates from the extraction devices is more time consuming in SPE compared to LLE because protic solvents (such as methanol) are used which have a lower vapour pressure than those of apolar solvents which are used in LLE

(Vas et al. 2004). Additionally, clotting, channelling and percolation are typical problems of SPE. Hence, LLE and SPE are always performed off-line. Automation of LLE and SPE is nevertheless complex, but these did not lead to a breakthrough in the economics of the sample preparation (Vas et al. 2004).

A recent and very successful new approach to sample preparation is solid-phase microextraction (SPME). Solid-phase microextraction is a solvent-free sample extraction technique that integrates, sampling, isolation and enrichment of analytes into one step. It was developed and implemented by Professor Janusz Pawliszyn from the University of Waterloo, Canada, in the 1990s. Analytes in the samples are directly extracted and concentrated on the extraction fibre. This method saves preparation time and on disposal costs and has the significant advantages of simplicity, speed, sensitivity and easy to operate techniques as compared to other extraction techniques like liquid-liquid extraction. It has been used routinely with gas chromatography (GC) and GC/mass spectrometry (GC/MS) and has been successfully applied to a wide variety of compounds (particularly for the extraction of volatile and semi-volatile organic compounds from environmental, biological and food samples). SPME can also be coupled with high-performance liquid chromatography (HPLC) and HPLC-MS in order to analyse weakly volatile or thermally labile compounds not amenable to GC or GC/MS. The main advantage of SPME is its good analytical performance combined with simplicity and low cost. SPME produces relatively clean and concentrated extracts and is ideal for MS applications (Pwaliszyn 2009). SPME combined with MS is increasingly gaining in popularity.

The SPME apparatus (Figure 1.17) is a very simple device consisting of a fibre holder and a fibre assembly, the latter containing a 1-2cm long retractable SPME fibre. The SPME fibre can be used as sampling gas (headspace(HS)-SPME) or as a sampling solution. In both cases, the SPME needle is inserted into the appropriate position (through a septum into the HS) and exposes the fibre to the environment by retracting the needle protecting the fibre. The analytes are concentrated on the coating by the absorption/adsorption processes. The sampling time are typically in the order of a few minutes. After sampling, the fibre is retracted into the metal needle and the next step is the transfer of the analytes from the fibre into the analytical instruments such as LC/MS or GC/MS for its analysis.

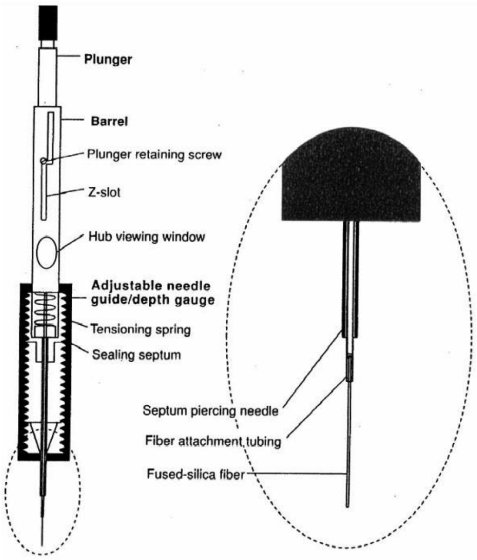

Figure 1.17: Schematic view of SPME manual fibre assembly holder (Picture from Sigma-Aldrich®).

In SPME based extraction techniques, a fused silica fibre coated with polymer is introduced into the sample or the headspace (HS) above the sample for a predetermined amount of time. The extraction process is completed when the analyte's concentration reaches equilibrium between the sample matrix and the fibre coating. In practice, this means that, once equilibrium is reached, the extracted amount is constant within the limit of experimental error and it is independent of a further increase in the extraction time (Lord & Pawliszyn 2000). The equilibrium can be as in equation 14.

$n=(K_{fs}V_fV_sCo)/(K_{fs}V_f+V_s)$——- equation (14).

where n = number of moles extracted by the coating, K_{fs} is the fibre coating /sample matrix distribution constant, V_f is the fibre coating volume, V_s is the sample volume and Co is the concentration of the analytes in the sample. In the above equation the amount of analytes extracted onto the coating (n) is directly proportional to the analytes concentration in the sample (Co) (Pwaliszyn 2009).

The SPME fibre coating is primarily responsible for the extraction of the analytes. Depending on the fibre coating SPME can be used to extract a wide range of analytes from volatile to non-volatile and from polar to non-polar. To accomplish this, different coating types have been developed which enable the extraction of a variety of analytes with enhanced selectivity. SPME coating can be classified primarily into four categories depending on the type of coating, coating thickness, polarity and whether the coating is

absorbent or adsorbent (Pwaliszyn 2009). A list of commercially available fibre is shown in Table 1.1.

Type of Coating	Extraction mechanism	Polarity
7 µm, 30 µm and 100 µm PDMS	Absorbent	Non-polar
85 µm PA	Absorbent	Polar
60 µm PEG (Carbowax)	Absorbent	Polar
15 µm Carbopack Z-PDMS	Adsorbent	Bi-polar
65 µm PDMS-DVB	Adsorbent	Bi-polar
55 µm/30 µm DVB/Carboxen-PDMS	Adsorbent	Bi-polar
85 µm Carboxen-PDMS	Adsorbent	Bi-polar

Table 1.1: Properties of commercially available SPME fibre coating.

The analytes attached to the fibre are then transferred into the analytical instruments, such as GC/MS for the analysis of the analytes. The combination of SPME with different chromatographic techniques has been investigated thoroughly by many researchers since the invention of the SPME technique. SPME coupled with GC/MS has been achieved by employing a GC-injection port as an interface, in which analytes are released by thermal desorption and carried into the GC column for separation and analysis. The choice of sampling and chromatography depends mainly on the polarity and volatility of the analytes. Volatile analytes are mostly studied by HS analysis followed by GC/MS. Polar and non-volatile samples are most often studied by direct immersion (DI) of the fibre in liquid, followed by GC or HPLC for the analysis. The sampling fibres can be used multiple times; hundreds of analyses in the case of HS analysis and dozens of times in the case of immersion analysis.

HS-SPME and GC/MS have been used in the detection of microbial VOCs (MVOCs) produced by indoor moulds. MVOCs produced from different sources such as malt extract agar, plasterboard and wallpaper have been compared (Van Lancker et al. 2008). SPME methods have been used to investigate water pollution, petroleum-related substances from refineries and refinery effluents in water (Comber et al. 2015). The techniques can also be used to screen environmental petrochemical contamination in seafood. VOC's fingerprinting of Listeria monocytogenes was detected by SPME/GC/MS and E-nose in a pure culture medium (Yu et al. 2014). Analysis of the VOC's fingerprint of microorganisms can be applied routinely in microbiology studies.

Metabolomics, the study of metabolites in biological samples, is critical in interpreting health status, medical diagnostics, disease conditions and treatments (Lord et al. 2011). Supported by many studies, SPME can be a reliable tool for early diagnosis. SPME study of rapid breath analysis was performed on cystic fibrosis patients and the results will help

the diagnosis of the disease in the near future (Kramer et al. 2015). HS-SPME analysis for VOC's in humans significantly reduces the background signal intensity with reproducible results. This method can be used to detect the biomarker for garlic intake and alcohol ingestion (Jiang et al. 2013).

The HS-SPME fibre has been used successfully in the extraction of the PBN trapped radical adducts from the Fenton reaction. The radicals generated in the Fenton reaction were trapped by using PBN derivatives, to form PBN adducts which are highly volatile, for example, the dimethyl PBN adduct was extracted by using HS-SPME and was analysed by GC/MS with an absorption time of less than three seconds. The HS-SPME method was developed to trap various radicals generated from acetaldehyde, propanal, methanol and DMSO and the resulting analysis analyses were very convincing suggesting that HS-SPME coupled with GC/MS can be a powerful tool for detecting free radical species.

1.7.3.2 Single Droplet Microextraction (SDME)

Single-drop micro-extraction was introduced in the mid-1990s (Liu & Dasgupta 1996, Jeannot & Cantwell 1997). SDME can be used as immersed SDME or headspace single-drop micro-extraction (HS-SDME). For immersed SDME, a drop of a few microliters of solvent is generated and held inside a liquid sample through a syringe which can be retracted and used for analysis. For HS-SDME, the analytes are extracted by suspending a 2-3 μL drop directly from the needle of a micro syringe. The needle passes through the septum of a vessel and the needle tip appears above the surface of the solution as shown in Figure 1.18. After the prescribed extraction time, the drop is drawn back into the syringe. The syringe is then removed and its content is injected directly into a gas chromatography column for analysis.

HS-SDME is a preferred choice and a powerful alternative to other techniques for volatile analytes as there is no contact between the solvent and the sample. The choice of solvent should be such that the octanol:water distribution coefficient of the analytes is low (Sramkova et al. 2014). Along with the extraction of analytes from the mixture, the acceptor phase drop can also be used as a derivatization reagent (Deng et al. 2005, Lin et al. 2013). The rate of mass transfer from the sample into the headspace and then into the acceptor phase, is vital for the method's sensitivity which can be enhanced by increasing temperature and agitation.

The SDME technique has been used for the extraction and analysis of nitroaromatics, dialkylphthalates, organochlorine compounds, polycyclic aromatic hydrocarbons, triazine herbicides, cocaine and endosulfans (Batlle & Neri 2004, Psillakis & Kalogerakis 2001, Hou & Lee 2002, De Jager & Anthony 2000, 2001). The SDME technique was developed by Buszewski and Ligor for the detection of trichlorobenzene, trichloromethane and

other chlorocompounds in water samples Ligor & Buszewski (2000). For the analysis of VOCs in dirty samples, Jeannot and coworkers developed HS-SDME (Theis et al. 2001). HS-SDME is widely used applied to pollutants in water and soils (Li et al. 2004, Colombini et al. 2004). The HS-SDME technique is inexpensive (as it does not involve a lot of solvent) and convenient and is a precise sample clean up and pre-concentration method for the detection of VOCs at trace levels (Deng et al. 2005). However, there are a few disadvantages in using HS-SDME such as the presence of large solvent peak in the chromatogram, presence of any impurities in the solvent and other contamination source (such as septum) can occur in the chromatogram.

In the present work, a novel technique of HS-SDME was developed, whereby analytes from the Fenton reaction mixture were extracted and concentrated by a suspended microdrop solvent (such as decane) and injected into GC/MS for its analysis.

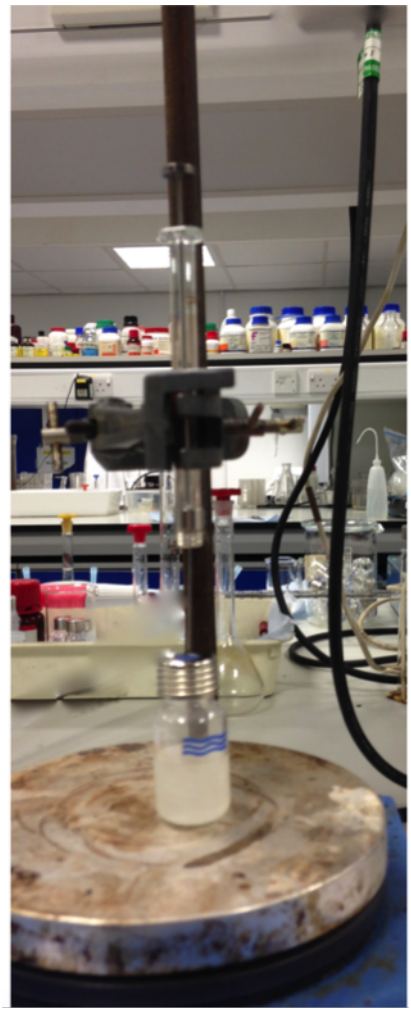

Figure 1.18: Setup used for HS-SDME.

1.7.4 Liquid chromatography/electron spin resonance (LC/ESR) and Liquid chromatography/mass spectrometry (LC/MS)

An ESR spin trap is a conventional and very reliable technique for the detection of free radicals, however, the characterization of free radicals and the knowledge of mechanisms have been restricted and the impact of many *in vivo* ESR studies has been hindered. For example, when POBN is used for lipid peroxidation studies in a cellular system, the POBN radical adducts formed showed an almost identical six-line ESR spectra for the many different carbon-centred radicals making it almost impossible to identify the detailed radical structure, thereby, limiting the knowledge to an understanding of the roles of radicals in lipid peroxidation and in lipid-peroxidation related human diseases (Qian et al. 2000). To overcome these problems and to improve the efficiency and reliability of the identification of the lipid-derived carbon-centred radicals, a combination of LC/ESR and LC/MS was used to detect, under identical chromatographic conditions, the peroxidation of two ω-6 PUFAs, linoleic acid and arachidonic acid, and this peroxidation was studied. Almost all the potential lipid derived carbon centred radical adducts formed from both PUFAs were detected (ESR) and identified (MS) (Qian et al. 2003).

LC/ESR and LC/MS was also used by Qian et al. (Qian et al. 2005) to characterize and quantify all the POBN-trapped free radicals from the interaction of $HO^{\bullet}$ and DMSO. In addition to identifying the two well-known radicals (methyl radical and methoxy radical detected by ESR), two additional radicals $^{\bullet}CH_2OH$ and $^{\bullet}CH_2S(O)CH_3$ were detected and identified by LC/ESR and LC/MS. Hence a combination of the analytical techniques LC/ESR and LC/MS provided fast, direct and reliable techniques for radical identification.

1.7.5 Other techniques

1.7.5.1 Assay of total antioxidant capacity

A high production of RS can decrease one or more antioxidant levels. The level of one or more of antioxidants can be measure and used as an index of oxidative stress. A decrease in antioxidant level does not necessarily mean that oxidative damage has taken place; it might mean that the defence mechanisms have removed the RS and protected the system. A concentration of different antioxidants can be measured, however, these methods can be very time consuming, laborious, costly and are complicated techniques. Hence, instead of measuring a single antioxidant level, the sum of the overall antioxidant levels can be measured, which is known as “total antioxidant capacity (TAC)”. The antioxidant capacity refers to the number of moles of a given oxidant scavenged by the sample studied. There are various assays for measuring TAC which can be broadly categorized into inhibi-

tion assays (such as TRAP (total (peroxyl) radical trapping antioxidant parameter assay), reduction assays (such as 1,1-diphenyl-2-picrazyl (DPPH)) and hydrophobic antioxidant assays (for antioxidants that are lipophilic).

The inhibition assay for antioxidants is where the oxidant reacts with the indicator (such as 2,2'-azobis(2-amidopropane) (ABAP), 2,2-azobis(2-amidinopropane) dihydrochloride (AAPH)) leading to a change in its absorbance, fluorescence, luminescence or other measurable properties. The first inhibition assay used was the TRAP assay. The TRAP assay is based on the oxidation of diluted blood plasma or serum by a free radicals' derived from decomposition of AAPH to peroxyl radicals that react with antioxidants in the blood plasma or serum. Once the antioxidant level has been depleted, lipid is added to the system (if not present) to check if any peroxyl radical is left as the presence of peroxyl radicals will cause lipid peroxidation. By measuring the lag period before the onset of peroxidation and by calibrating the assay with known antioxidant (such as Trolox C), a value of TRAP can be obtained as the micro moles of peroxyl radicals trapped per litre of fluid. Each Trolox molecule can trap two peroxyl radicals (Halliwell & Gutteridge 2007).

Reduction assay is based on the principle that antioxidants are reductants and the amounts of components able to reduce the indicator is equal to the amount of antioxidants present in the sample. However, there are exceptions to this as not all antioxidants have reducing properties. Some synthetic antioxidants such as nitroxides have oxidizing properties which cannot be measured by reduction assay. Also, those antioxidants which act via chelating reactive medical species will not be measured, but they do not contribute to the TAC as measured by various inhibition methods (especially those involving ABAP). There are several reductive assays which are mentioned here. There is the DPPH reduction method which involves the reduction of DPPH radicals by antioxidants and the results can be measured spectrophotometrically. There is the ABTS (2,2'-azinobis(3-ethylbenzthiazoline-6-sulfonic acid)) method in which the reduction of ABTS can be followed by ESR. Another widely used method is the ferric reducing activity of plasma (FRAP) method which measures the reduction of a ferric complex of 2,4,6-tripyridyltriazine to a coloured ferrous complex which can be measured by using spectrophotometry (Bartosz 2003).

1.7.5.2 Measurement of lipid peroxidation

ROS can react with lipids, termed as lipid peroxidation (LPO) and the measurement of LPO can be used to detect the oxidative stress. Lipid peroxidation is measured by measuring the intermediates (such as conjugated dienes) or end products of the process (e.g. hydrocarbons such as ethane and pentane as well as aldehydes such as acetaldehyde, malonaldehyde and propionaldehyde) which have been found during asthma, liver transplantation, aortic cross clamping, traumatic brain injury etc. (De Gruijl 1999).

There are specific and general methods available to detect these VOCs, for example, the detection of MDA can be done by reacting thiobarbituric acid (TBA) with MDA to form TBA-MDA adduct which can be measured by using the spectrophotometric assay method. MDA generated during reperfusion of the ischemic myocardium can be detected by derivatizing with 2,4-dinitrophenylhydrazine (DNPH) to form the corresponding DNPH derivatives which can be measured by using HPLC and GC/MS (Cordis et al. 1994). HNE can be detected by using pentafluorobenzyl-hydroxylamine to form the pentafluorobenzyl oxime (PFB-oxime) of HNE, followed by silylation (TMS) of the hydroxy group. This derivative can be analysed by GC/MS with negative ion chemical ionization. 1,3-Cyclohexanedione (CHD) is also used to detect the aldehyde; in this the aldehyde reacts with CHD to form fluorescent decahydroacridine derivatives which can be separated and identified by HPLC (Esterbauer & Zollern 1989).

Breath analysis is one of the efficient methods for the medical testing of lung diseases (such as asthma, cystic fibrosis (CF), bronchiectasis and interstitial lung disease), metabolic disorder (such as diabetes, potassium metabolism disorder), oxidative stress (such as diabetes mellitus and coronary artery disease), and gastro enteric diseases (such as lactase deficiency). A sampling device for breath exhaled via the mouth and nose and the air in the mouth cavity was developed by Smith and co-workers(Wang et al. 2008). Recently SPME has become a very popular method due to its simplicity. After sampling, the analytes can be detected by various analytical techniques such as GC coupled with flame ionization detection (FID), MS or ion-mobility spectrometry (IMS) (Lourenco & Turner 2014).

1.7.5.3 The deoxyribose assay

The hydroxyl radical reacts with 2-deoxyribose and produces a range of products. For example, the hydroxyl radical can be added to guanine at 4, 5 or 8 positions in the purine ring. Addition to C-8 produces a C-8 OH-adducts radical that can be reduced to 8-hydroxy-7,8-dihydroguanine, oxidized to 8-hydroxyguanine or undergo ring opening followed by one electron reduction and protonation to give 2,6-diamino-4-hydroxy-5-formamidopyrimidine (FAPyG) (Halliwell & Gutteridge 2007). On heating at a low pH some of these decompose to form MDA which can be detected by using the thiobarbituric acid (TBA) assay to generate pink $(TBA)_2$-MDA chromogen. This can be used to detect hydroxyl radical production.

1.8 Aims of this project

The aim of this project is to spin trap radicals generated from organic compounds such as methanol, DMSO, acetaldehyde and propionaldehyde by using PBN and its derivatives.

Extracting these free radical spin trapping adducts (PBN adducts) by different extraction techniques (such as liquid liquid extraction (chloroform solvent), HS-SDME (decane as solvent) and HS-SPME fibres) and its analysis by GC/MS.

For the detection of free radicals, EPR remains the traditional method; however, it cannot detect all free radicals, therefore, spin trapping compounds (such PBN, POBN, DMPO etc.) were developed which trap the free radicals to form a stable nitroxide compound that can be detected by the EPR spectroscopy. The combination of spin trap compound with EPR for the detection of free radicals was a major breakthrough for the detection of free radicals and the role of free radicals in diseases like cancer, neurological disorders, diabetes, ischemia/reperfusion and other ageing diseases. However, the EPR technique has limitations in the identification of free radicals as all radicals will generate a same signal pattern. Hence, the GC/MS technique was developed which is an alternative to EPR for the detection and identification of free radicals including hydroxyl radicals.

For the generation of free radicals the Fenton reaction system was used in which Fe^{2+} reacts with H_2O_2 to generate $HO^{\bullet}$ radicals which react with methanol, acetaldehyde, propionaldehyde and DMSO to generate radicals. These radicals were trapped by using spin trapping nitrone compounds such as PBN, PBN-d_6, 4-FPBN and 4-ClPBN. Nitrones are used to trap free radicals in chemical systems and biological systems. Nitrones such as PBN have a potent biological and anticancer activity in several experimental cancer models and have potential therapeutics in some cancers (Floyd et al. 2008). Studies have also shown that PBN related nitrones do decrease oxidative stress and oxidative damage and their potent biological anti-inflammatory activity (Floyd et al. 2008). PBN is the most common spin trap and it plays a unique role in the reaction of $HO^{\bullet}$ radicals and DMSO *in vivo/in vitro* (Chamulitrat et al. 1991). The nitroxide formed from highly reactive $HO^{\bullet}$ radicals is a setback in the case of hydroxyl spin trapping in biological systems. Hence, the presence of acetaldehyde, methanol etc. in the system results in the production of radicals which can be used in an indirect way to detect hydroxyl radicals in the system.

The Fenton system involves chemicals which can cause serious damage to the column, therefore, the reaction mixture is extracted in chloroform. The resulting chromatogram shows several peaks along with PBN adducts. Also, while extracting, it is possible to lose some of the analytes due to their highly volatile nature making the sampling method less precise. Hence, new extraction techniques, HS-SDME and HS-SPME, were developed for the analysis of PBN adducts formed during the Fenton reaction.

Chapter 2

Materials and methods

2.1 Chemicals

2.1.1 Synthesis of PBN derivatives

Materials used for the synthesis of PBN derivatives were obtained as follows:

4-Chlorobenzaldehyde (Alfa Aesar®, UK), 4-Fluorobenzaldehyde (Fluka®, China), 4-Bromobenzaldehyde (Sigma-Aldrich®, China), 4-Triflurobenzaldehyde (Sigma-Aldrich®, Germany), 4-Methyl- benzaldehyde (Lancaster,UK), 4-Methoxybenzaldehyde (Alfa Aesar®, UK), benzaldehyde-d_6 (CDN isotopes, UK), 2-Methyl-2-nitropropane (Sigma-Aldrich®, USA), Zinc (GPR, UK), acetic acid (Acros Organic, Belgium), ethanol and diethyl ether for synthesis (Instore bond from Salford University, UK), sodium bicarbonate (Sigma-Aldrich®, UK), Sodium sulfate (Sigma-Aldrich®, UK).

2.1.2 The Fenton reaction

Materials used for the generation of free radicals via Fenton type chemistry were obtained as follows:

Di-Potassium hydrogen phosphate anhydrous (Fluka®, BioChemika, CH), Ethylene-diaminetetraacetic acid disodium salt dihydrate (EDTA) (Sigma-Aldrich®, Germany), L-Ascorbic Acid (Sigma-Aldrich®, China), Hydrogen peroxide solution 30wt % in H_2O (Sigma-Aldrich®, Germany), Ammonium ferrous sulfate Hexahydrate ($FeH_8N_2O_8S_2.6H_2O$) (Fluka®, BioChemika, CH), Dimethyl sulfoxide (Alfa Aesar ®, UK), Dimethyl sulfoxide-d_6 (Sigma-Aldrich®, USA), N-*tert*-Butyl-α-phenylnitrone (PBN) (Sigma-Aldrich®, UK), acetaldehyde (Sigma-Aldrich®, Austria), Propanal (Sigma-Aldrich®, Austria), decane (Sigma-Aldrich®, UK), Methyl alcohol-d_4(CD_3OD), acetaldehyde-2,2,2-d_3(CD_3COH) all deuterated chemicals used in Fenton was purchased from CDN isotopes, UK.

2.2 Synthesis of PBN derivatives

The synthesis method was adopted from Hinton et. al. (Hinton & Janzen 1992). The desired substituted benzaldehyde (10 mmoles), 2-methyl-2-nitropropane (20 mmoles, 2.06 g) and zinc (30 mmoles, 19.96 g) were placed in round bottom flask along with 75 mL of 95% ethanol. The reaction mixture was kept in ice bath; acetic acid (60 mmoles, 3.79 g) was added slowly with continuous stirring, while keeping the mixture on ice. The solution was allowed to come to room temperature, stirred for an additional 1-2 hours and stored at 4°C overnight. The $Zn(OAc)_2$ was filtered out and the solution was concentrated on a rotary evaporator (Buchi,UK), leaving a colourless solid. The solid was dissolved in diethyl ether (50 mL) and was extracted with water with $NaHCO_3$ and again with water (50 mL each). The organic layer was dried with Na_2SO_4 and the ether was evaporated off. The resulting solid was purified by sublimation or by recrystallization. On many occasions an oil was obtained after final vaporization of the ether. The oil was solidified by storing at 4°C for 4-12 weeks.

The PBN derivatives synthesised were PBN, deuterated PBN (PBN-d_6), 4-FluoroPBN (4-FPBN) and 4-ChloroPBN (4-ClPBN). Their structures are shown in Figure 2.1.

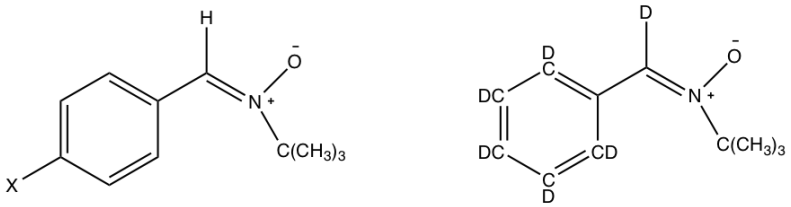

PBN derivatives:
(1) X=H, PBN
(2) X=F, 4-FPBN
(3) X=Cl, 4-ClPBN

(4) deuterated PBN-d_6

Figure 2.1: Structure of synthesised PBN and its derivatives.

2.3 The Fenton Reaction

2.3.1 Reagent Preparation:

Stock solutions were prepared in water for 100 mM potassium phosphate buffer (pH 7.4), 11 mM EDTA (sodium salt) solution, 50 mM PBN derivative, 3% H_2O_2 , 100 mM ascorbic acid and 10 mM $Fe(NH_4)_2(SO_2)_2$.

2.3.2 Fenton system

A standard method is used throughout the experiments for trapping free radicals by different PBN derivatives, unless stated otherwise. Various chemicals were used to generate different radicals as mentioned in Table 2.1.

Source	Volume (μL)
Acetaldehyde	135.0
Deuterated (d_4) acetaldehyde	135.0
Propanal	174.0
Methanol	96.0
Deuterated (d_4) methanol	96.0
DMSO	78.0
Deuterated (d_6) DMSO	78.0

Table 2.1: Volumes of chemicals used as the source of free radicals generated via Fenton type chemistry.

The reagents were added to a 25 mL beaker in specific order as mentioned below:
1) 100 mM phosphate buffer (pH 7.4) (5 mL)
2) 11 mM EDTA (1 mL)
3) 50 mM spin trap compound (1 mL)
4) 3% H_2O_2 (1 mL)
5) 100 mM Ascorbic acid (1 mL)
6) Second source of free radicals (see Table 2.1)

To initiate the reaction, 1 mL of 10 mM of ferrous ammonium sulphate $Fe(NH_4)_2(SO_4)_2$ was added to the reaction mixture and the reaction was typically carried out for 5 minutes.

2.4 Extraction Techniques

2.4.1 Direct chloroform extraction

1 mL of the Fenton reaction mixture was extracted into chloroform (2 mL) and kept aside for 5 minutes. The aqueous layer was removed carefully and the organic layer was subjected to GC-MS analysis.

2.4.2 Headspace Solid-Phase Microextraction (HS-SPME)

HS-SPME extraction was carried out to extract the volatile adducts using different SPME fibres, shown in Table 2.2. For extraction, 5 mL of the reaction mixture was transferred into an SPME vial and the adsorption of the analytes was done by placing the fibre into the headspace of the vial. For the GC-MS analysis, the analytes were desorbed from the fibre by exposing it in the injection port of the GC at 250°C.

SPME fibre	Needle size (ga)	Material	Selection guide for analyte
85 µm Carboxen/polydimethylsiloxane	24	StableFlex	Gases and low molecular weight compounds (MW 30-225)
75 µm Carboxen/polydimethylsiloxane	23	fused silica	Same as above
75 µm Carboxen/polydimethylsiloxane	24	fused silica	Same as above
100 µm polydimethylsiloxane	24	fused silica	Volatiles (MW 60-275)
50/30 µm divinylbenzene/Carboxen on polydimethylsiloxane	24	StableFlex	Flavor compounds: volatile and semi-volatiles, C3-C20
65 µm polydimethylsiloxane/divinylbenzene	24	StableFlex	Volatiles, amines and nitro-aromatic compounds (MW 50-300)
85 µm polyacrylate	24	fused silica	Polar semi-volatiles (MW 80-300)
60 µm Carbowax (PEG)	23	metal alloy	Alcohols and polar compounds (MW 40-275)

Table 2.2: Properties of different fibres used for HS-SPME extraction.

2.4.3 Headspace Single Droplet Microextraction (HS-SDME)

HS-SDME extraction was carried out to extract the volatile adducts from the Fenton reaction using 1-3 µL of the organic solvent decane at the tip of a microsyringe exposed to the reaction mixture. After extraction, the micro-drop is withdrawn back into the syringe

and injected into GC-MS for analysis.

2.5 Instrumentation

2.5.1 Gas chromatography - mass spectrometry

Gas chromatography - mass spectrometry (GC/MS) (Figure 2.2) is an instrumental technique that combines the features of gas chromatography and mass spectrometer by which complex mixtures can be separated, identified and quantified in their gaseous form. The GC is coupled to MS though the transfer line. The main features of the GC/MS system are briefly outlined below.

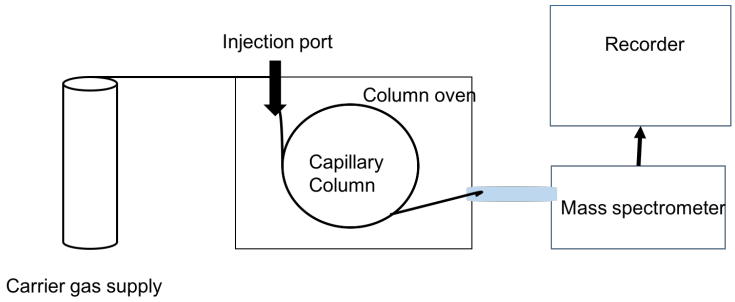

Figure 2.2: Diagram of gas chromatography mass spectrometry system (McMaster & McMaster 1998).

2.5.1.1 Gas Chromatography

Gas Chromatography (GC) is an analytical technique that measures the content of various components in a gaseous sample. In gas chromatography the sample mixture is injected into a heated injector port where it undergoes rapid heating and enters into the instrument in a gas stream which transports the sample into a separation tube known as the "column." Helium or nitrogen is used as the carrier gas. The various components are separated inside the glass column packed with silica that is coated with a liquid. The detector measures the quantity of the components that exit the column. To measure a sample with an unknown concentration, a standard sample with known concentration is injected into the instrument. The standard sample peak retention time (appearance time) and area are compared to the test sample to calculate the concentration. For futher information of regarding gas chromatography, readers are directed towards (McMaster & McMaster 1998).

2.5.1.2 Mass Spectrometry

The Electron-ionisation mass Spectrometer (MS) is the most useful detector for gas chromatography. The basic components of the EI-mass spectrometer are the pumping system, the interface to the gas chromatograph, the ionization chamber and electron sources, the focusing lens, the quadrupole analyzer, the detector and the data control system (McMaster & McMaster 1998).

In a GC/MS system, the mass spectrometer (mass analyzer) scans the masses continuously throughout the separation. When the sample exits the chromatography column, it is passed through a transfer line into the inlet of the mass spectrometer. The sample is then ionized and fragmented, typically by an electron-ionization ion source. During this process, the sample is bombarded by energetic electrons which ionize the molecule by causing them to lose an electron. Further bombardment causes the ions to fragment. The ions are then passed into a mass analyzer where the ions are sorted according to their m/z value, or mass-to-charge ratio. Most ions are only singly charged. The chromatogram will indicate the retention times of the separated components in the mixture and the mass spectrometer will determine what kind of molecules are present in the mixture (Hoffmann & Stroobant 2007).

2.5.1.3 Electron Ionization

The electron ionization (EI) source, formerly called electron impact, was devised by Dempster and improved by Bleakney and Nier (Hoffmann & Stroobant 2007). It is widely used in organic mass spectrometry. This ionization technique works well for many gas phase molecules but induces extensive fragmentation so that the molecular ions are not always observed. This ion source consists of a heated filament giving off electrons which are accelerated towards an anode and collide with the gaseous molecules of the sample injected into the source. Gases and samples with high vapour pressure are introduced directly into the sources, whereas, liquids and solids are usually heated to increase the vapour pressure for analysis.

In EI process, an electron from the analyte molecule (M) is expelled during the collision process to convert the molecule to a positive ion with an odd number of electrons as shown below (Davis & Frearson 1987), where M is the analyte molecule being ionised, e^- is the electron and $M^{+\bullet}$ is the resulting molecular ion.

$$M + e^- \rightarrow M^{+\bullet} + 2e^-$$

The EI source exposes the samples from the GC interface to a stream of 70 eV electrons from the filaments. The sample molecules have an electron expelled, leaving behind a molecular ion with a positive charge. The 70 eV is high enough not only to ionize the

sample molecule but also to cause many of them to fragment. The fragmentation pattern of the ions formed at a given electron energy is characteristic of the ionized molecules. Every time a molecule of the same compound is ionized under the same conditions, it forms the same quantity and pattern of ions. This fragments pattern becomes a finger-print that can be used to identify and quantify the molecule being analysed (Hoffmann & Stroobant 2007).

2.6 Instrument parameters

2.6.1 Standard GC/MS conditions

Two GC/MS instruments were used for the analysis:

(i) Varian 3800-MS quadrupole GC coupled with a Varian 1200 triple quadrupole MS/MS with EI source was utilized for this work. A Varian workstation with the advanced applications package was used for the data handling.

(ii) Shimadzu (GC-15A) GC coupled with QP 5050A MS. A Shimadzu workstation was used for data handling,

In all GC/MS studies, a Restek capillary column Poly(dimethylsiloxane) (PDMBS) was used with 30 metres length, an internal diameter of 0.25 mm and a stationary phase with a film coating thickness of 0.25 mm. Helium was used as the carrier gas with a flow rate of 1 mL/minute. 1 μL of sample was injected in the splitless mode with injector temperature 250 ºC injector temperature. The purge activation time was 3 minutes after injection. The initial column temperature was set to 100 °C. After sample injection it was maintained for one minute, and then increased at 15 ºC/minutes to 320 °C and held at 320 °C for two minutes. The detector temperature and the ion source temperature were maintained at 250 °C. Electron Ionization (EI) mass spectra were obtained over a typical scan range of 50-500 m/z using a single quadrupole and the total ion chromatogram was recorded from 3.0 minutes to 15.0 minutes. A 1300V photomultiplier voltage was used to detect all ions generated from the column effluent.

2.6.2 Standard HS-SPME-GC/MS conditions

The same GC/MS parameters were used to carry out the SPME analysis (see section 2.6.1). The SPME fibre was exposed in the injection port for desorption. The desorption time was 5 minutes at 250 °C and the injection port which was operated in splitless mode. The oven temperature program was set initially at 50 °C held for 5 minutes, this was then set to increase at a rate of 25 °C per minutes until a final temperature of 320 °C was reached and the temperature was then held for 5 minutes. The ionization energy was set at 70 eV and the photoelectron multiplier at 1320 volts with a scan range of 50-500 m/z.

2.6.3 Standard HS-SDME-GC/MS conditions

The same GC parameters were used to carry out the SDME analysis. For the MS analysis all parameters were same except there was a solvent delay time of 4 minutes. This is because intense decane peak elutes before the filament is turned on (i.e. long filament delay of 4 minutes).

2.7 EI mass spectra of PBN derivatives

Many of the chromatograms shown in this thesis contain a peak corresponding to the unreacted spin trap used in the Fenton reaction. The mass spectra for these compounds are shown and interpreted in this section.

2.7.1 PBN

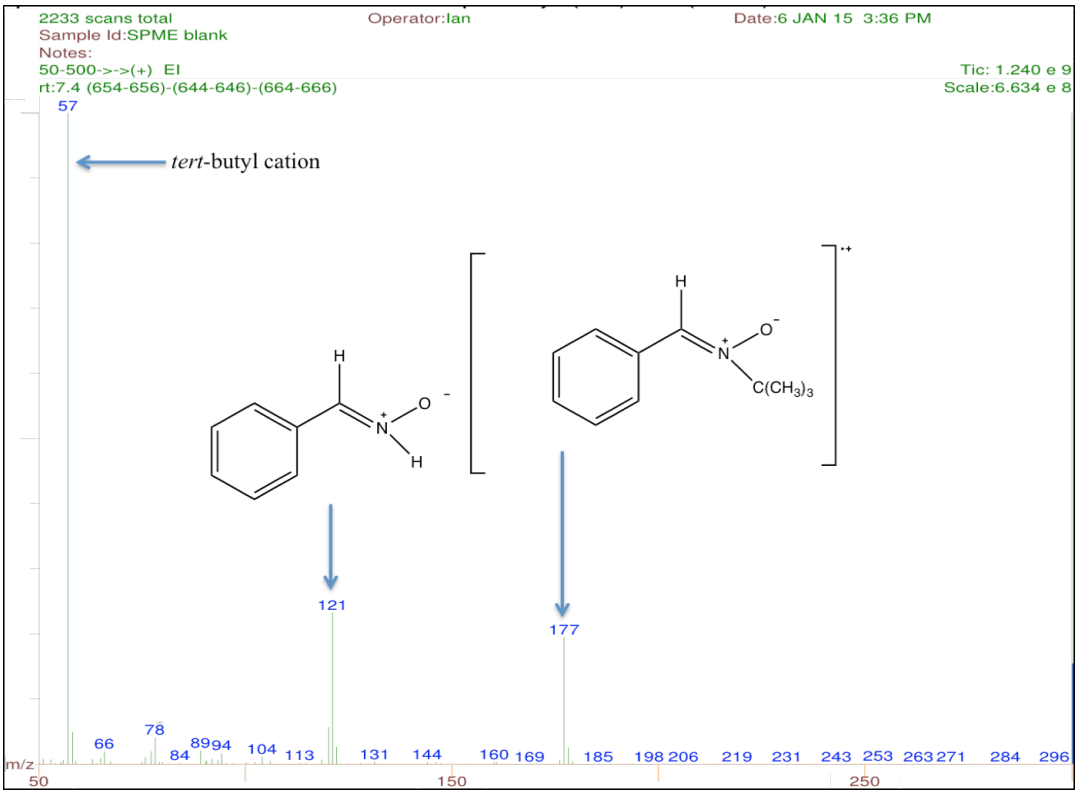

Figure 2.3: The EI mass Spectrum obtained for pure PBN, with a molecular ion 177 and base peak m/z 57.

The EI mass spectrum in Figure 2.3 shows a molecular ion at m/z 177. The fragment at m/z 121 is due to loss of 2-methyl-1-propene from the "molecular ion" (M-56) (Janzen & Dubose 1993), whilst the fragment at m/z 104 is loss of hydroxyl radical from m/z 121. The base peak fragment at m/z 57 corresponds to the *tert*-butyl cation.

2.7.2 Deuterated PBN-d_6

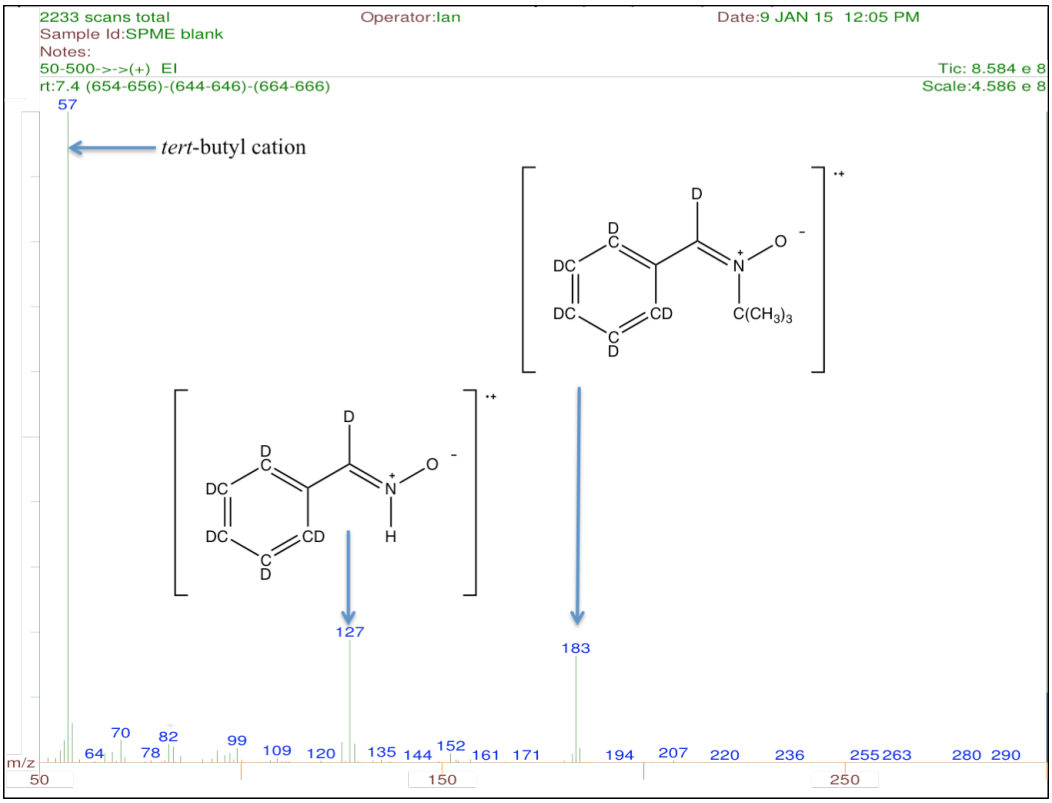

Figure 2.4: The EI mass Spectrum obtained for pure PBN-d_6, with a molecular ion 183 and base peak m/z 57.

The EI mass spectrum in Figure 2.4 shows a molecular ion at m/z 183 (an addition of 6 amu due to the presence of six deuterium atoms on the PBN) present in PBN. The fragment at m/z 127 is due to loss of 2-methyl-1-propene from the molecular ion (M-56), whereas the fragment at m/z 82 is due to the $C_6D_5^+$ cation and the base peak fragment at m/z 57 corresponds to the *tert*-butyl cation.

2.7.3 4-FPBN

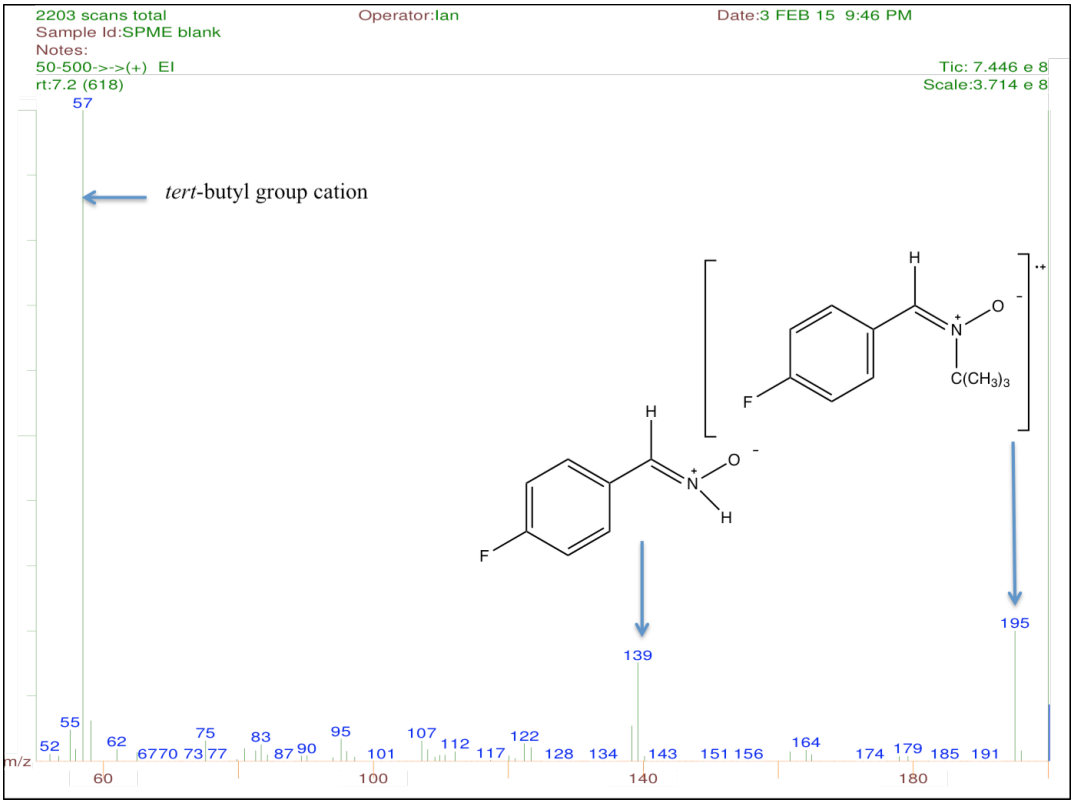

Figure 2.5: The EI mass Spectrum obtained for pure 4-FPBN, with a molecular ion at m/z 195 and base peak at m/z 57.

The EI mass spectrum in Figure 2.5 shows a molecular ion at 195 m/z. The fragment at m/z 139 (M-56) is due to loss of 2-methyl-1-propene from the molecular ion. The fragment at m/z 122 is due to loss of hydroxyl radical from m/z 139 and the base peak at 57 m/z shows the fragment for a *tert*-butyl cation.

2.7.4 4-ClPBN

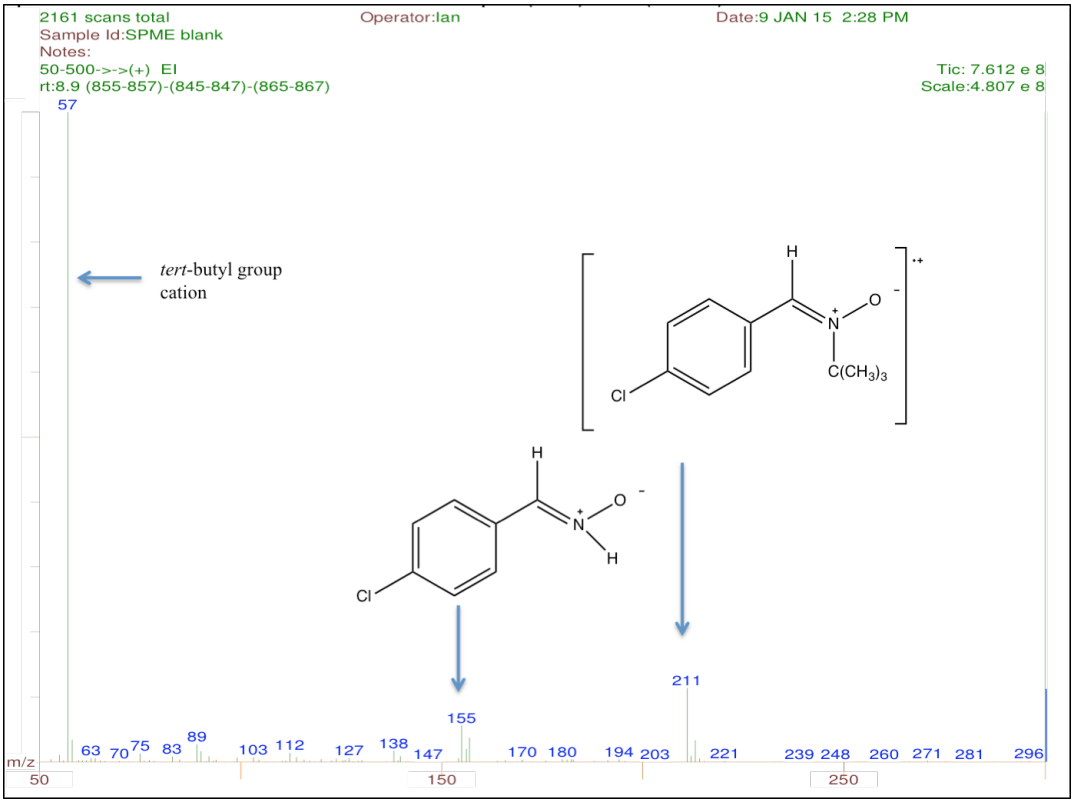

Figure 2.6: The EI mass Spectrum obtained for pure 4-ClPBN, with a molecular ion at m/z 211 and base peak at m/z 57.

The EI mass spectrum in Figure 2.6 shows a molecular ion at m/z 211 (^{35}Cl) with its corresponding isotope signal at m/z 213 (^{37}Cl). The fragment at 155/157 m/z is due to loss of 2-methyl-1-propene from the molecular ion. The base peak at 57 m/z corresponds to the *tert*-butyl cation.

2.8 Method Development

To validate the method described in section 2.3.2 a series of experiments was carried as detailed below.

2.8.1 GC-MS analysis of the Fenton reaction

2.8.1.1 PBN-OH adduct

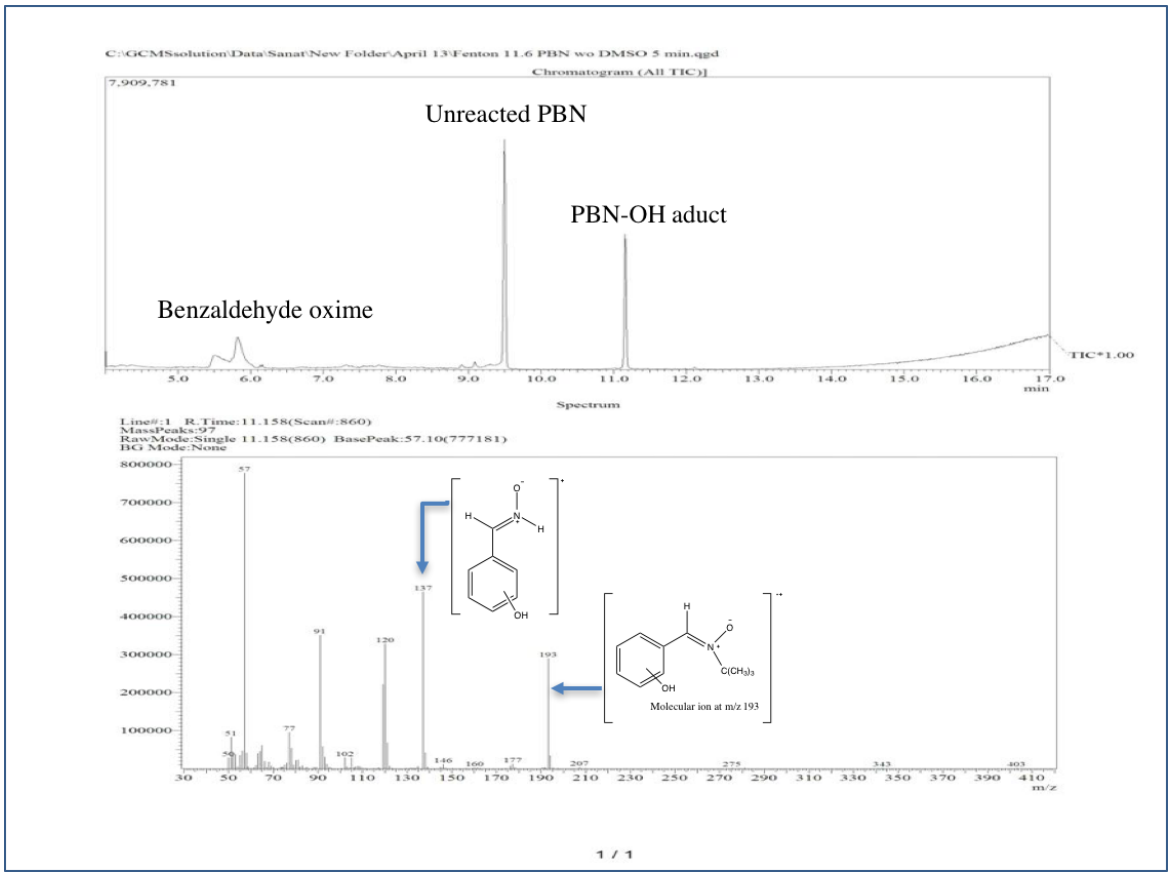

Figure 2.7: The GC total ion chromatogram and Electron ionization mass spectrum for the standard Fenton reaction. The mass spectrum corresponds to the a PBN-OH adduct.

To test the applicability of the GC/MS method to the study of spin trapped free radicals, the Fenton reaction was carried out as mentioned in section 2.3.2 in absence of a secondary source of free radicals. Hydroxyl radicals, generated in the Fenton reaction, were trapped by PBN to form a PBN-OH adduct (molecular ion at m/z 193, Figure 2.7) structure shown in Figure 2.8. Analysis of the mass spectrum and those of other PBN derivatives (data not shown) demonstrates that the hydroxyl radical has added to the 4

position on the benzene ring (Reinke et al. 2000). There is no peak in the chromatogram for the hydroxyl radical adduct to the carbon (C=N). However, from previous studies the decay kinetics of the hydroxyl adduct of PBN at this site in aqueous phosphate buffer has been found to be 1st order with half-life of 1 minute (approximately) (Janzen et al. 1992), and therefore cannot be detected directly.

The GC-EIMS TIC (Figure 2.7) shows the presence of three peaks for benzaldehyde oxime, unreacted PBN retained at 9.5 minutes (see section 2.3) and PBN-OH adducts (11.15 minutes).

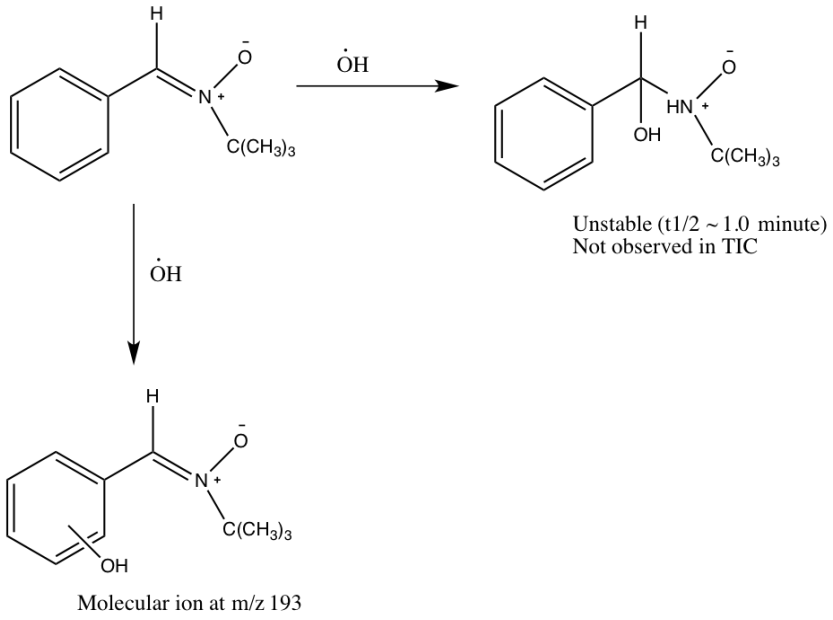

Figure 2.8: Possible sites of OH addition to PBN.

The EI mass spectrum shown in Figure 2.7 corresponds to the peak retained at 11.15 minutes with a strong molecular ion at m/z 193, an addition of 16 Da to the PBN. The only possibility for having a molecular ion at m/z 193 is the addition of a hydroxy radical ($HO^{\bullet}$) to PBN resulting in the formation of a PBN-OH adducts. The fragment at m/z 137 is due to loss of 2-methyl-1-propene from $M^{\bullet+}$. The fragment at m/z 120 is due to loss hydroxyl radical from m/z 137; m/z 91 corresponds to the tropylium cation, whereas m/z 77 corresponds to the phenyl cation and base peak at m/z 57 is for the *tert*-butyl cation.

Reinke et al. (2000) showed the preferred site for the PBN-OH adduct is the para position on the benzene ring (Reinke et al. 2000), however, PBN-OH adduct was also found when the 4-substituted PBN derivatives (Table 2.3) were used suggesting the OH may have added to ortho or meta position on the benzene ring.

Identity	Retention time (minutes)	Base peak (m/z)	Molecular ion (m/z)
PBN-OH	11.15	57	193
PBN-d_6 OH	9.0	57	198
4-FPBN-OH	8.9	57	211
4-ClPBN-OH	10.4	57	227/229

Table 2.3: PBN-OH adducts for different PBN derivatives with their retention time, molecular ion and base peak.

2.8.1.2 Benzaldehyde oxime

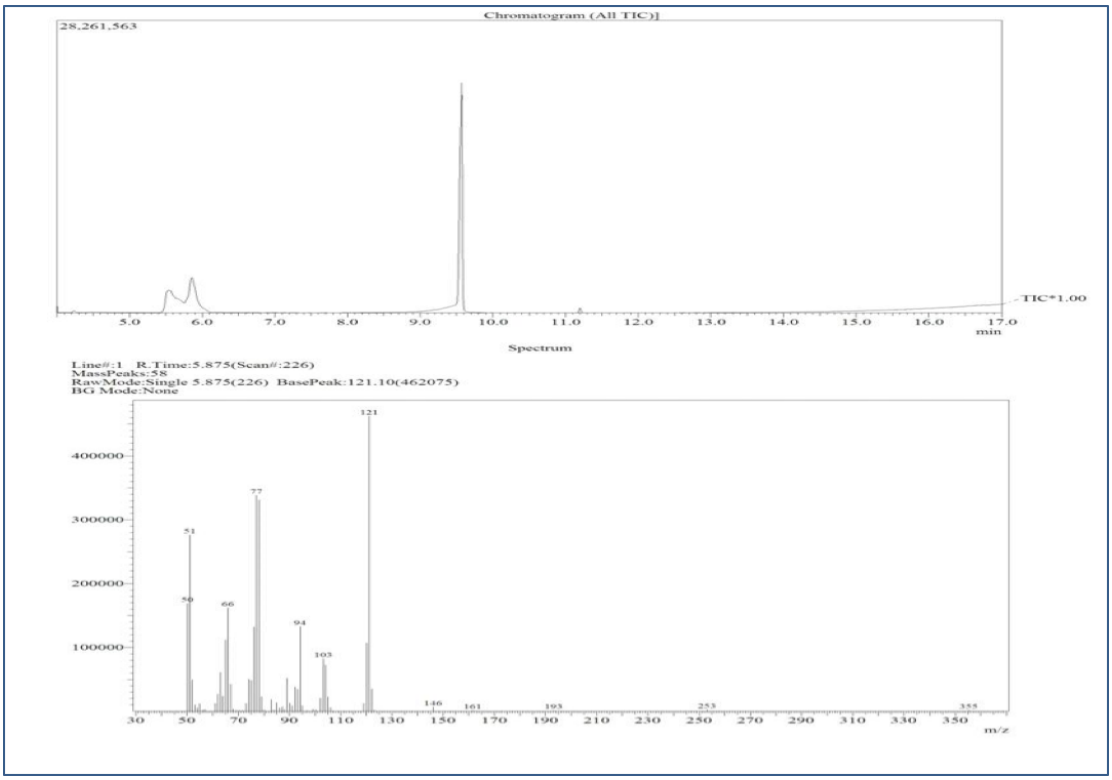

Figure 2.9: The GC total ion chromatogram and Electron ionization mass spectrum for the standard Fenton reaction. The EI mass spectrum corresponds to the benzaldehyde oxime.

The GC-EIMS TIC (Figure 2.9) shows presence of three peaks: one for benzaldehyde oxime (5.5-6.0 minutes), PBN retained at 9.5 minutes (see section 2.3) and a PBN-OH adduct (11.15 minutes).

The mass spectrum (Figure 2.9) for the peak retained at 5.5-6.0 minutes corresponds to the benzaldehyde oxime (Figure 2.10) with a "molecular ion" at m/z 121. The fragment

at m/z 77 corresponds to the phenyl cation and is formed due to loss of a CH=NOH from the molecular ion. Depending on the PBN derivative, the corresponding benzaldehyde oxime has been found in all the Fenton reactions, summarized in Table 2.4.

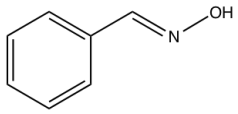

Figure 2.10: Structure of benzaldehyde oxime.

Compound	Retention time (minutes)	Molecular ion
Benzaldehyde oxime	5.5-6.0	121
Benzaldehyde oxime-d_6	4.3-4.5	127
4-Fluorobenzaldehyde oxime	4.3-4.5	139
4-Chlorobenzaldehyde oxime	5.9-6.2	155

Table 2.4: Retention times and molecular ions for benzaldehyde oxime.

2.8.2 GC-MS analysis of the Fenton reaction in the presence of DMSO

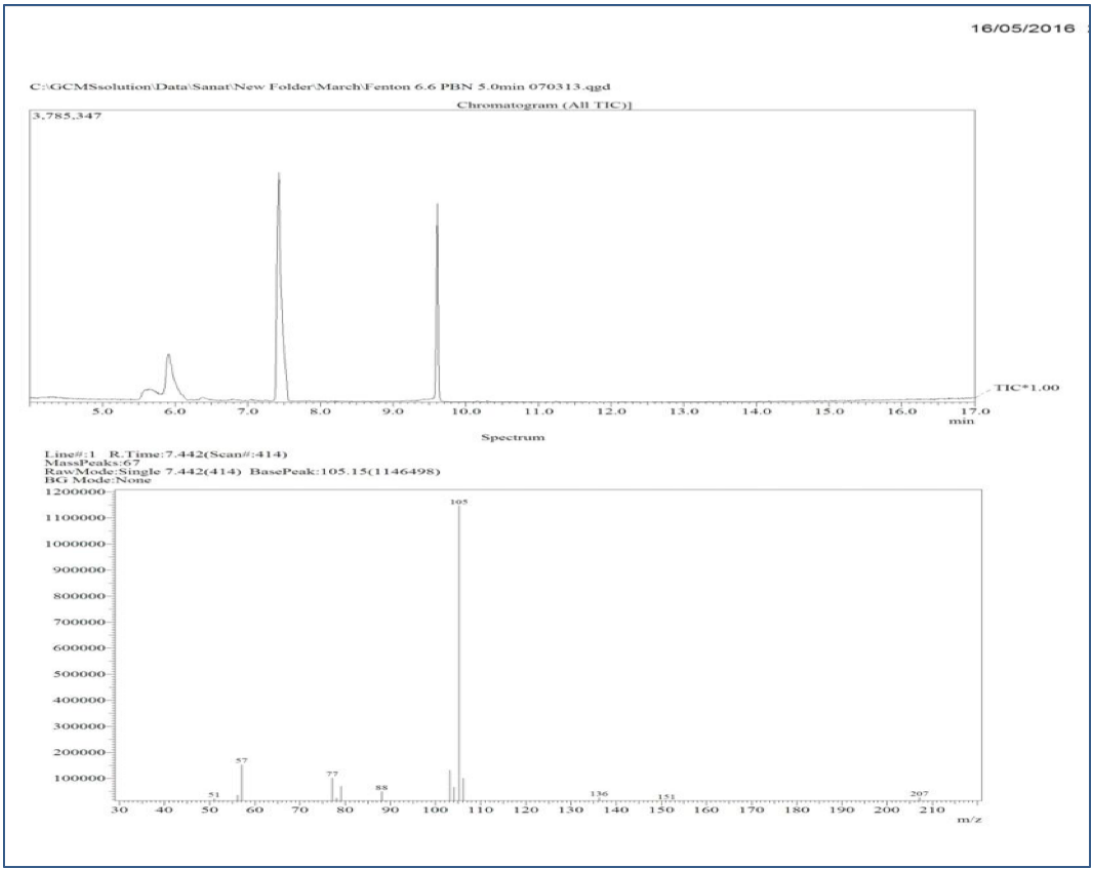

Figure 2.11: The GC total ion chromatogram and Electron ionization mass spectrum for the "Fenton" reaction carried out in the presence of DMSO. The mass spectrum shown is for the PBN$(CH_3)_2$ adduct.

The GC-EIMS TIC (Figure 2.11) shows presence of strong peak retained at 7.5 minutes correspond to the PBN$(CH_3)_2$ adduct with "molecular ion" at m/z 207. The base peak is at m/z 105. This corresponds to the ion generated as a result of dissociation of the molecular ion at the C-N bond; fragment at m/z 77 is for the phenyl cation; and m/z 57 is for the *tert*-butyl cation.

This result suggests two methyl radicals generated are from DMSO in the Fenton reaction which are trapped by PBN to form PBN$(CH_3)_2$ adduct. The mass spectrum of the PBN dimethyl adduct is exactly the same as that shown by Janzen et al. formed by chemical methods (Janzen et al. 1985). Also, trapping of two methyl radicals by a nitrone spin trap has been shown previously as an indirect approach to detecting hydroxyl radicals (Mistry et al. 2008).

The other peaks in the chromatogram (Figure 2.11) correspond to benzaldehyde oxime (Rt 5.5 minutes) and unreacted PBN (Rt = 9.75 minutes).

2.8.3 GC-MS analysis of the Fenton reaction in the absence of Fe (II) and EDTA

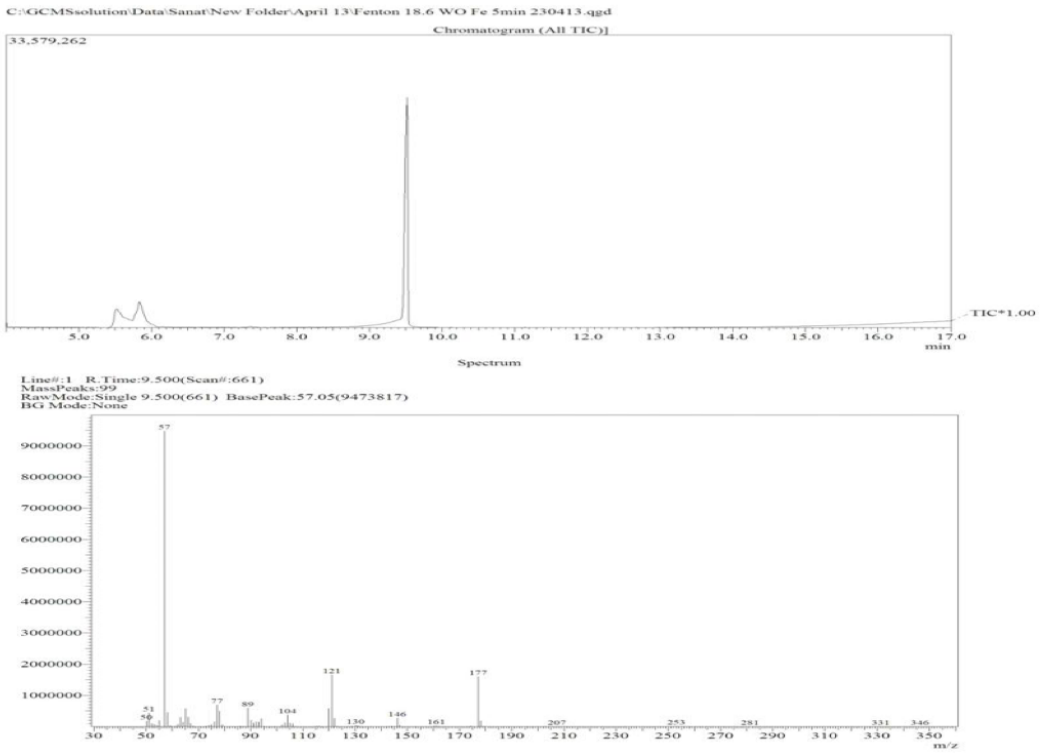

Figure 2.12: The GC total ion chromatogram and Electron ionization mass spectrum for the "Fenton" reaction carried out in the absence of Fe^{2+} and EDTA.

Chelated Fe^{2+} is an important component of the Fenton reaction system as it reduces hydrogen peroxide to generate hydroxyl radicals which, in turn, may react with other compounds (such as acetaldehyde, propanal, methanol etc.) to form other free radicals. These free radicals are trapped by the nitrone PBN to form stable adducts which can then be detected by GC/MS. To further confirm that hydroxyl free radicals are generated in our Fenton system, the Fenton reaction was carried out in absence of Fe^{2+} and EDTA.

The GC-EIMS TIC (Figure 2.12) shows only 3 peaks. The first two are believed to correspond to benzaldehyde oxime (Rt= 5.5 and 6.0 minutes, see section 2.8.1.2). The third peak corresponds to unreacted PBN (identified from its EI mass spectrum section 2.7.1).

This result suggests that neither hydroxyl radicals nor methyl radicals are generated in absence of Fe^{2+} and EDTA making them essential components required for generation of the radicals.

2.8.4 GC-MS analysis of the Fenton reaction in the absence of PBN

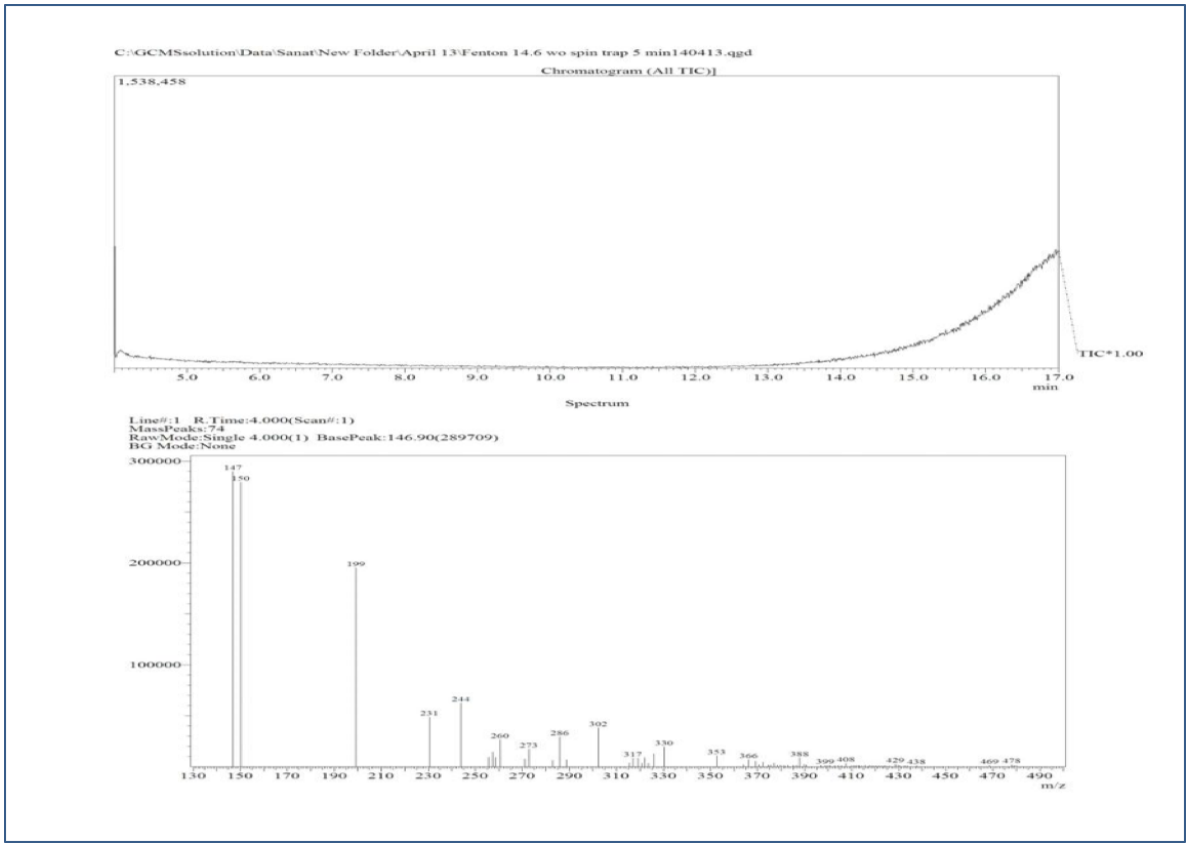

Figure 2.13: The GC total ion chromatogram and Electron ionization mass spectrum for "Fenton" reaction carried out in the absence of PBN.

The GC-EIMS TIC (Figure 2.13) shows shows the "background" ions present at that point in the chromatogram (these are probably derived from the column and hence their intensity increases as the temperature increases). This result demonstrates that all peaks in the subsequent chromatograms are derived from PBN and its derivative.

2.8.5 Analysis of the Fenton reaction in the absence of H_2O_2 and secondary sources of free radicals

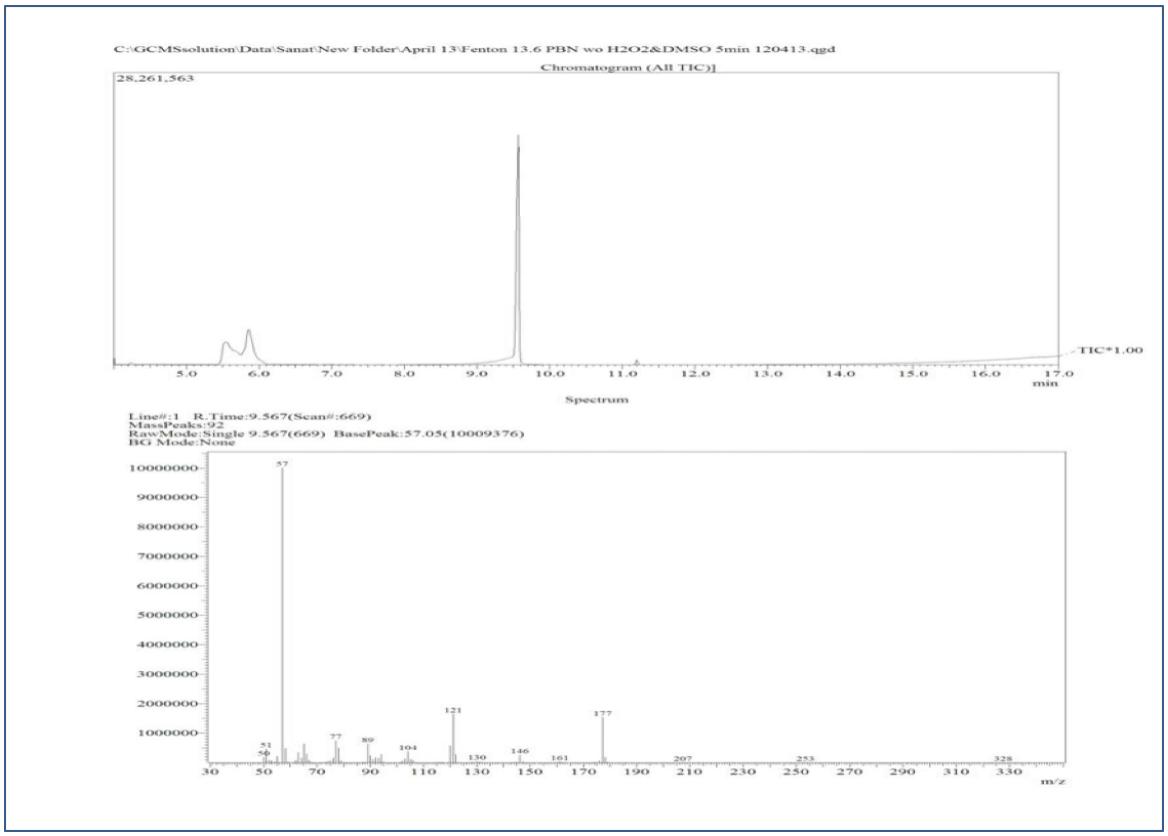

Figure 2.14: The GC total ion chromatogram of the Fenton reaction in the absence of H_2O_2 and DMSO.

To confirm H_2O_2 is the only source of hydroxyl radicals, which may then react with a secondary source of free radicals (such as acetaldehyde, propanal, methanol etc.), an experiment was carried out in absence of these chemicals and keeping the other conditions the same. The TIC (Figure 2.14) shows no peaks other than those corresponding to the PBN (retention time = 9.5 minutes) and benzaldehyde oxime (retention time= 5.5-6.0 minutes), confirming H_2O_2 as the source of the hydroxyl radical. This hydroxyl radical may then react to form other secondary radicals in the presence of other compounds which, in turn, may be trapped by PBN and detected by GC/MS.

2.8.6 Analysis of the Fenton reaction in the absence of ascorbate

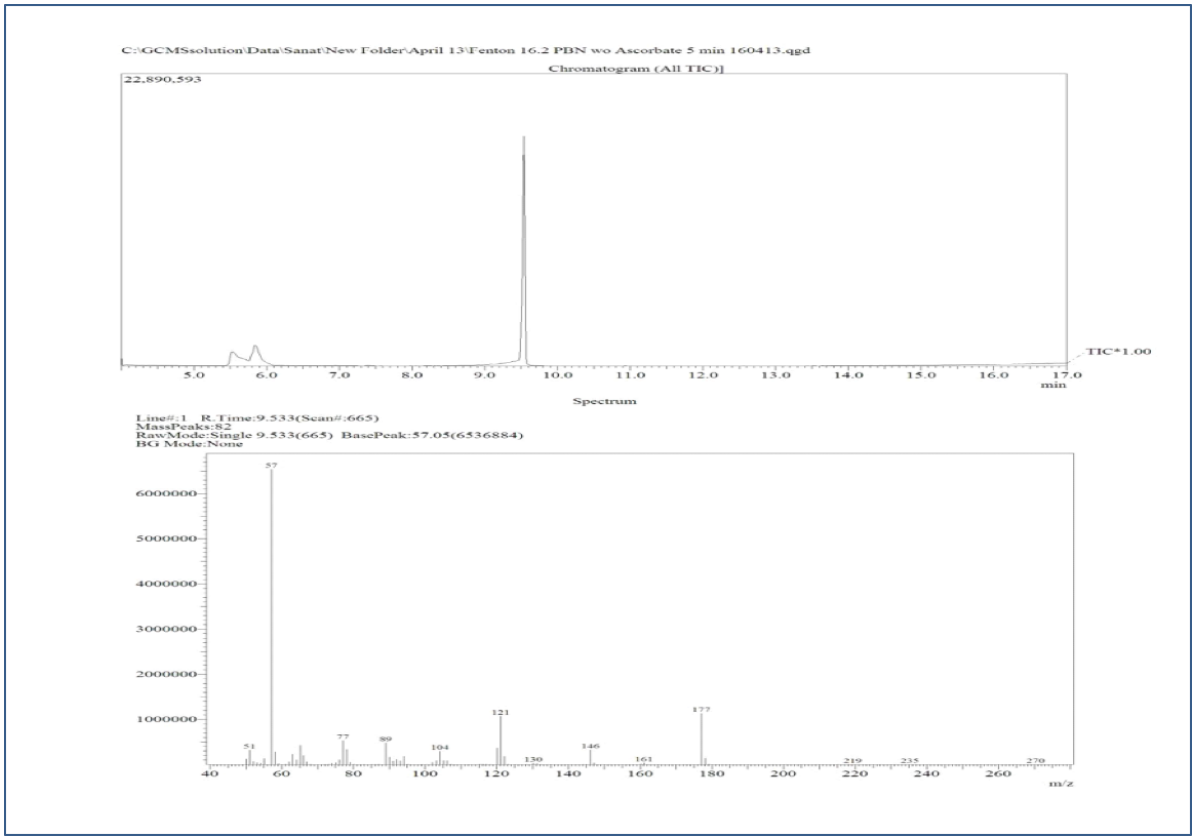

Figure 2.15: The GC total ion chromatogram of the Fenton reaction in the absence of ascorbate.

The role of ascorbate in the Fenton reaction is to redox recycle Fe^{3+} to Fe^{2+} and thereby maintaining the availability of Fe^{2+} for further reaction with hydrogen peroxide. This appears to increase the yield of hydroxyl radicals in the Fenton reaction. To confirm this, the Fenton reaction was carried out in absence of ascorbate. The TIC (Figure 2.15) only shows peaks corresponding to PBN and benzaldehyde oxime peak. This demonstrates that ascorbate does indeed play a significant role in generating sufficient levels of hydroxyl radicals for "trapping" by PBN (on the benzene ring) see section 2.8.1.1.

Chapter 3

Analysis of spin trapped hydroxymethyl radical from methanol

3.1 Introduction

Methanol is an industrial solvent which is used as a chemical intermediate for the production of various chemical compounds like formaldehyde and glycol ethers. It is also a denaturation product of ethanol. Reports suggest acute exposure to methanol causes toxicity in humans. Routes of methanol exposures are by inhalation, ingestion and through skin. On absorption methanol is metabolized by alcohol dehydrogenase to toxic metabolites. Fishbein et al. demonstrated oxidation of methanol in the hepatic microsomal mixed-function oxidase system. Skrzydlewska et al. (2000) reported that lipid peroxidation and protein oxidation can occurred due to methanol intoxication (Skrzydlewska et al. 2000). This was confirmed from the ESR studies which showed a significant increase in liver extracts from poisoned animals, of a g=2.003 signal attributed to the free radicals (in general) among others semiquinones**.** Further studies (Albano et al. 1988) showed that alcohol (e.g. ethanol) on oxidation produces free radical intermediates which were trapped and detected by ESR spin trapping. Mason et al. also showed *in vivo* trapping of methanol metabolite ($^{\bullet}CH_2OH$) by α-(4-pyridyl 1-oxide)-N-*tert*-butylnitrone (POBN) spin trap to form POBN/$^{\bullet}CH_2OH$ adducts which was detected and identified by ESR (Kadiiska & Mason 2000). The kinetics reaction of the hydroxyl radical with methanol has been studied and showed that H-atom abstraction takes place primarily at the methyl site of methanol (Jimenez et al. 2003).

The other methods for detection of hydroxymethyl radical are extraction of PBN radical adducts from the Fenton reaction. The organic phase was evaporated under N_2 and then derivatized by trimethylsilylation and analysed by GC/MS (Castro et al. 1997). The PBN radical adducts can also be derivatized by (trimethylsilyl)trifluoracetamide (BSTFA)

(Diaz Gomez et al. 2000). Hydroxymethyl radical was also generated in FAD-NADPH model system (Castro et al. 2002). The generation of hydroxymethyl radical was confirmed when reaction mixture from the system was extracted with toluene and the organic phase was dried. The residue was silylated with BSTFA:acetonitrile (1:1) and analysed by GC/MS (Diaz Gomez et al. 2000, Castro et al. 2002). The other techniques which can be used to detect the hydroxymethyl radical is by ^{19}F-NMR, however, in this technique specific spin trap having fluorine in the structure such as 4-hydroxy-5,5-dimethyl-2-trifluoromethylpyrroline-1-oxide (F-DMPO) is required. The adducts formed FDMPO/CH_2OH were extremely stable to degradation and the ^{19}F-NMR showed -74.6 and -76.75 ppm. However, a potential disadvantage is the reduced sensitivity (by 1000 folds or more) compared to the ESR and GC/MS (Khramtsov et al. 2001).

A different approach has been developed where PBN trapped radical generated from methanol to form PBN-hydroxylmethyl adducts in the Fenton reaction which was methylated from methyl radical generated from DMSO in the same Fenton reaction. These adducts were extracted by using headspace solid-phase microextraction techniques (HS-SPME) and analysed by GC/MS. To our best knowledge there have been no reports on spin trapping hydroxymethyl radical in presence of methyl radical by PBN and there extraction and analysis by HS-SPME/GC/MS.

3.2 Spin trapping of radical from methanol

Trapping of methanol radicals was carried out by the Fenton type chemistry as mentioned in chapter 2 and the reaction mixture was extracted into chloroform and analysed by GC/MS. The chromatograms obtained for PBN and 4-FPBN are shown below.

3.2.1 PBN

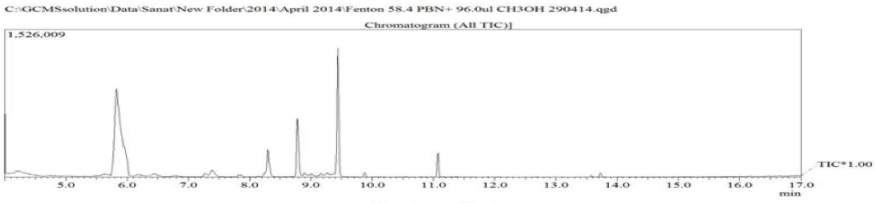

Figure 3.1: GC-EIMS total ion chromatogram (TIC) obtained from the "Fenton" reaction mixture which includes PBN and methanol (see materials and methods for details).

The GC-EIMS TIC (Figure 3.1) shows a peak corresponding to benzaldehyde oxime (8.3-8.8 minutes), unreacted PBN at 9.4 minutes (identified in section 2.7.1), PBN-OH at 11.0 minutes (identified in section 2.8.1.1). The mass spectrum for peak at 6.0 minutes shows molecular ion at m/z 161 and is believed to correspond to a compound derived from PBN by loss of the oxygen atom from the nitroxide group (PBN-O). This compound may be formed during the reaction or possibly when the mixture was injected into the GC. Nitroxides are known to easily lose the nitroxide oxygen on heating (Mistry et al. 2008). The remaining peaks are believed to derive from the trapping of methanol radicals. .

3.2.2 4-FPBN

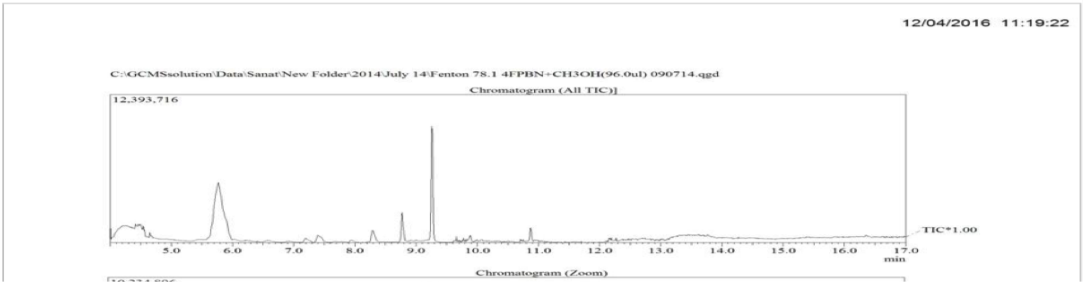

Figure 3.2: GC-EIMS total ion chromatogram (TIC) obtained from the "Fenton" reaction mixture which includes 4-FPBN and methanol (see materials and methods for details).

3. Analysis of spin trapped hydroxymethyl radical from methanol

The GC-EIMS TIC (Figure 3.2) shows a peak corresponding to 4-Fluorobenzaldehyde oxime (8.3-8.8 minutes), unreacted 4-FPBN at 9.25 minutes (identified in section 2.7.3) and 4-FPBN-OH adducts at 11.0 minutes (identified in section 2.8.1.1). The peak at 5.75 minutes is believed to be a compound derived from the spin trap which has lost the oxygen atom from the nitroxide group. The remaining peaks in the mass spectrum are believed to derive from the trapping of methanol radicals, however, in order to help identify these adducts a series of experiments were conducted involving the use of mixtures of methanol and DMSO.

3.3 Spin trapping of radicals from a mixture of methanol and DMSO

3.3.1 Chromatogram

Chromatogram obtained from analysis of Fenton reaction containing methanol and DMSO (3:1 by molar ratio) with different PBN derivatives is shown below.

3.3.1.1 PBN

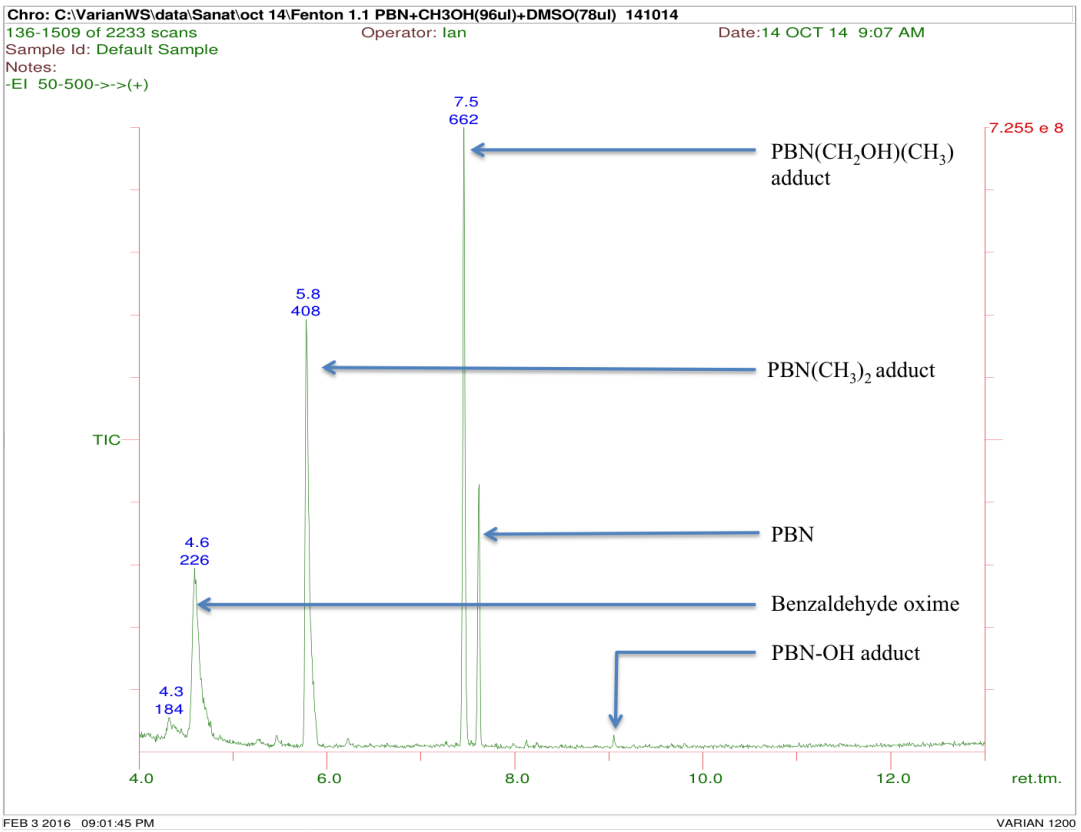

Figure 3.3: Total ion chromatogram (TIC) obtained from the analysis of the reaction mixture between PBN, methanol and DMSO in Fenton reaction.

TIC (Figure 3.3) shows a benzaldehyde oxime peak (4.3-4.6 minutes), PBN dimethyl adducts (5.8 minutes, section 3.3.3.1), PBN $(CH_2OH)(CH_3)$ adducts (7.5 minutes, section 3.3.2.1), unreacted PBN (7.6 minutes, section 2.7.1) and PBN-OH adducts (9.1 minutes, section 2.8.1.1).

3.3.1.2 Deuterated PBN-d_6

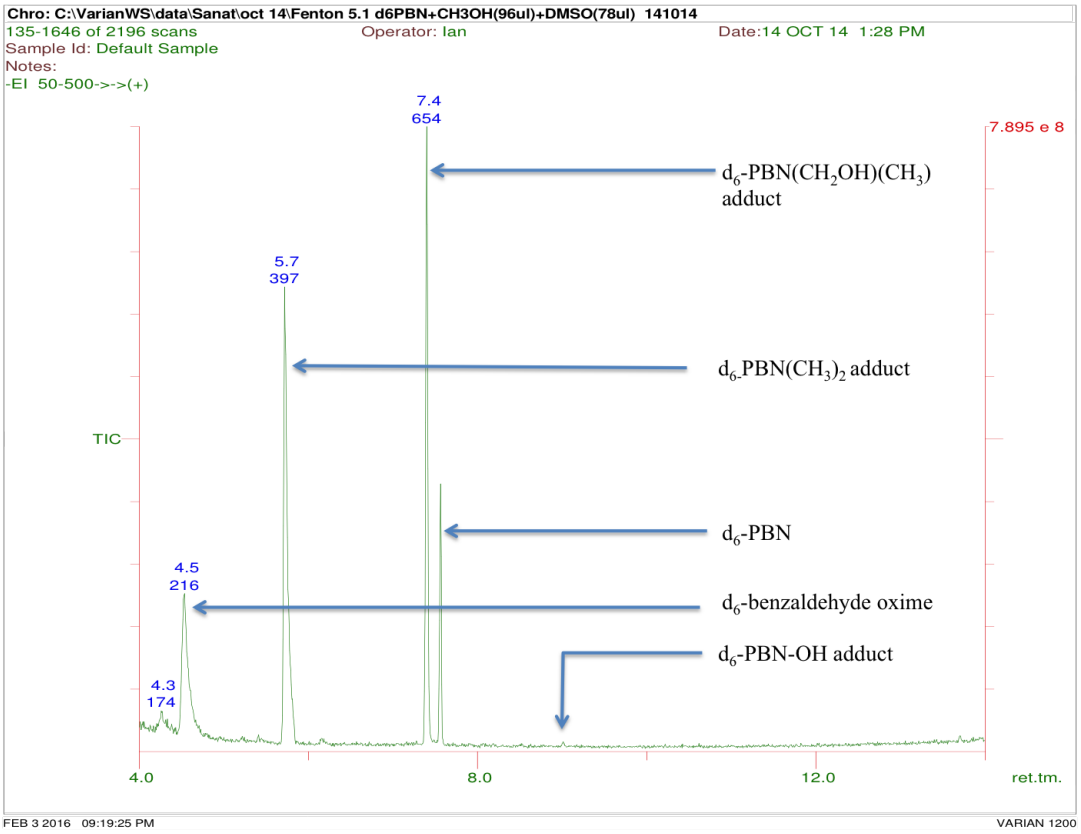

Figure 3.4: Total ion chromatogram (TIC) obtained from the analysis of the reaction mixture between PBN-d_6, methanol and DMSO in Fenton reaction.

TIC (Figure 3.4) shows a benzaldehyde-d_6 oxime peak (4.3-4.5 minutes), PBN-d_6 dimethyl adducts (5.7 minutes, section 3.3.3.2), PBN-d_6 (CH_2OH)(CH_3) adducts (7.4 minutes, section 3.3.2.2), unreacted PBN-d_6 (7.6 minutes, section 2.7.2) and PBN-d_6OH adducts (9.0 minutes, section 2.8.1.1).

3.3.1.3 4-FPBN

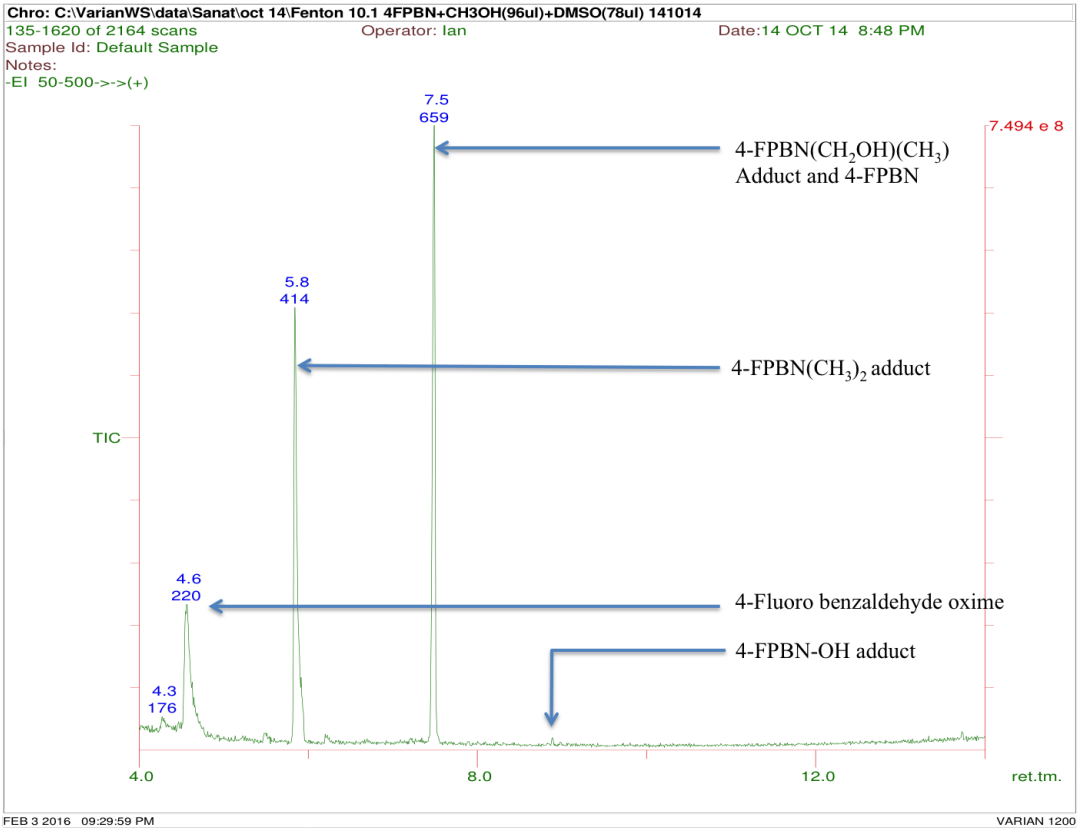

Figure 3.5: Total ion chromatogram (TIC) obtained from the analysis of the reaction mixture between 4-FPBN, methanol and DMSO in Fenton reaction.

TIC (Figure 3.5) shows a 4-Fluorobenzaldehyde oxime peak (4.3-4.6 minutes), 4-FPBN dimethyl adducts (5.8 minutes, section 3.3.3.3) and 4-FPBN-OH adducts (9.0 minutes, section 2.8.1.1). The unreacted 4-FPBN peak (section 2.7.3) and the 4-FPBN $(CH_2OH)(CH_3)$ adducts peak (section 3.3.2.3) is overlapping at 7.5 minutes.

3.3.1.4 4-ClPBN

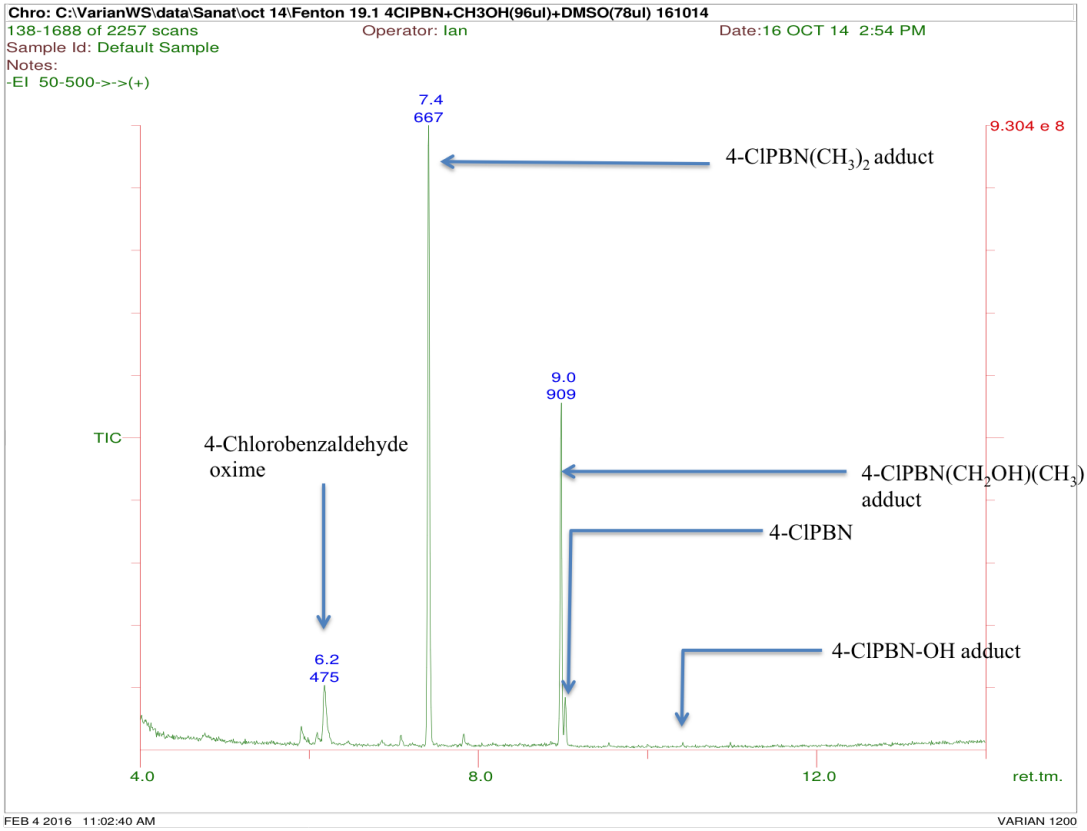

Figure 3.6: Total ion chromatogram (TIC) obtained from the analysis of the reaction mixture between 4-ClPBN, methanol and DMSO in Fenton reaction.

TIC (Figure 3.6) shows a 4-Chlorobenzaldehyde oxime peak (5.9-6.2 minutes), 4-ClPBN dimethyl adducts (7.4 minutes, section 3.3.3.4), 4-ClPBN (CH_2OH)(CH_3) adducts (9.0 minutes, section 3.3.2.4), unreacted 4-ClPBN (9.0 minutes, section 2.7.4) and 4-ClPBN-OH adducts (10.4 minutes, section 2.8.1.1).

3.3.2 Hydroxymethyl(CH_2OH)-methyl(CH_3) adduct mass spectra for different PBN derivatives

3.3.2.1 PBN(CH_2OH)(CH_3) adduct

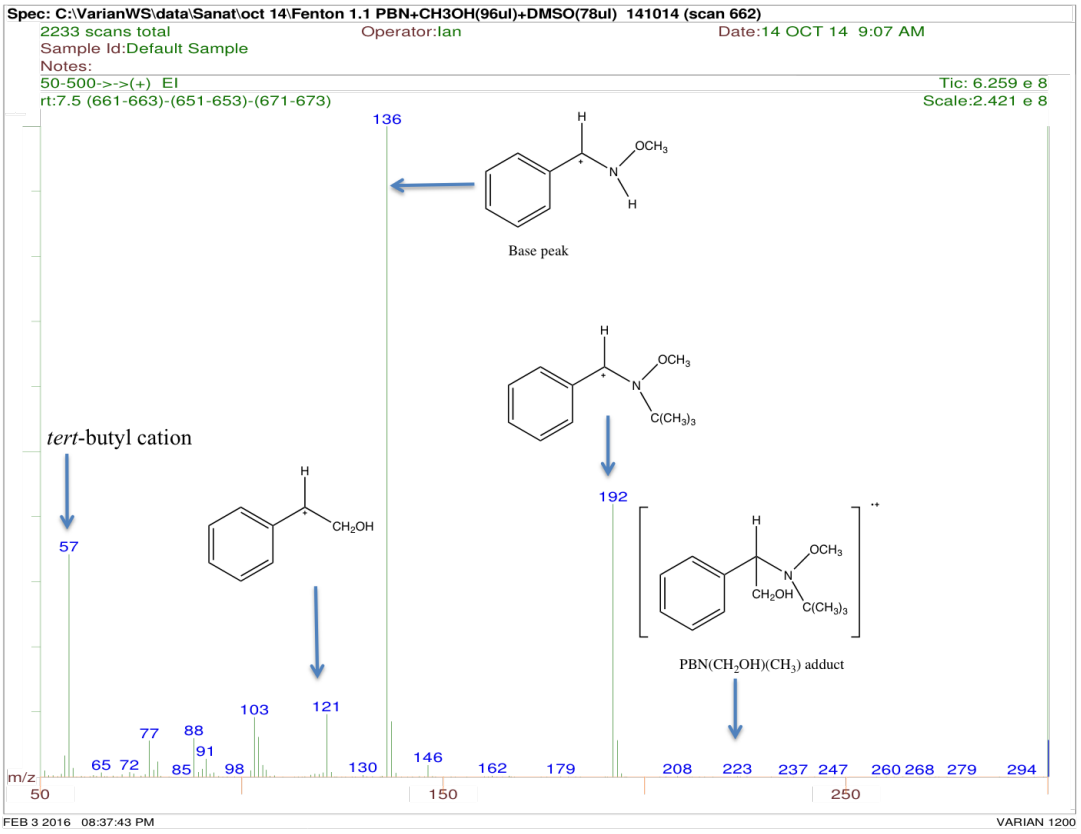

Figure 3.7: Mass spectrum for PBN(CH_2OH)(CH_3) adducts retained at 7.5 minutes (from chromatogram in Figure 3.3).

The mass spectrum (Figure 3.7) corresponds to the peak retained at 7.5 minutes in GC chromatogram (Figure 3.3). The mass spectrum shows weak molecular ion at m/z 223. The fragmentation pattern (Figure 3.8) shows a fragment at m/z 208 (M-15) loss of methyl from $M^{\bullet+}$, m/z 192 (M-31) is loss of a hydroxymethyl radical from $M^{\bullet+}$. Base peak at m/z 136 is for cation shown in Figure 3.7 formed due to loss of 2-methyl-1-propene from m/z 192. Fragment at m/z 121 is due to C_6H_5-$^+$CH-CH_2OH cation, m/z 91 is for the tropylium cation, m/z 77 is for phenyl cation and m/z 57 is for the *tert*-butyl cation.

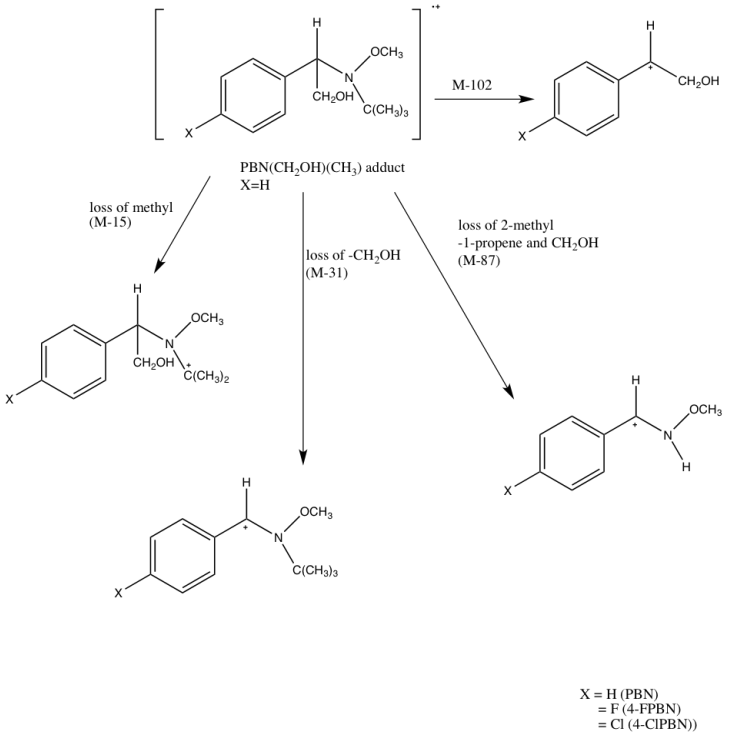

Figure 3.8: Fragmentation pattern for X-PBN(CH_2OH)(CH_3) molecular ion.

3.3.2.2 PBN-$d_6(CH_2OH)(CH_3)$ adduct

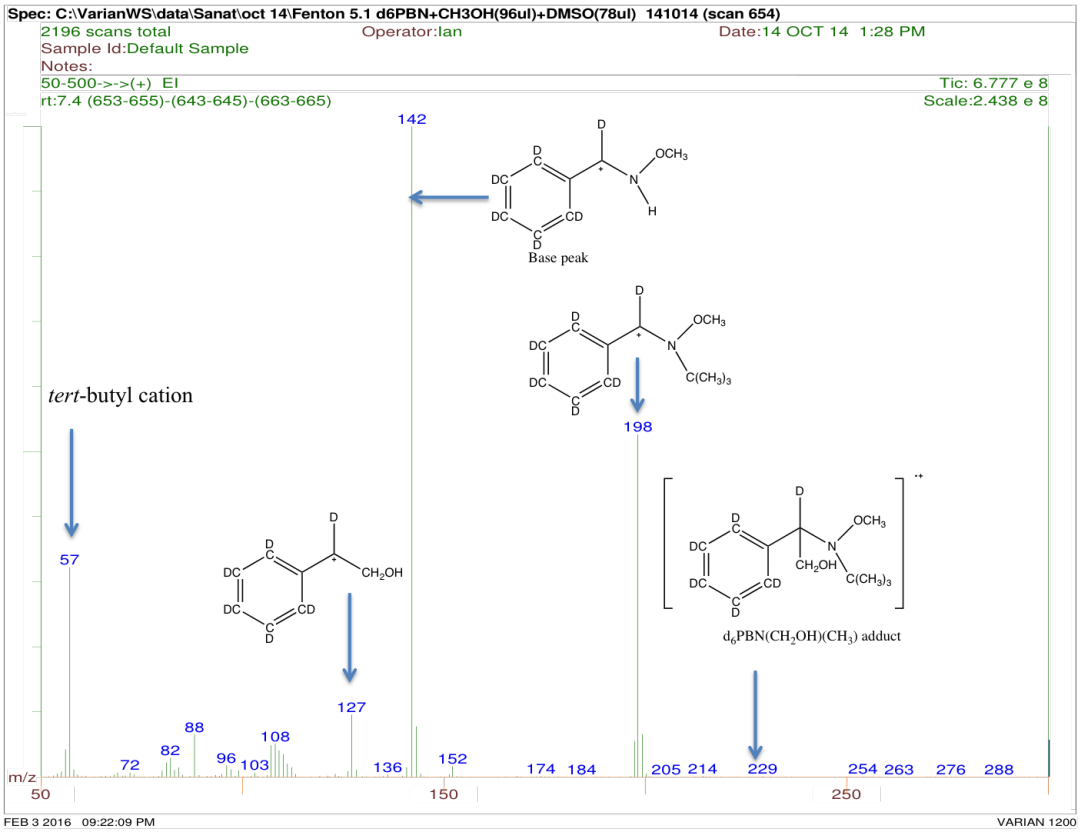

Figure 3.9: Mass spectrum for PBN-$d_6(CH_2OH)(CH_3)$ adduct retained at 7.4 minutes (from chromatogram in Figure 3.4).

The mass spectrum (Figure 3.9) corresponds to the peak retained at 7.4 minutes in GC chromatogram (Figure 3.4). The mass spectrum shows weak molecular ion at m/z 229 for PBN-$d_6(CH_2OH)(CH_3)$ adducts. The fragmentation pattern (Figure 3.8) shows a fragment at m/z 214 (M-15) loss of methyl from $M^{\bullet+}$, m/z 198 (M-31) is loss of a hydroxymethyl radical from $M^{\bullet+}$. Base peak at m/z 142 is for cation (Figure 3.9) formed due to loss of 2-methyl-1-propene from m/z 198. Fragment at m/z 127 is for C_6D_5-$^+$CD-CH_2OH cation, m/z 96 is for the $d_5$tropylium cation ($C_7D_5H_2^+$), m/z 82 is for $C_6D_5^+$ and m/z 57 is for the *tert*-butyl cation.

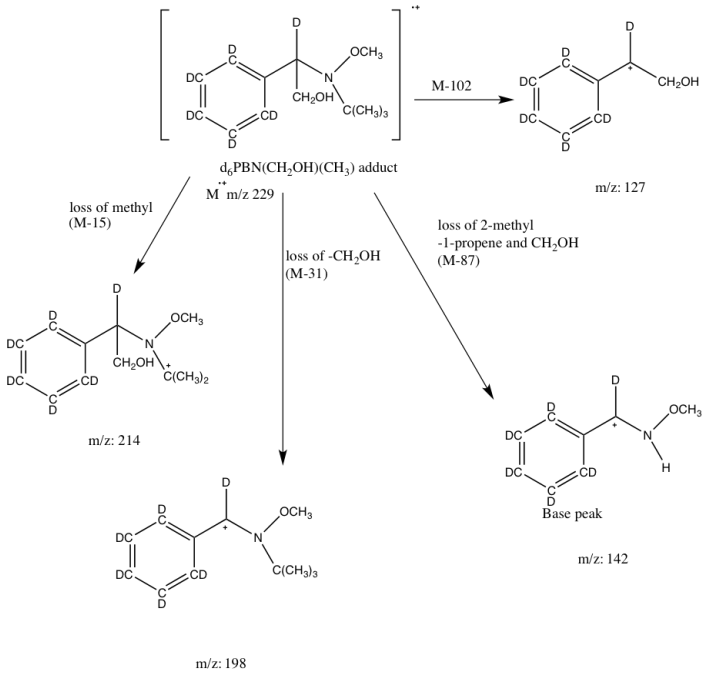

Figure 3.10: Fragmentation pattern for PBN-d_6(CH_2OH)(CH_3) molecular ion.

3.3.2.3 4-FPBN(CH_2OH)(CH_3) adduct

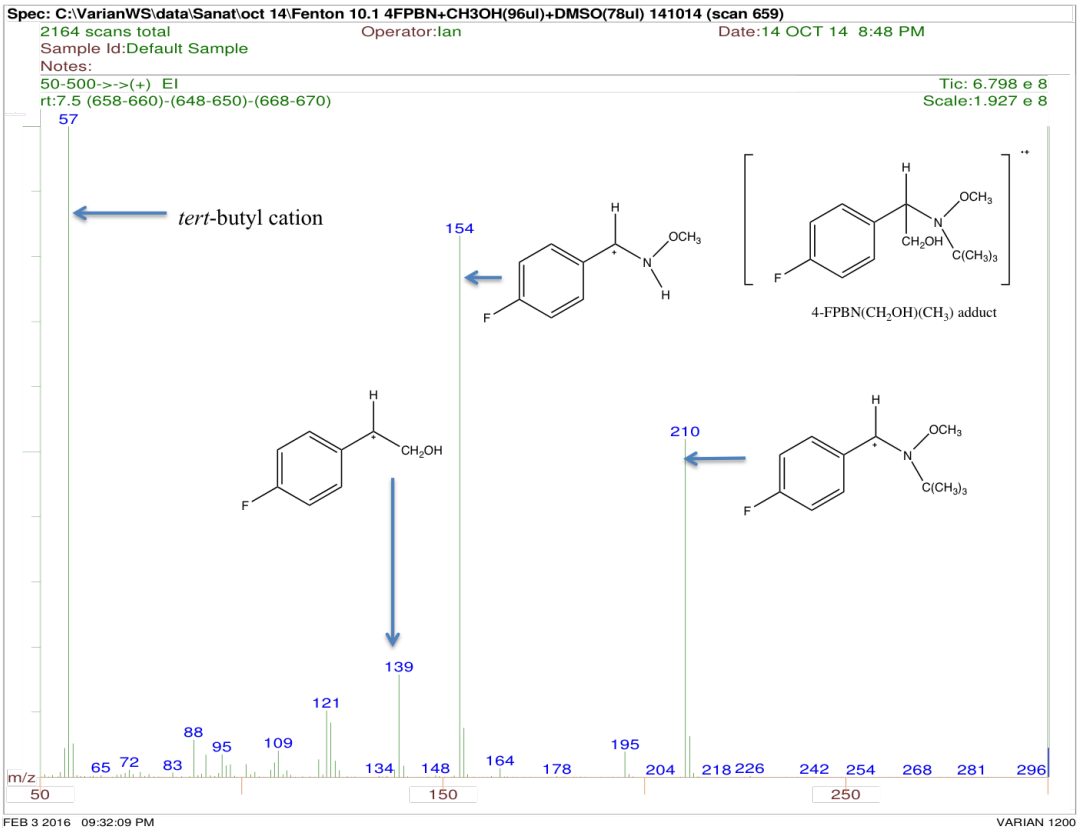

Figure 3.11: Mass spectrum for 4-FPBN(CH_2OH)(CH_3) adduct retained at 7.5 minutes (from chromatogram in Figure 3.5).

The mass spectrum (Figure 3.11) corresponds to the peak retained at 7.5 minutes in GC chromatogram (Figure 3.5). The mass spectrum doesn't show a molecular ion at m/z 241, addition of hydroxymethyl radical from methanol and methyl radical from DMSO to 4-FPBN forming 4-FPBN(CH_2OH)(CH_3) adducts as expected. However, the fragmentation shows a similar fragment pattern for PBN(CH_2OH)(CH_3) adducts (Figure 3.8) with expected mass difference due to the presence of fluorine at para position. The fragmentation pattern shows a fragment at m/z 226 (M-15) loss of methyl from $M^{\bullet+}$, m/z 210 (M-31) is loss of a hydroxymethyl radical from $M^{\bullet+}$, fragment at m/z 154 is for cation shown in Figure 3.11 formed due to loss of 2-methyl-1-propene from m/z 210. Fragment at m/z 139 is due to 4-FC_6H_4-$^{+}$CH-CH_2OH cation (shown in Figure 3.11), m/z 109 is for the 4-Fluoro tropylium cation, m/z 95 is for 4-$FC_6H_4^{+}$ and base peak at m/z 57 is for the *tert*-butyl cation.

3.3.2.4 4-ClPBN(CH_2OH)(CH_3) adduct

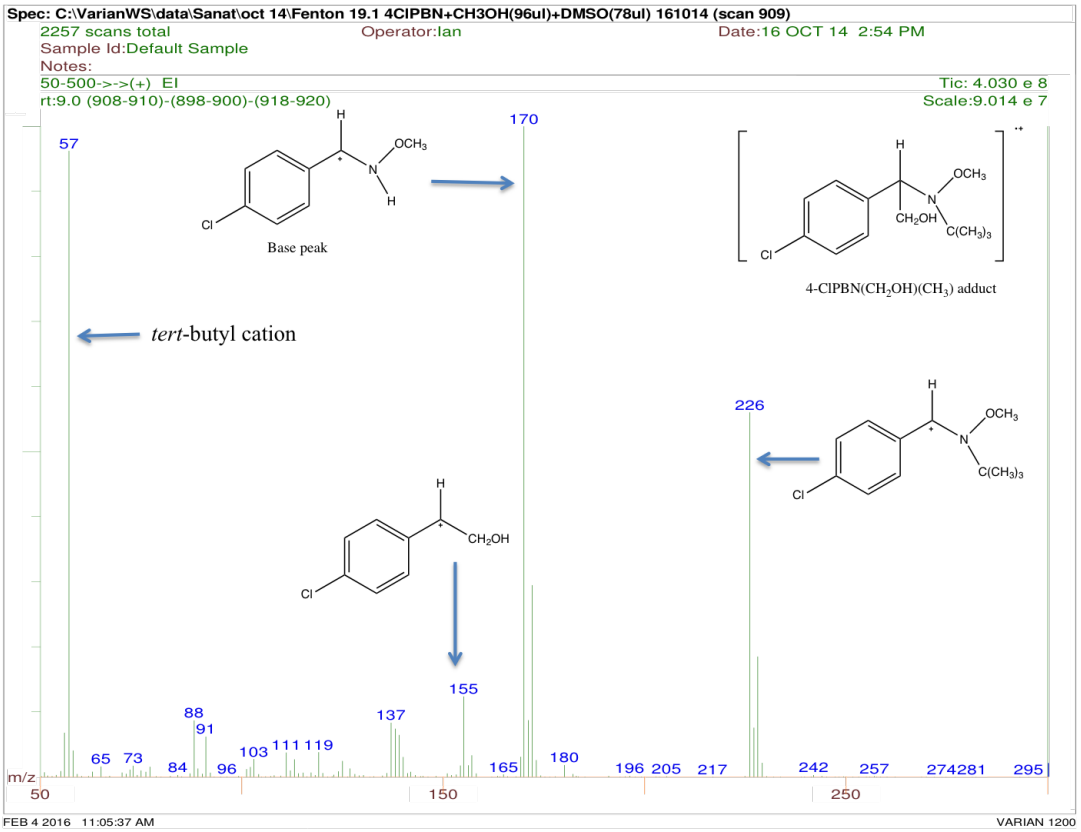

Figure 3.12: Mass spectrum for 4-ClPBN(CH_2OH)(CH_3) adduct retained at 9.0 minutes (from chromatogram in Figure 3.6).

The mass spectrum (Figure 3.12) corresponds to the peak retained at 9.0 minutes in GC chromatogram (Figure 3.6). The mass spectrum shows a weak molecular ion for 4-ClPBN(CH_2OH)(CH_3) adducts at m/z 257/259. The fragmentation shows a similar fragment pattern for PBN(CH_2OH)(CH_3) adducts (Figure 3.8). Fragments at m/z 242/244 (M-15) loss of methyl from $M^{\bullet+}$, m/z 226/228 (M-31) is loss of a hydroxymethyl radical from $M^{\bullet+}$. Base peak fragment at m/z 170 is for cation shown in Figure 3.12 formed due to loss of 2-methyl-1-propene from m/z 226. Fragment at m/z 155 is due to 4-ClC_6H_4-$^+$CH-CH_2OH cation (shown in Figure 3.12), m/z 111 is for 4-$ClC_6H_4^+$ and m/z 57 is for the *tert*-butyl cation.

3.3.3 Dimethyl adduct mass spectra for different PBN derivatives

3.3.3.1 PBN$(CH_3)_2$ adduct

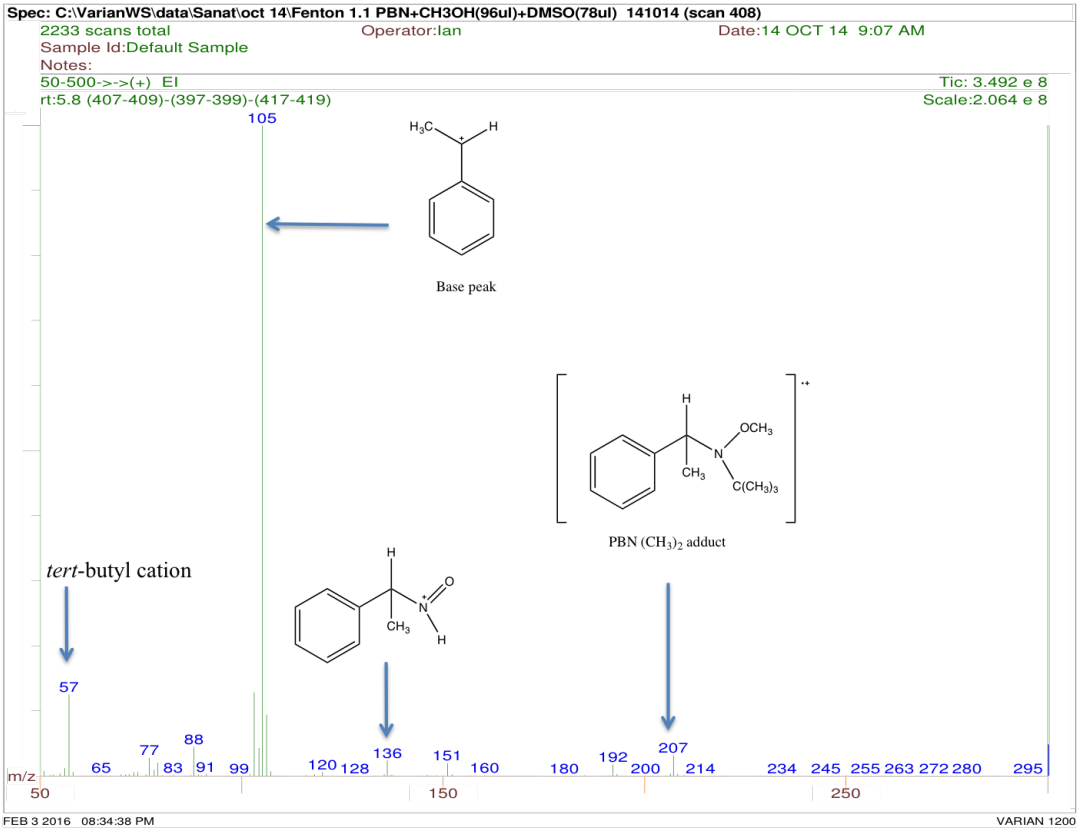

Figure 3.13: Electron ionization (EI) mass spectrum of peak at 5.8 minutes corresponding to PBN$(CH_3)_2$ (from chromatogram in Figure 3.1).

The EI mass spectrum in Figure 3.13 corresponds to the PBN dimethyl adducts (PBN $(CH_3)_2$). The mass spectrum shows a weak molecular ion at m/z 207. The fragment at m/z 192 is due to the loss of a methyl radical (M-15) and m/z 151 is due to the loss of 2-methyl-1-propene (M-56), both from the molecular ion. The fragment at m/z 136 could be due to loss of a methyl radical from the ion at m/z 151. The base peak at m/z 105 corresponds to the cation shown in Figure 3.13, resulting from dissociation of the molecular ion between the C-N bond. The fragment at m/z 77 is for the phenyl cation ($C_6H_5^+$) and m/z 57 is for the *tert*-butyl cation. The fragmentation pattern is showed in Figure 3.14.

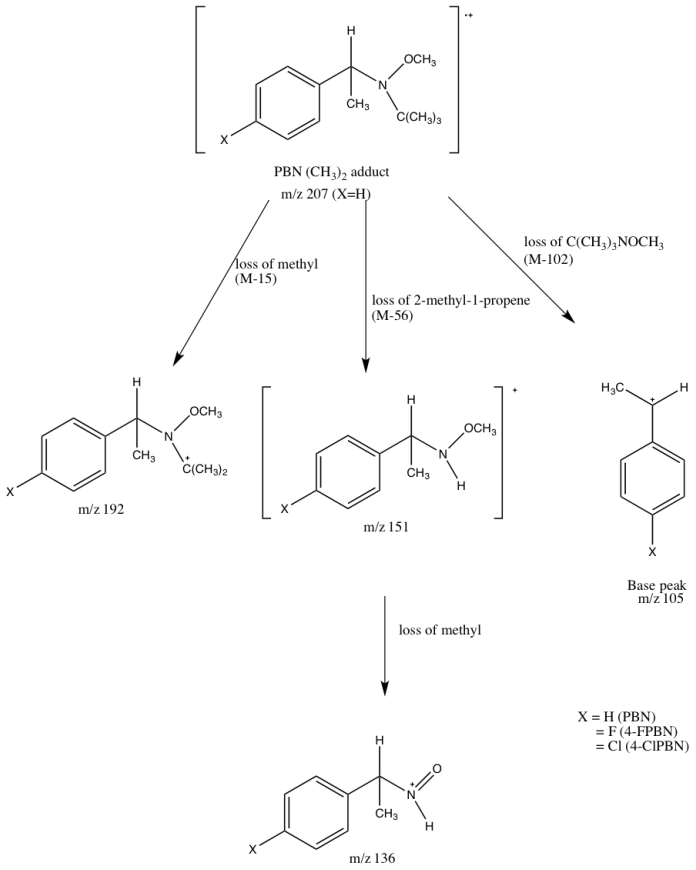

Figure 3.14: Scheme showing possible fragmentation pattern for PBN dimethyl derivatives generated by EI mass spectrometry.

3.3.3.2 Deuterated-PBN$(CH_3)_2$ adduct

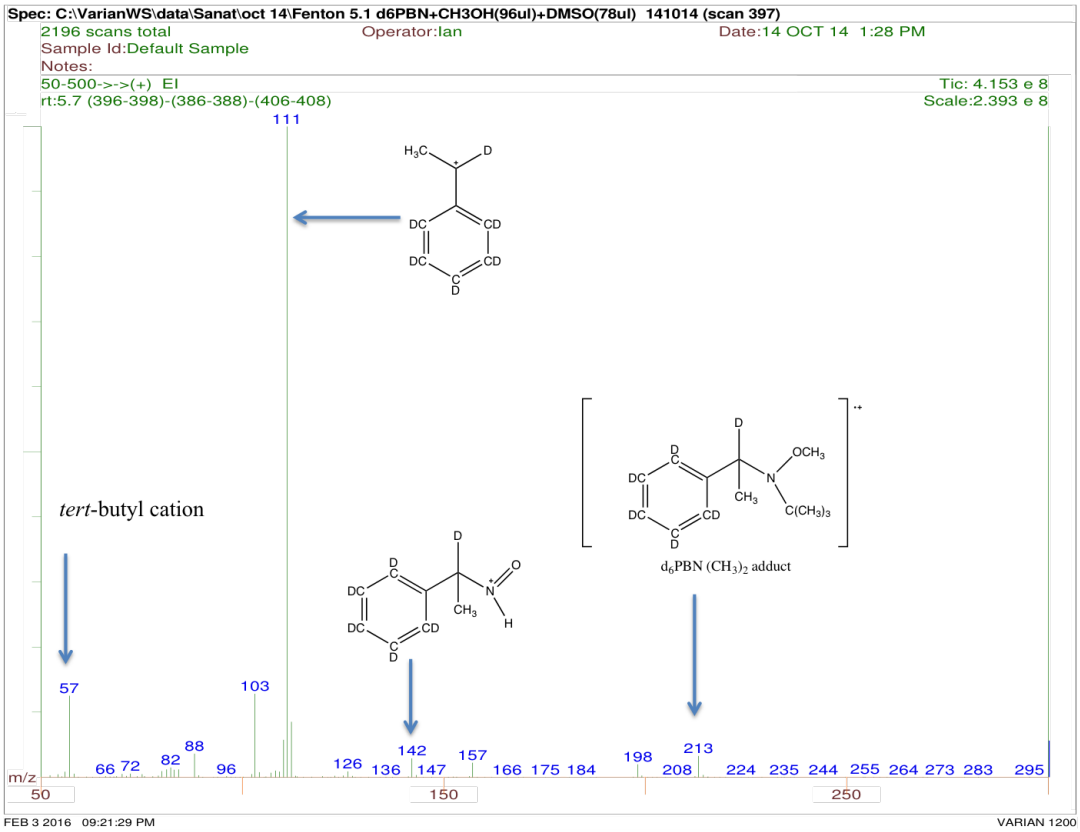

Figure 3.15: Electron ionization (EI) mass spectrum of peak at 5.7 minutes (from chromatogram in Figure 3.4) corresponding to PBN-d_6 dimethyl adduct.

The EI mass spectrum in Figure 3.15 is for the peak with retention time 5.7 minutes in GC chromatogram (Figure 3.4) with a molecular ion m/z 213. Fragment at m/z 198 is due to the loss of methyl from molecular ion. Fragment at m/z 157 is due to the loss of 2-methyl-1-propene (M-56) from a molecular ion. Fragment at m/z 142 is likely to be loss of a methyl radical from the ion at m/z 157. The base peak at m/z 111 corresponds to dissociation of the molecular ion at the C-N bond as shown in Figure 3.16, m/z 82 and 57 correspond to the deuterated phenyl cation and the *tert*-butyl cation.

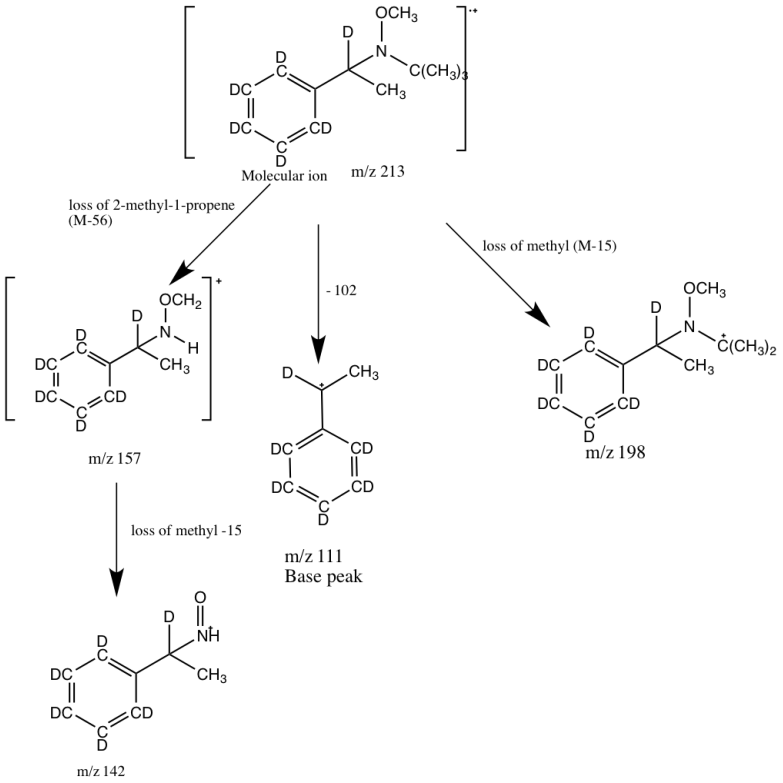

Figure 3.16: Scheme showing possible fragmentation pattern for PBN-d_6 dimethyl derivatives generated by EI mass spectrometry.

3.3.3.3 4-FPBN(CH_3)$_2$ adduct

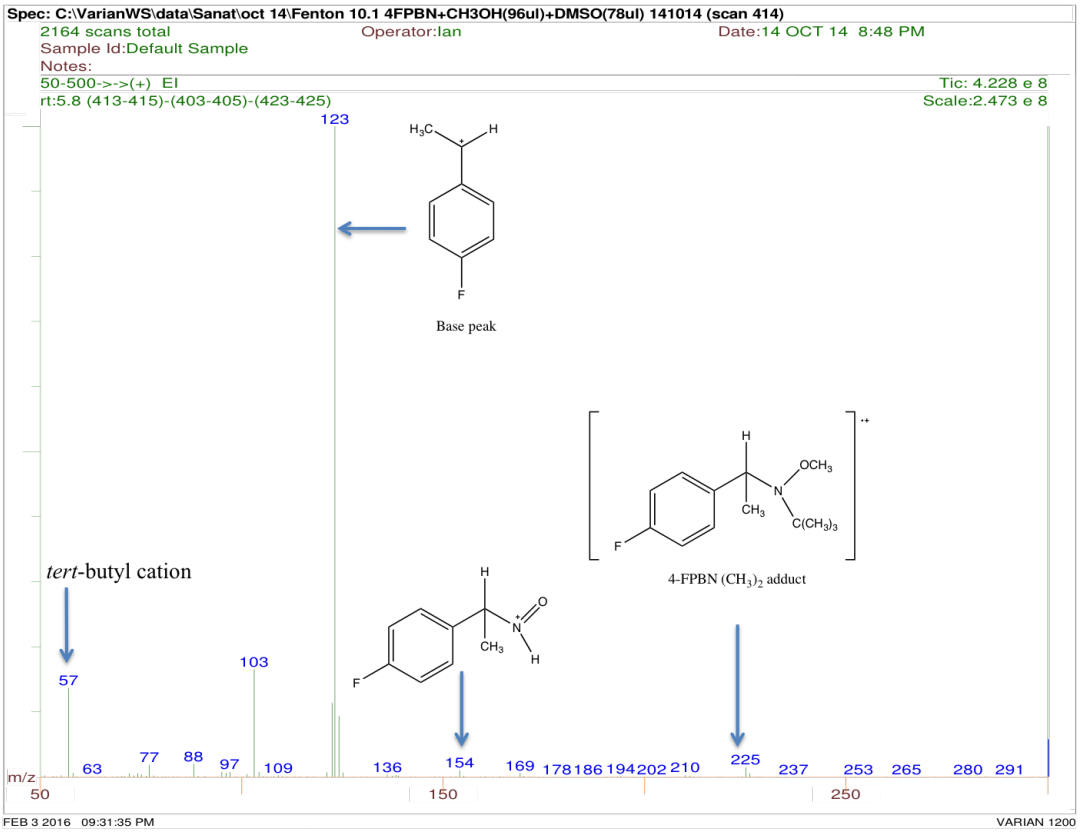

Figure 3.17: Electron ionization (EI) mass spectrum of peak at 5.8 minutes (from the chromatogram in Figure 3.5) corresponding to the 4-FPBN dimethyl adduct.

The EI mass spectrum for peak with retention time 5.8 minutes (from the chromatogram in Figure 3.5) is shown in Figure 3.17. The mass spectrum shows a molecular ion at m/z 225. The fragment pattern is similar to that of the PBN dimethyl adducts with a peak at m/z 169 is due to the loss of 2-methyl-1-propene from $M^{+\bullet}$ (M-56). The base peak m/z 123 is due to the cation shown in Figure 3.17 and corresponds to dissociation of the molecular ion at the C-N bond. Other fragments are m/z 103 is due to loss of HF from the base peak, m/z 95 is for the 4-$FC_6H_4^+$ and m/z 57 is for the *tert*-butyl cation.

3.3.3.4 4-ClPBN$(CH_3)_2$ adduct

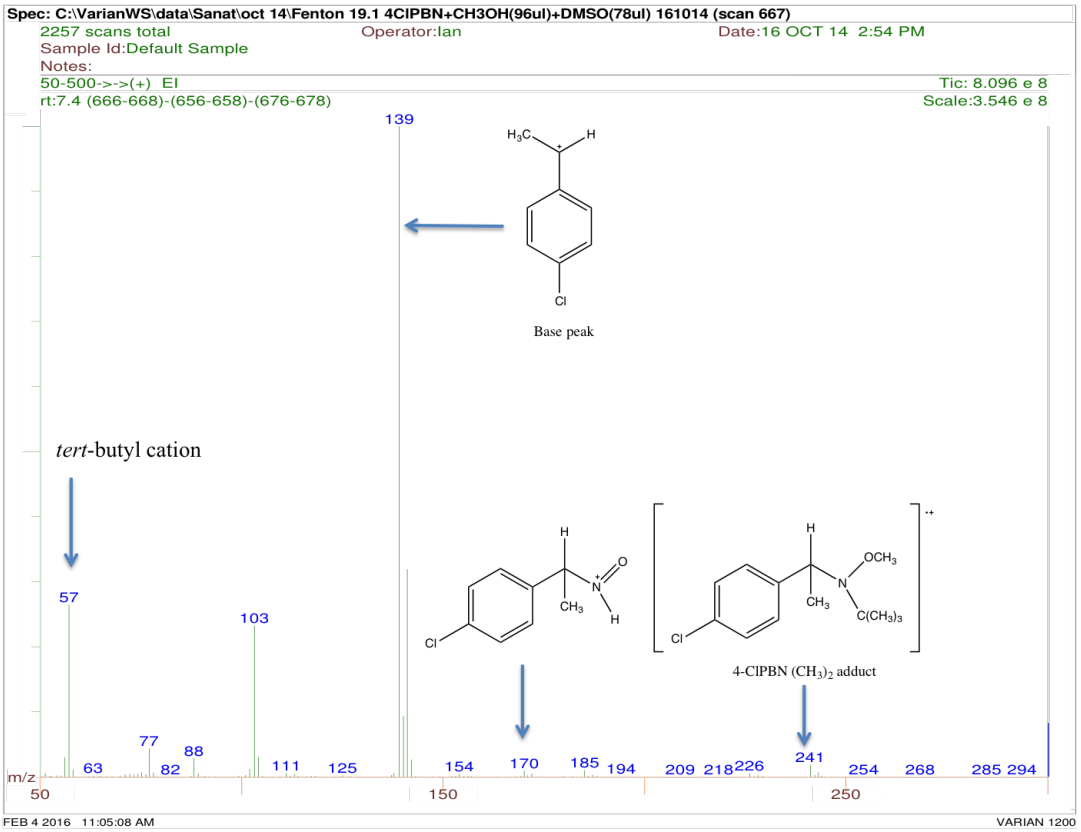

Figure 3.18: Electron ionization (EI) mass spectrum of peak at 7.4 minutes (from the chromatogram in Figure 3.6) corresponding to the 4-ClPBN dimethyl adduct.

The EI mass spectrum for peak with retention time 7.4 minutes (from the chromatogram in Figure 3.6) is shown in (Figure 3.18). The mass spectrum showed a weak molecular ion at m/z 241/243. Fragments at m/z 226 is due to the loss of methyl from a molecular ion, m/z 185 is due to the loss of 2-methyl-1-propene from $M^{+\bullet}$ (M-56). Fragment at m/z 170 is loss of methyl from the ion at m/z 185. The base peak at m/z 139/141 is for the cation shown in Figure 3.18 and corresponds to dissociation of the molecular ion at the C-N bond. Fragement at m/z 103 is due to the loss of HCl from the base peak, fragment at m/z 77 is for the phenyl cation and m/z 57 is for the *tert-butyl* cation.

3.4 Spin trapping of radicals from a mixture of deuterated methanol (CD_3OH) and DMSO

The experiments described in the previous section (3.3.2) were repeated using deuterated methanol (CD_3OH) and DMSO in order to confirm the interpretation of the EI mass spectra and the overall mechanism. The mass spectrum of dimethyl adducts and the OH adducts were identical and interpreted in section 3.3.3 and 2.8.1.1 respectively.

3.4.1 PBN(CD_2OH)(CH_3) adduct

The chromatogram and mass spectrum (Figures not shown) obtained from the Fenton reaction involving the deuterated methanol and DMSO showed PBN(CH_3)$_2$ adducts (5.8 minutes) with molecular ion m/z 207, PBN-CD_2OH-CH_3 adducts (7.4 minutes) and PBN-OH adducts (9.0 minutes) with molecular ion at m/z 193.

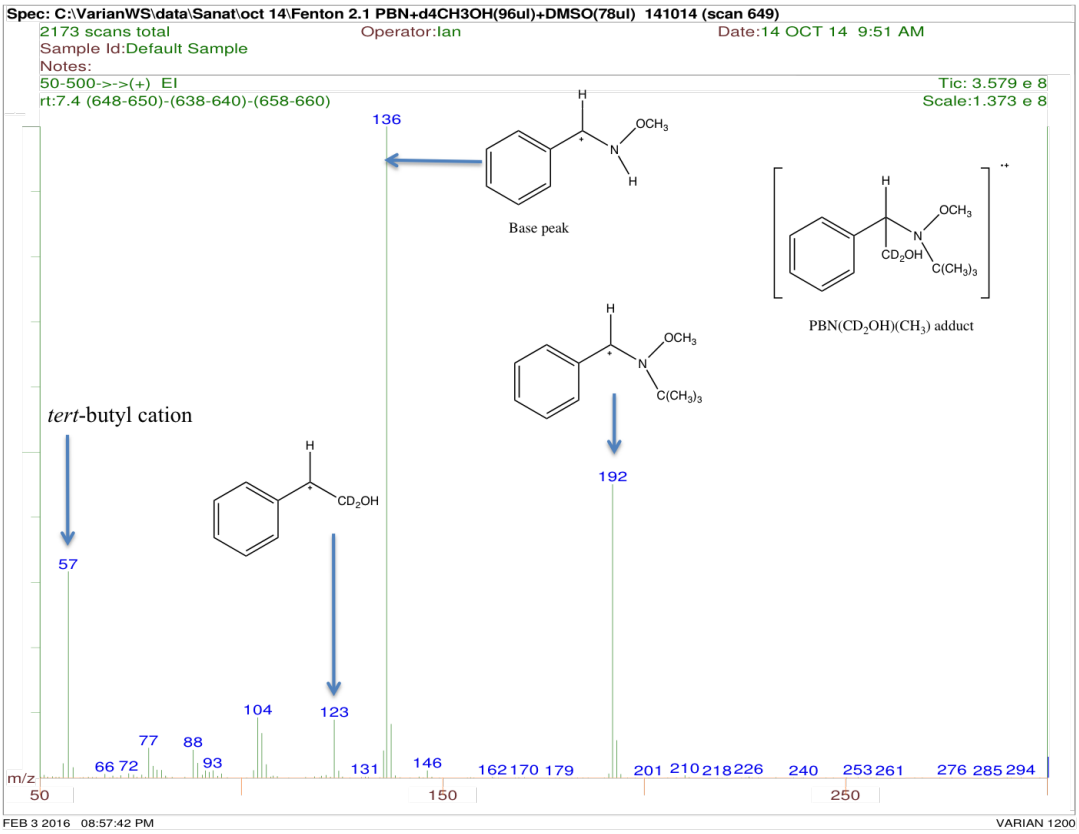

Figure 3.19: Mass spectrum for PBN(CD_2OH)(CH_3) adduct retained at 7.4 minutes.

The mass spectrum (Figure 3.19) corresponds to the peak retained at 7.4 minutes. The

mass spectrum doesn't show a molecular ion for the PBN(CD_2OH)(CH_3) (MW=225) adducts. However, the fragmentation pattern is exactly the same as shown in Figure 3.20 with expected mass difference due to the presence of deuterated methanol. The fragment pattern shows a fragment at m/z 210 (M-15) loss of methyl from $M^{\bullet+}$, m/z 192 (M-33) is due to loss of a $^{\bullet}CD_2OH$ radical from $M^{\bullet+}$. Base peak at m/z 136 is for cation shown in Figure 3.19 formed due to loss of 2-methyl-1-propene from m/z 192. Fragment at m/z 123 is due to C_6H_5-$^{+}$CH-CD_2OH cation, m/z 93 is for the $C_7H_5D_2^{+}$, m/z 77 is for phenyl cation and m/z 57 is for the *tert*-butyl cation.

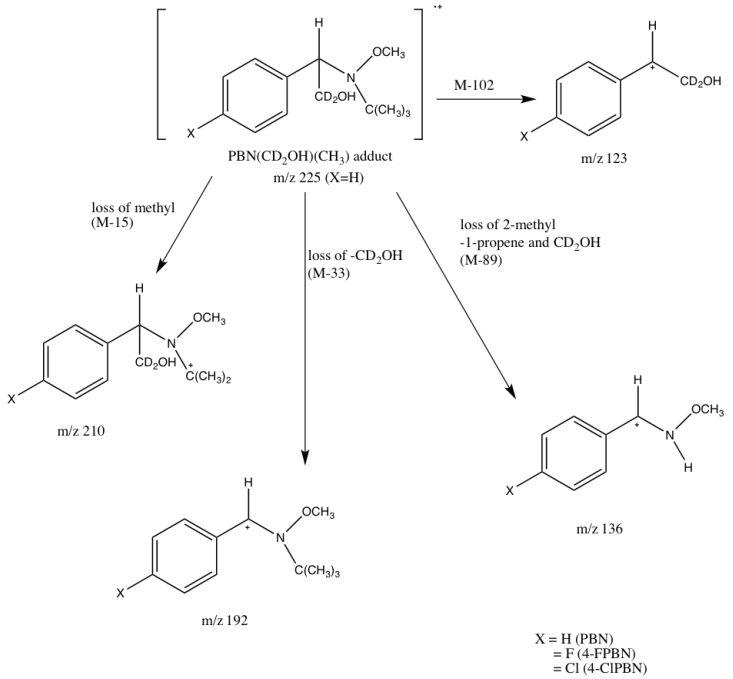

Figure 3.20: Fragment pattern for X-PBN (CD_2OH)(CD_3) molecular ion.

3.4.2 PBN-d_6(CD_2OH)(CH_3) adduct

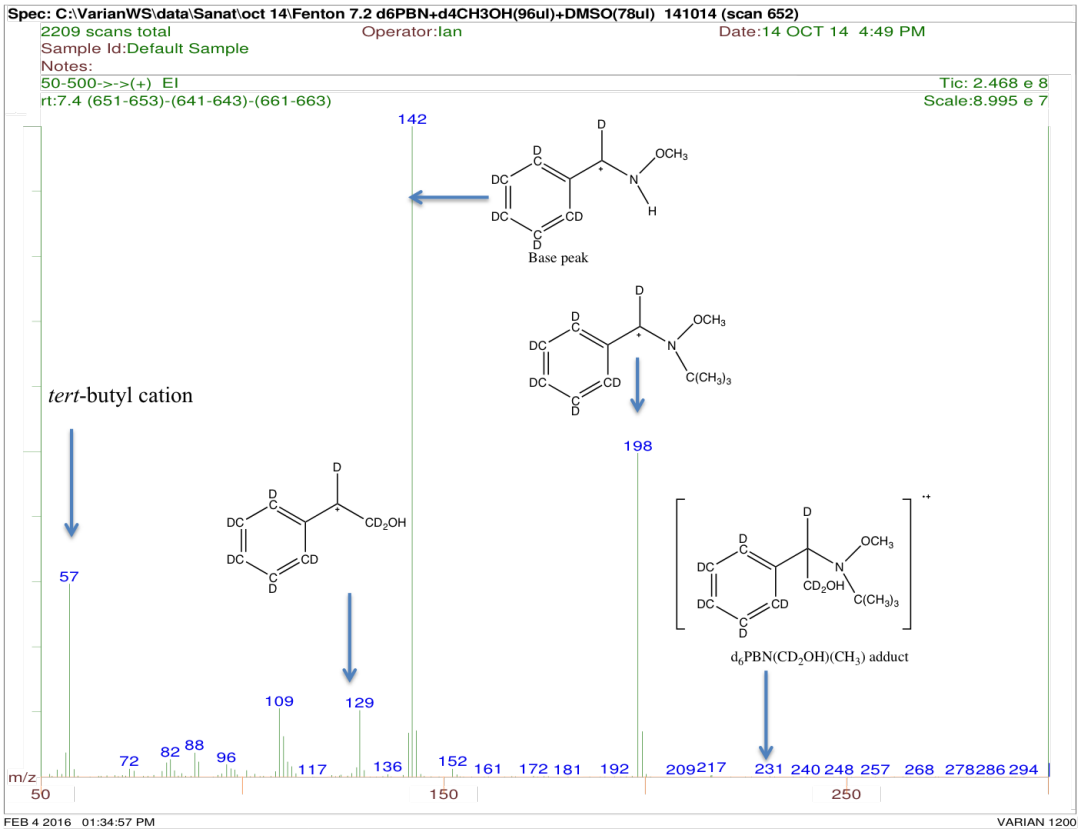

Figure 3.21: Mass spectrum for PBN-d_6(CD_2OH)(CH_3) adduct retained at 7.4 minutes.

The mass spectrum (Figure 3.21) corresponds to the peak retained at 7.4 minutes. The mass spectrum show a weak molecular ion for the PBN-d_6(CD_2OH)(CH_3) (MW=231) adducts. The fragmentation pattern is exact the same as shown in Figure 3.22 with expected mass difference due to the presence of deuterated methanol. The fragment pattern shows a fragment at m/z 198 (M-33) is due to loss of a $^{\bullet}CD_2OH$ radical from $M^{\bullet+}$. Base peak at m/z 142 is for cation shown in Figure 3.21 formed due to loss of 2-methyl-1-propene from m/z 198. Fragment at m/z 129 is due to C_6D_5-$^{+}$CD-CD_2OH cation, m/z 82 is for phenyl-d_6 cation and m/z 57 is for the *tert*-butyl cation.

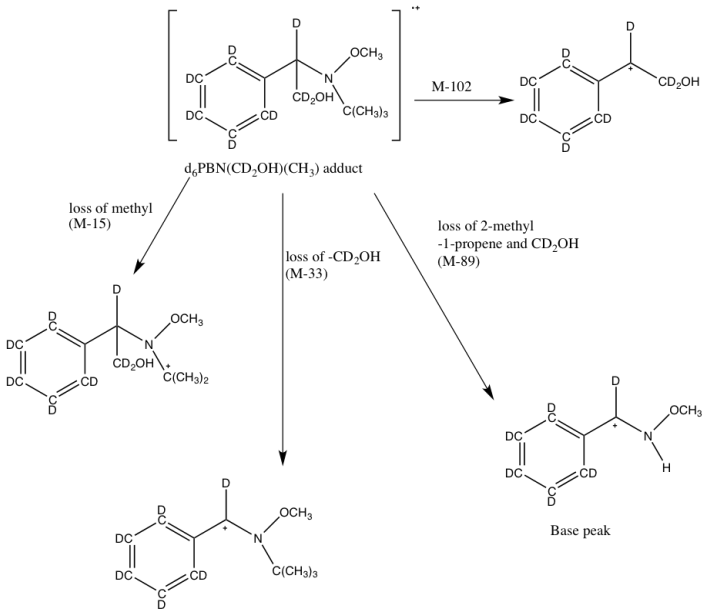

Figure 3.22: Fragment pattern for PBN-$d_6(CD_2OH)(CH_3)$ molecular ion.

3.4.3 4-FPBN(CD_2OH)(CH_3) adduct

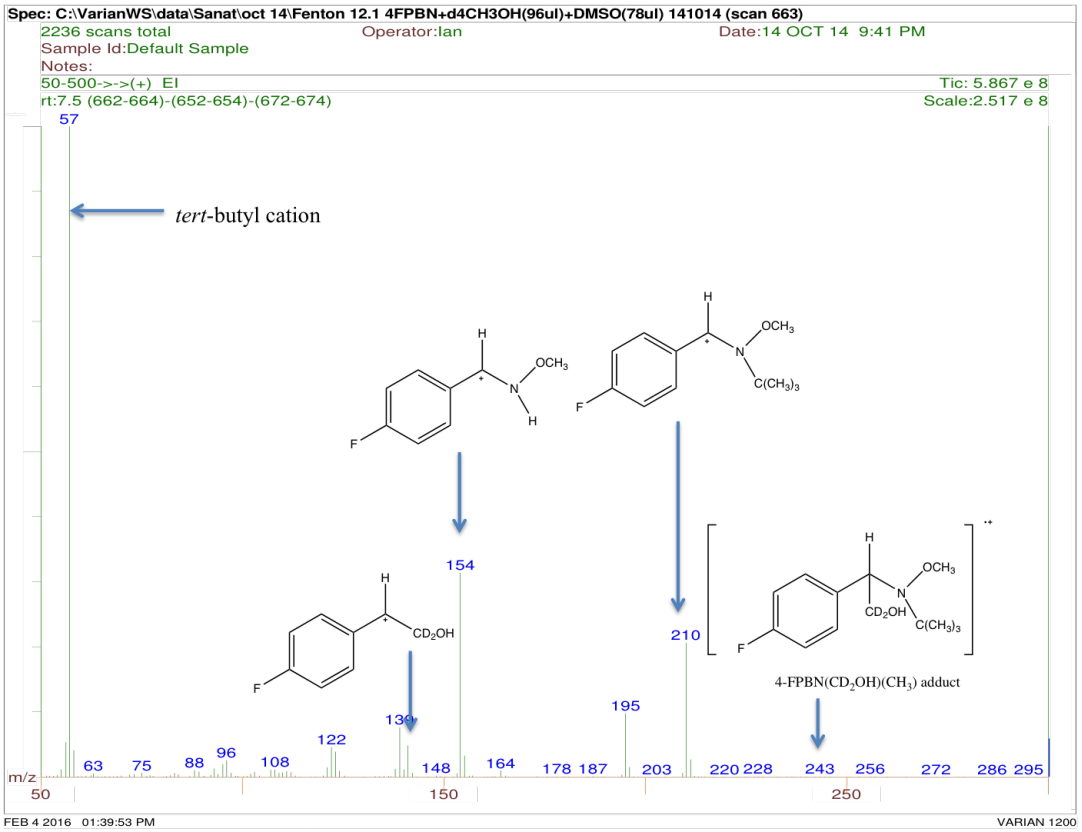

Figure 3.23: Mass spectrum for 4-FPBN(CD_2OH)(CH_3) adduct retained at 7.5 minutes.

The mass spectrum (Figure 3.23) corresponds to the peak retained at 7.5 minutes. The mass spectrum show a weak molecular ion for the 4-FPBN(CD_2OH)(CH_3) (MW=243) adducts. The mass spectrum shows a fragment at m/z 228 formed due to loss of methyl from the molecular ion, fragment at m/z 210 (M-33) is due to loss of $^{\bullet}CD_2OH$ radical from $M^{\bullet+}$, m/z 154 is for cation shown in Figure 3.23 formed due to loss of 2-methyl-1-propene from m/z 210. Fragment at m/z 141 is due to 4-FC_6H_4-^{+}CH-CD_2OH cation, m/z 95 is for 4-$FC_6H_4^{+}$ and base peak at m/z 57 is for the *tert*-butyl cation. The presence of m/z 195 and fragment at m/z 139 is from the 4-FPBN as the peak for unreacted 4-FPBN and 4-FPBN(CD_2OH)(CH_3) adducts are overlapping.

3.4.4 4-ClPBN(CD_2OH)(CH_3) adduct

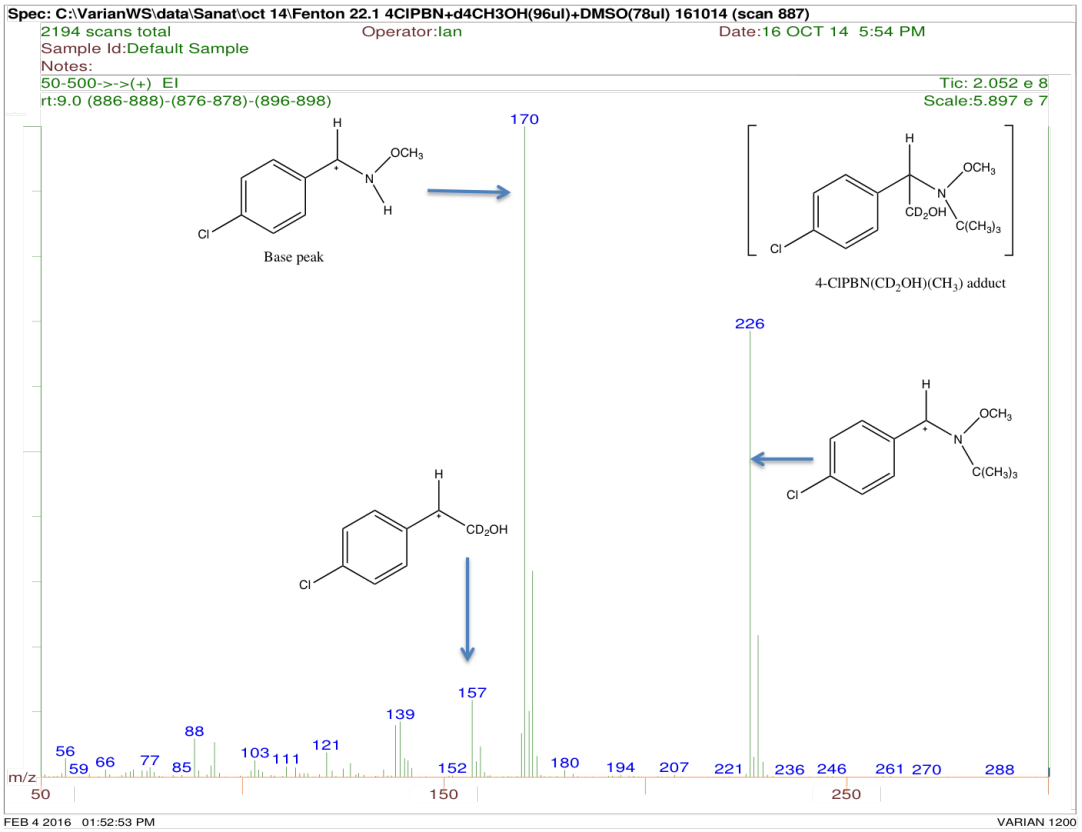

Figure 3.24: Mass spectrum for 4-ClPBN(CD_2OH)(CH_3) adduct retained at 9.0 minutes.

The mass spectrum (Figure 3.24) corresponds to the peak retained at 9.0 minutes. The mass spectrum doesn't show a molecular ion for the 4-ClPBN(CD_2OH)(CH_3) (MW=243) adducts, however, a weak fragment at m/z 261 is the isotope signal containing ^{37}Cl . The mass spectrum shows a fragment at m/z 246 formed due to loss of methyl from the isotope molecular ion m/z 261, fragment at m/z 226/228 (M-33) is due to loss of $^{\bullet}CD_2OH$ radical from $M^{\bullet+}$. Base peak fragment at m/z 170 is for cation shown in Figure 3.24 formed due to loss of 2-methyl-1-propene from m/z 226. Fragment at m/z 157 is due to 4-ClC_6H_4-$^{+}$CH-CD_2OH cation and m/z 111 is for 4-$ClC_6H_4^{+}$.

3.5 Spin trapping of radicals from a mixture of methanol (CH_3OH) and deuterated DMSO (C_2D_6SO)

In these set of experiment DMSO was replaced by deuterated DMSO whereas other experimental conditions remain unchanged. This Fenton system will yield $^{\bullet}CD_3$ radical, $^{\bullet}CH_2OH$ radical and hydroxyl radical which was trapped by PBN and its derivative to form deuterated dimethyl ($(CD_3)_2$) adducts, hydroxymethyl-deuterated methyl (CH_2OH-CD_3) adducts and hydroxyl adducts. In this section, only the deuterated dimethyl ($(CD_3)_2$) adducts and the hydroxymethyl-deuterated methyl (CH_2OH-CD_3) adducts mass spectrum are analysed from this set of experiments.

3.5.1 PBN(CH_2OH)(CD_3) adduct

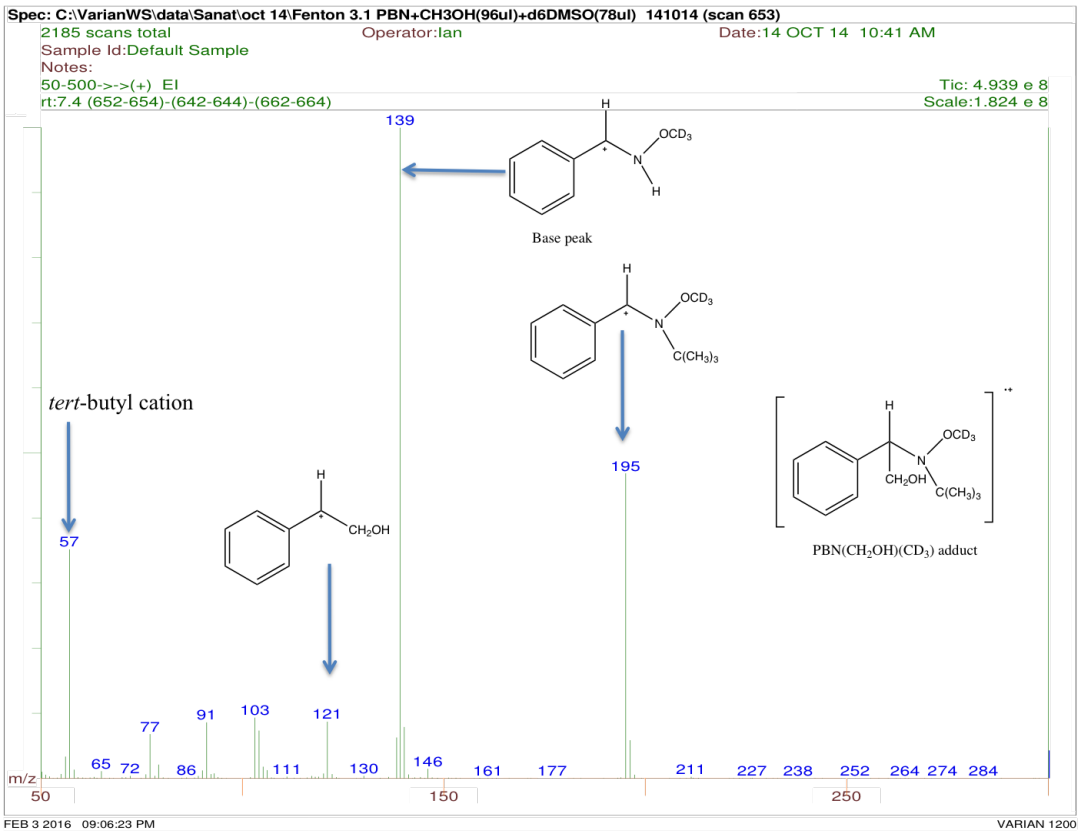

Figure 3.25: Mass spectrum for PBN(CH_2OH)(CD_3) adduct retained at 7.4 minutes.

The mass spectrum (Figure 3.25) corresponds to the peak retained at 7.4 minutes. The mass spectrum doesn't shows a molecular ion at m/z 226, addition of hydroxymethyl

radical from methanol and deuterated methyl radical from DMSO-d_6 to PBN forming PBN(CH_2OH)(CD_3) adducts. The fragmentation shows a weak fragment at m/z 211 (M-15) loss of methyl from $M^{\bullet+}$, m/z 195 (M-31) is loss of a hydroxymethyl radical from $M^{\bullet+}$. Base peak at m/z 139 is for cation shown in Figure 3.25 formed due to loss of 2-methyl-1-propene from m/z 195. Fragment at m/z 121 is due to C_6H_5-$^+$CH-CH_2OH cation, m/z 91 is for the tropylium cation, m/z 77 is for phenyl cation and m/z 57 is for the *tert*-butyl cation. The general fragmentation pattern is shown in Figure 3.26.

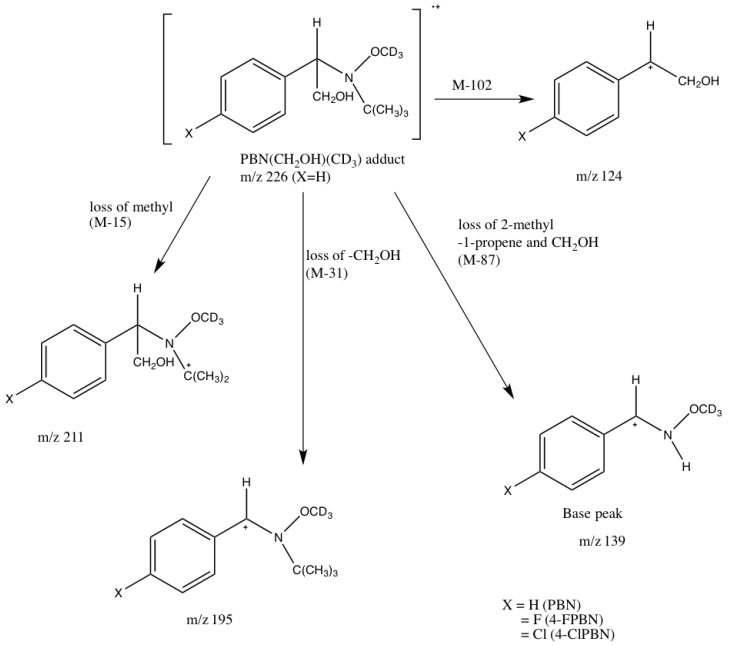

Figure 3.26: Fragmentation pattern for X-PBN (CH_2OH)(CD_3) molecular ion.

3.5.2 PBN-d_6(CH_2OH)(CD_3) adduct

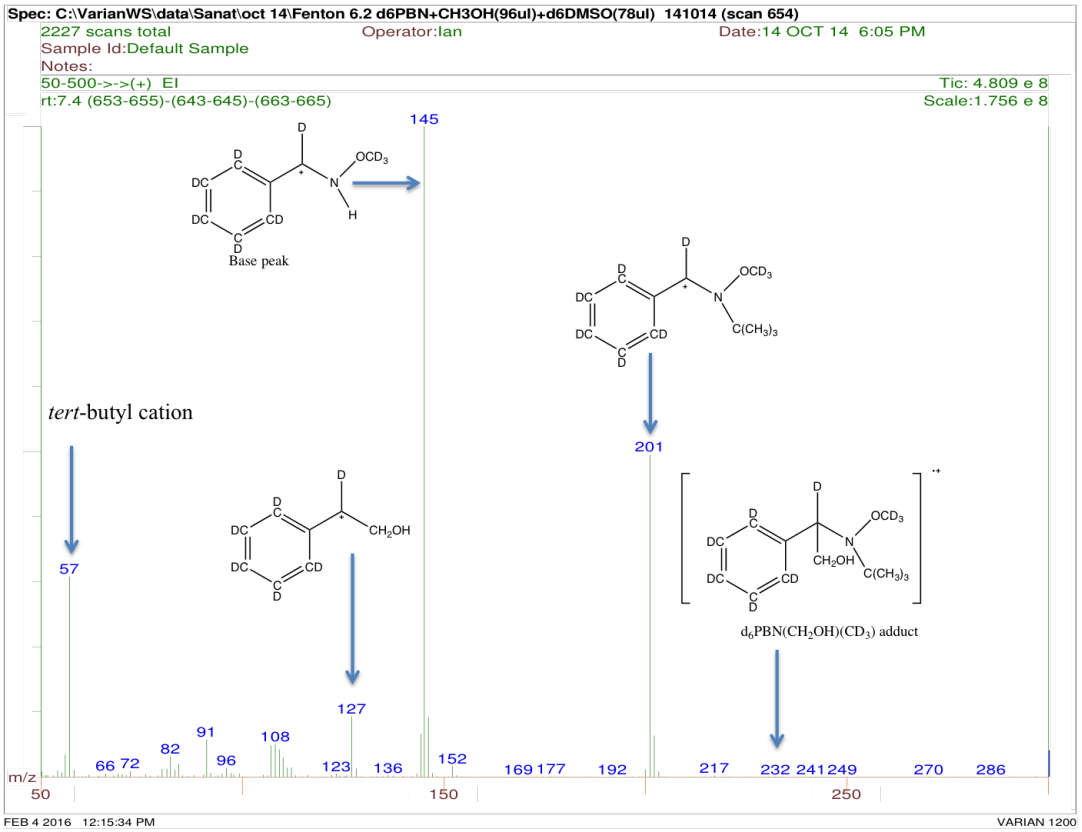

Figure 3.27: Mass spectrum for PBN-d_6(CH_2OH)(CD_3) adduct retained at 7.4 minutes.

The mass spectrum (Figure 3.27) corresponds to the peak retained at 7.4 minutes. The mass spectrum shows weak molecular ion at m/z 232 for PBN-d_6(CH_2OH)(CD_3) adducts. The fragmentation pattern (Figure 3.28) shows a fragment at m/z 217 (M-15) loss of methyl from $M^{\bullet+}$, m/z 201 (M-31) is loss of a hydroxymethyl radical from $M^{\bullet+}$. Base peak at m/z 145 is for cation (shown in Figure 3.27) formed due to loss of 2-methyl-1-propene from m/z 201. Fragment at m/z 127 is for C_6D_5-$^+$CD-CH_2OH cation, m/z 96 is for the d_5 tropylium cation, m/z 82 is for $C_6D_5^+$ and m/z 57 is for the *tert*-butyl cation.

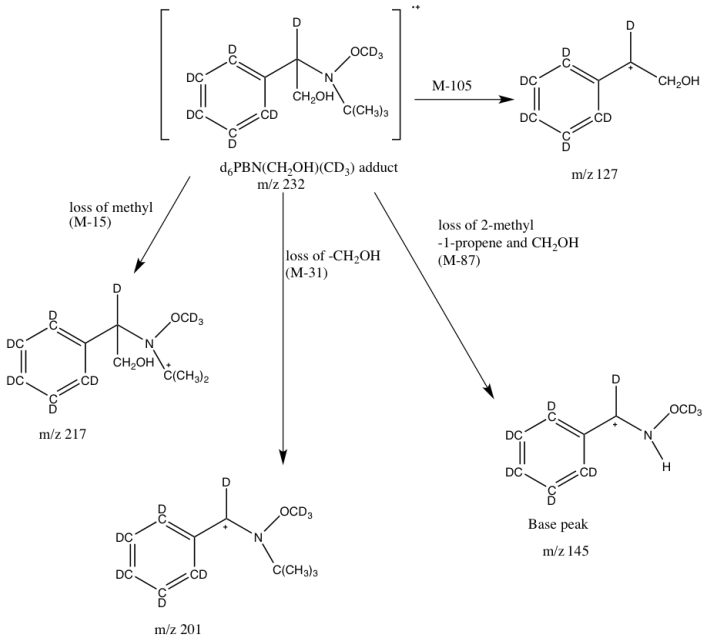

Figure 3.28: Fragmentation pattern for PBN-$d_6(CH_2OH)(CD_3)$ molecular ions.

3.5.3 4-FPBN(CH_2OH)(CD_3) adduct

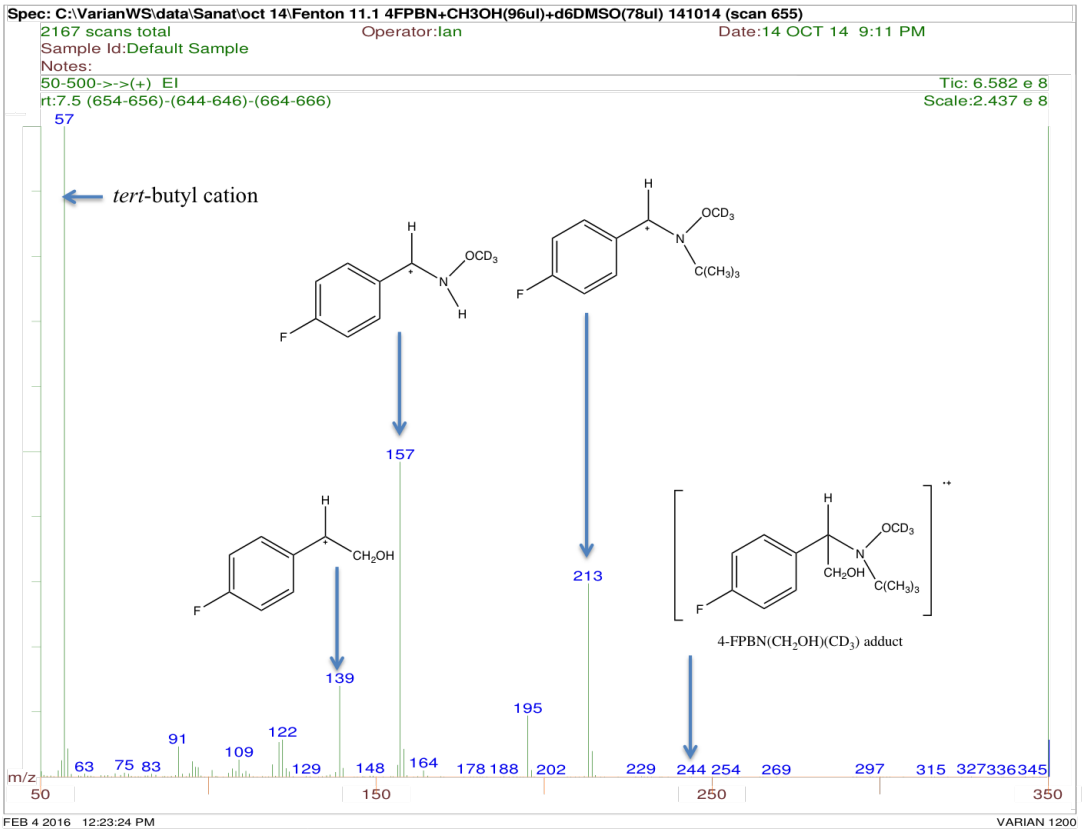

Figure 3.29: Mass spectrum for 4-FPBN(CH_2OH)(CD_3) adduct retained at 7.5 minutes.

The mass spectrum (Figure 3.29) corresponds to the peak retained at 7.5 minutes. The mass spectrum shows a weak molecular ion at m/z 244, addition of hydroxymethyl radical from methanol and CD_3 radical from d_6-DMSO to 4-FPBN forming 4-FPBN (CH_2OH) (CD_3) adducts as expected. The fragmentation pattern is similar to other X-PBN (CH_2OH) (CD_3) adducts shown in Figure 3.26. In this mass spectrum fragment at m/z 229 (M-15) loss of methyl from $M^{\bullet+}$, m/z 213 (M-31) is loss of a hydroxymethyl radical from $M^{\bullet+}$, fragment at m/z 157 is for cation shown in Figure 3.29 formed due to loss of 2-methyl-1-propene from m/z 213. Fragment at m/z 139 is due to 4-FC_6H_4-$^+$CH-CH_2OH cation (shown in Figure 3.29), m/z 109 is for the 4-fluoro tropylium cation, m/z 95 is for 4-$FC_6H_4^+$ and base peak at m/z 57 is for the *tert*-butyl cation.

3.5.4 4-ClPBN(CH_2OH)(CD_3) adduct

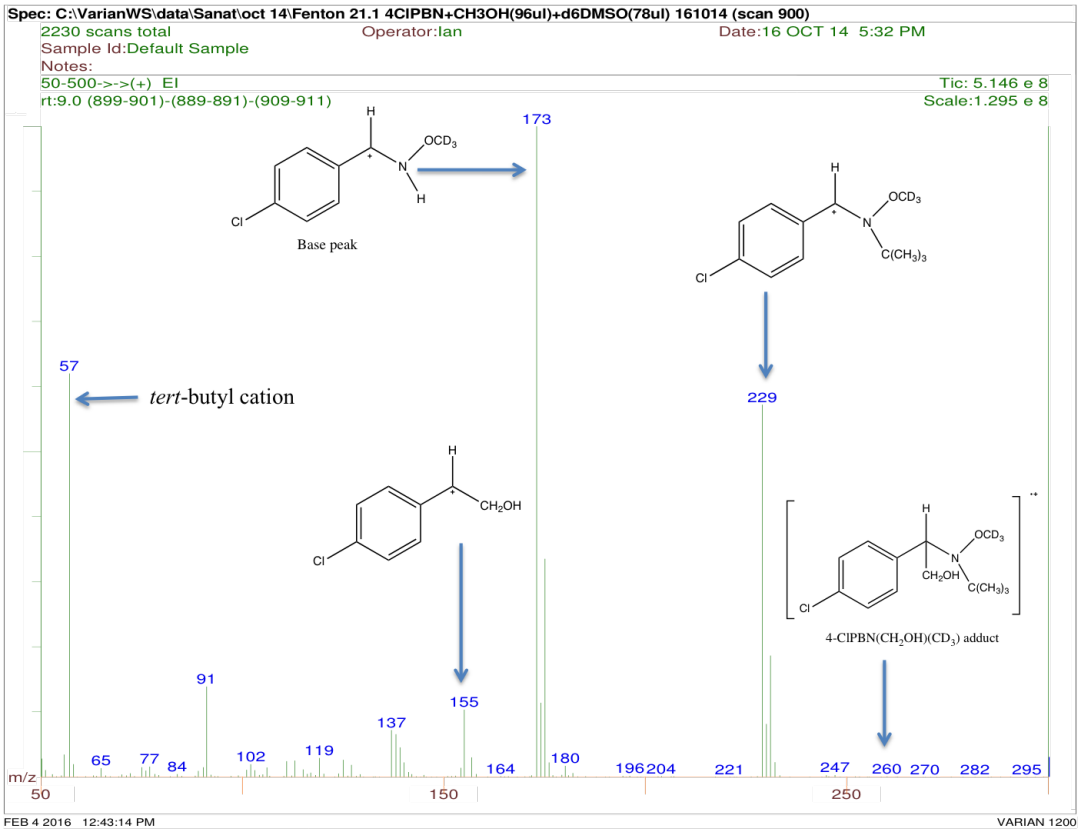

Figure 3.30: Mass spectrum for 4-ClPBN(CH_2OH)(CD_3) adduct retained at 9.0 minutes.

The mass spectrum (Figure 3.30) corresponds to the peak retained at 9.0 minutes. The mass spectrum shows a weak molecular ion for 4-ClPBN(CH_2OH)(CD_3) adducts at m/z 260. The fragmentation shows a similar fragment pattern for PBN(CH_2OH)(CD_3) adducts (Figure 3.26). Fragment at m/z 245 and isotope signal at m/z 247 is formed due to loss of methyl from $M^{\bullet+}$, m/z 229/231 (M-31) is loss of a hydroxymethyl radical from $M^{\bullet+}$. Base peak fragment at m/z 173 (^{35}Cl) and its isotope signal at m/z 175 (^{37}Cl) is for cation shown in Figure 3.30 formed due to loss of 2-methyl-1-propene from m/z 229. Fragment at m/z 155 is due to 4-ClC_6H_4-$^{+}$CH-CH_2OH cation (shown in Figure 3.30) and m/z 57 is for the *tert*-butyl cation.

3.6 Spin trapping of radicals from a mixture of deuterated methanol (CD_3OH) and deuterated DMSO (C_2D_6SO)

In this set of experiments methanol and DMSO was replaced by deuterated methanol and DMSO whereas other experimental conditions remain unchanged. This Fenton system will yield $^{\bullet}CD_3$ radical, $^{\bullet}CD_2OH$ radical and hydroxyl radical which was trapped by PBN and its derivative to form deuterated dimethyl ($(CD_3)_2$) adducts, hydroxymethyl-deuterated methyl (CD_2OH-CD_3) adducts and hydroxyl adducts. The chromatogram shows a major peak for corresponding benzaldehyde oxime, $(CD_3)_2$ adducts, CD_2OH-CD_3 adducts, unreacted PBN (derivatives) and the hydroxyl adducts. The interpretation of the deuterated dimethyl ($(CD_3)_2$) adducts (Section 4.7.2), unreacted PBN (Section 2.7.1) and hydroxyl adducts (Section 2.8.1.1) have been done in previous sections. Hence, only the deuterated hydroxymethyl-deuterated methyl (CD_2OH-CD_3) adducts mass spectrum are interpreted from this set experiment.

3.6.1 PBN(CD_2OH)(CD_3) adduct

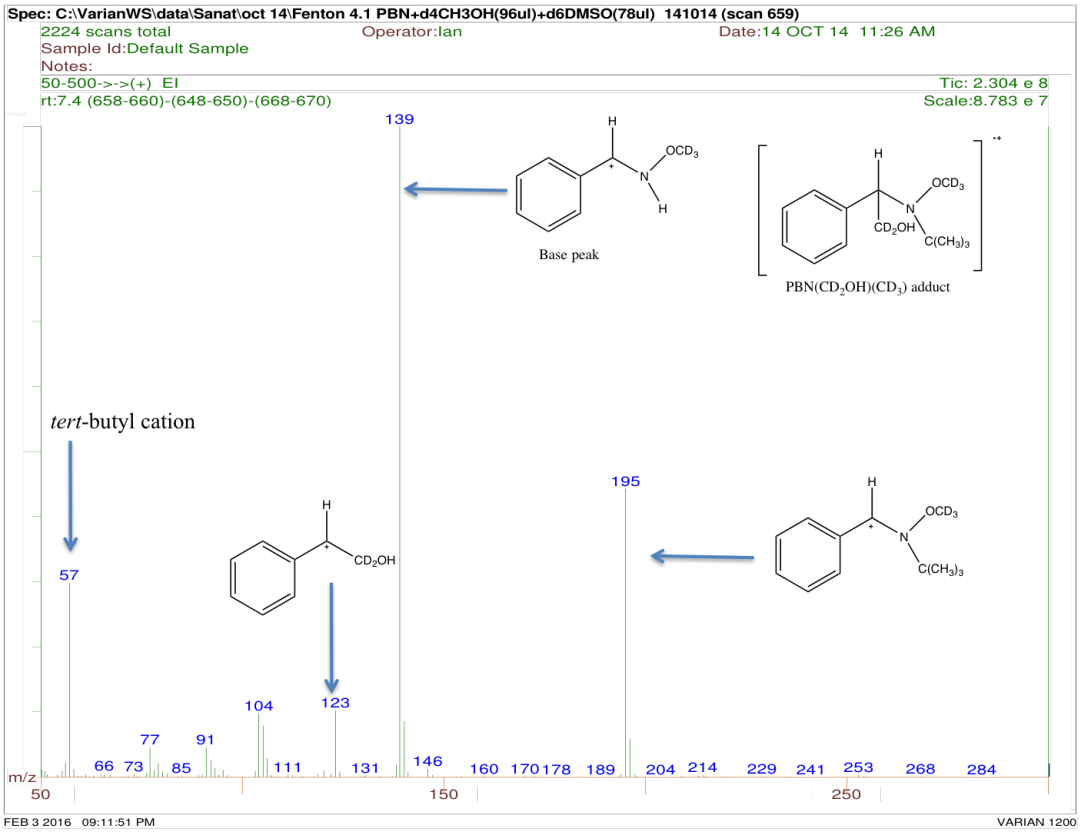

Figure 3.31: Mass spectrum for PBN(CD_2OH)(CD_3) adduct retained at 7.4 minutes.

The mass spectrum (Figure 3.31) corresponds to the peak retained at 7.4 minutes. The mass spectrum doesn't show a molecular ion at m/z 228, addition of deuterated hydroxymethyl radical from deuterated methanol and deuterated methyl radical from DMSO-d_6 to PBN forming PBN(CD_2OH)(CD_3) adducts. The fragment at m/z 195 (M-33) is loss of a deuterated hydroxymethyl radical from $M^{\bullet+}$. Base peak at m/z 139 is for cation shown in Figure 3.31 formed due to loss of 2-methyl-1-propene from m/z 195. Fragment at m/z 123 is due to C_6H_5-$^{+}$CH-CD_2OH cation, m/z 91 is for the tropylium cation, m/z 77 is for phenyl cation and m/z 57 is for the *tert*-butyl cation. The general fragmentation pattern is shown in Figure 3.32.

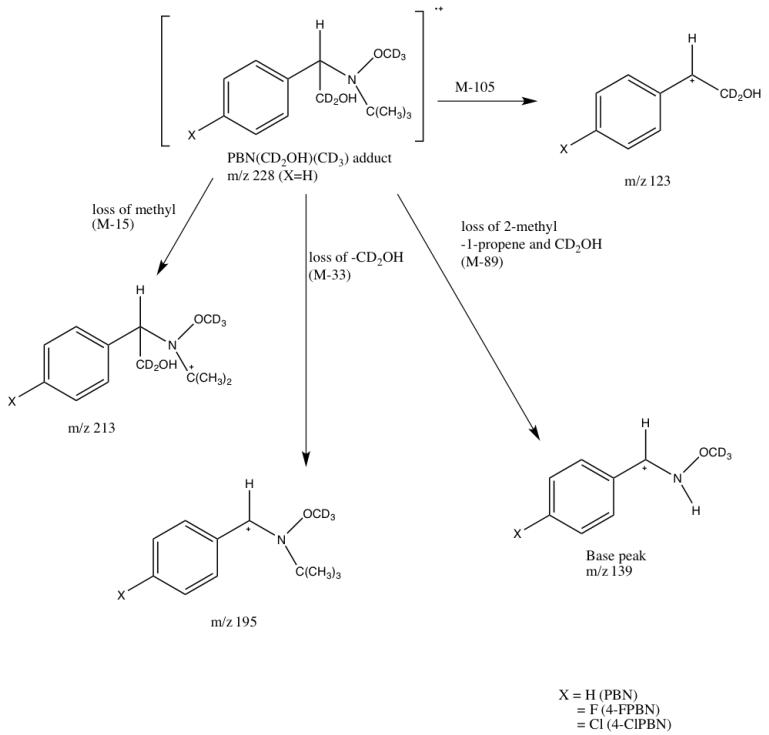

Figure 3.32: Fragmentation pattern for X-PBN (derivatives) CD_2OH-CD_3 molecular ion.

3.6.2 PBN-d_6(CD_2OH)(CD_3) adduct

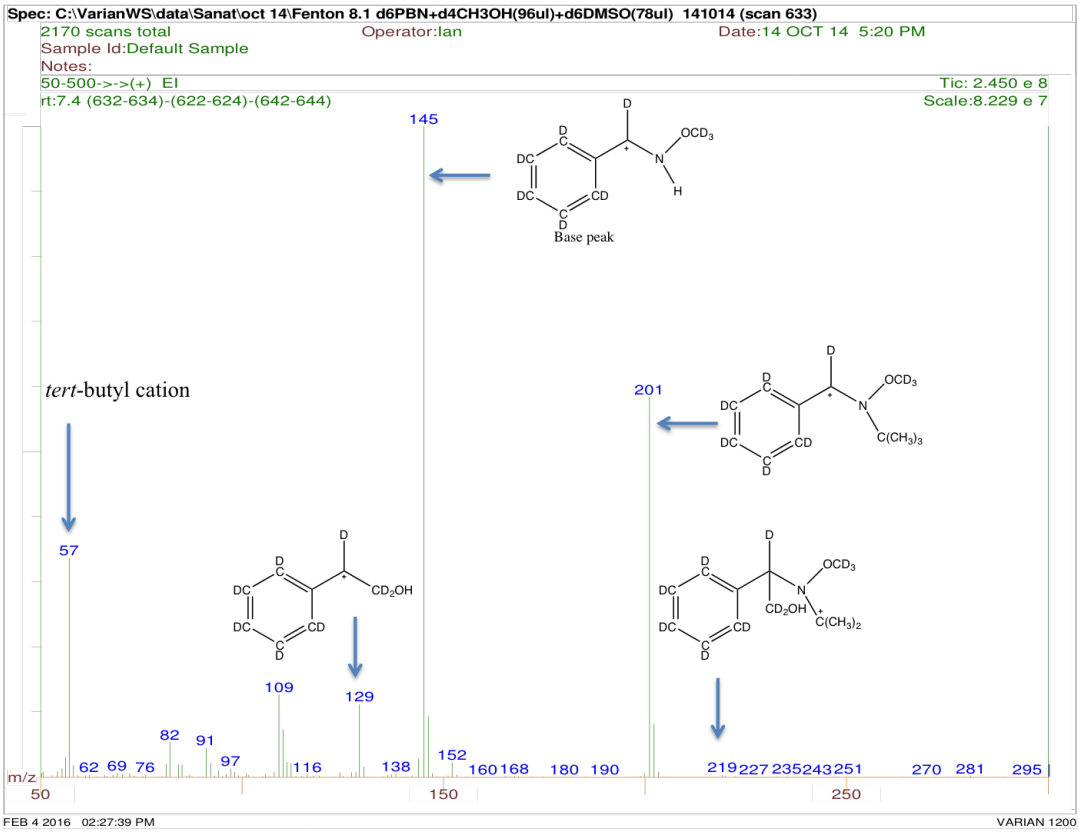

Figure 3.33: Mass spectrum for PBN-d_6(CD_2OH)(CD_3) adduct retained at 7.4 minutes.

The mass spectrum (Figure 3.33) corresponds to the peak retained at 7.4 minutes. The mass spectrum doesn't show a molecular ion at m/z 234 for PBN-d_6(CD_2OH)(CD_3) adducts. The fragmentation pattern (Figure 3.34) shows a fragment at m/z 219 (M-15) loss of methyl from $M^{\bullet+}$, m/z 201 (M-33) is loss of a deuterated hydroxymethyl radical from $M^{\bullet+}$. Base peak at m/z 145 is for cation (shown in Figure 3.33) formed due to loss of 2-methyl-1-propene from m/z 201. Fragment at m/z 129 is for C_6D_5-$^+$CD-CD_2OH cation, m/z 82 is for $C_6D_5^+$ and m/z 57 is for the *tert*-butyl cation.

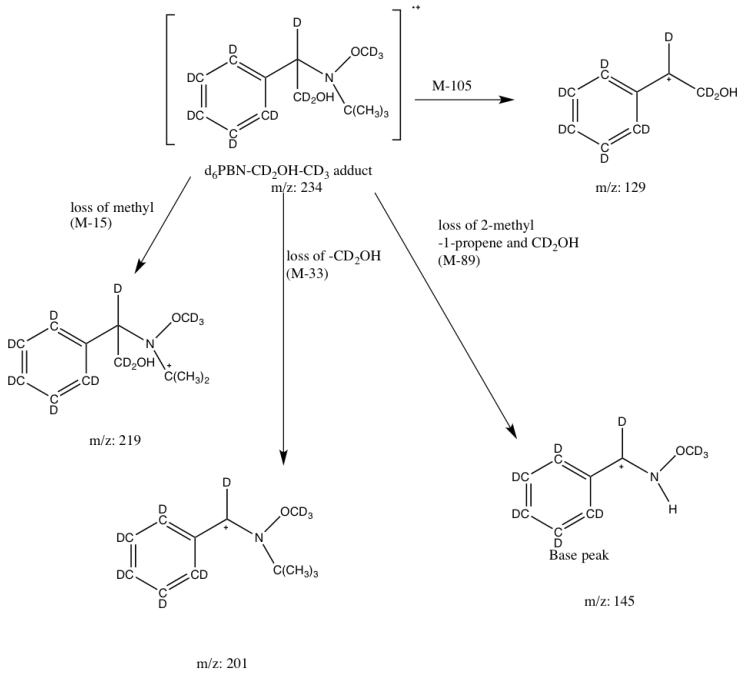

Figure 3.34: Fragmentation pattern for PBN-d_6(CD_2OH)(CD_3) molecular ion.

3.6.3 4-FPBN(CD_2OH)(CD_3) adduct

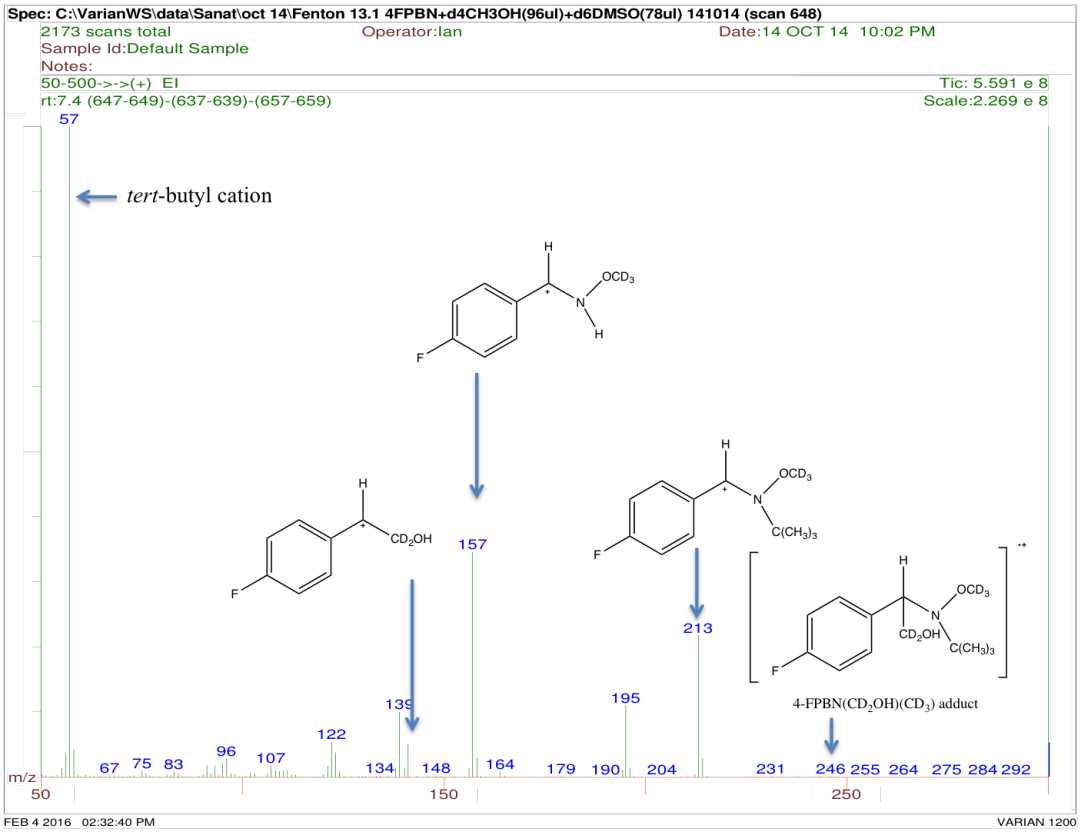

Figure 3.35: Mass spectrum for 4-FPBN(CD_2OH)(CD_3) adduct retained at 7.4 minutes.

The mass spectrum (Figure 3.35) corresponds to the peak retained at 7.4 minutes. The mass spectrum shows a weak molecular ion at m/z 246, addition of deuterated hydroxymethyl radical from deuterated methanol and CD_3 radical from d_6-DMSO to 4-FPBN forming 4-FPBN(CD_2OH)(CD_3) adducts as expected. The fragmentation pattern is similar to other X-PBN(CD_2OH)(CD_3) adducts as shown in Figure 3.32. In this mass spectrum fragment at m/z 231 (M-15) loss of methyl from $M^{\bullet+}$, m/z 213 (M-33) is loss of a deuterated hydroxymethyl radical from $M^{\bullet+}$, fragment at m/z 157 is for cation shown in Figure 3.35 formed due to loss of 2-methyl-1-propene from m/z 213, fragment at m/z 141 is due to 4-FC_6H_4-$^+$CH-CD_2OH cation (shown in Figure 3.35) and base peak at m/z 57 is for the *tert*-butyl cation.

This mass spectrum also shows a presence of 4-FPBN at m/z 195 and its fragment m/z 139 formed due to loss of 2-methyl-1-propene from m/z 195. This is possible because the 4-FPBN(CD_2OH)(CD_3) adducts and 4-FPBN have very similar retention time.

3.6.4 4-ClPBN(CD_2OH)(CD_3) adduct

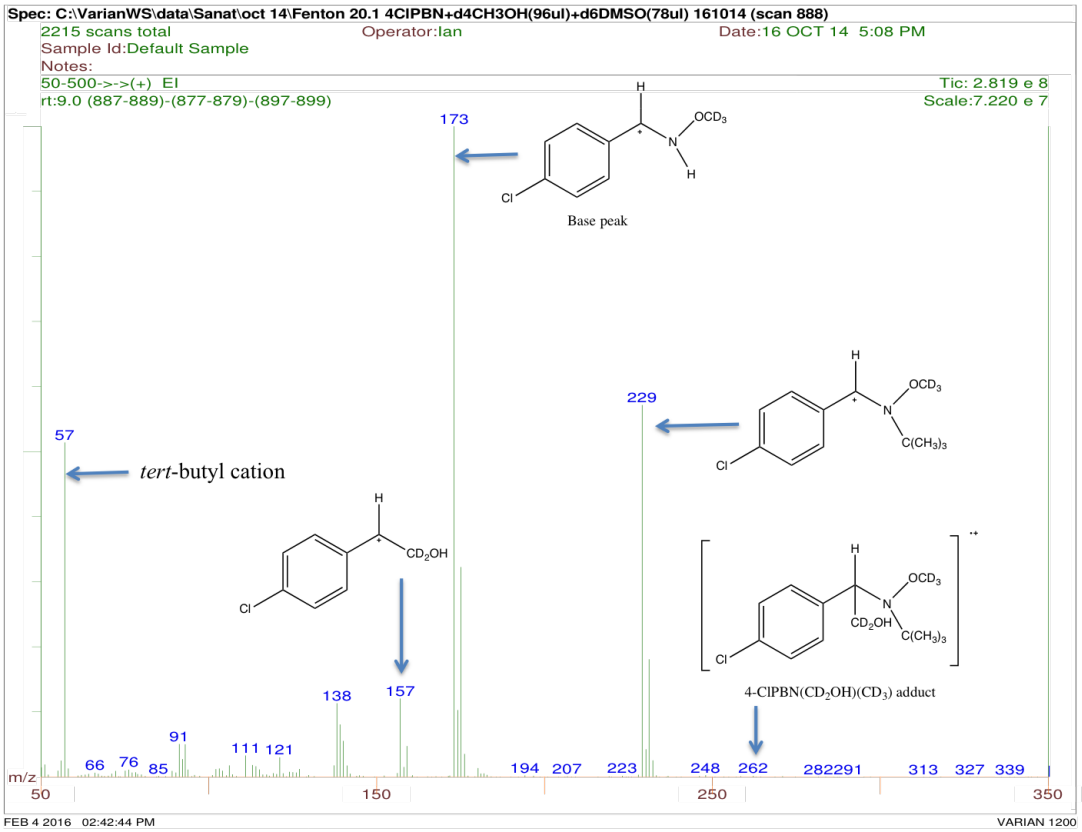

Figure 3.36: Mass spectrum for 4-ClPBN(CD_2OH)(CD_3) adduct retained at 9.0 minutes.

The mass spectrum (Figure 3.36) corresponds to the peak retained at 9.0 minutes. The mass spectrum shows a weak molecular ion for 4-ClPBN(CH_2OH)(CD_3) adducts at m/z 262. The fragmentation shows a similar fragment pattern for PBN(CD_2OH)(CD_3) adducts (Figure 3.32). The fragment at m/z 229 and its isotope signal m/z 231 is loss of a deuterated hydroxymethyl radical from $M^{\bullet+}$(M-31). Base peak fragment at m/z 173 (^{35}Cl) and its isotope signal at m/z 175 (^{37}Cl) is for cation shown in Figure 3.36 formed due to loss of 2-methyl-1-propene from m/z 229. Fragment at m/z 157 is due to 4-ClC_6H_4-$^{+}$CH-CD_2OH cation (shown in Figure 3.36), m/z 111 is for the 4-$ClC_6H_4^{+}$ and m/z 57 is for the *tert*-butyl cation.

3.7 Headspace Solid-Phase MicroExtraction Gas Chromatography (HS-SPME-GC/MS)

Owing to the potential volatility of many of the PBN adducts observed in the previous experiments, the headspace SPME-GC/MS technique was applied to the analysis of radicals generated by the Fenton system and trapped by PBN and its derivatives. To test the potential of this technique standard Carboxen®/Polydimethylsiloxane (CAR/PDMS) fibres were used.

3.7.1 Analysis of trapped radicals from the Fenton system containing methanol

3.7.1.1 Chromatogram

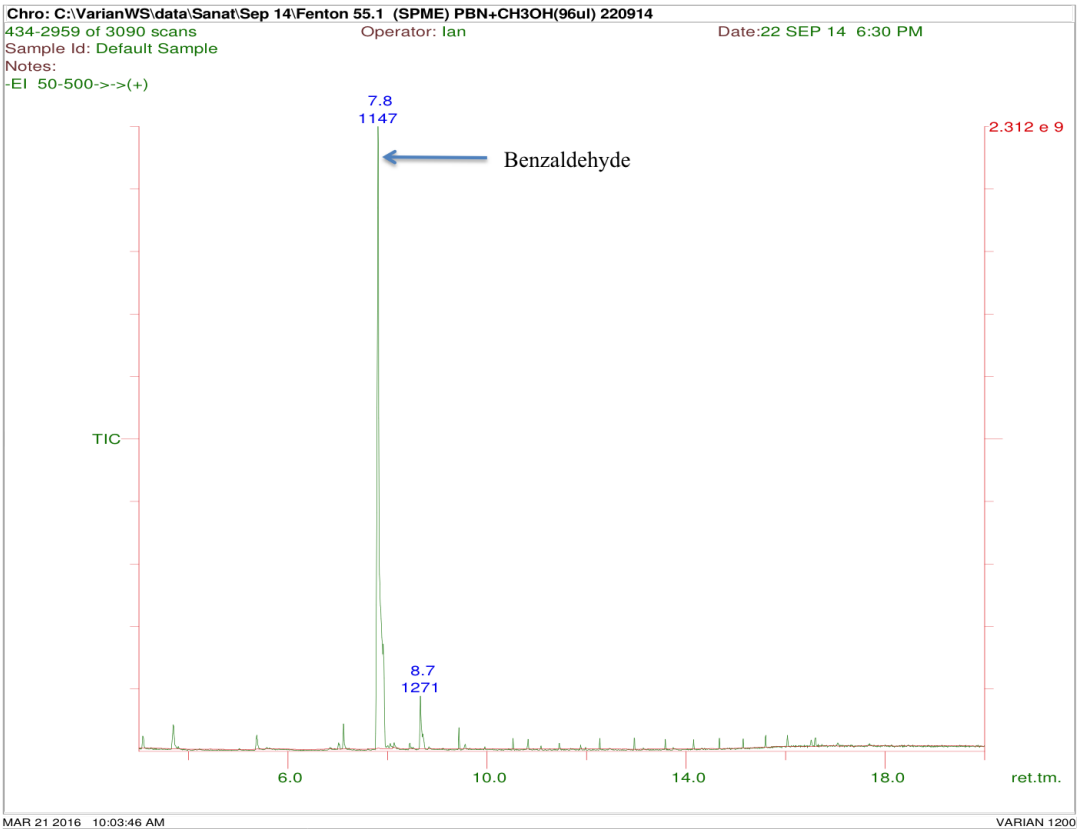

Figure 3.37: Total ion chromatogram (TIC) obtained from the HS-SPME-GC/MS analysis of the reaction mixture between PBN and methanol in Fenton reaction.

TIC in Figure 3.37 shows a intense peak at 7.8 minutes (Benzaldehyde mass spectrum Figure 3.38). Peak at 8.7 minutes corresponds to the salicylaldehyde (mass spectrum Figure 3.39) and the various small peaks seems to be coming from the fibre which could be due to the degradation of the fibre, hence mass spectrum not included.

3.7.1.2 Benzaldehyde peak at 7.8 minutes

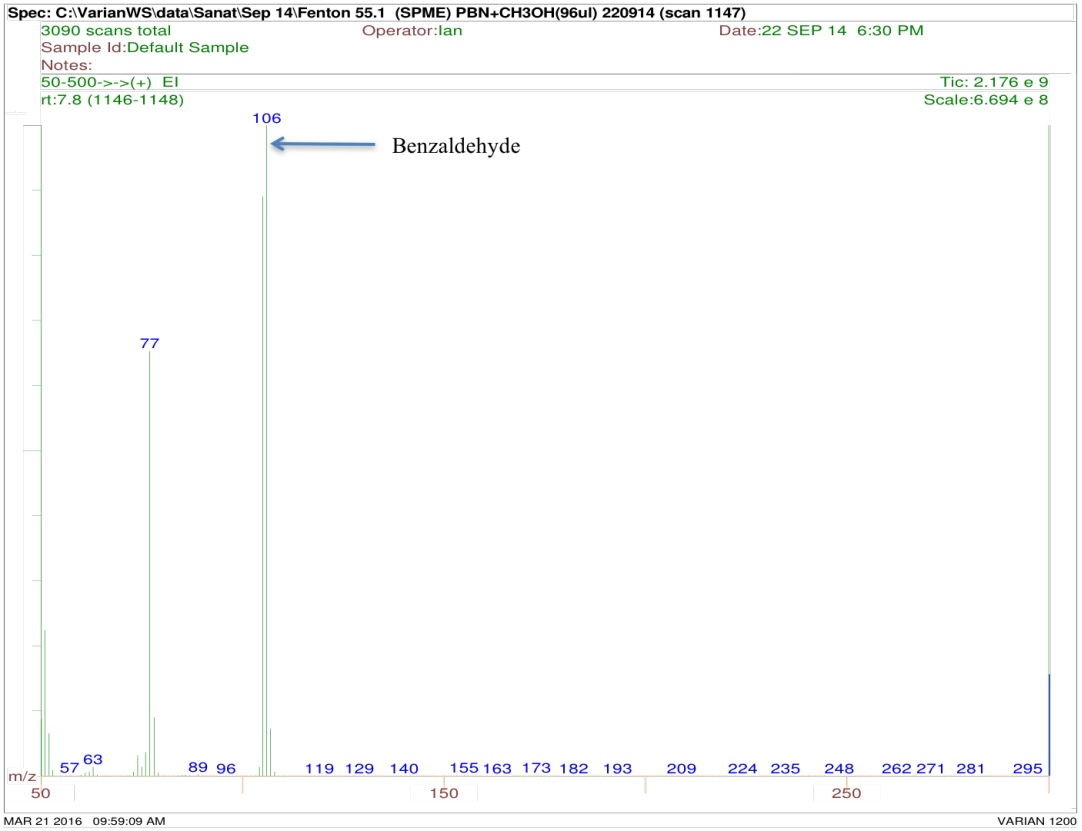

Figure 3.38: Mass spectrum for benzaldehyde retained at 7.8 minutes (Figure 3.37).

The mass spectrum shown in Figure 3.38 corresponds to the peak retained at 7.8 minutes (Figure 3.37). The mass spectrum shows a strong molecular ion at m/z 106 which correspond to benzaldehyde (MW=106) and fragment at m/z 77 is for the phenyl cation. Benzaldehyde could be the decomposed products of the PBN which has been formed as a result of the reaction of the hydroxyl radical with the PBN at the site (C=N). Hydroxyl radical adds to the C site (C=N) of the PBN and the resulting spin adduct has a half-life of less than 1 minute at pH 7.0, and decomposes to release benzaldehyde (Reinke et al. 2000).

3.7.1.3 Peak at 8.7 minutes

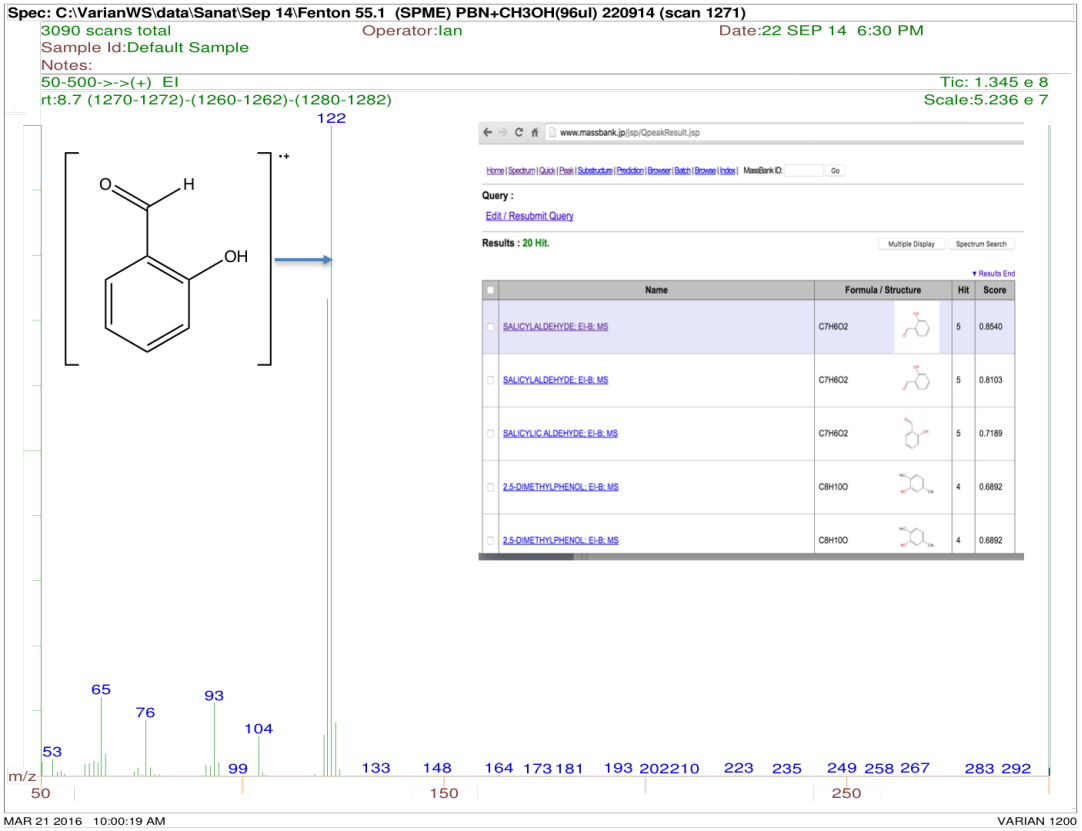

Figure 3.39: Mass spectrum for peak retained at 8.7 minutes.

The mass spectrum for peak retained at 8.7 minutes shows a strong molecular ion at m/z 122. To identify the molecular ion the mass spectrum was searched in mass bank database and the search result showed presence of salicylaldehyde (Figure 3.39).

3.7.2 Analysis of trapped radicals from the Fenton system containing methanol and DMSO

3.7.2.1 Chromatogram

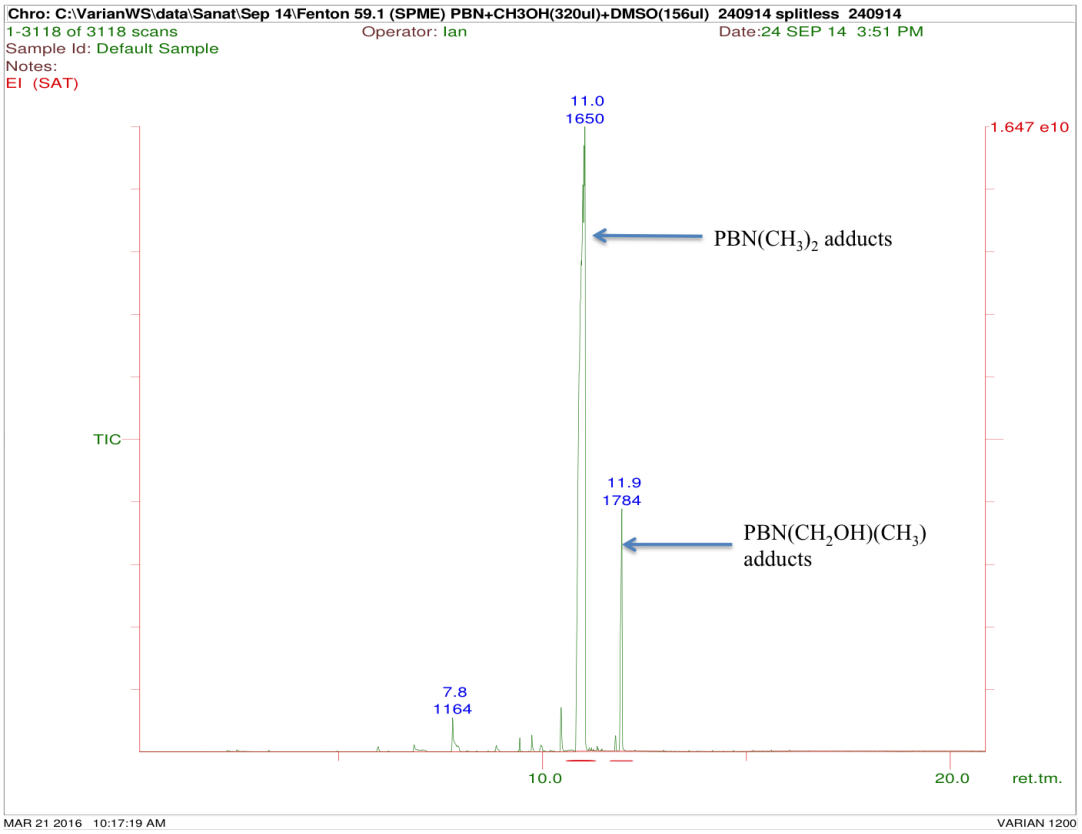

Figure 3.40: Total ion chromatogram (TIC) obtained from the HS-SPME-GC/MS analysis of the reaction mixture between PBN, methanol and DMSO in Fenton reaction.

TIC shown in Figure 3.40 shows a intense peak at 11.0 minutes for the $PBN(CH_3)_2$ adducts (identified in section 3.3.3.1) and 11.9 minutes for $PBN(CH_2OH)(CH_3)$ adducts. The other peak at 7.8 minutes is for benzaldehyde (interpretation shown in section 3.7.1).

3.7.2.2 PBN$(CH_3)_2$ adduct

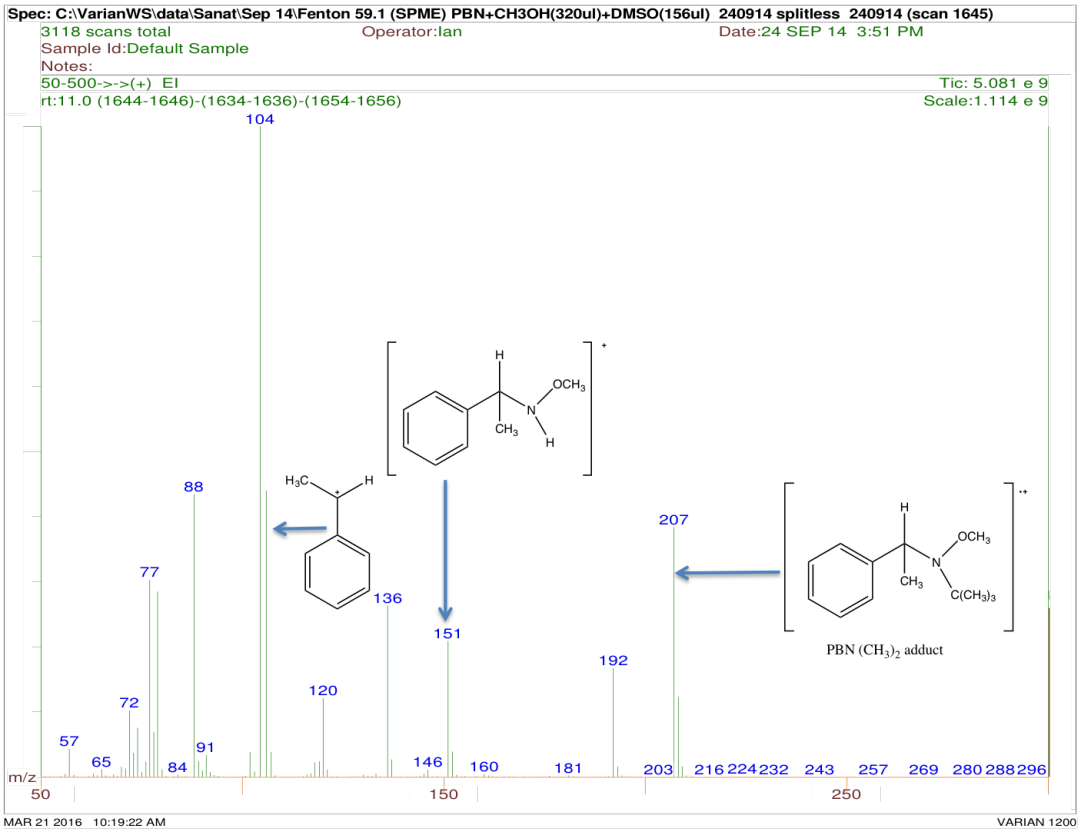

Figure 3.41: Mass spectrum for PBN$(CH_3)_2$ adduct peak at 11.0 min (Figure 3.40).

The mass spectrum (shown in Figure 3.41) corresponds to a dimethyl adduct of PBN (PBN$(CH_3)_2$) with a molecular ion at m/z 207. The interpretation of the EI mass spectrum of the PBN$(CH_3)_2$ adduct have been given in section 3.3.3.1.

Different synthesised PBN derivatives were used to confirm the formation of dimethyl adducts. Within all cases molecular ions were observed at the expected m/z values, with the mass difference due to the presence of a different substituent at the 4 (para) position of the benzene ring of PBN. Retention times and m/z values for the molecular ions of the different PBN dimethyl adducts are given in Table 3.1.

PBN (PBN(CH_3)$_2$	Retention time ($R_t$in minutes)	Molecular ion (m/z)
PBN	11.0	207
4-FPBN	11.0	225
4-ClPBN	11.9	241

Table 3.1: Dimethyl adducts for different PBN derivatives with their retention time (R_t) and molecular ion.

3.7.2.3 PBN(CH_2OH)(CH_3) adduct at 11.9 minutes

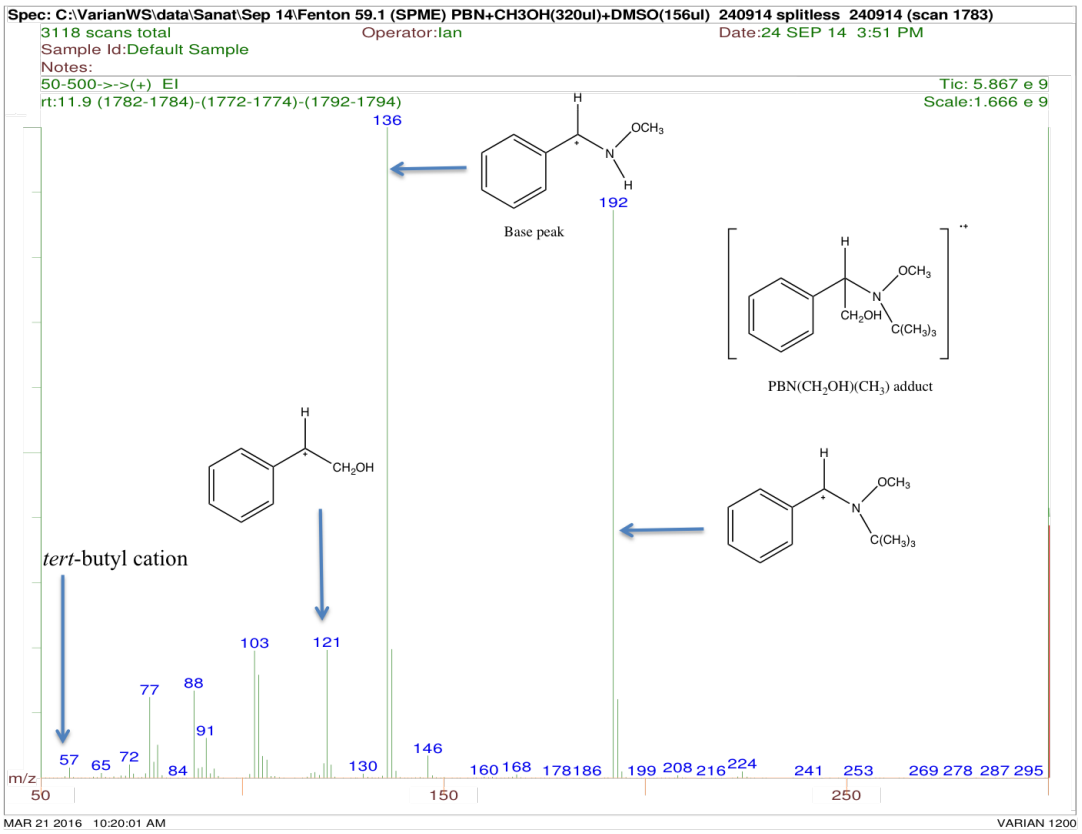

Figure 3.42: Mass spectrum for PBN(CH_2OH)(CH_3) adduct peak at 11.9 minutes (Figure 3.40).

The mass spectrum shown in Figure 3.42 correspond to the peak retained at 11.9 minutes (Figure 3.40) for PBN(CH_2OH)(CH_3) adducts. The mass spectrum does not show a molecular ion or it is very weak, however, the fragment pattern is identical to the PBN(CH_2OH)(CH_3) adducts as seen in Figure 3.8. For interpretation of the

PBN(CH_2OH)(CH_3) adducts mass spectrum see section 3.3.2.1. Different PBN derivatives were used to confirm the formation of PBN(CH_2OH)(CH_3) adducts and, in each case, no molecular ion was seen in the mass spectrum, hence m/z for 4-XPBN(CH_3) cation has been shown in Table 3.2.

X-PBN derivatives	Retention time (R_t in minutes) PBN(CH_2OH)(CH_3) adducts	4-X-PBN(CH_3) cation (m/z) ($M^{\bullet+}$- 31)
PBN	11.9	192
4-FPBN	11.9	210
4-ClPBN	12.9	226

Table 3.2: Retention times (R_t) and m/z values for the M-31 peak of different hydroxymethyl methyl adducts of PBN.

3.7.2.4 PBN(CH_2OH)(CH_3) adduct at 11.8 minutes

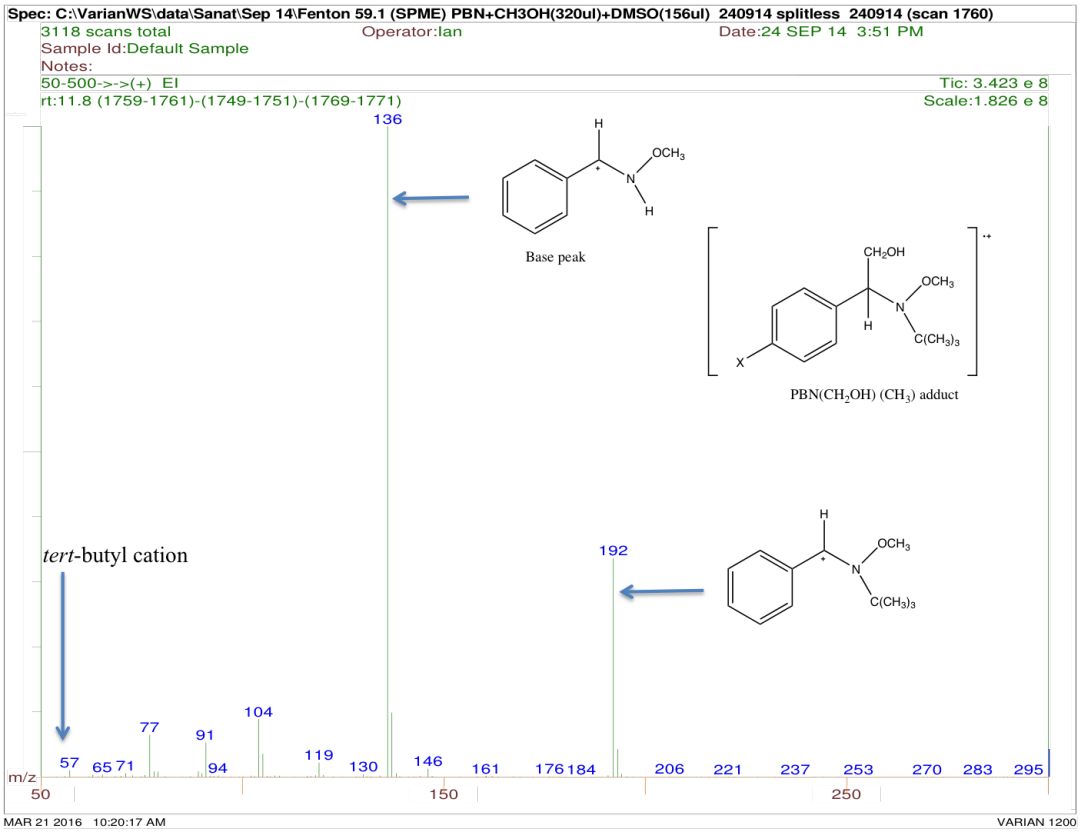

Figure 3.43: Mass spectrum for PBN(CH_2OH)(CH_3) adduct peak at 11.8 minutes (Figure 3.40).

The mass spectrum in Figure 3.43 correspond to the peak retained at 11.8 minutes (Figure 3.40) for PBN(CH_2OH)(CH_3) adduct. This peak is very weak compared to the peak at 11.9 minutes. This PBN(CH_2OH)(CH_3) adduct at 11.8 minutes could be the isomers of the PBN(CH_2OH)(CH_3) adduct. For interpretation of PBN(CH_2OH)(CH_3) adduct mass spectrum see section 3.3.2.1.

3.7.2.5 Peak at 9.4 minutes

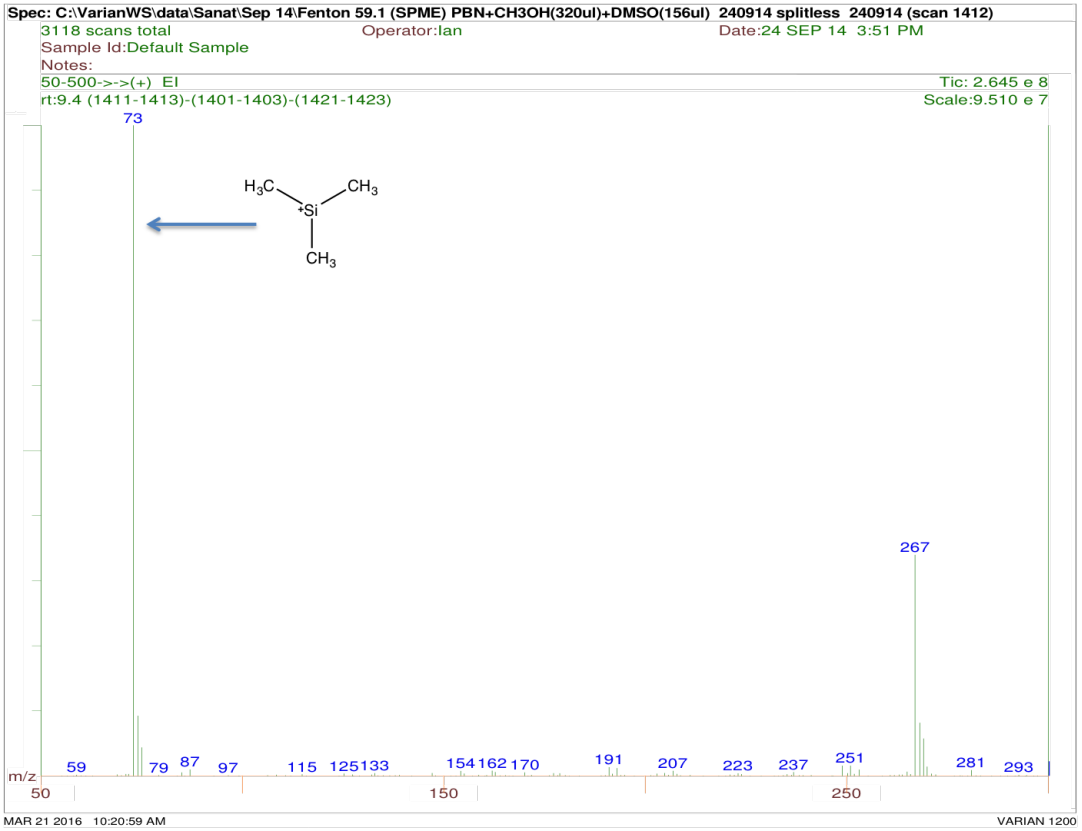

Figure 3.44: Mass spectrum a for peak at 9.4 minutes (Figure 3.40).

Mass spectrum in Figure 3.44 correspond to the peak retained at 9.4 minutes for the siloxane polymer of the stationary phase or from the SPME fibre, polydimethylsiloxane (PDMS) ($Si(CH_3)_3$, MW=73). This peak could be due to the degradation of the PDMS chain and subsequent loss of methyl terminated group.

3.7.3 Spin trapping of deuterated methanol (CD_3OH) and DMSO radicals

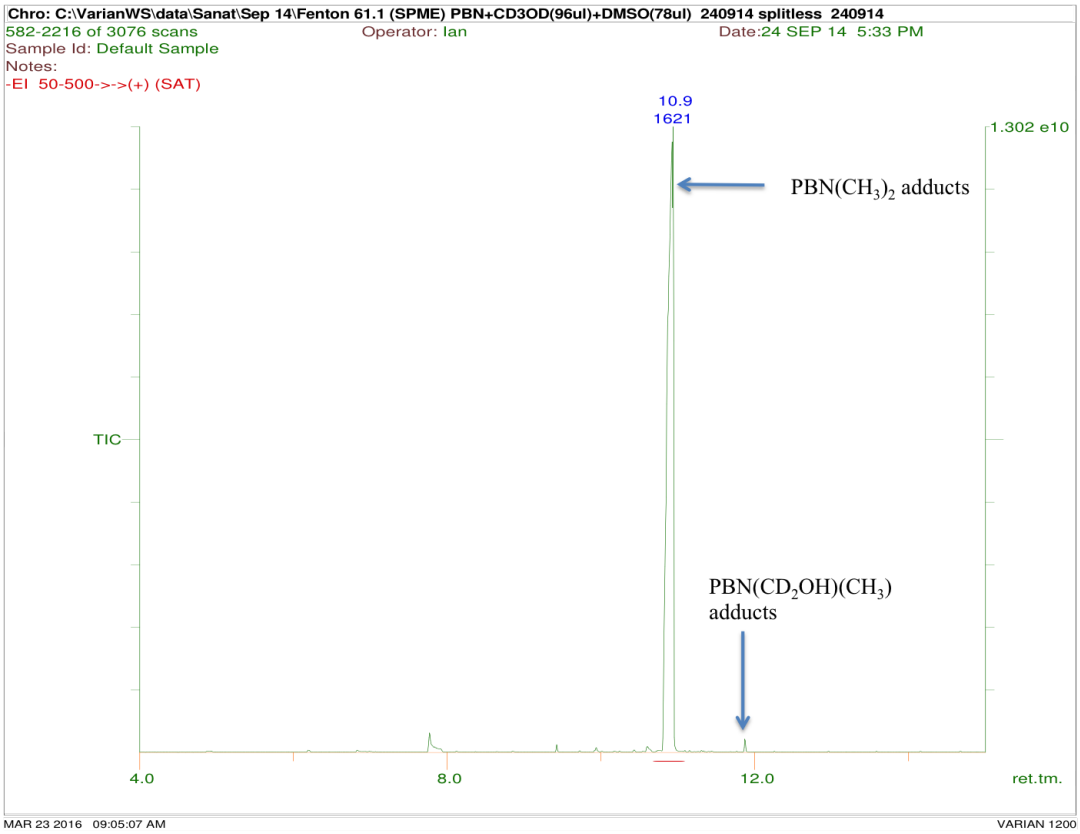

Figure 3.45: Total ion chromatogram (TIC) obtained from the HS-SPME-GC/MS analysis of the Fenton reaction mixture containing PBN, deuterated methanol (CD_3OH) and DMSO (3:1 by molar mass) .

The TIC shown in Figure 3.45 is similar to the chromatogram shown in Figure 3.40 with a very intense peak at 10.9 minutes for the PBN dimethyl adduct whose mass spectrum has been shown in section 3.3.3.1. The peak at 12.0 minutes is for a PBN(CD_2OH)(CH_3) adduct; its EI mass spectrum has been analysed previously in section 3.4.1. Confirmation of the hydroxy-deuteromethyl methyl adducts was done by using different PBN derivatives and the adducts formed which have been tabulated in Table 3.3.

X-PBN derivatives	Retention time (R_t in minutes) $PBN(CD_2OH)(CH_3)$ adducts	4-X-$PBN(CH_3)$ cation (m/z) ($M^{\bullet+}$- 33)
PBN	12.0	192
4-FPBN	11.9	210
4-ClPBN	12.8	226

Table 3.3: Retention times (R_t) and m/z values for the M-33 peak of different hydroxy-deuteromethyl methyl adducts of PBN.

3.7.4 Spin trapping of methanol (CH_3OH) and DMSO-d_6 radicals

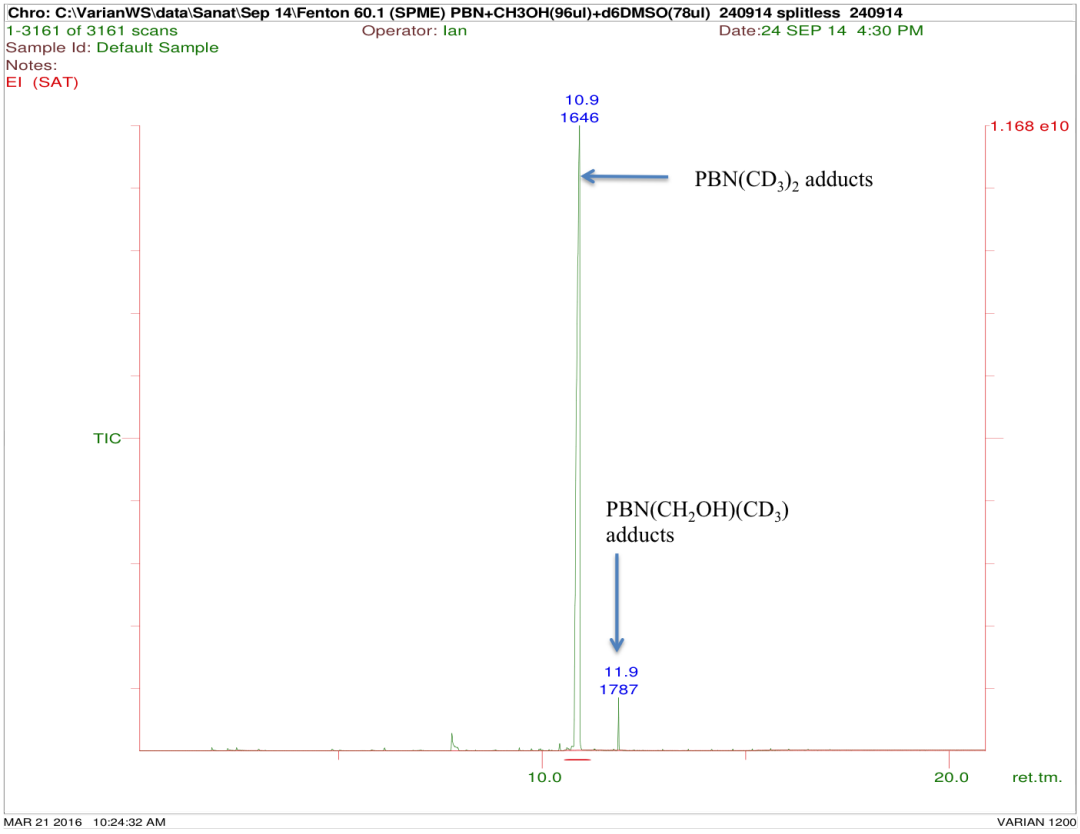

Figure 3.46: Total ion chromatogram (TIC) obtained from the HS-SPME-GC/MS analysis of the Fenton reaction mixture containing PBN, methanol and deuterated DMSO (3:1 by molar mass).

TIC shown in Figure 3.46 shows a intense peak 10.9 minutes for $PBN(CD_3)_2$ adduct. The mass spectrum shows a strong molecular ion peak at m/z 213 for the $PBN(CD_3)_2$

adduct which has been interpreted in section 4.7.2. The dimethyl adduct obtained for different PBN derivatives has been summarised in Table 3.4. The chromatogram also shows peak at 11.9 minutes for PBN(CH_2OH)(CD_3) adduct and the corresponding mass spectrum doesn't show any molecular ion, however, there is a strong peak at 195 for the PBN(CD_3)$^+$ cation which is formed due to loss of a hydroxymethyl radical from the PBN(CH_2OH)(CD_3) adduct. A similar pattern was seen with different PBN derivatives which have been tabulated in Table 3.4 with the retention time and m/z for PBN(CD_3) cation.

PBN derivatives	4-X-PBN(CD_3)$_2$ adducts		4-X-PBN(CH_2OH)(CD_3) adducts	
	R_t (minutes)	$M^{\bullet+}$ (m/z)	R_t (minutes)	m/z ($M^{\bullet+}$- 31)
PBN	10.9	213	11.9	195
4-FPBN	10.9	231	11.9	213
4-ClPBN	11.9	247	12.8	229

Table 3.4: Retention times (R_t), molecular ion (m/z) for deuterated dimethyl adducts and m/z values for the M-31 peak for hydroxymethyl methyl adducts of 4-X-PBN derivatives.

3.7.5 Spin trapping of deuterated methanol (CD_3OH) and DMSO-d_6 radicals

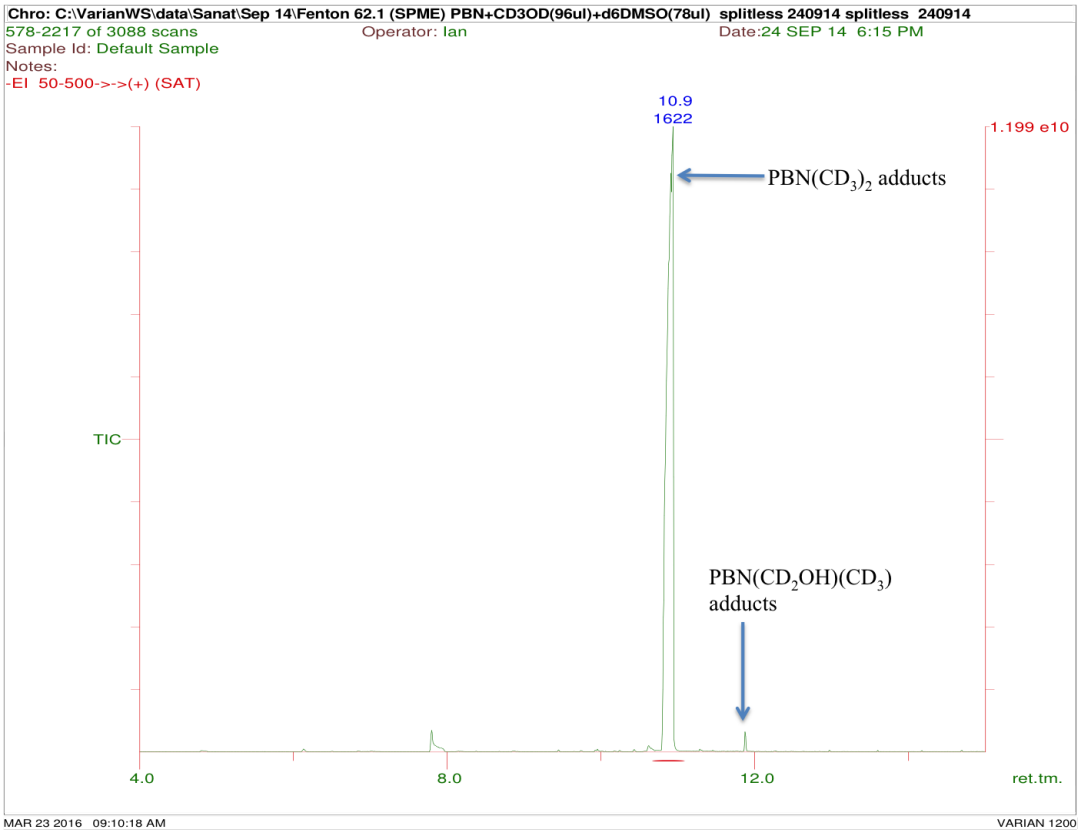

Figure 3.47: Total ion chromatogram (TIC) obtained from the HS-SPME-GC/MS analysis of the Fenton reaction mixture containing PBN, deuterated methanol and deuterated DMSO (3:1 by molar mass).

TIC shown in Figure 3.47 shows a intense peak 10.9 minutes for $PBN(CD_3)_2$ adduct and $PBN(CD_2OH)(CD_3)$ adduct at 11.9 minutes. The mass spectrum for this adducts is similarly found in other experiments which have been tabulated in Table 3.5.

PBN derivatives	4-X-PBN(CD_3)$_2$ adducts		4-X-PBN(CD_2OH)(CD_3) adducts	
	R_t (minutes)	$M^{\bullet+}$ (m/z)	R_t (minutes)	m/z ($M^{\bullet+}$- 31)
PBN	10.9	213	11.9	195
4-FPBN	10.9	231	11.9	213
4-ClPBN	11.9	247	12.8	229

Table 3.5: Retention times (R_t), molecular ion (m/z) for deuterated dimethyl adducts and m/z values for the M-33 peak for hydroxy-deuteromethyl methyl adducts of 4-X-PBN derivatives..

3.7.6 Comparison of SPME fibres for the trapping of methanol and DMSO radicals

Four different fibres were used in identical conditions to check the affinity of the PBN hydroxymethyl methyl adducts towards the fibre. The different fibres used were polyacrylate (PA), carbowax-polyethylene glyco (PEG), polydimethylsiloxane/Divinylbenzene

(PDMS/DVB) and Carboxen/Polydimethylsiloxane(CAR/PDMS). All these fibres were able to absorb PBN hydroxymethyl methyl adducts from the head space with varying sensitivity. TIC in Figure 3.48 shows the peak of interest for PBN dimethyl adducts and PBN hydroxymethyl methyl adducts obtained from different SPME fibres. The peak area for PBN hydroxylmethyl methyl adducts was compared and it was found CAR/PDMS fibre showed more affinity for the PBN hydroxylmethyl methyl adducts compared to other fibres (Figure 3.49). Hence, CAR/PDMS fibre was used to extract the hydroxymethyl methyl adducts for different PBN derivatives.

3. Analysis of spin trapped hydroxymethyl radical from methanol

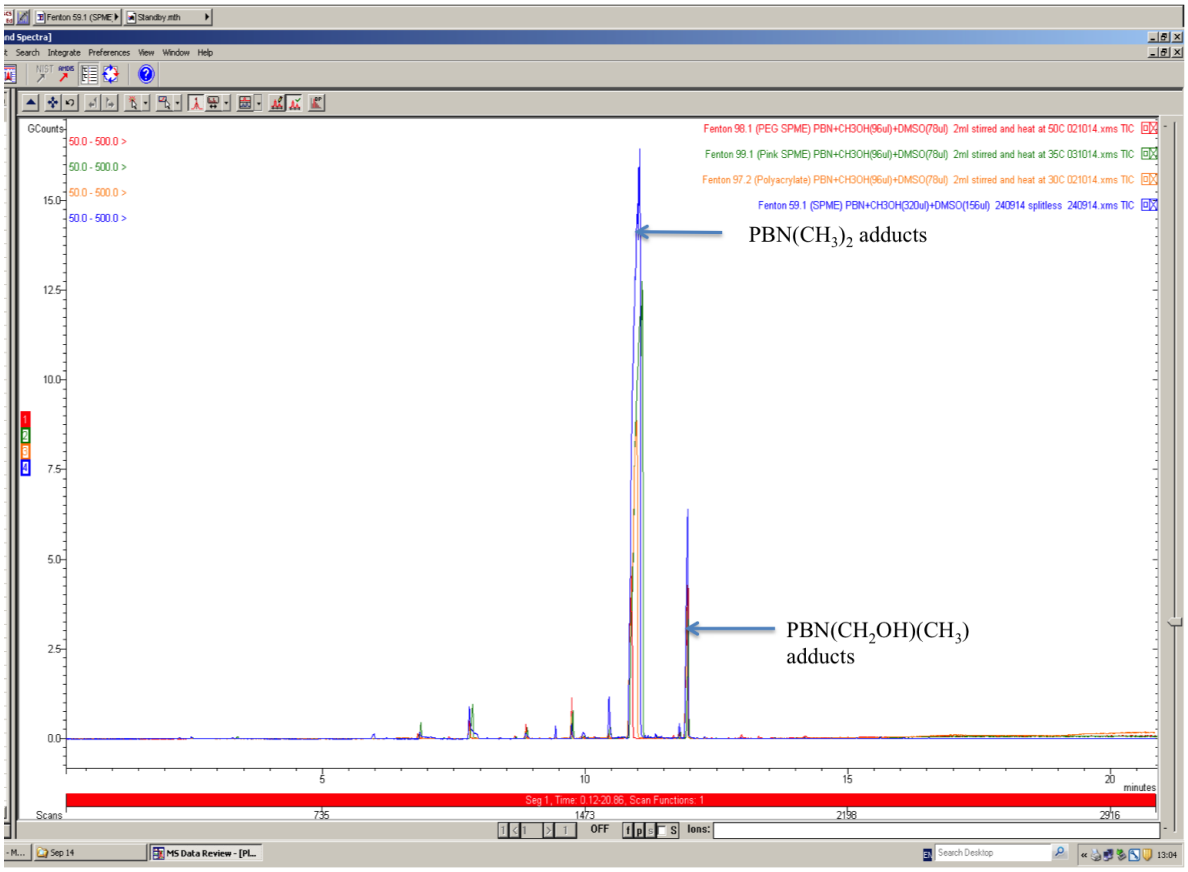

Figure 3.48: Overlaid TIC for $PBN(CH_3)_2$ adduct and $PBN(CH_2OH)(CH_3)$ adduct obtained from carboxen/polydimethylsiloxane fibre (CAR/PDMS), Polyethylene Glycol fibre (PEG), Polyacrylate fibre and Polydimethylsiloxane/Divinylbenzene (PDMS/DVB) fibre.

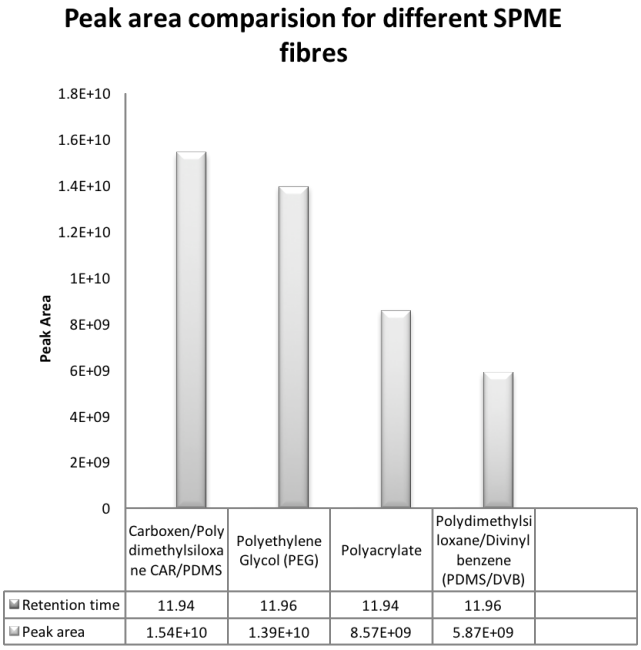

Figure 3.49: $PBN(CH_2OH)(CH_3)$ adduct peak comparision for carboxen/polydimethylsiloxane fibre (CAR/PDMS), Polyethylene Glycol fibre (PEG), Polyacrylate fibre and Polydimethylsiloxane/Divinylbenzene (PDMS/DVB) fibre.

3.8 Discussion

The main aim of this chapter was to trap and identify the radicals generated from the reaction of the hydroxyl radical with methanol by trapping with PBN and some of of its para-substituted derivatives. In the Fenton reaction Fe(II) reacts with hydrogen peroxide to generate hydroxyl radicals which react with methanol to form hydroxymethyl and methoxy radicals as seen in Figure 3.50 (a and b) (Halpern 1984, Nakagawa 2016). These radicals which are trapped by PBN and the resulting adducts are extracted into chloroform for analysis by GC/MS. The chromatogram (Figure 3.1) shows several peaks which are not present when the experiment is carried out in the absence of methanol, thus confirming that these peaks derived from methanol. However, the corresponding mass spectrum for the methanol radicals does not show the expected molecular ion at m/z 208 (PBN will trap either the hydroxymethyl or methoxy radical at the carbon site). This could be due to the PBN-CH_2OH (or PBN-OCH_3) adducts being highly unstable in the ion source and therefore heavily fragments. Hence, in order to make the PBN methanol adducts more stable, a methyl radical was generated from DMSO (Figure 3.50 (c)) in the same Fenton system. The hydroxylmethyl radicals and methyl radicals in the presence of PBN will react to form $PBN(CH_2OH)(CH_3)$ or $PBN(OCH_3)(CH_3)$ and $PBN(CH_3)_2$ adducts as shown

in Figure 3.50.

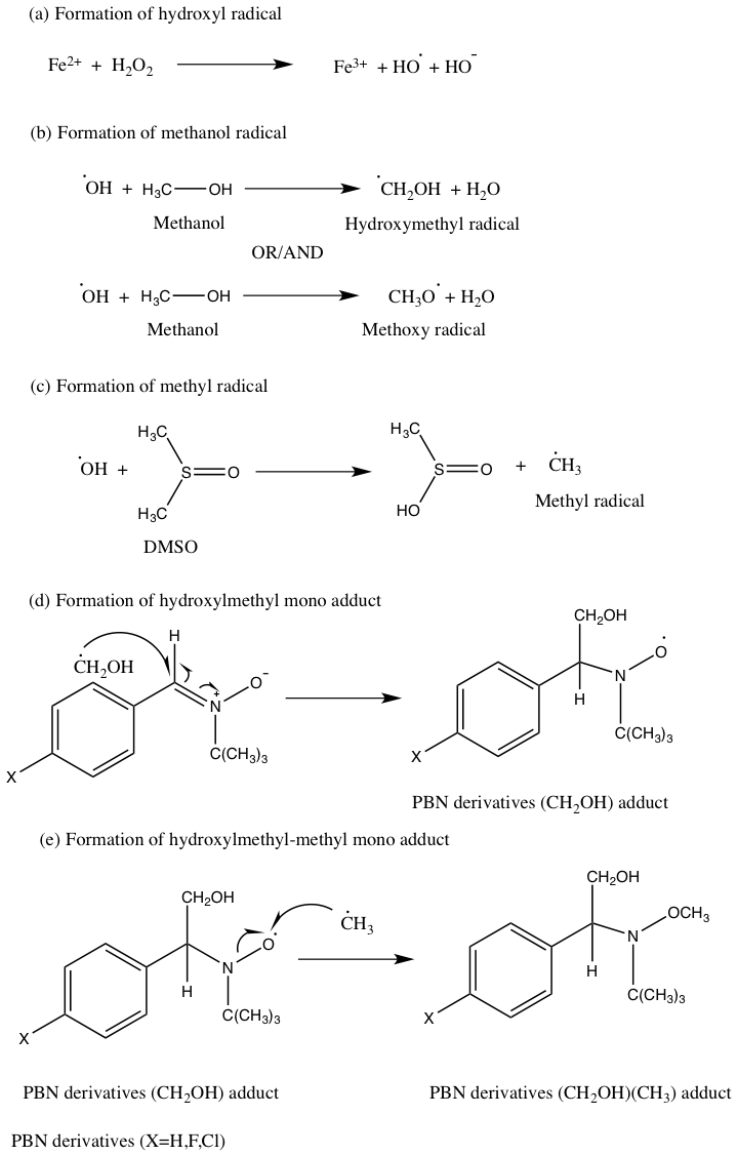

Figure 3.50: (a) Fe(II) reacts with hydrogen peroxide to form hydroxyl radicals and hydroxide ions, (b) hydroxyl radicals react with methanol to form hydroxymethyl radicals and methoxy radicals, (c) hydroxyl radicals react with DMSO to form methyl radicals, (d) hydroxymethyl radicals generated from methanol are trapped by PBN to form PBN hydroxymethyl adducts, and (e) methyl radicals generated from DMSO react with PBN hydroxymethyl adducts to form PBN(CH_2OH)(CH_3) adducts.

The chromatogram (Figure 3.3) for the experiment involving PBN, methanol and DMSO along with other Fenton chemicals shows a strong peak for PBN(CH_3)$_2$ adducts at 5.8 minutes; PBN(CH_2OH)(CH_3) adducts peak at 7.5 minutes. The formation of PBN

dimethyl adducts from acetaldehyde have been been discussed in chapter 4. The mechanism for the formation of dimethyl adducts is same as for the DMSO, hence this section is focused on PBN(CH_2OH)(CH_3) adducts.

The formation of the PBN(CH_2OH)(CH_3) adducts is a two-step mechanism. In the first step hydroxymethyl radicals are trapped by PBN (derivatives) at the carbon site to form PBN(CH_2OH) adducts (Figure 3.50). In the second step methyl radicals are added to the oxygen site to form PBN(CH_2OH)(CH_3) adducts as shown in Figure 3.50. The mass spectrum for PBN(CH_2OH)(CH_3) adducts (Figure 3.7) shows a weak molecular ion at 223 and the fragmentation at m/z 192 is due to loss of hydroxymethyl from the molecular ion. To confirm the formation PBN(CH_2OH)(CH_3) adducts deuterated methanol and deuterated DMSO was used in the Fenton reaction to form PBN(CD_2OH)(CD_3) adducts and the corresponding chromatogram shows a PBN(CD_2OH)(CD_3) adduct peak at 7.4 minutes. The mass spectrum (Figure 3.31) shows a fragment peak m/z 195 and a base peak m/z 139 which is three mass units higher confirming the presence of deuterated methyl and fragment at m/z 123 which is two mass unit higher confirming the presence of CD_2OH when compared to the PBN(CH_2OH)(CH_3) adducts mass spectrum (Figure 3.7). The formation of $^{\bullet}CH_2OH$ adduct and not $^{\bullet}OCH_3$ adduct is in agreement with the previous studies where researchers have detected and identified PBN-CH_2OH and POBN-CH_2OH adducts using GC/MS and ESR spectroscopy has been done (Kadiiska & Mason 2000, Skrzydlewska et al. 2000, Castro et al. 2002). Mason et al. have also identified and quantified spin trapped radicals generated from DMSO my using POBN, LC/ESR and LC/MS (Qian et al. 2005).

Further to confirm the formation of PBN(CH_2OH)(CH_3) adducts deuterated methanol (CD_3OD) and deuterated DMSO (DMSO-d_6) was used in different combinations (such as CD_3OD & DMSO, CH_3OH & DMSO-d_6) with PBN derivatives. The chromatogram (Figure 3.4.1) for the experiment involving CD_3OD & DMSO showed a PBN(CD_2OH)(CH_3) adducts peak at 7.4 minutes and the corresponding mass spectrum 3.4.1 shows a strong fragment at m/z 192 for the PBN(CH_3) cation. When the mass spectrum of the PBN-(CD_2OH)(CH_3) adducts was compared to the PBN(CH_2OH)(CH_3) adducts the only difference was a fragment at m/z 123 which is 2 mass units higher, confirming the presence of two deuterium from the deuterated methanol. From the mass spectrum interpretation, a fragment at m/z 123 was identified as C_6H_5-$^{+}$CH-CD_2OH (section 3.4.1). Hence, it can be confirmed that CH_2OH radicals are generated from the methanol and trapped by PBN to form PBN(CH_2OH)(CH_3) adducts.

To confirm $^{\bullet}CH_3$ radicals are generated from DMSO deuterated DMSO was used. Deuterated DMSO will generate $^{\bullet}CD_3$ radicals which are trapped by PBN to form PBN-(CH_2OH)(CD_3) adducts. The mass spectrum (Figure 3.25) shows a peak at m/z 195 which is three mass units higher than the PBN(CH_2OH)(CH_3) adducts confirming the generation

of $^{\bullet}CH_3$ radicals and the formation of PBN(CH_2OH)(CH_3) adducts. The base peak at m/z 139 is also three mass units higher confirming the presence of deuterated methyl in the base peak. Different PBN derivatives such PBN-d_6, 4-FPBN and 4-ClPBN were used to confirm the formation of hydroxymethyl methyl adducts and all showed similar results.

The chromatogram (Figure 3.3) shows other peaks of unreacted PBN, PBN-OH adducts and benzaldehyde oxime peaks. Corresponding unreacted PBN and the oxime peaks have been found in all the experiments involving PBN and its derivatives. However, the presence of PBN-OH adducts is not very commonly seen unless there is no secondary source of radicals (methanol and DMSO in this case) as seen in the method development (section 2.8) . In this experiment hydroxyl radicals generated from hydrogen peroxide react with PBN to form hydroxyl adducts. The mass spectrum (Figure 2.8.1.1) for the PBN-OH adducts shows a molecular ion at m/z 193 suggesting that the hydroxyl radical is not trapped at the preferred carbon site or at the oxygen site. The other possibility would be the removal of hydrogen from the ortho or meta position of the ring and, subsequently, the addition of OH to the ring. The OH radicals were not added to the para position of the PBN as OH adducts were seen with the other PBN derivatives as having para substitution (section 2.8.1.1). A similar result was observed with the PBN-d_6 with the molecular ion at m/z 198 for PBN-d_6-OH adducts suggesting a loss of deuterium from the ring and, subsequently, the addition of a hydroxyl radical. Hence, it can be confirmed the OH adducts can be either 2-hydroxy PBN or 3-hydroxy PBN. The formation of PBN-OH adduct in the Fenton reaction was shown by Mason et al., however, the major product in this instance was identified as 4-hydroxyPBN and 2-hydroxyPBN as minor product (Reinke et al. 2000).

Hence these results suggest that the methanol radicals can forms stable PBN adducts in presence of methyl radicals which can be easily analysed by GC/MS by liquid liquid extraction using chloroform as the solvent. However, the chromatogram shows the presence of other products from the reaction and also, if the Fenton reaction mixture is not carefully extracted in chloroform, it can deteriorate the column. Hence, to achieve accurate sample analysis, a combined method of continuous quick sampling and extraction is required. HS-SPME integrates sampling, extraction and concentration into a single solvent-free step which was used for the analysis of hydroxymethyl methyl adducts.

To check the sensitivity of HS-SPME for the PBN(CH_2OH)(CH_3) adduct different SPME fibres such as polyethylene Glyco (PEG), polyacrylate and polydimethylsiloxane/ divinylbenzene (PDMS/DVB) along with CARB/PDMS were used to collect the sample from the headspace. All these fibres showed a varying affinity towards the PBN(CH_2OH)(CH_3) adducts; however, the CARB/PDMS showed a higher affinity compared to others when peak areas for PBN (CH_2OH)(CH_3) adducts obtained from different fibres were compared (Figure 3.49). CARB/PDMS fibre is used to trap a wide range of volatile compounds.

This fibre was used to extract the PBN(CH_2OH)(CH_3) adducts and the chromatogram (Figure 3.40) showed the presence of the PBN dimethyl adducts and PBN hydroymethyl methyl adducts which was confirmed by using the deuterated methanol and DMSO as described in section 3.7.6. The mass spectrum for the PBN(CH_2OH)(CH_3) adducts and the PBN(CD_2OH)(CD_3) adducts was identical with the expected mass difference due to the presence of deuterium. The chromatogram also showed the presence of other peaks such as benzaldehyde and peaks that occurred due to the fibre. However, the intensity of these peaks was very low compared to the dimethyl and hydroxymethyl methyl adducts. Due to its limited life span and number of usages the fibre can degrade with time and can interfere in the analysis.

This novel technique for trapping methanol radicals in presence of methyl radicals, when combined with HS-SPME GC/MS, has the potential to be a powerful technique for the detection of free radicals generated in a range of environmental and biological systems.

Chapter 4

Analysis of spin trapped methyl radical from acetaldehyde

4.1 Introduction

Acetaldehyde (ethanal) is a highly reactive and toxic molecule which can cause damage to cells and the genome. Acetaldehyde has been classified as a class 1 toxin (human carcinogen) by the World Health Organization. The sources of acetaldehyde can be both natural and manufactured. The main source of acetaldehyde is the consumption of ethanol as *in vivo* ethanol is absorbed by the gastrointestinal tract and 90% of it is metabolized in the liver to acetaldehyde by alcohol dehydrogenase. Acetaldehyde may then be further converted into acetate by acetaldehyde dehydrogenase. These processes are considered to be a detoxification as acetate is a relatively innocuous compound. There are other routes of alcohol and acetaldehyde metabolism which are associated with the production of free radicals. For example ethanol oxidation by hepatic microsomal P450 enzymes is associated with the production of the superoxide anion and 1-hydroxyethyl radical. Similarly, it is has been shown that acetaldehyde oxidation to acetate can generate free radicals either by some chemical and enzymatic systems. Systems that can oxidize acetaldehyde to free radical intermediates include xanthine oxidase (Puntarulo & Cederbaum 1989), aldehyde oxidase (Rajasinghe et al. 1990), mitochondria (Boh et al. 1982), and microsomes (Gonthier et al. 1991). The importance of free radical mechanisms in the toxic effects of ethanol is now apparent as acetaldehyde is ubiquitously present and increased levels are linked with neurological pathologies such as stroke and Alzheimer's disease.

Initially, only acetyl radical and hydroxyl radicals were detected from the oxidation of acetaldehyde (Albano et al. 1994), however, Nakao et al. (2000) successfully showed the presence of methyl radicals by enzymatic oxidation of acetaldehyde in presence of Fe(II)/EDTA. They also showed that oxidation of acetaldehyde by xanthine oxidase and

in presence of Fe(II)/EDTA generates hydroxyl radicals which react with acetaldehyde to generate acetyl radicals which on decarbonylation produce methyl radicals (Nakao et al. 2000*a*). These radicals (methyl, acetyl and hydroxyl) were trapped by using the spin trap POBN and identified by EPR spectroscopy. The EPR spectrum generated similar hyperfine splitting constants for the different trapped radicals. Thus, to confirm trapping of the methyl radical ^{13}C acetaldehyde was used. This generated an additional line resulting from coupling to the ^{13}C (I=1/2) atom. These radicals were also detected by using LC/MS/MS (Nakao et al. 2000*b*). Podmore et al. generated methyl radical from DMSO which was trapped by POBN and the POBN methyl adducts was detected by GC/MS (Mistry et al. 2008).

In this chapter methyl radicals have been generated from acetaldehyde and trapped by PBN using Fenton type chemistry. The resulting adduct formed in the Fenton reaction was extracted by three different methods, which are: (i) Direct chloroform extraction, (ii) Solid Phase MicroExtraction (SPME) and (iii) Single Droplet MicroExtraction (SDME). As described in the material and methods, the extract was subjected to GC/MS for analysis and the interpretation of the results is mentioned below.

4.2 Chloroform Extraction

Selected PBN derivatives were used in a Fenton system for trapping of radicals generated from acetaldehyde. A portion of the sample was extracted into chloroform for analysis, as described in the materials and methods section. GC/MS analysis showed a peak corresponding to a PBN dimethyl adduct (X-PBN-$(CH_3)_2$; described previously in chapter 3) along with unreacted PBN and other adducts/byproduct formed during the reaction. To confirm the identity of the adduct deuterated acetaldehyde was used which showed a shift in m/z in the EI mass spectrum due to the presence of deuterium. The analysis and interpretation of the results are shown below.

4.2.1 Chromatogram

Methyl radicals generated from acetaldehyde in the Fenton system as described in Chapter 2 (Materials and Methods) was trapped by PBN. The reaction mixture was extracted in chloroform and injected in GC/MS for its analysis.

4.2.1.1 PBN

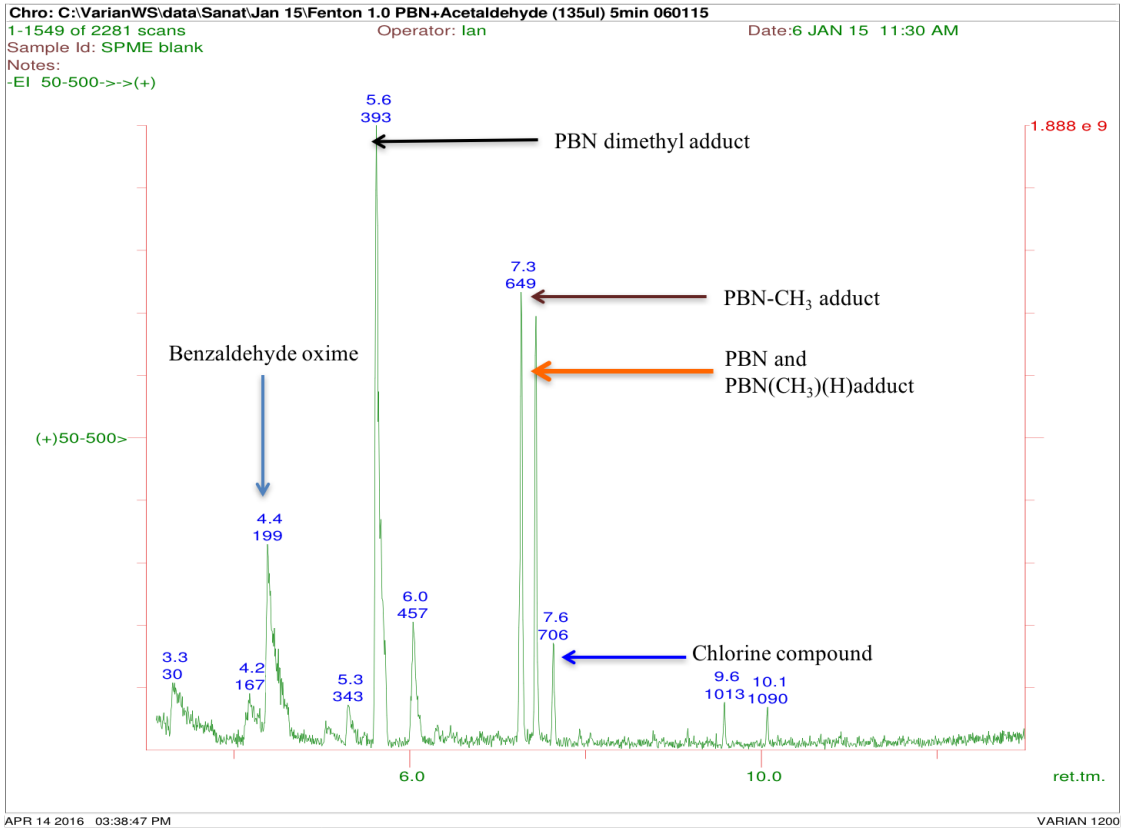

Figure 4.1: Total ion chromatogram (TIC) obtained from the GC/MS analysis of the Fenton reaction mixture containing PBN and acetaldehyde.

TIC (Figure 4.1) shows the presence of benzaldehyde oxime (R_t 4.4 minutes, see section 2.8.1.2), PBN dimethyl adduct ($PBN(CH_3)_2$; R_t 5.6 minutes; see section 3.3.3.1), PBN-CH_3 adduct (R_t 7.3; see section 4.4.1), $PBN(CH_3)(H)$ adduct (R_t 7.4 minutes; 4.5.1), PBN (R_t 7.4 minutes; see section 2.7.1) and a dichlorinated compound (1,1-dichloro-2-phenylethene) (R_t 7.6 minutes; see section 4.6.1).

4.2.1.2 Deuterated PBN-d_6

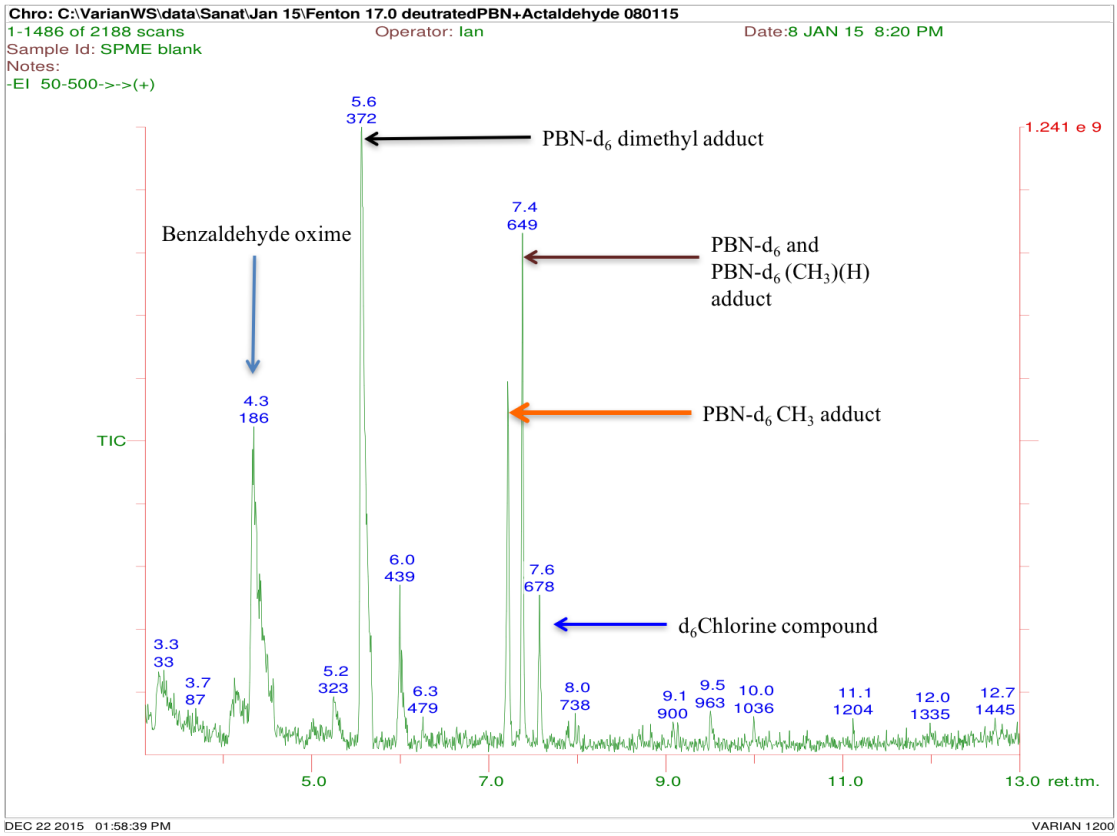

Figure 4.2: Total ion chromatogram (TIC) obtained from the GC/MS analysis of the Fenton reaction mixture containing PBN-d_6 and acetaldehyde.

The TIC (Figure 4.2) obtained from the GC/MS analysis of the Fenton reaction mixture containing PBN-d_6 and acetaldehyde shows the presence of deuterated benzaldehyde oxime (R_t 4.4 minutes; see section 2.8.1.2), PBN-d_6 dimethyl adducts (PBN-$d_6(CH_3)_2$; R_t 5.6 minutes; see section 3.3.3.2), PBN-d_6 monomethyl adducts (PBN-d_6CH_3; R_t 7.2 minutes; 4.4.2), PBN-$d_6(CH_3)(H)$ (R_t 7.4 minutes; see section 4.5.1), PBN-d_6 (R_t 7.4 minutes; see section 2.7.2) and a deuterated dichlorinated compound (R_t 7.6 minutes; 4.6.1).

4.2.1.3 4-FPBN

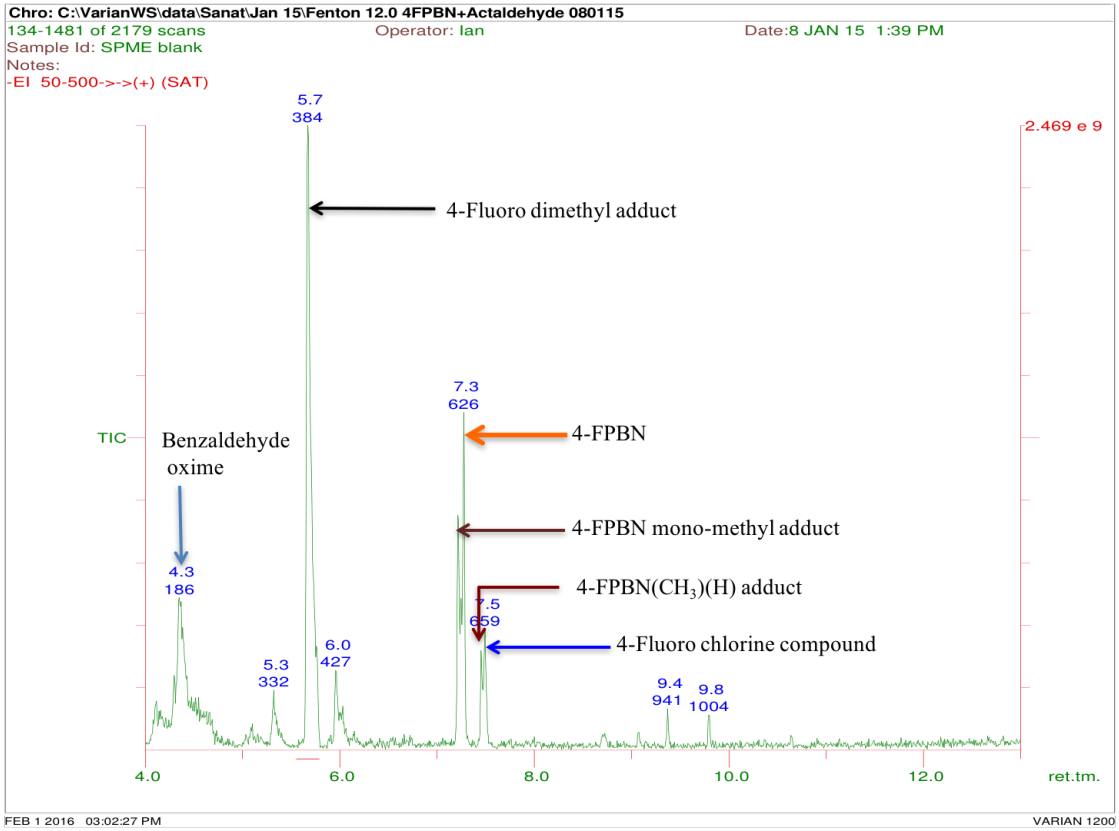

Figure 4.3: Total ion chromatogram (TIC) obtained from the GC/MS analysis of the Fenton reaction mixture containing 4-FPBN and acetaldehyde.

TIC (Figure 4.3) shows presence of 4-fluorobenzaldehyde oxime (R_t 4.3 minutes; see section 2.8.1.2), 4-FPBN dimethyl adducts (4-FPBN$(CH_3)_2$; R_t 5.7 minutes; see section 3.3.3.3), 4-FPBN monomethyl adducts (4-FPBN-CH_3; R_t 7.2 minutes; section 4.4.3), 4-FPBN(CH_3)(H) adducts (R_t 7.5 minutes; 4.5.3), 4-FPBN (R_t 7.3 minutes; section 2.7.3) and 4-fluoro dichlorinated compound (R_t 7.5 minutes; section 4.6.1).

4.2.1.4 4-ClPBN

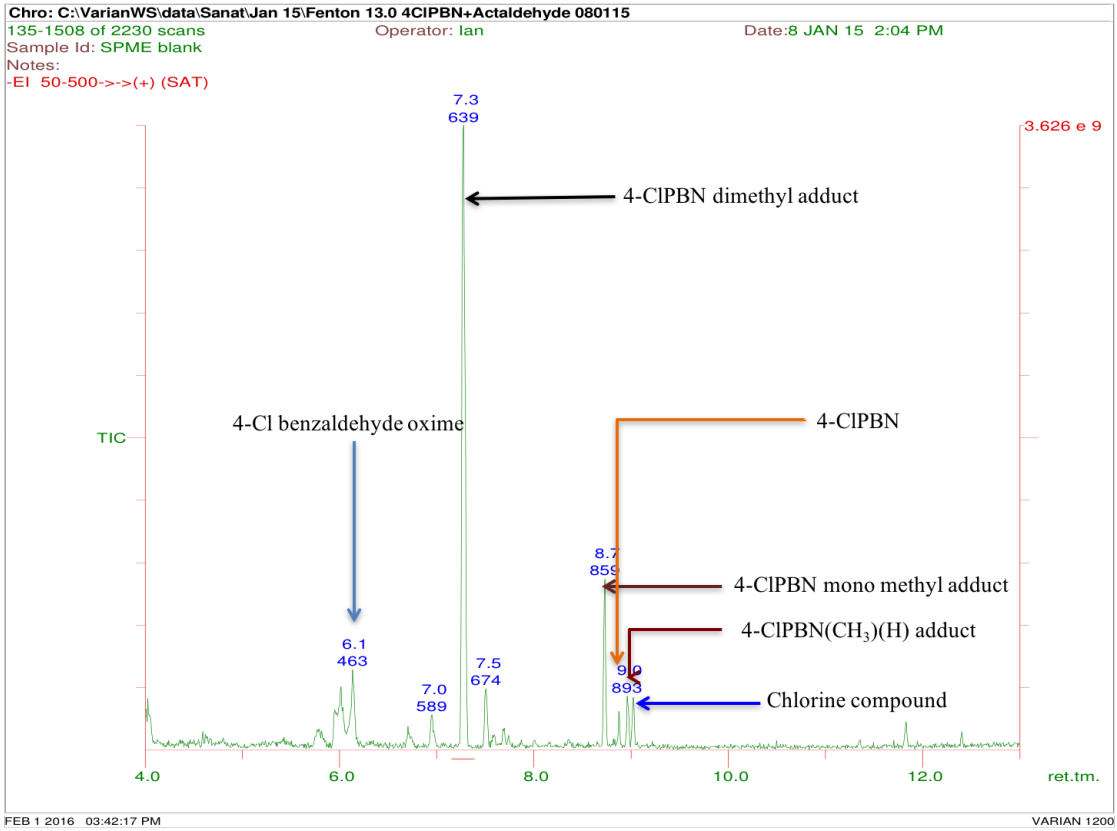

Figure 4.4: Total ion chromatogram (TIC) obtained from the GC/MS analysis of the Fenton reaction mixture containing 4-ClPBN and acetaldehyde.

TIC Figure 4.4 shows presence of 4-chlorobenzaldehyde oxime (R_t 6.1 minutes; see section 2.8.1.2), 4-ClPBN dimethyl adducts (4-ClPBN$(CH_3)_2$; R_t 7.3 minutes; see section 3.3.3.4), 4-ClPBN monomethyl adducts (4-ClPBN-CH_3; R_t 8.7 minutes; section 4.4.4), 4-ClPBN(CH_3)(H) adducts (R_t 9.0 minutes; section 4.5.4), 4-ClPBN (R_t 9.0 minutes; section 2.7.4) and 4-chloro dichlorinated compound (R_t 9.0 minutes; section 4.6.1).

4.3 EI mass spectra of dimethyl adduct

4.3.1 $PBN(CH_3)_2$ adduct

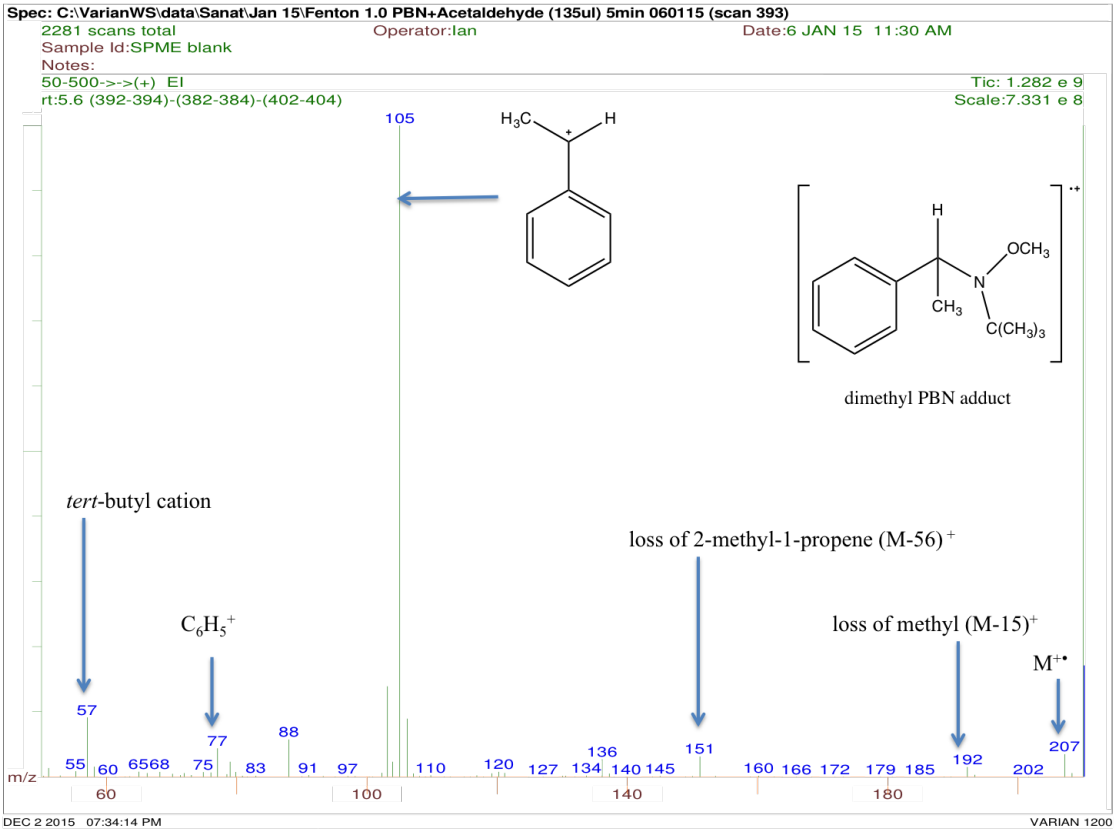

Figure 4.5: Electron ionization (EI) mass spectrum of peak at 5.6 minutes (from chromatogram in Figure 4.1) corresponding to $PBN(CH_3)_2$. Structure structure given in the top right is the molecular ion of $PBN(CH_3)_2$, i.e. corresponding to the peak at m/z 207.

The EI mass spectrum shown in Figure 4.5 corresponds to the PBN dimethyl adduct ($PBN(CH_3)_2$). As discussed in chapter 3, section 3.3.3.1 the mass spectrum for the PBN dimethyl adduct from acetaldehyde and DMSO shows a exact fragments.

4.3.2 Deuterated PBN-$d_6(CH_3)_2$ adduct

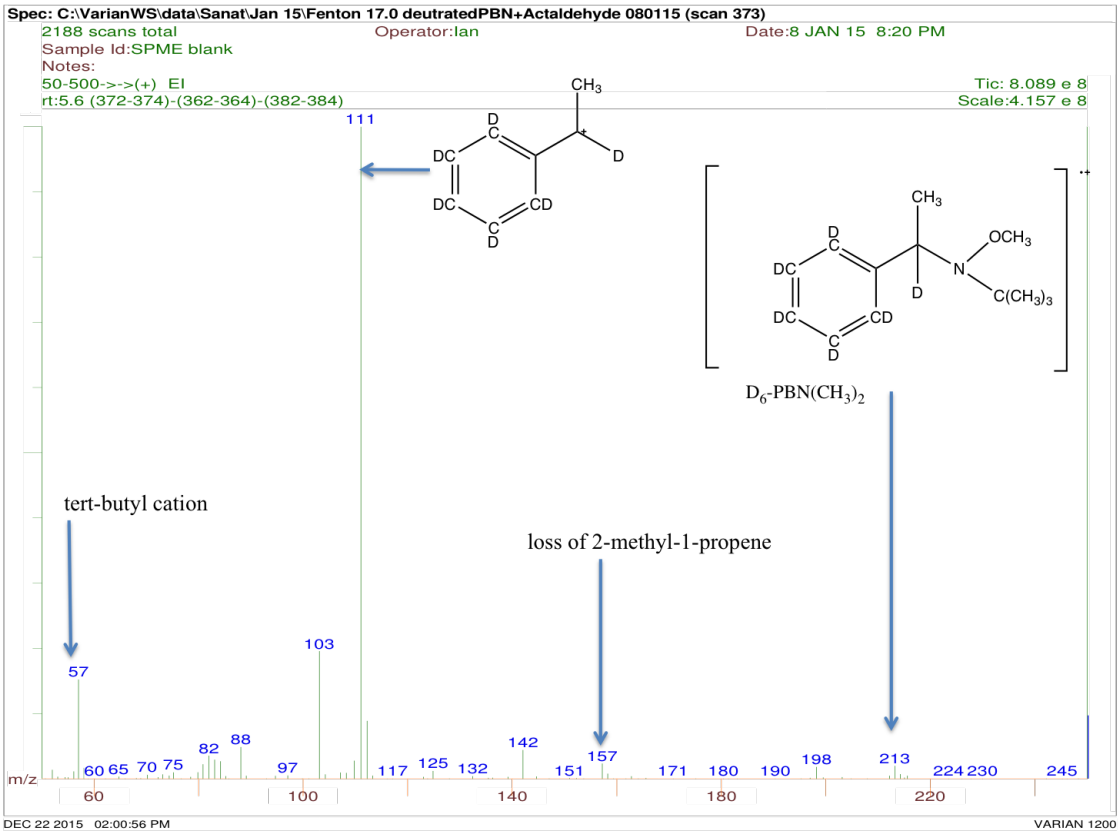

Figure 4.6: Electron ionization (EI) mass spectrum of peak at 5.6 minutes (from chromatogram in Figure 4.2) corresponding to PBN-$d_6(CH_3)_2$.

The EI mass spectrum shown in Figure 4.6 is for the PBN-d_6 dimethyl adduct. As discussed in chapter 3, section 3.3.3.2 the mass spectrum for the PBN-d_6 dimethyl adduct from acetaldehyde and DMSO shows exact fragments.

4.3.3 4-FPBN$(CH_3)_2$ adduct

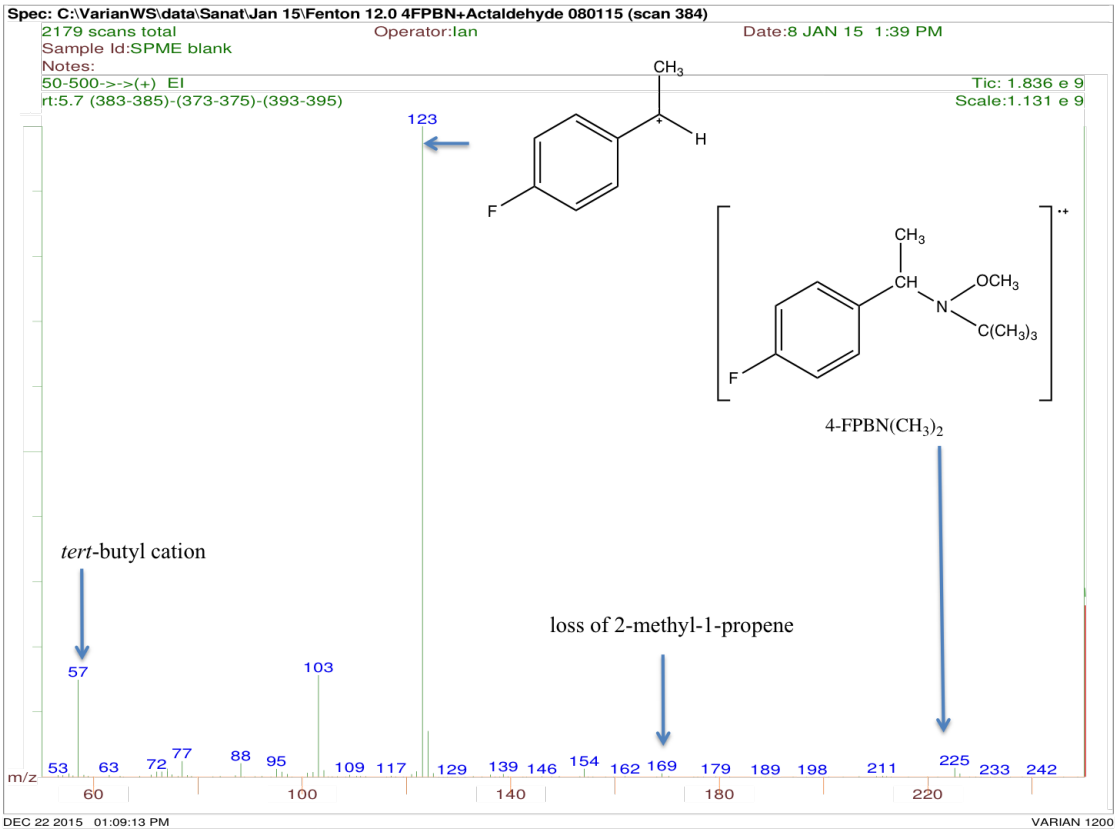

Figure 4.7: Electron ionization (EI) mass spectrum of peak at 5.7 minutes (from chromatogram in Figure 4.3) corresponding to 4-FPBN $(CH_3)_2$.

The EI mass spectrum shown in Figure 4.7 is for the 4-FPBN dimethyl adduct. As discussed in chapter 3, section 3.3.3.3 the mass spectrum for the 4-FPBN dimethyl adduct from acetaldehyde and DMSO shows exact fragments.

4.3.4 4-ClPBN$(CH_3)_2$ adduct

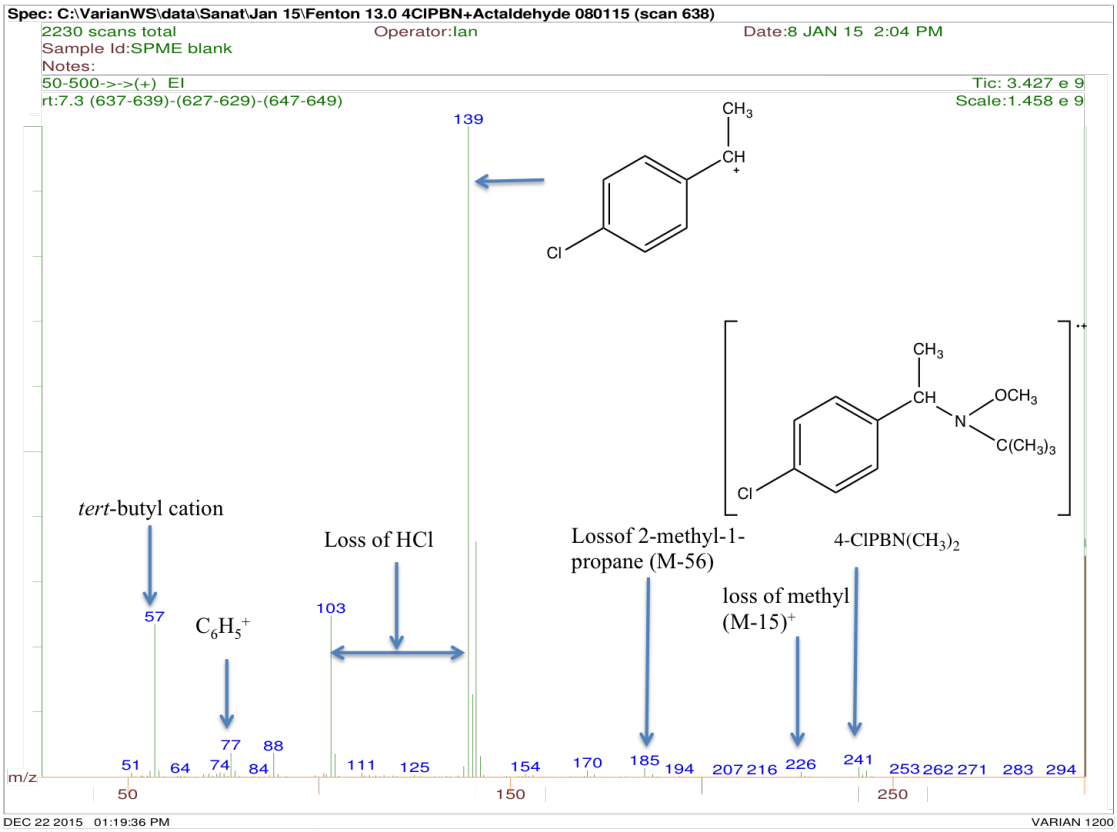

Figure 4.8: Electron ionization (EI) mass spectrum of peak at 7.3 minutes (from chromatogram in Figure 4.4) corresponding to 4-ClPBN $(CH_3)_2$.

The EI mass spectrum shown in Figure 4.8 is for the 4-PBN dimethyl adduct. As discussed in chapter 3, section 3.3.3.4 the mass spectrum for the 4-ClPBN dimethyl adduct from acetaldehyde and DMSO shows exact fragments.

4.4 EI mass spectrum of monomethyl adduct

4.4.1 PBN-CH_3 adduct at 7.3 minutes

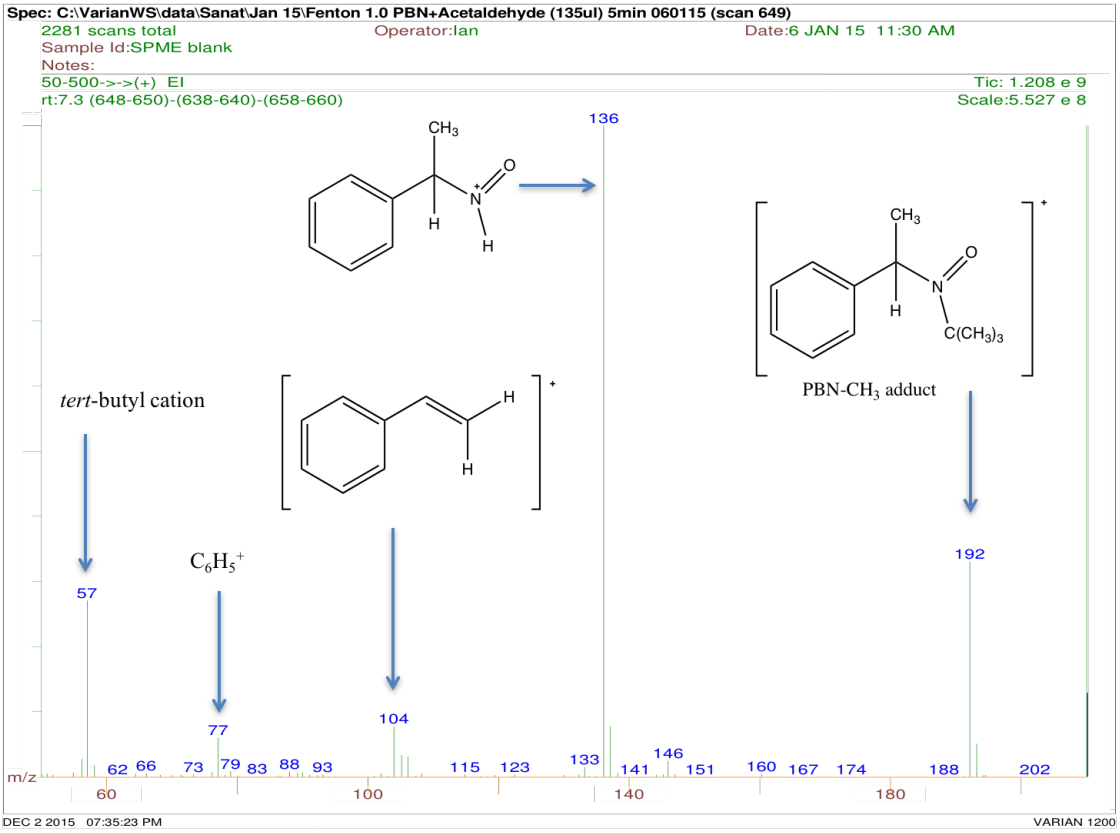

Figure 4.9: Electron ionization (EI) mass spectrum of the peak at 7.3 minutes (from the chromatogram in Figure 4.1) believed to correspond to a PBN monomethyl adduct.

The EI mass spectrum in Figure 4.9 is from the peak with retention time 7.3 minutes (from the chromatogram in Figure 4.1). Assuming the "molecular ion" is present at m/z 192 then the PBN adduct must contain an unpaired electron and thus is likely to be a nitroxide. The peak at m/z 193 is clearly an isotope peak as it has approx. 14% of the intensity of that at m/z 192 (due to ^{12}C and ^{14}N atom). The species responsible for this peak in the chromatogram is also clearly a methyl adduct to PBN (see subsequent section 4.7.3 for proof). The base peak fragment at m/z 136 is due to the loss of 2-methyl-1-propene from the "molecular ion". Fragment at m/z 146 could be possible due to the loss of NOH and some unusual rearrangement of *tert*-butyl group attaching to the chiral carbon, fragment at m/z 104 is probably due to dissociation of the "molecular ion" at the

C-N bond with additional loss of a hydrogen atom (loss of tBuNOH from the molecular ion). The fragments at m/z 77 and m/z 57 are for the phenyl cation and *tert*-butyl cation respectively.

4.4.2 PBN-d_6CH_3 adduct at 7.2 minutes

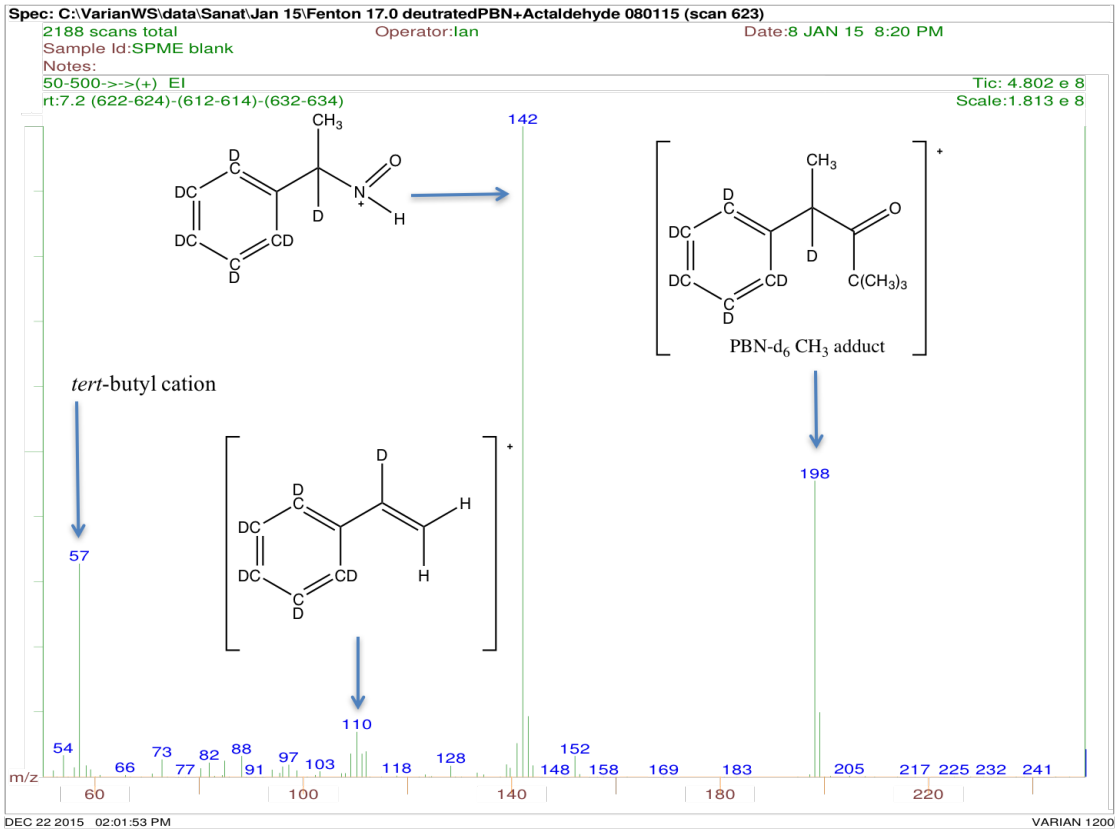

Figure 4.10: Electron ionization (EI) mass spectrum of the peak at 7.2 minutes (from the chromatogram in Figure 4.2) corresponding to PBN-d_6 monomethyl adduct.

The EI mass spectrum showed in Figure 4.10 corresponds to the peak with retention time 7.2 minutes (from the chromatogram in Figure 4.2) with a "molecular ion" at m/z 198. The peak at m/z 198 corresponds to a PBN-d_6 monomethyl adduct with a fragmentation pattern similar to that of the PBN-CH_3 adduct shown in section 4.4.1. Fragment m/z 152 is possibly due to the loss of methyl and NOH from m/z 198. The base peak at m/z 142 is due to the loss of 2-methyl-1-propene from m/z 198; m/z 82 corresponds to deuterated phenyl cation and m/z 57 to the *tert*-butyl cation.

4.4.3 4-FPBN CH_3 adduct at 7.2 minutes

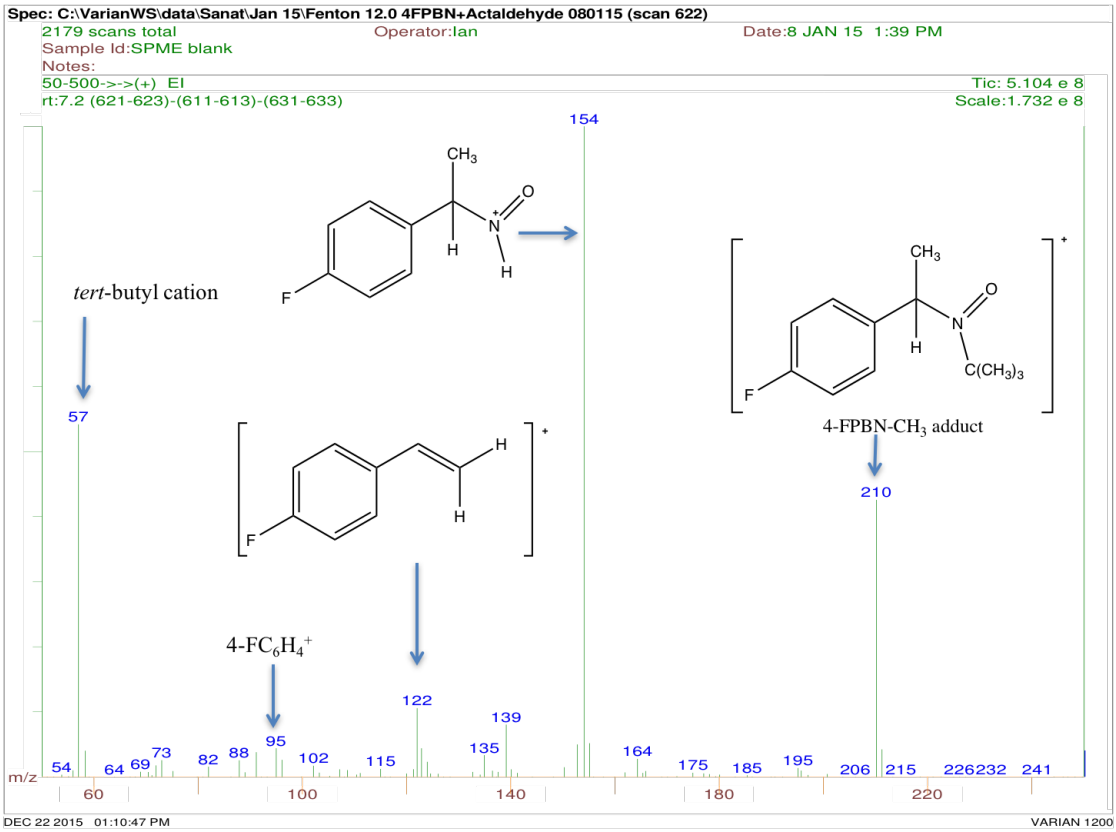

Figure 4.11: Electron ionization (EI) mass spectrum of the peak at 7.2 minutes (from the chromatogram in Figure 4.3) corresponding to 4-FPBN monomethyl adduct.

The EI mass spectrum for peak with retention time 7.2 minutes (from the chromatogram in Figure 4.3) is shown in Figure 4.11. The mass spectrum shows a "molecular ion" at m/z 210. This is in agreement with the previous mass spectra for PBN-CH_3 and PBN-d_6CH_3 (an increase of 18 m/z units from PBN-CH_3). The fragment at m/z 195 is due to the loss of a methyl radical from m/z 210, with m/z 164 possibly being due to the loss of methyl and NOH from m/z 210. The base peak at m/z 154 is due to the loss of 2-methyl-1-propene from the "molecular ion" (M-56). The fragment at m/z 139 is possibly due to the loss of a methyl radical from base peak, whereas the fragment at m/z 122 corresponds to the cation showed in Figure 4.11; m/z 95 may be assigned to 4-$FC_6H_4^+$ and m/z 57 to the *tert*-butyl cation.

4.4.4 4-ClPBN-CH_3 adduct at 8.7 minutes

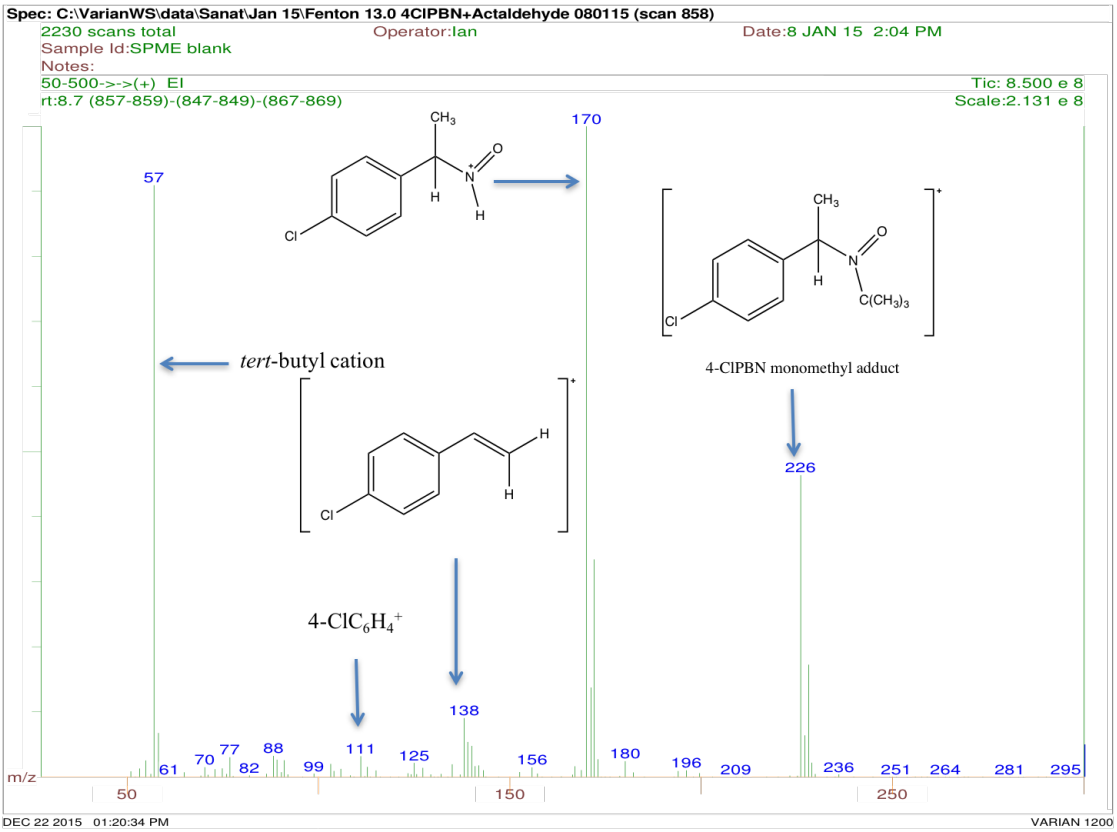

Figure 4.12: Electron ionization (EI) mass spectrum of the peak at 8.7 minutes (from the chromatogram in Figure 4.4) corresponding to 4-ClPBN monomethyl adduct.

The EI mass spectrum for peak with retention time 8.7 minutes (from the chromatogram in Figure 4.4) is shown in Figure 4.12. The mass spectrum shows a "molecular ion" at m/z 226/228. This is in agreement with the previous mass spectra for PBN-CH_3 and PBN-d_6CH_3 (an increase of 34 m/z units from PBN-CH_3). The fragment at m/z 180/182 possibly being due to the loss of methyl and NOH from m/z 226. The base peak at m/z 170/172 is due to the loss of 2-methyl-1-propene from the "molecular ion" (M-56). The fragment at m/z 122 corresponds to the cation showed in Figure 4.11; m/z 111/113 may be assigned to 4-$ClC_6H_4^+$ and m/z 57 to the *tert*-butyl cation

4.5 EI mass spectrum of other methyl adducts

The chromatogram for the Fenton reaction involving PBN derivatives and acetaldehyde shows more than one peak corresponding to a monomethyl adduct. However, these peaks having identical mass spectra but different retention times suggest they are different PBN adducts. Presumably PBN methyl adduct eluted later have trapped methyl radical at the benzyl carbon site and hydrogen at the oxygen site. By coincidence the other methyl peaks in some cases appear to overlap those of unreacted starting material.

4.5.1 PBN(CH_3)(H) adduct at 7.4 minutes

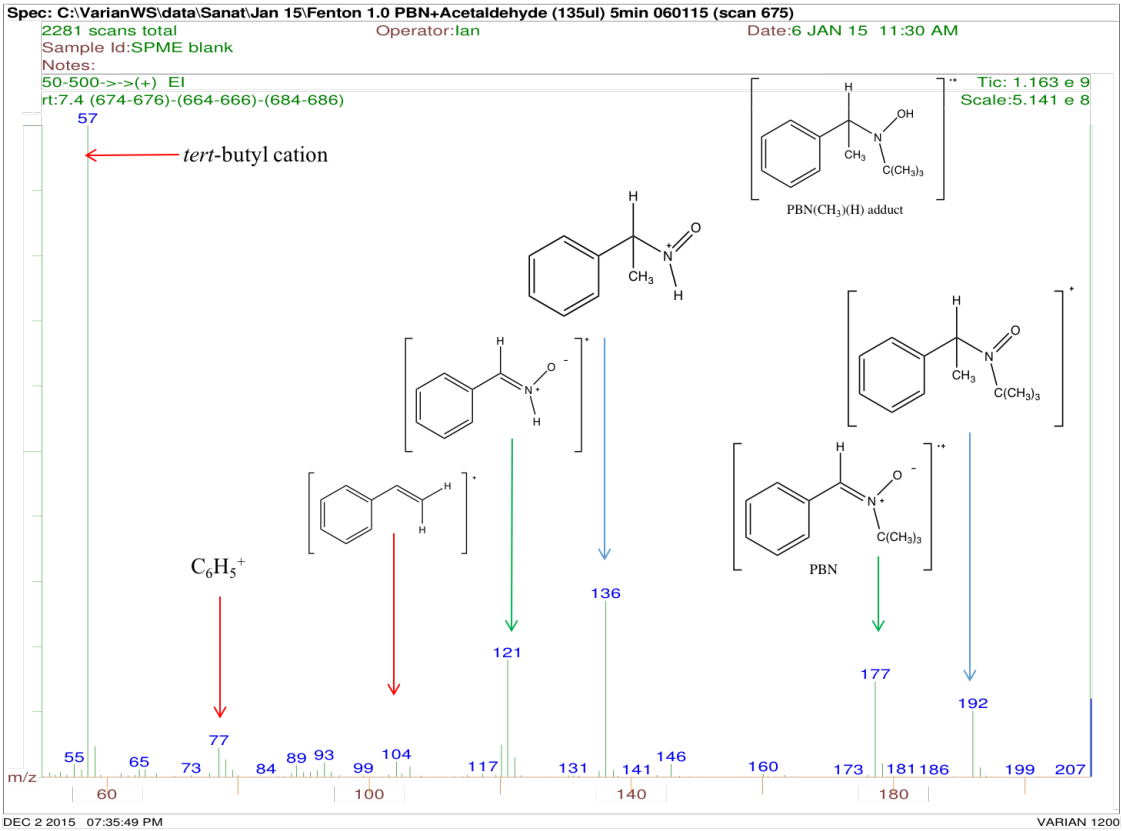

Figure 4.13: Electron ionization (EI) mass spectrum of peak at 7.4 minutes (from the chromatogram in Figure 4.1) believed to correspond to a PBN (CH_3)(H) adduct (structure shown in top right) and unreacted PBN. Peaks labelled in blue are for the PBN(CH_3)(H) adduct, peaks labelled in green are for PBN and peaks labelled in red are common peaks.

The EI mass spectrum in Figure 4.13 is from the peak with retention time 7.4 minutes (from the chromatogram in Figure 4.1). The mass spectra correspond to the PBN(CH_3)(H) adduct structure shown in top right in Figure 4.13. The mass spectrum doesn't show a molecular ion at m/z 193. The fragment at m/z 192 is for the cation shown in Figure 4.13 formed due to loss of hydrogen from the oxygen site. The fragment pattern has a peak at m/z 136 corresponding to loss of 2-methyl-1-propene from the peak at m/z 192. The peak at m/z 121 may be derived from the EI mass spectra of both unreacted PBN and PBN(CH_3)(H) adduct. The peak at m/z 77 corresponds to the phenyl cation and the base peak at m/z 57 to the *tert*-butyl cation both are derived from the EI mass spectra of PBN and PBN(CH_3)(H) adduct. As this PBN(CH_3)(H) adduct and unreacted PBN (section 2.7.1) appear to have the same retention time they overlap.

4.5.2 PBN-d_6 (CH_3)(H) adduct at 7.4 minutes

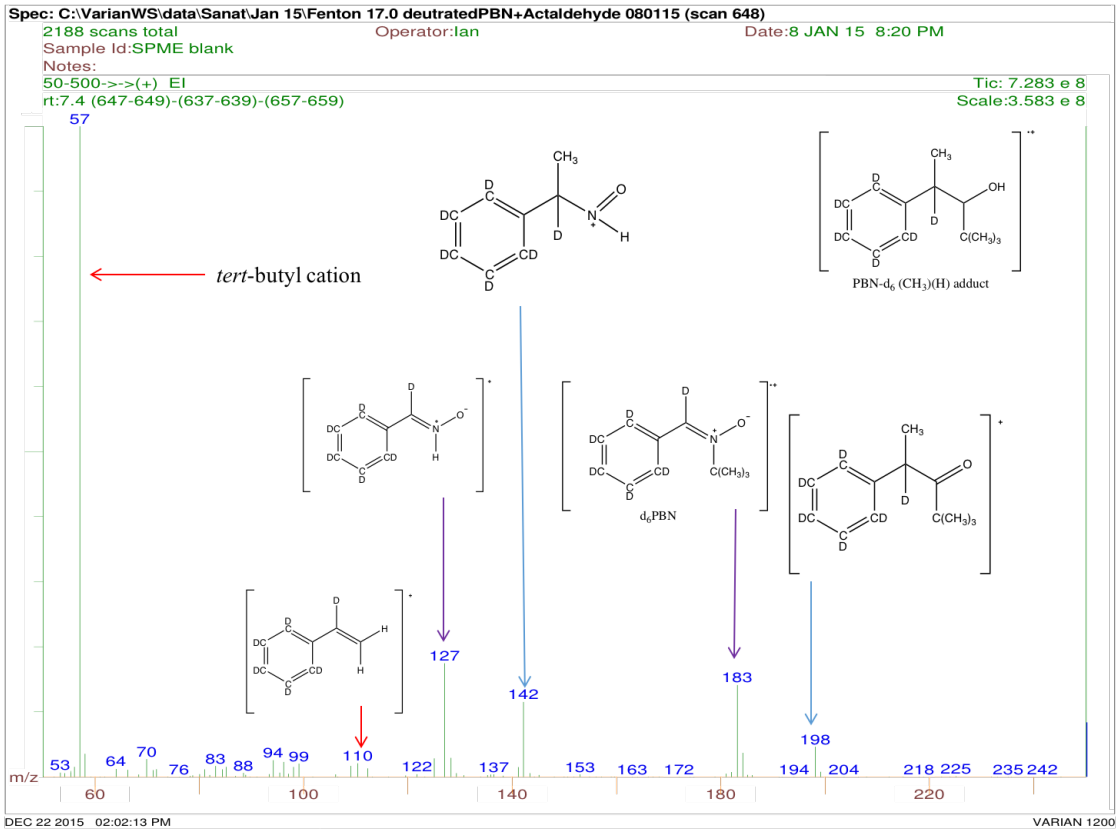

Figure 4.14: Electron ionization (EI) mass spectrum of peak at 7.4 minutes (from the chromatogram in Figure 4.2) believed to correspond to a PBN-d_6(CH_3)(H) adduct (structure shown in top right). Peaks labelled in blue are for the PBN-d_6(CH_3)(H) adduct, peaks labelled in purple are for PBN-d_6 and peaks labelled in red are the common peaks.

The EI mass spectrum in Figure 4.14 is from the peak with retention time 7.4 minutes (from the chromatogram in Figure 4.2). The mass spectrum corresponds to the PBN-d_6 (CH_3)(H) adduct structure shown in top right in Figure 4.14 and doesn't show a molecular ion at m/z 199. The fragment at m/z 198 is for the cation shown in Figure 4.14 formed due to loss of hydrogen from the oxygen site. The fragmentation pattern shows a peak at m/z 142 is due to loss of 2-methyl-1-propene from the m/z 198. The peak at m/z 127 is derived from the EI mass spectra of both unreacted PBN-d_6 and PBN-d_6(CH_3)(H). The base peak at m/z 57 corresponds to the *tert*-butyl cation. As the PBN-d_6 (CH_3)(H) adduct and unreacted PBN-d_6 (section 2.7.2) appear to have same retention time they overlap.

4.5.3 4-FPBN(CH_3)(H) adduct at 7.5 minutes

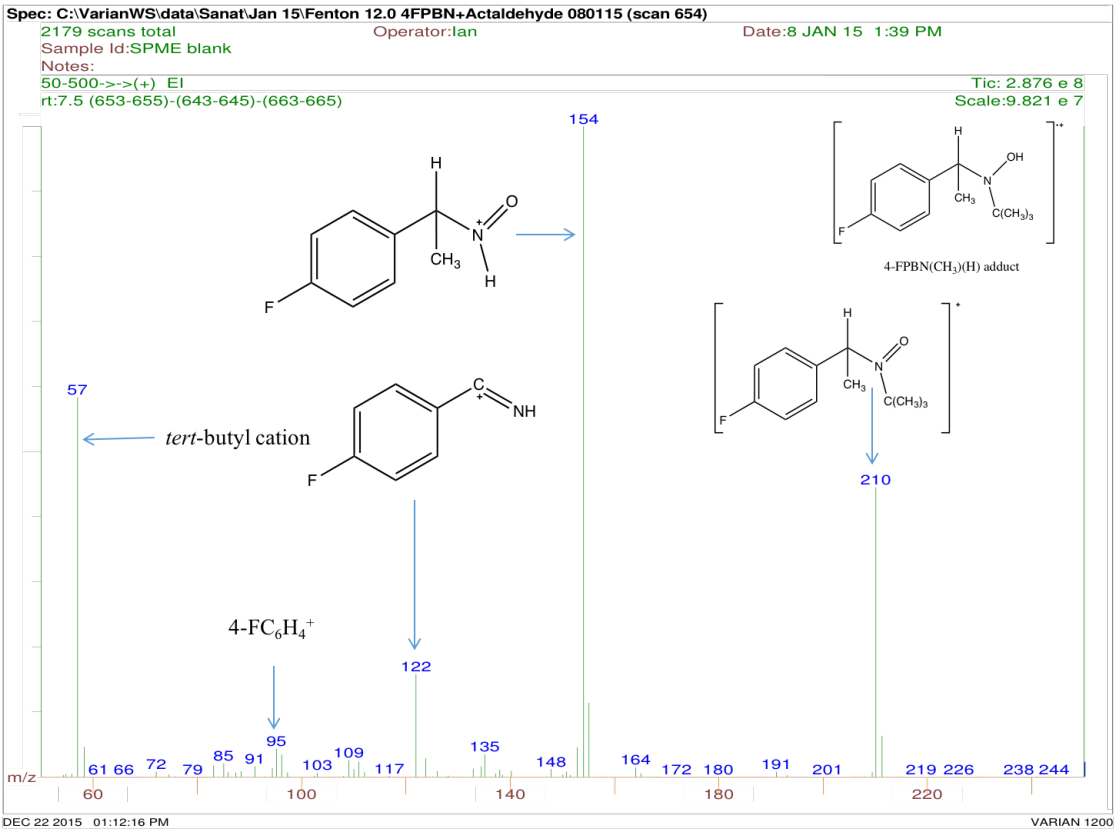

Figure 4.15: Electron ionization (EI) mass spectrum of the peak at 7.5 minutes (from the chromatogram in Figure 4.3) corresponding to 4-FPBN(CH_3)(H) adduct (structure shown in top right).

The EI mass spectrum for peak with retention time 7.5 minutes (from the chromatogram in Figure 4.3) is shown in Figure 4.15. The mass spectrum doesn't shows a molecular ion at m/z 211 for 4-FPBN(CH_3)(H) adduct. The fragment at m/z 210 is for structure shown in Figure 4.15 formed due to loss of hydrogen from the oxygen site. The base peak at m/z 154 is due to the loss of 2-methyl-1-propene from the m/z 210; the fragment at m/z 122 is due to the cation shown in Figure 4.15; m/z 95 corresponds to 4-$FC_6H_4^+$ and m/z 57 to the *tert*-butyl cation. It is clear that there is no contribution from unreacted 4FPBN in this EI mass spectrum. This is due to the fact that unreacted 4-FPBN has clearly separated from this methyl adduct on the chromatogram.

4.5.4 4-ClPBN(CH_3)(H) adduct at 9.0 minutes

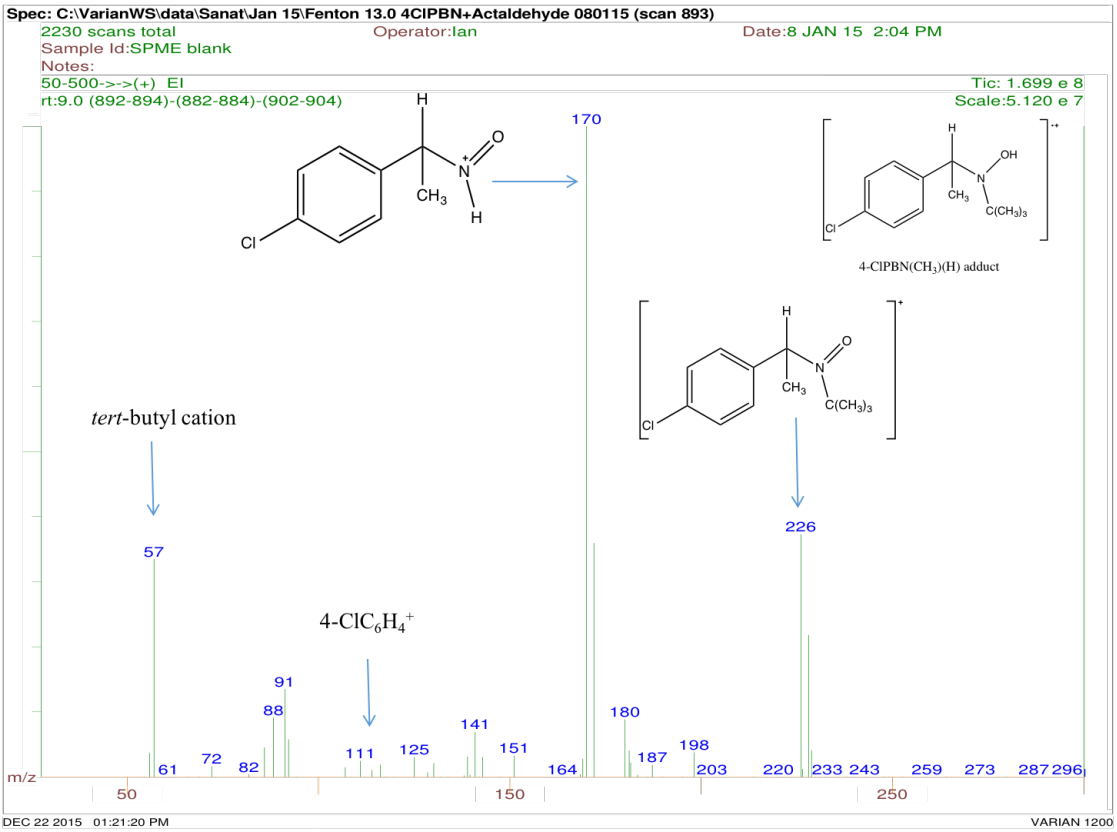

Figure 4.16: Electron ionization (EI) mass spectrum of the peak at 9.0 minutes (from the chromatogram in Figure 4.4) corresponding to 4-ClPBN(CH_3)(H) adduct (structure shown in top right).

The EI mass spectrum for peak with retention time 9.0 minutes (from the chromatogram in Figure 4.4) is shown in Figure 4.16. The mass spectrum doesn't shows a molecular ions for 4-ClPBN(CH_3)(H) adduct (structure shown in top right in Figure 4.16) at m/z 227/229. The fragment at m/z 226/228 is for structure shown in Figure 4.16, formed due to loss of hydrogen from the oxygen site from the 4-ClPBN(CH_3)(H) adduct. The base peak fragment at m/z 170/172 is due to the loss of 2-methyl-1-propene from m/z 226/228; m/z 111/113 corresponds to 4-$ClC_6H_4^+$ and m/z 57 to the *tert*-butyl cation.

4.6 Miscellaneous peaks

4.6.1 Chromatographic peaks for Chlorine compounds

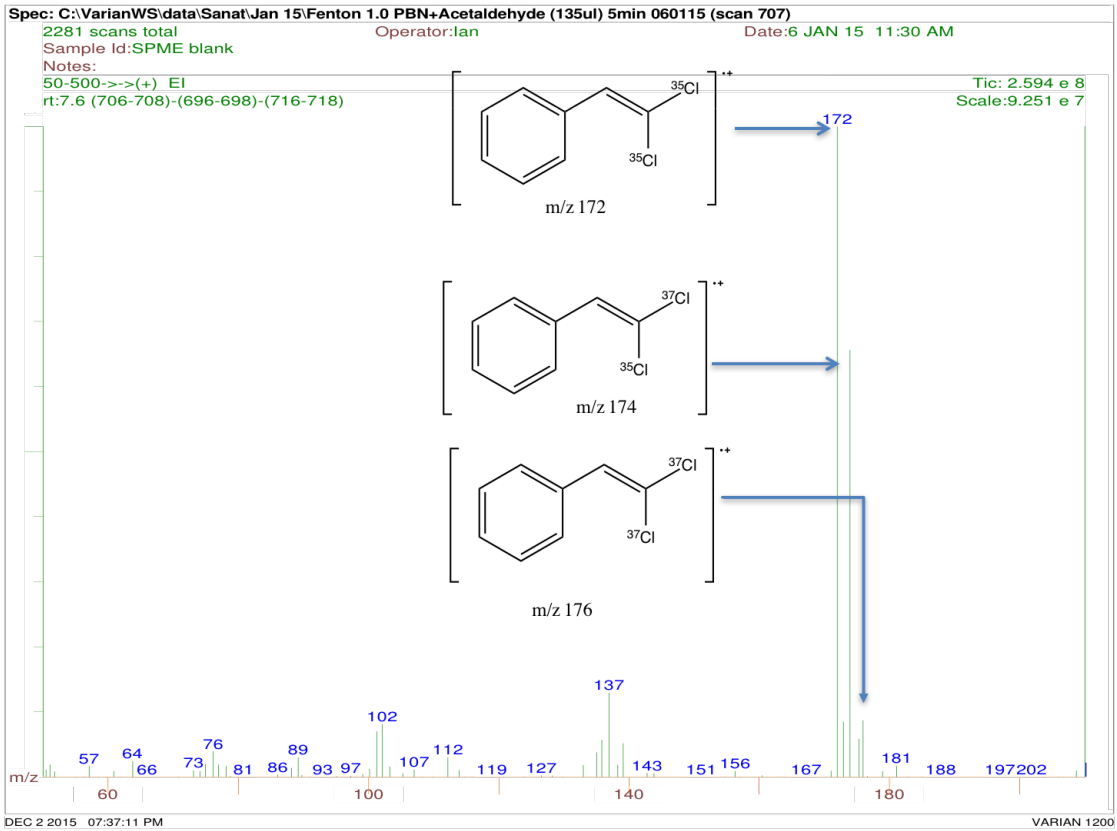

Figure 4.17: Electron ionization (EI) mass spectrum of the peak at 7.6 minutes (from the chromatogram in Figure 4.1) tentatively assigned to 1,1-dichloro-2-phenylethene adduct at 7.6 minutes.

The mass spectrum in Figure 4.17 corresponds to the peak retained at 7.6 minutes (from the chromatogram in Figure 4.1) and shows a presence of two chlorine atoms with the fragment pattern at m/z 172, m/z 174 and m/z 176 and the height intensity in ratio 9:6:1. Assuming the molecular ion for this peak is at m/z 172/174/176 then it may be assigned to the compound 1,1-dichloro-2-phenylethene. The fragment at m/z 137 is due to loss of a ^{35}Cl atom from the molecular ion, and m/z 102 is loss of a second ^{35}Cl from the peak at m/z 137. The mass spectrum also shows the corresponding isotope peaks for ^{37}Cl. The presence of fragment at m/z 57 is unknown. If this peak corresponds to the *tert*-butyl cation then clearly the peaks at m/z 172/174/176 are not the molecular ion; however, there are no clearly identifiable peaks in the mass spectrum above these values. Similar peaks

to those in Figure 4.17 were observed when the Fenton reaction was carried with other PBN derivatives, which have been tabulated in Table 4.1.

Identity	Retention time (minutes)	Molecular ion (m/z)
C_6H_5-CH-$CHCl_2$	7.6	172/174/176
C_6D_5-CD-$CHCl_2$	7.6	178/180/182
4-FC_6H_4-CH-$CHCl_2$	7.5	190/192/194
4-ClC_6H_4-CH-$CHCl_2$	9.0	206/208/210/212

Table 4.1: Molecular ion values and retention times for the chlorine containing compound observed with the PBN derivatives.

4.6.2 Chromatographic peak at 6.0 minutes

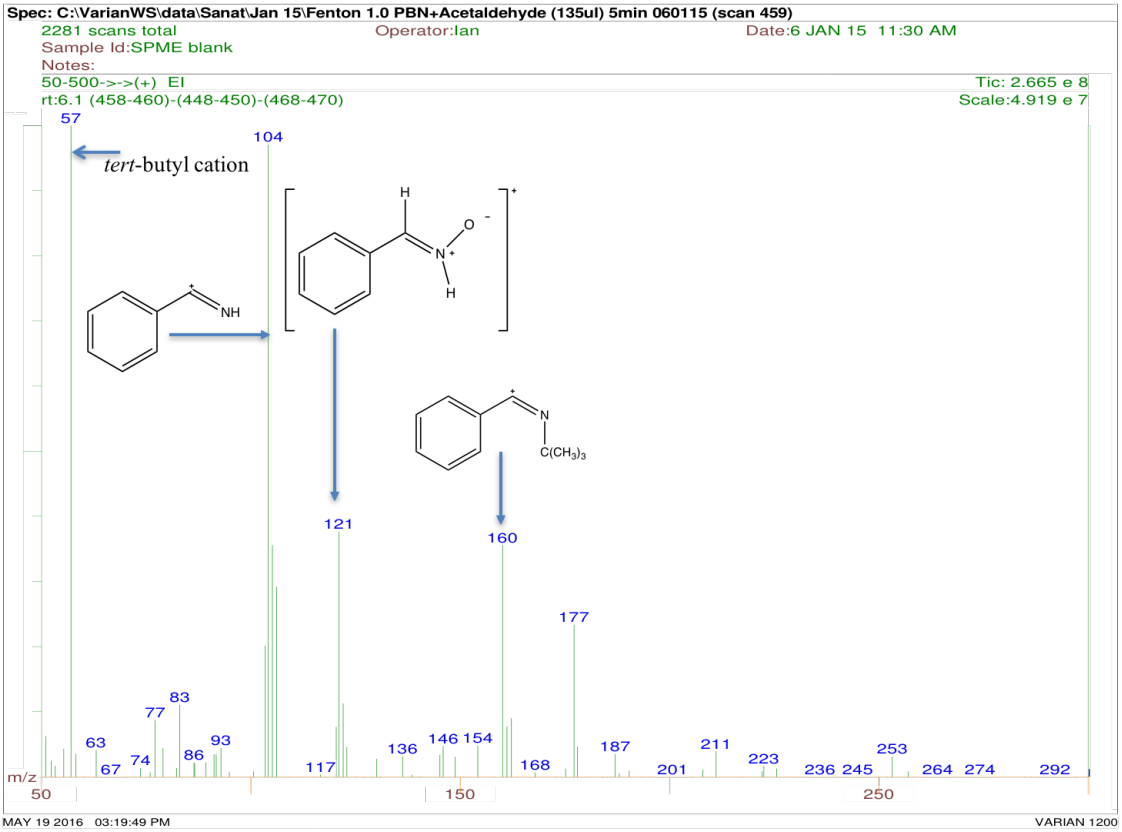

Figure 4.18: Electron ionization (EI) mass spectrum of the peak at 6.0 minutes (from the chromatogram in Figure 4.1).

The mass spectrum shown in Figure 4.18 corresponds to the peak retained at 6.0 minutes (from the chromatogram in Figure 4.1). The mass spectrum shows a strong ion at m/z 177 and a similar fragmentation pattern to that seen for PBN mass spectrum (Figure 2.3), however, they have different retention times suggesting this peak is not unreacted PBN. Indeed, the PBN can be seen as co-eluting with a PBN$(CH_3)_2$ adduct later in the chromatogram (Figure 4.1). The mass spectrum does not appear to show a molecular ion. The mass spectral analysis shows a fragments at m/z 160 (possibly due loss of $HO^{\bullet}$ from m/z 177), m/z 121 (due to loss of 2-methyl-1-propene from m/z 177) and m/z 104 (due to loss of tBuNOH from the molecular ion). The base peak at m/z 57 corresponds to the *tert*-butyl cation.

Similar peaks were observed when the Fenton reaction was carried out with other PBN derivatives, summarised in Table 4.2. The EI-MS from different PBN derivatives shows that the ion at m/z 160 has the structure shown in Figure 4.19. This fragment peak was also observed in the Fenton reaction involving the use of deuterated acetaldehyde, however, no change in the mass spectrum was seen, showing that it is not derived from acetaldehyde.

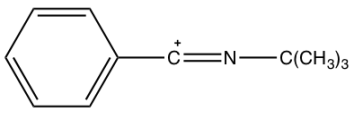

Figure 4.19: Possible structure of ion at m/z 160.

PBN derivatives	Retention time (mins)	Characteristic fragment (m/z)
PBN	5.9	177, 160, 121, 104, 57
PBN-d_6	6.0	182, 165, 126, 109, 57
4-FPBN	6.0	178, 122, 57
4-ClPBN	7.5	194/196, 138

Table 4.2: Retention times and m/z values for fragments for the unknown compound observed with the PBN derivatives.

The structure of the compound corresponding to the peak at 6.0 minutes is not known; from the fragments in the mass spectra we can deduce that it is a PBN adduct. However, there appears to be no molecular ion peak to help determine the adduct's identity. Since it is clearly not unreacted PBN (based upon its relatively low retention time compared to PBN) and has a retention time similar to PBN$(CH_3)_2$, this PBN adduct must be relatively volatile.

4.6.3 Chromatographic peaks retained at 9.6 and 10.1 minutes

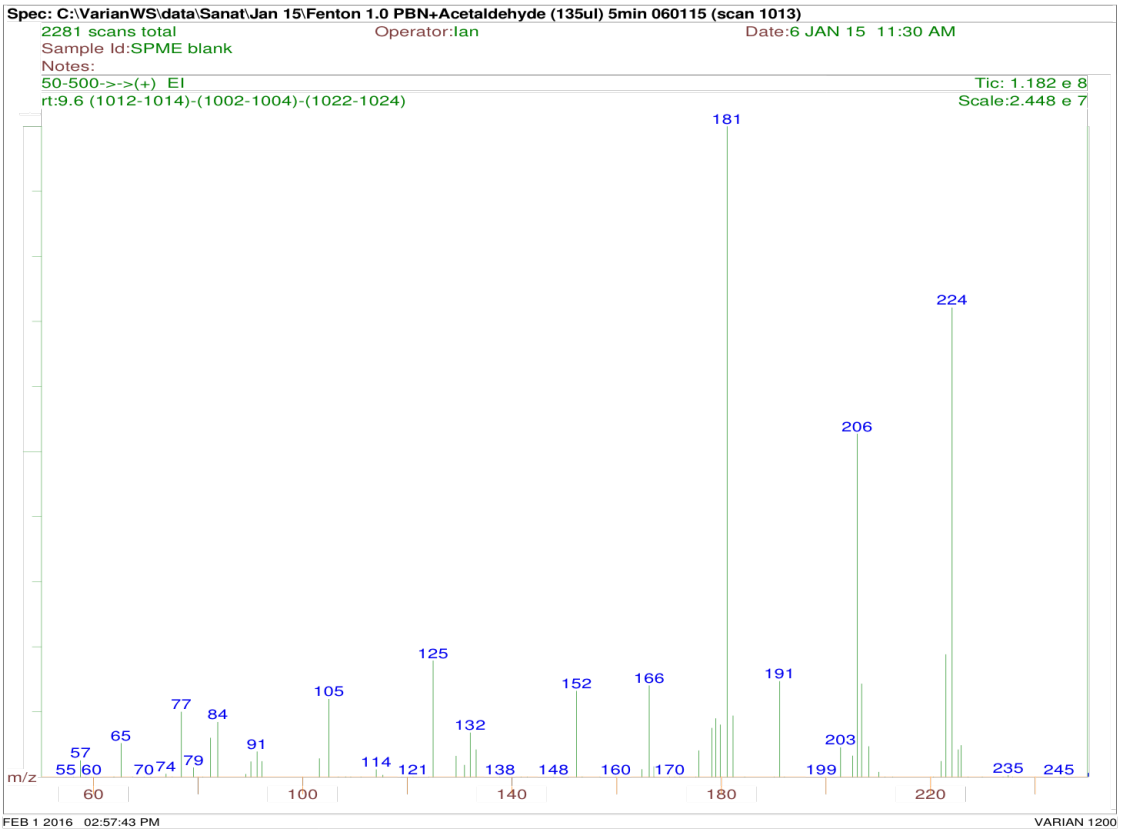

Figure 4.20: Electron ionization (EI) mass spectrum of the peak at 9.6 minutes (from the chromatogram in Figure 4.1).

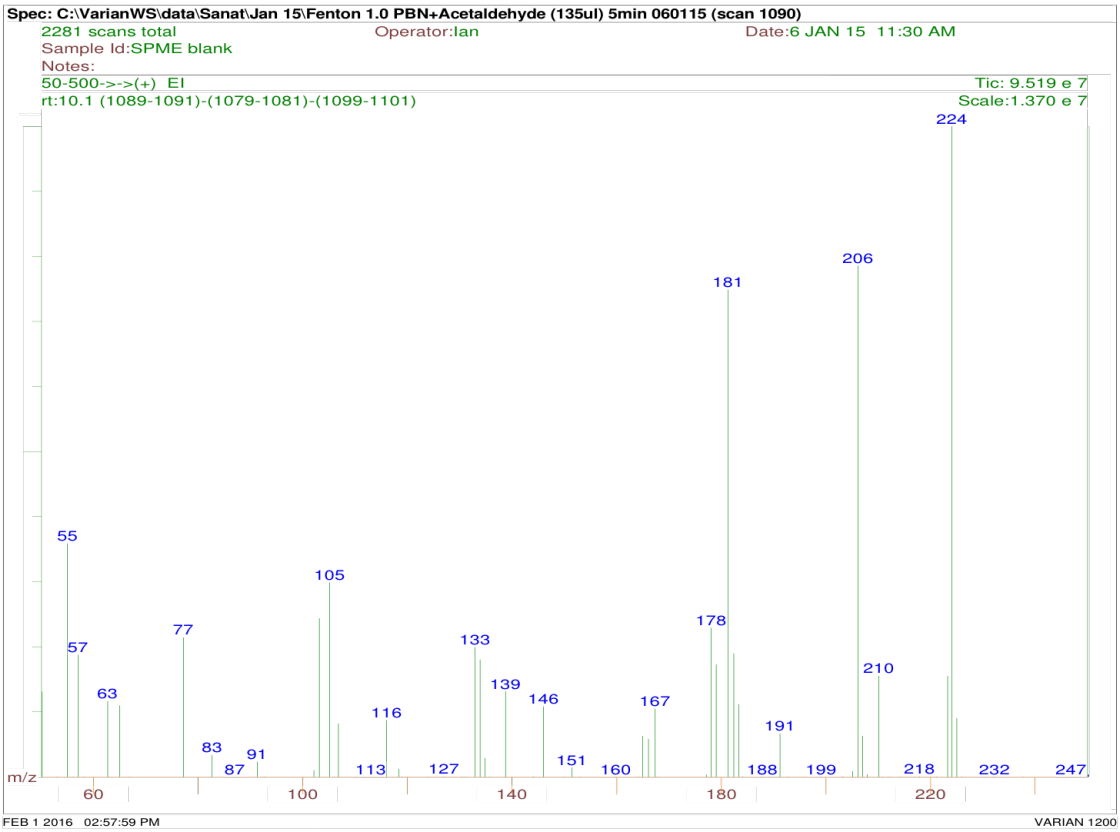

Figure 4.21: Electron ionization (EI) mass spectrum of the peak at 10.1 minutes (from the chromatogram in Figure 4.1).

The mass spectrum shown in Figure 4.20 corresponds to the peak retained at 9.6 minutes (from the chromatogram in Figure 4.1). The mass spectrum shows strong ions at m/z 181, 206 and m/z 224. Similar fragments pattern were seen with PBN-d_6, 4-FPBN and 4-ClPBN (Table 4.3). The fragment at m/z 224 loses a water molecule (18 m/z) to form m/z 206. The fragment at m/z 224 may also lose an acetyl radical ($CH_3CO^{\bullet}$) (43 m/z) to generate fragment at m/z 181. This was confirmed from the PBN and deuterated acetaldehyde mass spectrum which showed a loss of 46 m/z due to presence of deuterium acetyl radical ($CD_3CO^{\bullet}$).

For identification of the ions present in this mass spectrum different PBN derivatives were used. The ions observed suggested the presence of two X-C_6H_4-CH- units in the structure. For example, the corresponding mass spectrum for the fluorine derivative shows an increase of 36 m/z (217-181) suggesting the presence of two fluorine atoms in the structure (each fluorine atom replaces a hydrogen atom on the benzene ring). Similar results were also found with deuterated PBN which shows difference of 12 m/z when compared to PBN, thus confirming presence of two C_6D_5-CD- units in the structure.

From the above information the possible structure is shown in Figure 4.22. A similar mass spectrum (Figure 4.21) was observed for the peak at 10.1 minutes in chromatogram Figure 4.1 suggesting the presence of a stereoisomer due to the presence of chiral carbon attached to benzene ring.

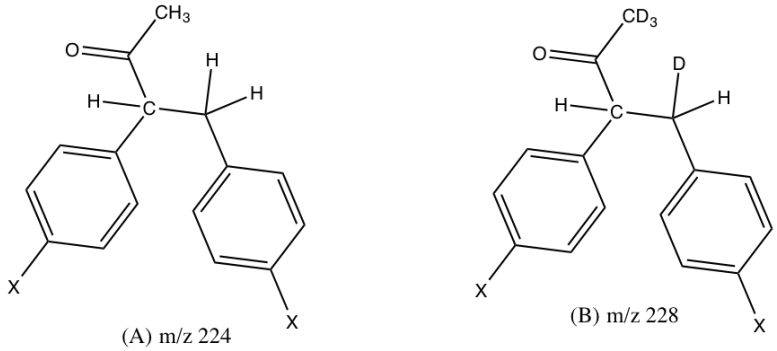

Figure 4.22: Possible structures for the compound retained at 9.6 and 10.1 minutes (A) compound from the Fenton reaction containing acetaldehyde, (B) compound from the Fenton reaction containing deuterated acetaldehyde.

PBN derivatives	Retention time (minutes)	Fragments (m/z)
PBN	9.6, 10.1	181, 206, 224
PBN-d_6	9.5, 10.0	193, 218, 236
4-FPBN	9.4, 9.8	217, 242, 260
4-ClPBN	11.8, 12.4	249/251, 274/276, 292/280

Table 4.3: Retention times and m/z values for for the compounds observed with the PBN derivatives.

4.7 Confirmation of methyl adduct

4.7.1 PBN Acetaldehyde-d_3 Chromatogram

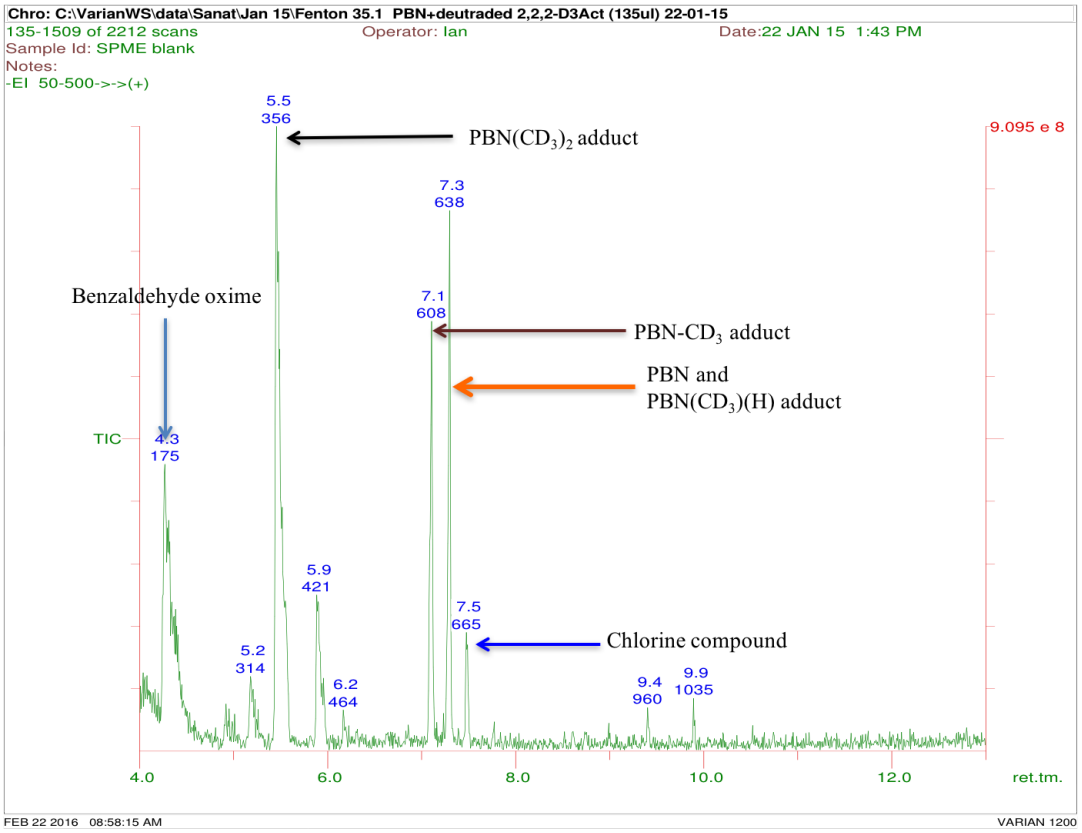

Figure 4.23: Total ion chromatogram (TIC) obtained from the GC/MS analysis of the Fenton reaction mixture containing PBN and deuterated acetaldehyde.

The TIC (Figure 4.23) obtained from the GC/MS analysis of the Fenton reaction mixture in the presence of PBN and acetaldehyde-d_3 (structure shown in Figure 4.24) shows the presence of the benzaldehydeoxime (R_t 4.3 minutes; 2.8.1.2), the PBN $(CD_3)_2$ adducts (R_t 5.5 minutes; see section 4.7.2), PBN-CD_3 adducts (R_t 7.1; see section 4.7.3), PBN (CD_3)(H) adduct (R_t 7.3 minutes; see section 4.7.4), unreacted PBN (R_t 7.3 minutes; see section 2.7.1) and a dichlorinated compound (1,1-dichloro-2-phenylethene) (R_t 7.5 minutes; see section 4.6.1).

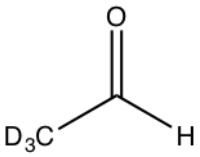

Figure 4.24: Structure of deuterated acetaldehyde.

4.7.2 PBN$(CD_3)_2$ adduct

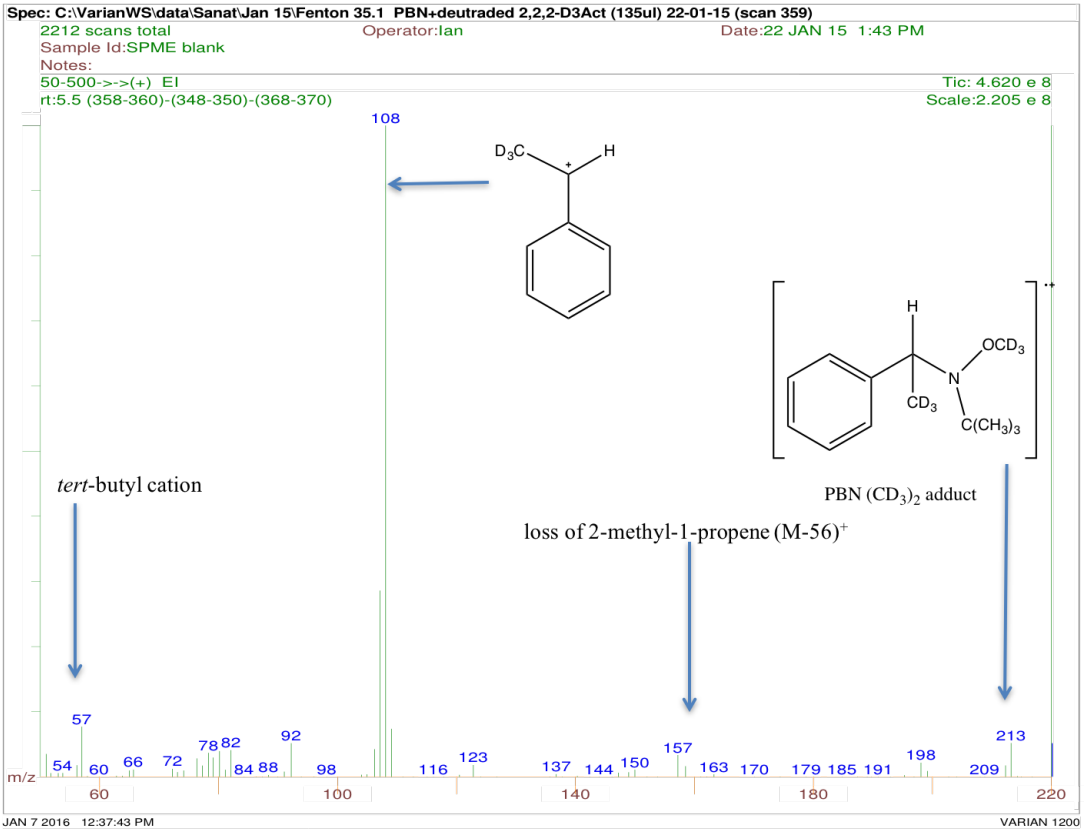

Figure 4.25: Electron ionization (EI) mass spectrum of peak at 5.6 minutes (from the chromatogram in Figure 4.23) corresponding to a PBN$(CD_3)_2$ adduct.

The EI mass spectrum for the peak with retention time 7.1 minutes (from the chromatogram in Figure 4.23) is shown in Figure 4.25. The mass spectrum shows a weak molecular ion at m/z 213. The fragment at m/z 198 is due to the loss of methyl radical (M-15) from the "molecular ion". The peak at m/z 157 is due to the loss of 2-methyl-1-propene from the molecular ion (M-56). The base peak at m/z 108 corresponds to the

cation showed in Figure 4.25, formed by dissociation of the molecular ion at the C-N bond. The fragment at m/z 57 corresponds to the *tert*-butyl cation. The fragmentation pattern is similar to the PBN dimethyl adduct (except CH_3 has been replaced by CD_3); this can be seen in Figure 3.14.

4.7.3 PBN-CD_3 adduct at 7.1 minutes

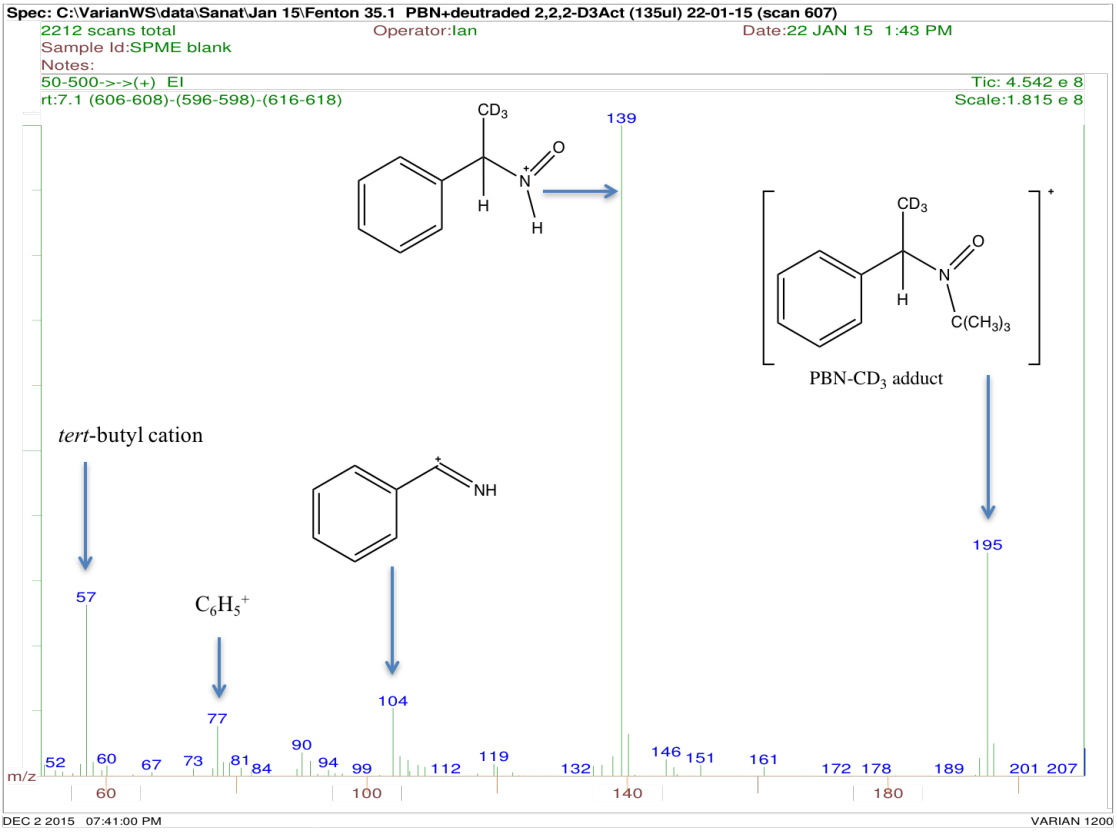

Figure 4.26: Electron ionization (EI) mass spectrum of peak at 7.1 minutes (from the chromatogram in Figure 4.23) corresponding to a PBN-CD_3 adduct.

The EI mass spectrum for the peak with retention time 7.1 minutes (from the chromatogram in Figure 4.23) is shown in Figure 4.26. The mass spectrum shows a "molecular ion" at m/z 195 corresponding to a PBN-CD_3 adduct. The base peak at m/z 139 is due to the loss of 2-methyl-1-propene from the "molecular ion" (M-56). The fragment at m/z 77 may be assigned to the phenyl cation and that at m/z 57 to the *tert*-butyl cation.

4.7.4 PBN(CD_3)(H) adduct at 7.3 minutes

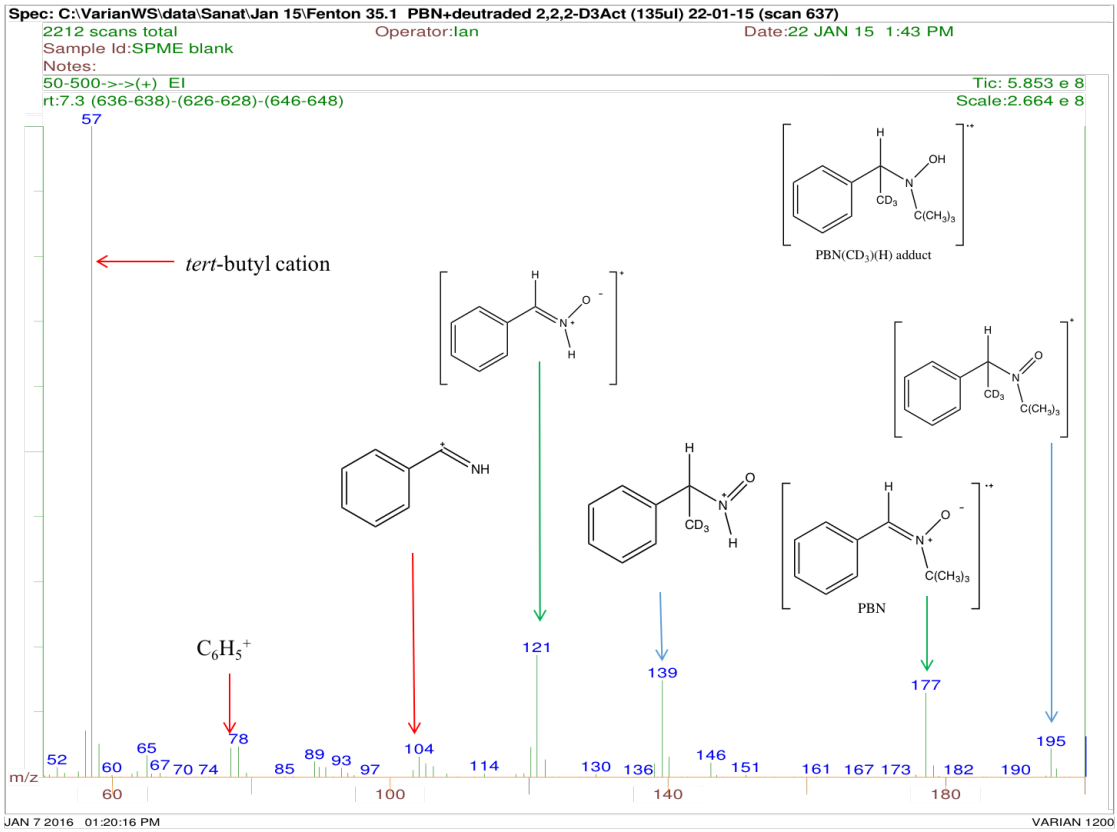

Figure 4.27: Electron ionization (EI) mass spectrum of peak at 7.3 minutes (from the chromatogram in Figure 4.23) corresponding to a PBN(CD_3)(H) adduct (structure shown in top right) and unreacted PBN. Peaks labelled in blue are for the PBN(CD_3)(H) adduct, peaks labelled in green are for unreacted PBN and peaks labelled in red are the common.

The EI mass spectrum for the peak with retention time 7.3 minutes (from the chromatogram in Figure 4.23) is shown in Figure 4.27. The mass spectrum showed presence of two compounds which are PBN(CD_3)(H) adduct (structure shown in Figure 4.27) and unreacted PBN ($M^{+\bullet}$ at m/z 177). For the PBN(CD_3)(H) adduct the mass spectrum is identical to the mass spectrum for the peak retained at 7.4 min (for further interpretation refer to section 4.5.1).

4.8 Analysis of spin trapped methyl radical generated from acetaldehyde by Single Droplet Microextraction (SDME)

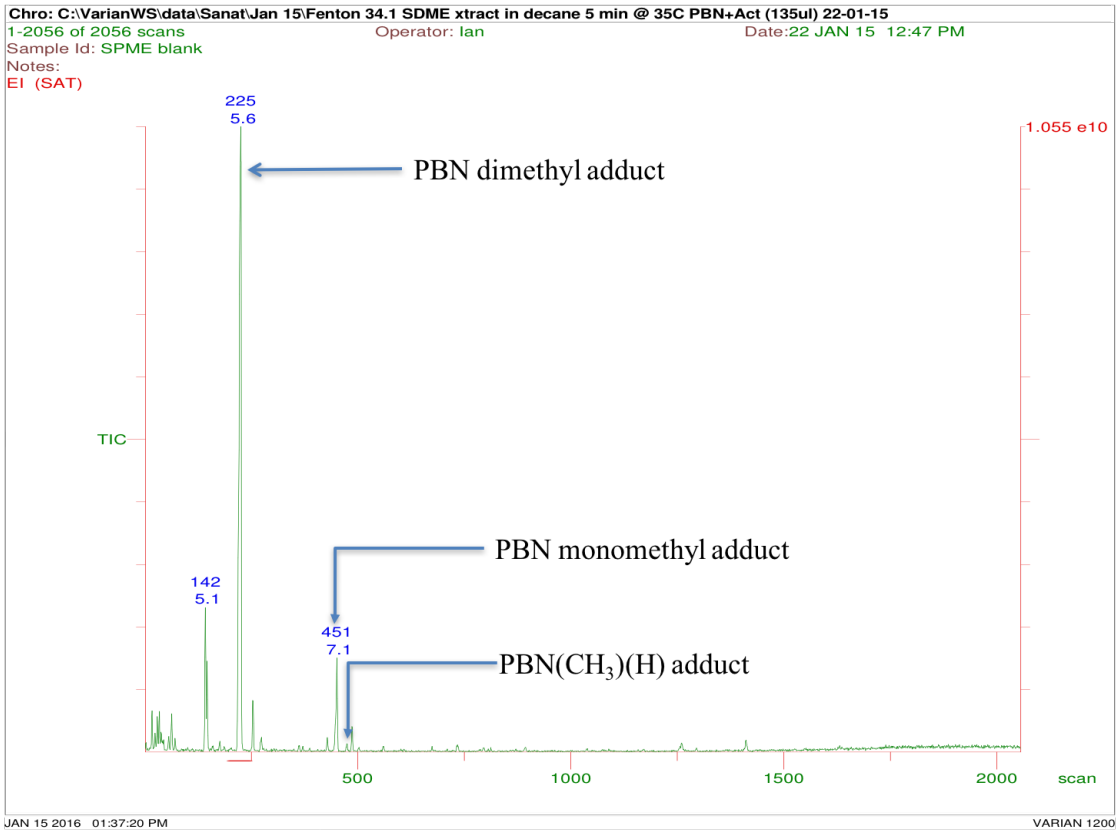

Figure 4.28: Total ion chromatogram (TIC) obtained from the SDME GC/MS analysis of the Fenton reaction mixture containing PBN and acetaldehyde.

The TIC obtained from the GC/MS analysis of the Fenton reaction mixture containing PBN and acetaldehyde extracted into decane and sampled using the SDME technique. The chromatogram shows various peaks for hydrocarbons which are probably alkane impurities dissolved in the decane. These hydrocarbon peaks have been identified in the chapter 5 (section 5.3.3). The data is summarised in Table 4.4. The mass spectrum for the dimethyl and mono-methyl adducts have been interpreted. The mass spectrum for the dimethyl and mono-methyl adducts have been discussed earlier in this chapter.

Retention time (R_t)	Molecular ion (m/z)	Identity
5.1 minutes	184	Tridecane
5.6 minutes	207	$PBN(CH_3)_2$
5.8 minutes	198	Tetradecane
7.1 minutes	192	$PBN\text{-}CH_3$
7.3 minutes	193	$PBN(CH_3)(H)$
7.4 minutes	226	Hexadecane

Table 4.4: Retention times and molecular ion values (m/z) for compounds obtained from the SDME sampling and GC/MS analysis of the Fenton reaction involving PBN and acetaldehyde.

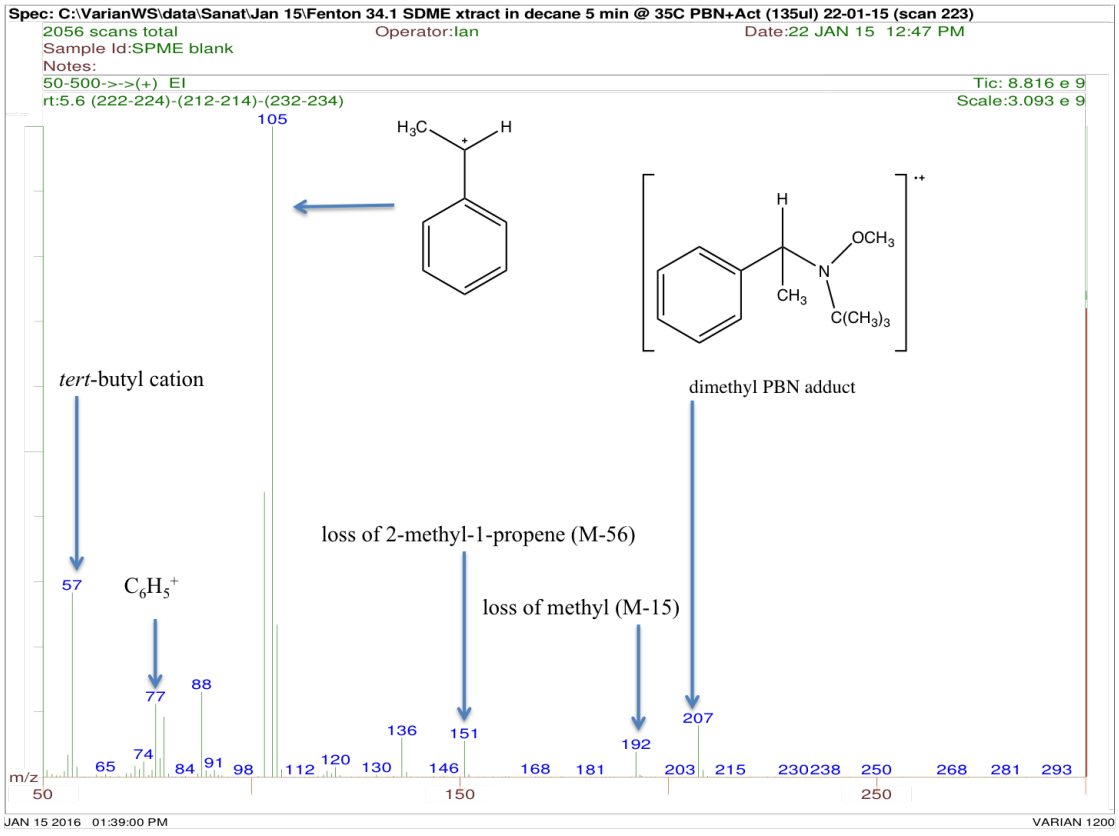

Figure 4.29: Electron ionization (EI) mass spectrum obtained for peak at 5.6 minutes (from the chromatogram in Figure 4.28) corresponding to a $PBN(CH_3)_2$ adduct with "molecular ion" at m/z 207.

The mass spectrum of the peak at 5.6 minutes is shown in Figure 4.29 clearly demonstrates the presence of the PBN dimethyl adduct (previously interpreted in chapter 3).

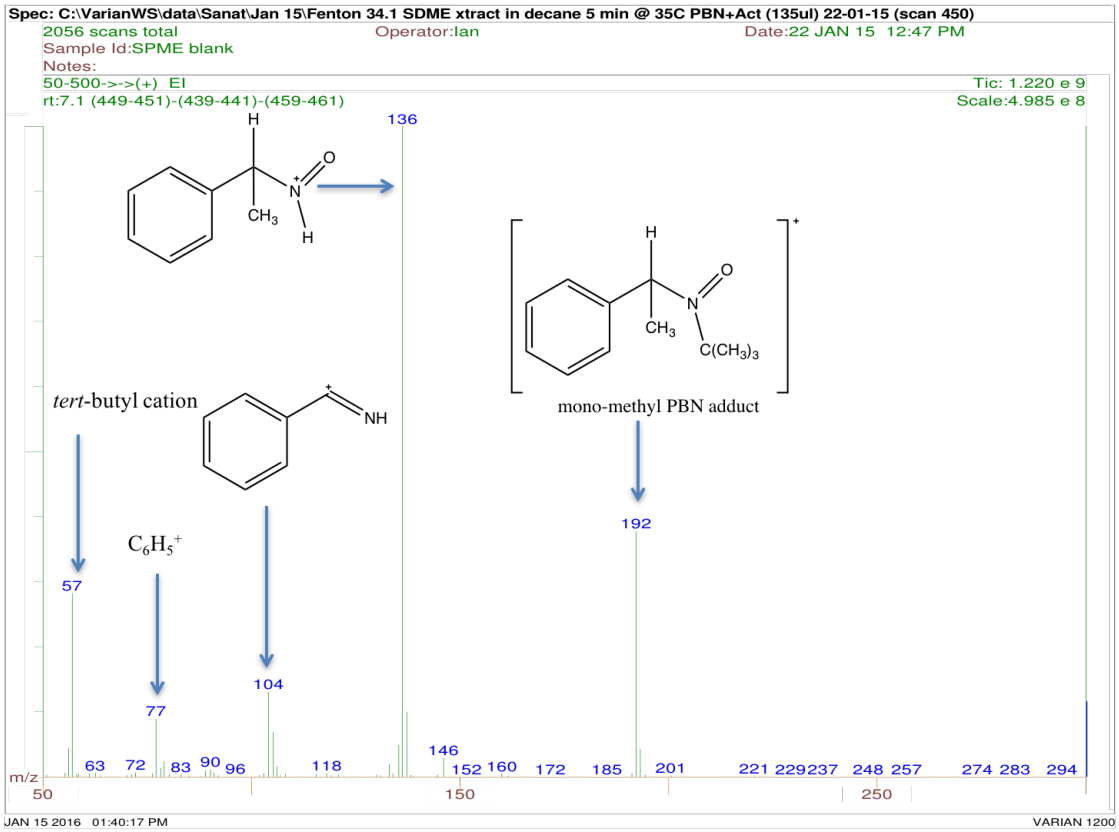

Figure 4.30: Electron ionization (EI) mass spectrum obtained for peak at 7.1 minutes (from the chromatogram in Figure 4.28) corresponding to a monomethyl PBN adduct with a "molecular ion" at m/z 192.

The mass spectrum for peak at 7.1 minutes is shown in Figure 4.30 clearly demonstrates the prescence of a monomethyl PBN adduct. This spectrum has been interpreted earlier in the chapter (see section 4.4.1).

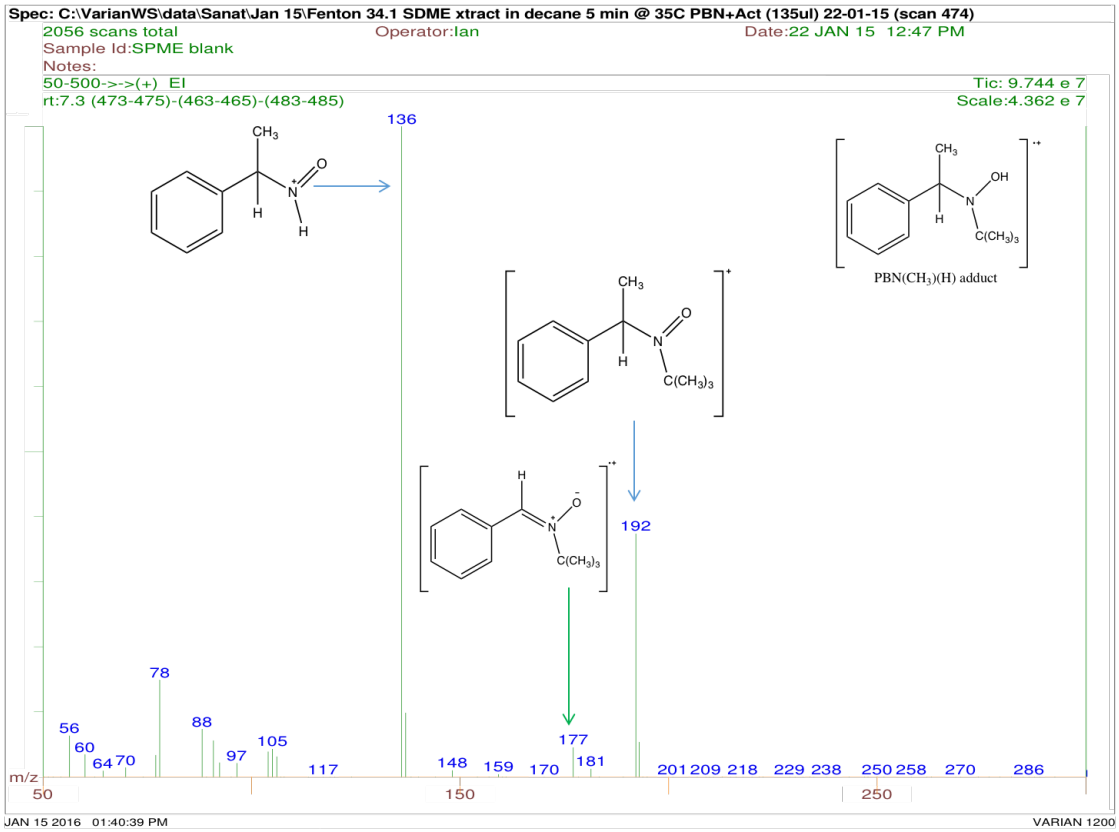

Figure 4.31: Electron ionization (EI) mass spectrum obtained for peak at 7.3 minutes (from the chromatogram in Figure 4.28) corresponding to PBN(CH_3)(H) adduct (structure shown in top right) with the presence of a small amount of unreacted PBN. Peaks labelled in blue are for PBN(CH_3)(H) adduct and peaks labelled in green are for unreacted PBN.

The mass spectrum for peak at 7.3 minutes (from the chromatogram in Figure 4.28) is shown in Figure 4.31. As was seen previously this peak is derived from two separate compounds: PBN(CH_3)(H) and unreacted PBN (see section 4.5.1).

To confirm the formation of dimethyl and mono-methyl PBN adduct in the Fenton reaction and its extraction by the SDME technique deuterated acetaldehyde-d_3 was used. As expected the dimethyl PBN adduct showed an increase of six m/z units due to the presence of six deuterium atoms in the molecular ion and the mono-methyl PBN adducts both showed an increase of three m/z units for their "molecular ions". The mass spectra followed the same fragment pattern with expected changes in m/z values when the deuteromethyl was present in the fragment. The adduct peaks have been summarized in Table 4.5.

Acetaldehyde			Deuterated acetaldehyde		
Retention time (minutes)	Fragments (m/z)	Molecular ion (m/z)	Fragments (m/z)	Molecular ion (m/z)	Identity
5.6	57,77,105, 136,151, 192,207	207	57,108,139, 157,177, 198,213	213	PBN dimethyl adduct
7.1	57,77,104, 136,192	192	57,77,104, 139,195	195	mono-methyl adduct
7.3	57,104,136, 177,192	193	57,77,139, 195	196	$(CH_3)(H)$ adduct

Table 4.5: Retention times and m/z values of fragments and molecular ions for compounds obtained from GC/MS analysis of SDME extracted Fenton systems involving PBN and acetaldehyde /deuterated acetaldehyde.

4.9 Discussion

The first objective of these experiments was to trap the radicals generated from acetaldehyde using PBN derivatives in the Fenton reaction and identifying them by GC/MS. The second objective was to develop and compare two different extraction techniques for the radicals trapped by PBN.

In the Fenton reaction Fe^{2+} reacts with H_2O_2 to generate hydroxyl radicals which then react with acetaldehyde to form acetyl radicals. These then undergo decarbonylation to form methyl radicals (Nakao et al. 2000*b*) as shown in Figure 4.32. Formation of PBN dimethyl adducts is a two-step mechanism (Figure 4.32). In the first step the methyl radical generated is trapped at the carbon site of the PBN to form a mono-methyl PBN adducts and, in the second step, another methyl radical is added to the oxygen site of the PBN to form a stable dimethyl adduct.

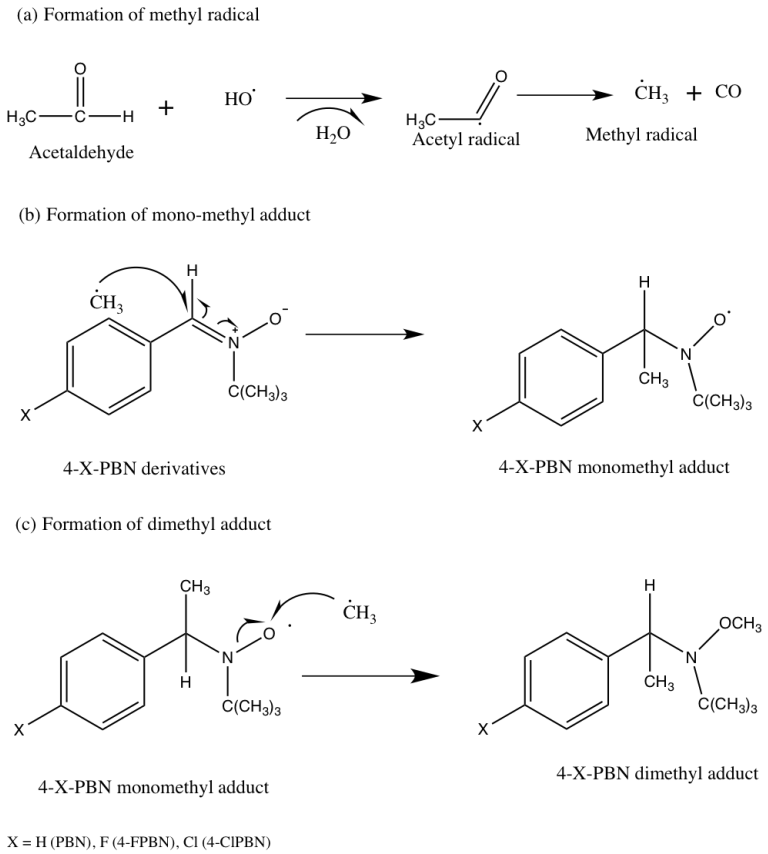

Figure 4.32: Schematic representation for (a) formation of methyl radicals from acetaldehyde through the Fenton mechanism, (b) the methyl radical is trapped by PBN (derivatives) at the carbon site to form a monomethyl PBN adducts, (c) a second methyl radical is added to the oxygen site of the monomethyl PBN adducts to form a dimethyl PBN adducts.

The TIC of the chloroform extracted Fenton reaction mixture containing acetaldehyde shows various peaks and, to confirm the peaks generated in the Fenton reaction the chromatogram was compared to the controls (Section 2.8). On comparison it was found that peaks retained at 5.6 minutes and 7.3 minutes are generated from the reaction mixture as these peaks were not present when acetaldehyde was not used in the Fenton reaction. The peak retained at 4.4 minutes is for the benzaldehyde oxime. The peak at 7.4 minutes contains unreacted PBN as seen from the control experiments and also the mass spectrum shows the presence of a molecular ion at m/z 177 and characteristic fragments at m/z 57 for *tert*-butyl cation for the PBN as mentioned by Janzen and Dubose (Janzen & Dubose 1993); however, the mass spectrum also shows presence of a PBN monomethyl adduct with a "molecular ion" at m/z 192. It should be noted that the molecular ion for this species is in fact a cation (not a radical cation, as is usual) since the adduct is a nitroxide

free radical and therefore contains an unpaired electron.

The chromatogram (Figure 4.1) obtained for the reaction mixture shows an intense peak retained at 5.6 minutes and the corresponding mass spectrum (Figure 3.13) shows a molecular ion at m/z 207 corresponding to the PBN dimethyl adducts. This mass spectrum also shows a fragment at m/z 151 formed due to loss of the 2-methyl-1-propene from the molecular ion and a base peak at m/z 105 for a cation $C_8H_9^+$ formed by the dissociation of the molecular ion at the C-N bond. This fragmentation pattern was exactly the same as the fragment pattern for synthesised PBN$(CH_3)_2$ adducts showed by Janzen et al. (Janzen et al. 1985). For confirmation and interpretation of the mass spectrum of the dimethyl adducts, different PBN derivatives, such as PBN-d_6, 4-FPBN and 4-ClPBN were used in the Fenton reaction and all the PBN derivatives showed dimethyl adducts in the chromatogram and the mass spectrum showed an identical fragmentation pattern (Table 4.6).

Further, to confirm acetaldehyde was the only source for the methyl radicals trapped by PBN, deuterated acetaldehyde was used. Deuteromethyl radicals ($^{\bullet}CD_3$) were generated from the deuterated acetaldehyde which were then trapped by PBN to form PBN$(CD_3)_2$ adducts and the mass spectrum showed a molecular ion at m/z 213 - a shift of 6 m/z due to the presence of six deuterium atoms in the molecular ion. As expected, the PBN$(CD_3)_2$ adduct was retained at 5.6 minutes (under the chromatographic conditions used) (Figure 4.23). Fragments at m/z 157 and the base peak at m/z 108 also confirm acetaldehyde as the source of the free radicals. Hence, potentially this method may be used for the indirect detection of hydroxyl radicals through detection and identification of methyl radicals from acetaldehyde.

Dimethyl adducts	Retention time (minutes)	Molecular ion and fragments (m/z)
PBN$(CH_3)_2$	5.6	207, 151, 105
PBN-$d_6(CH_3)_2$	5.6	213, 157, 111
4-FPBN$(CH_3)_2$	5.7	225, 169, 123
4-ClPBN$(CH_3)_2$	7.3	241, 185, 139

Table 4.6: Dimethyl adducts for different PBN derivatives with their retention time, molecular ion and characteristic fragments.

The TIC (Figure 4.1) shows a peak retained at 7.3 minutes and the corresponding mass spectrum (Figure 4.9) shows a strong peak at m/z 192. This peak corresponds to a PBN monomethyl adduct (structure shown in Figure 4.33). The presence of PBN monomethyl adduct was confirmed by using deuterated acetaldehyde. The GC chromatogram for PBN and deuterated experiment showed the presence of PBN-CD_3 adduct and the corresponding mass spectrum was similar to the PBN-CH_3 adduct with expected mass difference (Figure 4.26).

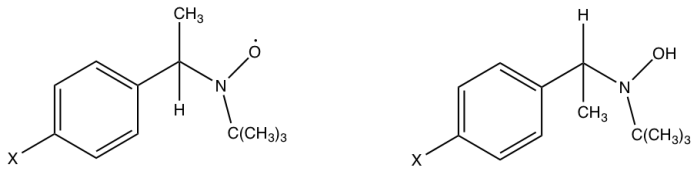

(A) 4-X-PBN monomethyl adduct peak retained at 7.3 min. (X=H))

(B) 4-X-PBN(CH_3)(H) adduct peak retained at 7.4 min. (X=H)

Figure 4.33: Structure of PBN methyl adducts (X = F and Cl) (A) the PBN monomethyl adduct at 7.3 minutes and (B) the PBN(CH_3)(H) adduct at 7.4 minutes.

The TIC (Figure 4.1) and the mass spectrum (Figure 4.13) for the peak retained at 7.4 minutes showed the presence of unreacted PBN and PBN(CH_3)(H) adducts. For the PBN(CH_3)(H) adducts (structure B shown in Figure 4.33), the mass spectrum doesn't show a molecular ion at m/z 193 which could be because the adduct loses the hydrogen attached to oxygen rapidly or the adduct rapidly decomposes to monomethyl adducts. The fragment at m/z 192 is due to loss of hydrogen and the fragments at m/z 136 is due to the loss of 2-methyl-1-propene from the m/z 192; this was confirmed when deuterated acetaldehyde was used and the corresponding mass spectrum showed a strong cation at m/z 195 and a fragment at m/z 139, an addition of 3 m/z units due to the presence of the deuterated methyl group. Different PBN derivatives were also used to confirm the formation of monomethyl adducts and all the derivatives showed the presence of PBN methyl adducts. If both the peaks retained at 7.3 minutes and 7.4 minutes have a "molecular ion" m/z 192, it can be considered that the methyl radical is added to different position or different adduct or they are isomers. However, stereoisomers should have same retention time, hence the two peaks are different PBN methyl adduct. The second possibility would be if a methyl radical is added to the oxygen site, although this seems highly unlikely. The presence of PBN monomethyl adduct in the Fenton reaction involving acetaldehyde its absence in the Fenton system containing methanol and DMSO, is due to the difference in the rate constant. The rate constant for methyl from acetaldehyde is 10^{-2} $M^{-1}s^{-1}$ (Nakao et al. 2000*a*), whereas for DMSO is $7x10^{9}$ $M^{-1}s^{-1}$ (Qian et al. 2003), shows that methyl radical from acetaldehyde is slow which results in a steady build of PBN-CH_3 adducts enough to be detected by GC/MS.

The chromatogram (Figure 4.1) shows a peak at 6.0 minutes and its mass spectrum shows a very similar mass spectrum compared to the unreacted PBN suggest this is PBN derived compound. However, based on retention time of unreacted PBN and PBN dimethyl adduct it suggest this PBN derived compound is fairly volatile.

The chromatogram (Figure 4.1) also shows two peaks with similar mass spectrum retained at 9.4 minutes and 10.1 minutes suggesting they are isomers. Information obtained from their mass spectrum confirms presence of an acetyl radical (CH_3-C=O), a hydrogen

atom (from acetaldehyde) and two units of (X-C_6H_5-CH-) derived from the PBN. These units were confirmed from experiments involving deuterated acetaldehyde and different PBN derivatives. The possible structure obtained for these peaks is shown in Figure 4.22. This result suggests that acetyl radical is trapped by PBN to form (PBN-$COCH_3$) adduct, however this adduct is unstable and can react with other adducts in the Fenton reaction to form the suggested compound. This finding can be supported from the result of Nakao et al. were they showed acetaldehyde metabolised to acetyl radicals which can be spin trapped by POBN to form POBN acetyl radical adduct which is unstable (Nakao et al. 2000*a*).

The chromatogram also shows the presence of dichlorinated compound retained at 7.6 minutes which could be the by-product of a reaction involving PBN (as similar mass spectrum was obtained for other PBN derivatives). If m/z 172/174/176 is considered as molecular ion, then the suggested structure to the compound is 1,1-dichloro-2-phenylethene. This peak is not related to acetaldehyde as the same peak was observed when deuterated acetaldehyde was used. However, there is evidence in the mass spectrum (Figure 4.17) fragment at m/z 57 is *tert*-butyl cation then m/z 172/174/176 is not the molecular ion.

The method was developed to detect and identify the radicals generated from acetaldehyde. However, the chromatogram shows the presence of other peaks along with the PBN dimethyl adducts. Hence, an alternative extraction technique which did not involve direct contact with the reaction mixture (HS-SDME) was used to extract the PBN adducts from the Fenton reaction mixture.

Extraction techniques	Methyl adduct	Retention time (minutes)	Molecular ion (m/z)	Base peak (m/z)
Chloroform	$PBN(CH_3)_2$	5.6	207	105
	$PBN(CH_3)_2$	5.6	213	111
	4-$FPBN(CH_3)_2$	5.7	225	123
	4-$ClPBN(CH_3)_2$	7.3	241	139
	$PBN(CD_3)_2$	5.6	213	108
HS-SDME	$PBN(CH_3)_2$	5.6	207	105
	$PBN(CD_3)_2$	5.6	213	108

Table 4.7: Retention times and m/z values of molecular ions and base peaks for dimethyl obtained from GC/MS analysis of chloroform and HS-SDME extracted Fenton systems involving PBN derivatives and acetaldehyde /deuterated acetaldehyde.

For HS-SDME, the adducts from the Fenton reaction mixture were headspace extracted and concentrated by a microdrop of the solvent decane. The chromatogram (Figure 4.28) showed the presence of a PBN dimethyl adduct at 5.6 minutes along with PBN

monomethyl adducts at 7.1 minutes and 7.3 minutes, identification of which was confirmed by using deuterated acetaldehyde. The chromatogram also showed the presence of other alkanes (Table 4.4) which could be impurities present in the decane. The dimethyl adduct from the chloroform and HS-SDME extraction is summarized in Table 4.7.

The detection of PBN dimethyl adduct and PBN monomethyl adduct can be used to study the toxic effect of acetaldehyde which is the primary metabolite of ethanol (Zhang et al. 2004). Also this method can also be used as an indirect approach for detection of hydroxyl radicals. The use HS-SDME GC/MS can very useful in detection and identification of spin trapped radicals as it is simple and does not involve contact with the Fenton reaction mixture and also uses much less solvent and is more cost effective.

Chapter 5

Analysis of spin trapped ethyl radical from propionaldehyde (propanal)

5.1 Introduction

Lipid peroxidation (LPO) is a chain reaction which involves reaction of ROS with lipids. During the process it releases intermediate and end products which can be measured to quantify the ROS. The end products released during the LPO are hydrocarbons such as ethane and pentane as well as aldehydes like acetaldehyde, malondialdehyde and propionaldehyde. Among these ethane, pentane and malondialdehyde have been extensively found during asthma, aortic cross sampling, cystic fibrosis, liver transplantation and traumatic brain injury. However, the role of propionaldehyde in LPO is limited to experimental myocardial I/R injury and ultraviolet radiation-induced skin LPO. Propionaldehyde has been used in biomarker for LPO in olives oils, sunflower oils and other food products and its presence in biological samples is very complex and their concentration is very low (Steeghs et al. 2006). The method for detection of propionaldehyde was through derivatization of propionaldehyde with 2,4-dinitrophenylhydrazine (DNPH) and extraction with pentane and its analysis by GC/MS, however, this method is laborious and time consuming. There are other methods for detection of propionaldehyde which are highly sensitive such as laser-based photoacoustic detection (LPD) and proton transfer reaction mass spectrometry (PTR-MS) (Moeskops et al. 2006). Propionaldehyde has been quantified from breath analysis which results from spontaneous fragmentation of LPO after I/R injury in patient after lung or heart lung transplantation by ion-molecule reaction mass spectrometry (IMR-MS) instruments (Dolch et al. 2015).

The purpose of this experiment is to spin trap the radicals generated from propionaldehyde by PBN and its derivatives. Then to extract the PBN trapped radicals by using liquid-liquid extraction, SDME and SPME and to analyse the extract by GC/MS.

5.2 Chloroform extraction

5.2.1 Chromatogram

5.2.1.1 PBN

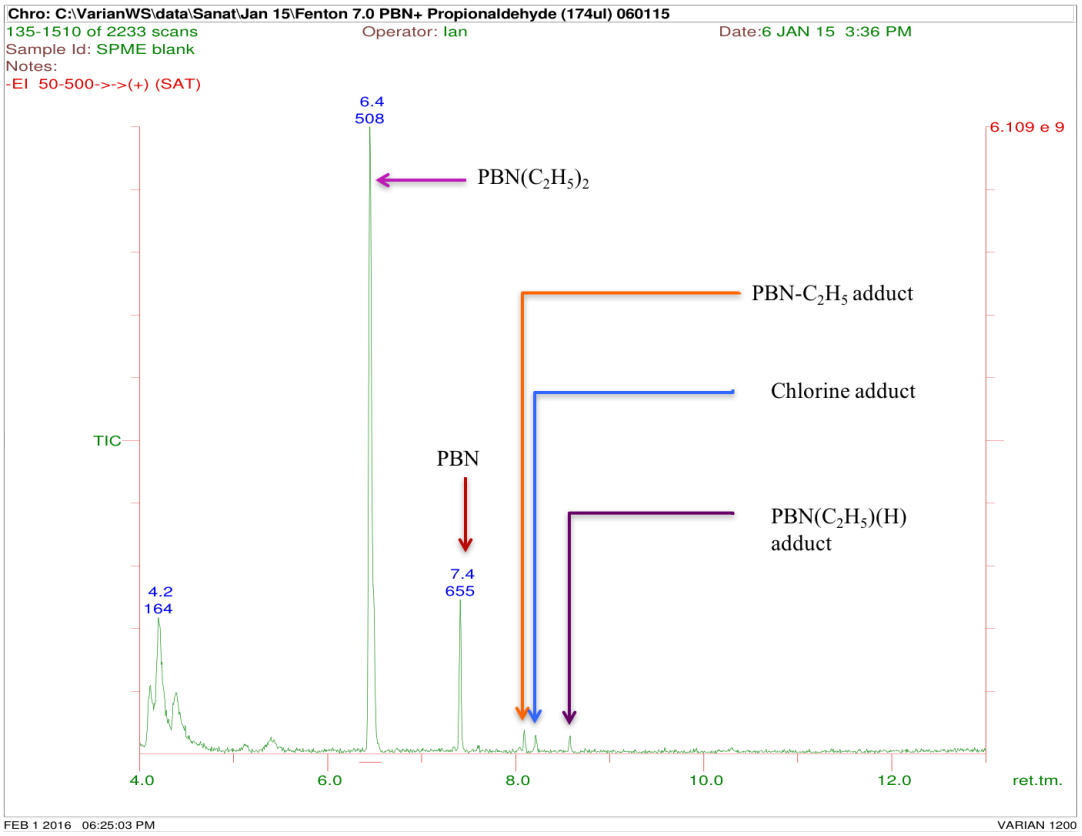

Figure 5.1: Total ion chromatogram (TIC) obtained from the GC/MS analysis of the Fenton reaction mixture containing PBN and propanal and extracted directly with chloroform.

Total ion chromatogram (TIC) obtained for the reaction mixture involving the Fenton chemical, PBN and propanal extracted into chloroform is shown in Figure 5.1. Identified peaks with their retention time, molecular ion and base peak are shown in Table 5.1 below.

Retention time (minutes)	Molecular ion (m/z)	Base Peak (m/z)	Identity
4.1 - 4.3	121	121	Benzaldehyde oxime
6.4	235	119	$PBN(C_2H_5)_2$
7.4	177	57	PBN
8.1	206	150	$PBN\text{-}C_2H_5$
8.2	172	172	$C_6H_5\text{-}CH\text{-}CHCl_2$
8.6	207	147	$PBN(C_2H_5)(H)$

Table 5.1: Retention, molecular ion, base peak with their identity for peaks obtained in chromatogram (Figure 5.1).

5.2.1.2 Deuterated PBN-d_6

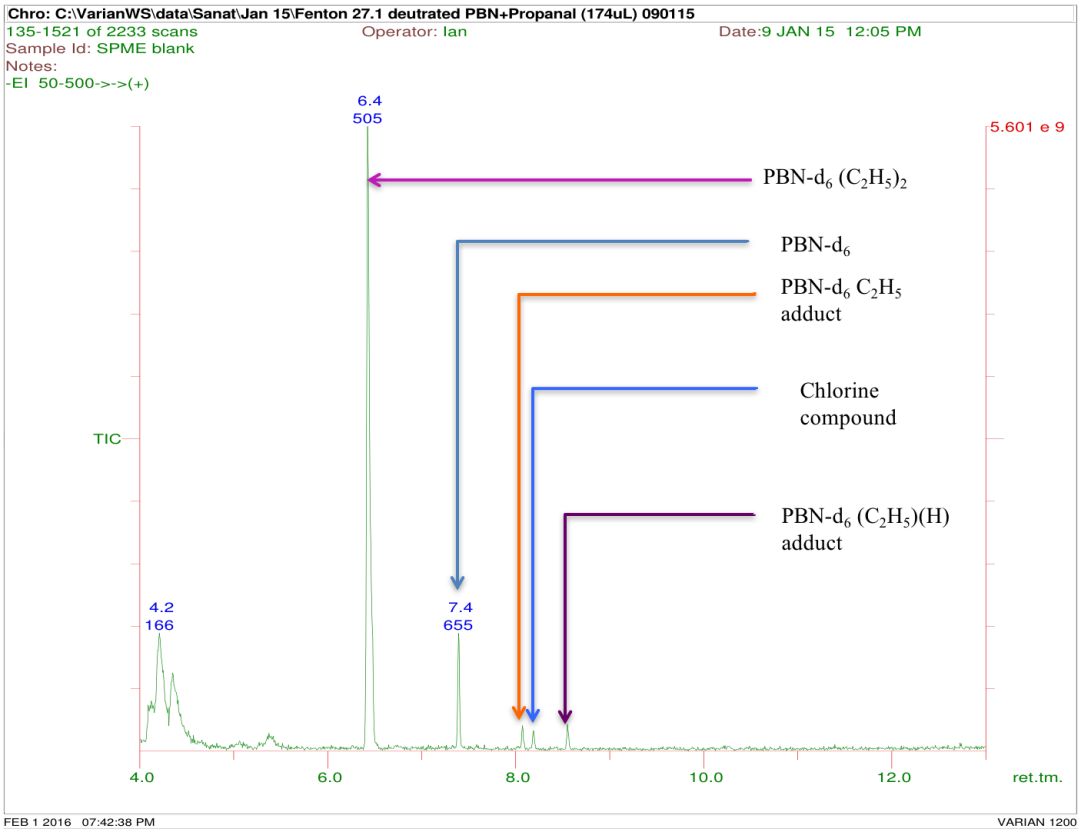

Figure 5.2: Total ion chromatogram (TIC) obtained from the GC/MS analysis of the Fenton reaction mixture containing PBN-d_6 and propanal and extracted directly with chloroform.

TIC obtained for the reaction mixture involving Fenton chemistry, PBN-d_6 and propanal extracted into chloroform is shown in Figure 5.2. Identified peaks with their retention times, molecular ions and base peaks are given in Table 5.2.

Retention time (minutes)	Molecular ion (m/z)	Base Peak (m/z)	Identity
4.1 - 4.3	127	127	Benzaldehyde oxime-d_6
6.4	241	125	PBN-d_6(C_2H_5)$_2$
7.4	183	57	PBN-d_6
8.1	212	156	PBN-d_6 C_2H_5
8.2	178	178	C_6D_5-CD-$CHCl_2$
8.6	213	153	PBN-d_6 (C_2H_5)(H)

Table 5.2: Retention, molecular ion, base peak with their identity for peaks obtained in chromatogram (Figure 5.2).

5.2.1.3 4-FPBN

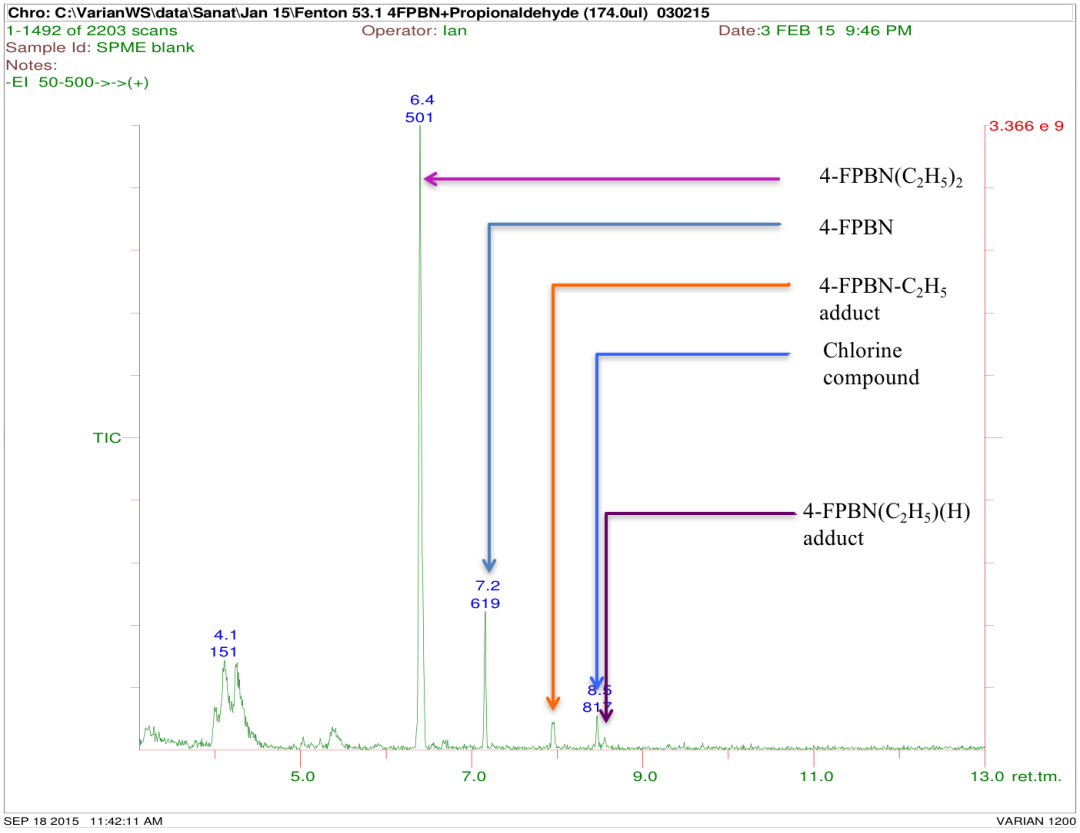

Figure 5.3: Total ion chromatogram (TIC) obtained from the GC/MS analysis of the Fenton reaction mixture containing 4-FPBN and propanal and extracted directly with chloroform.

5. Analysis of spin trapped ethyl radical from propionaldehyde (propanal)

TIC obtained for the reaction mixture involving Fenton chemistry, 4-FPBN and propanal extracted into chloroform is shown in Figure 5.3. Identified peaks with their retention times, molecular ions and base peaks are given in Table 5.3.

Retention time (minutes)	Molecular ion (m/z)	Base Peak (m/z)	Identity
4.0 - 4.4	139	55	4-Fluoro benzaldehyde oxime
6.4	253	137	4-FPBN(C_2H_5)$_2$
7.2	195	57	4-FPBN
7.9	224	168	4-FPBN-C_2H_5
8.0	190	190	4-FC_6H4-CH-$CHCl_2$
8.5	225	165	4-FPBN(C_2H_5)(H)

Table 5.3: Retention, molecular ion, base peak with their identity for peaks obtained in chromatogram (Figure 5.3).

5.2.1.4 4-ClPBN

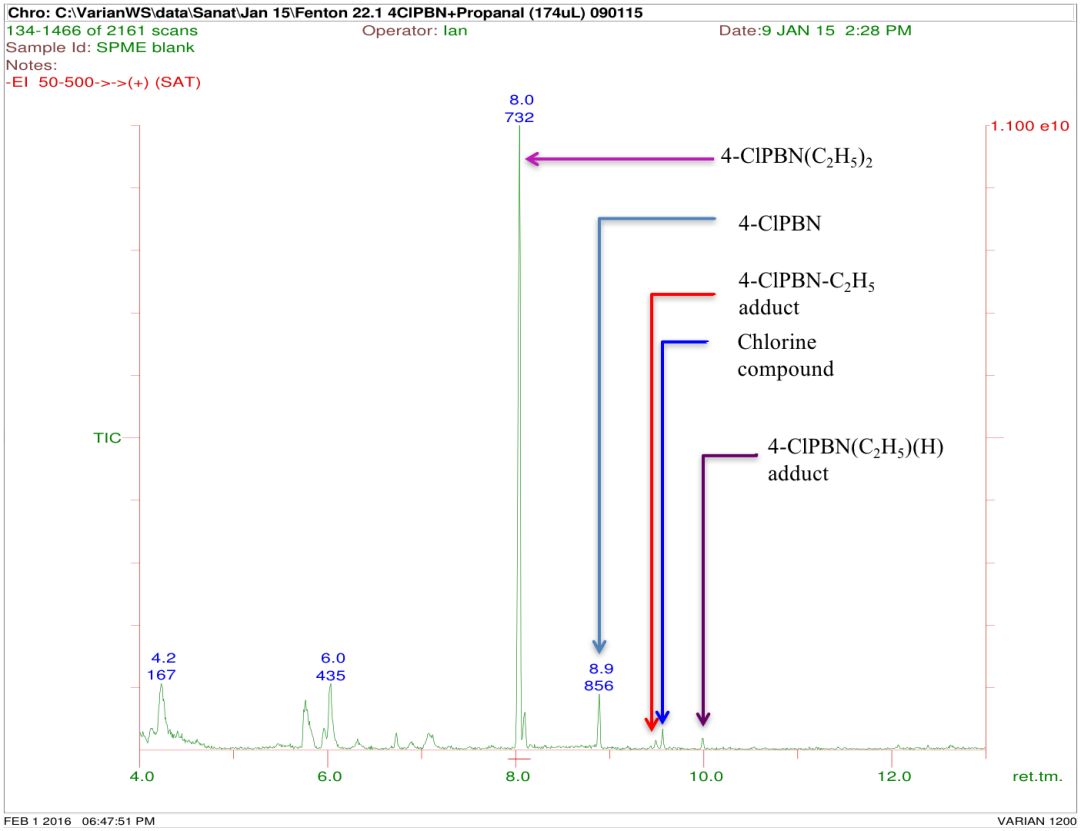

Figure 5.4: Total ion chromatogram (TIC) obtained from the GC/MS analysis of the Fenton reaction mixture containing 4-ClPBN and propanal and extracted directly with chloroform.

TIC obtained for the reaction mixture involving Fenton chemistry, 4-ClPBN and propanal extracted into chloroform is shown in Figure 5.4. Identified peaks with their retention times, molecular ions and base peaks are given in Table 5.4.

Retention time (minutes)	Molecular ion (m/z)	Base Peak (m/z)	Identity
5.8-6.0	155	155	4-Chloro benzaldehyde oxime
8.0	269	153	4-ClPBN$(C_2H_5)_2$
8.9	211	57	4-ClPBN
9.5	240	184	4-ClPBN-C_2H_5
9.6	206	206	4-ClC_6H4-CH-$CHCl_2$
10.0	241	181	4-ClPBN(C_2H_5)(H)

Table 5.4: Retention, molecular ion, base peak with their identity for peaks obtained in chromatogram (Figure 5.4).

5.2.2 Analysis and interpretation of diethyl adduct

5.2.2.1 PBN$(C_2H_5)_2$ adduct

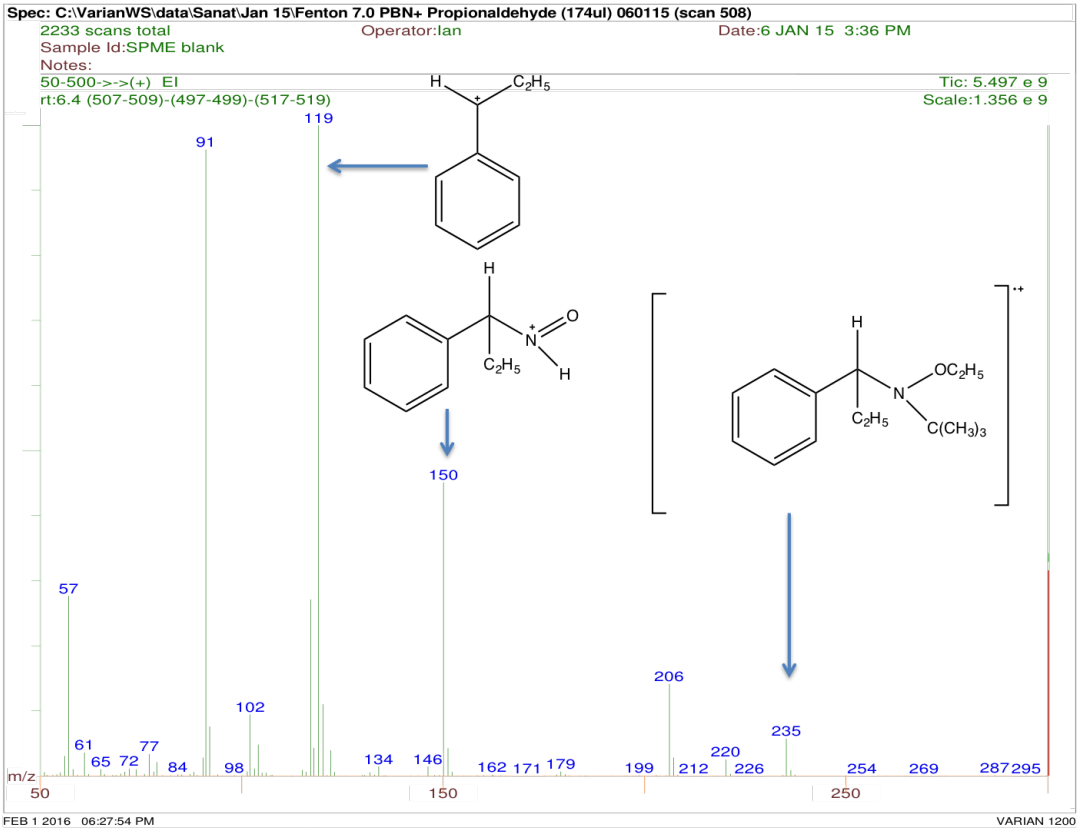

Figure 5.5: Mass spectrum obtained for PBN-diethyl adduct at 6.4 minutes (from the chromatogram in Figure 5.1) with a molecular ion at m/z 235.

The TIC chromatogram (shown in Figure 5.1) shows an intense peak at 6.4 minutes and its corresponding mass spectrum (Figure 5.5) shows a molecular ion at m/z 235 for a PBN$(C_2H_5)_2^{\bullet+}$ adduct (MW=235). The fragmentation pattern is shown in Figure 5.6. Loss of a methyl radical from the molecular ion results in a peak at m/z 220, whereas loss of an ethyl radical from the molecular ion results in a peak at m/z 206. The fragment at m/z 179 and m/z 150 are due to loss of 2-methyl-1-propene (56 Da) from the molecular ion and the ion at m/z 206, respectively. The base peak at m/z 119 is due to the presence of the cation shown in Figure 5.5, and resulting from dissociation of the molecular ion at the C-N bond. The fragment at m/z 91 may be assigned to the tropylium ion ($C_7H_7^+$) and that at m/z 57 to the *tert*-butyl cation.

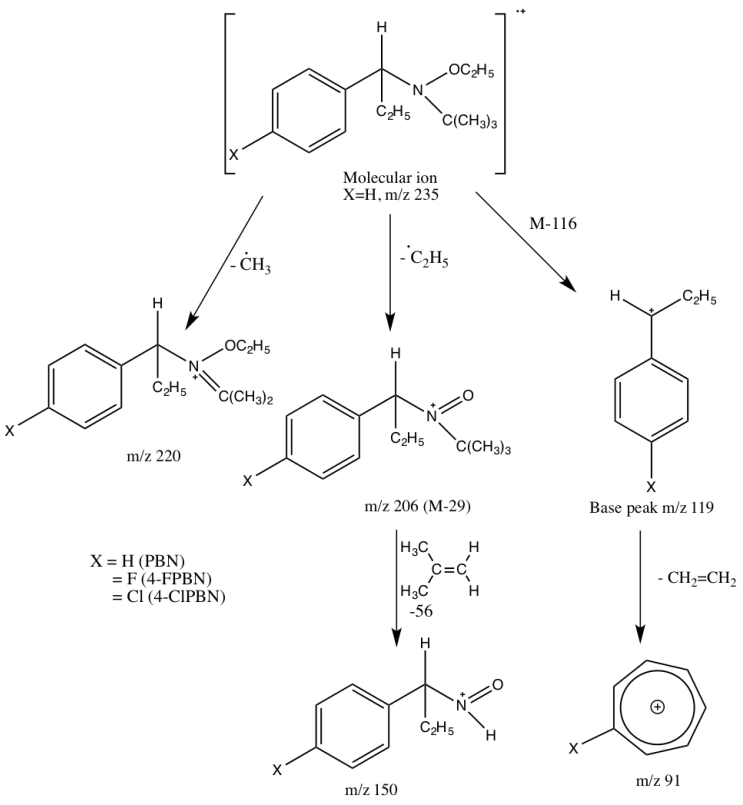

Figure 5.6: EI-MS fragmentation pattern for the PBN-diethyl adduct.

5.2.2.2 Deuterated PBN-$d_6(C_2H_5)_2$ adduct

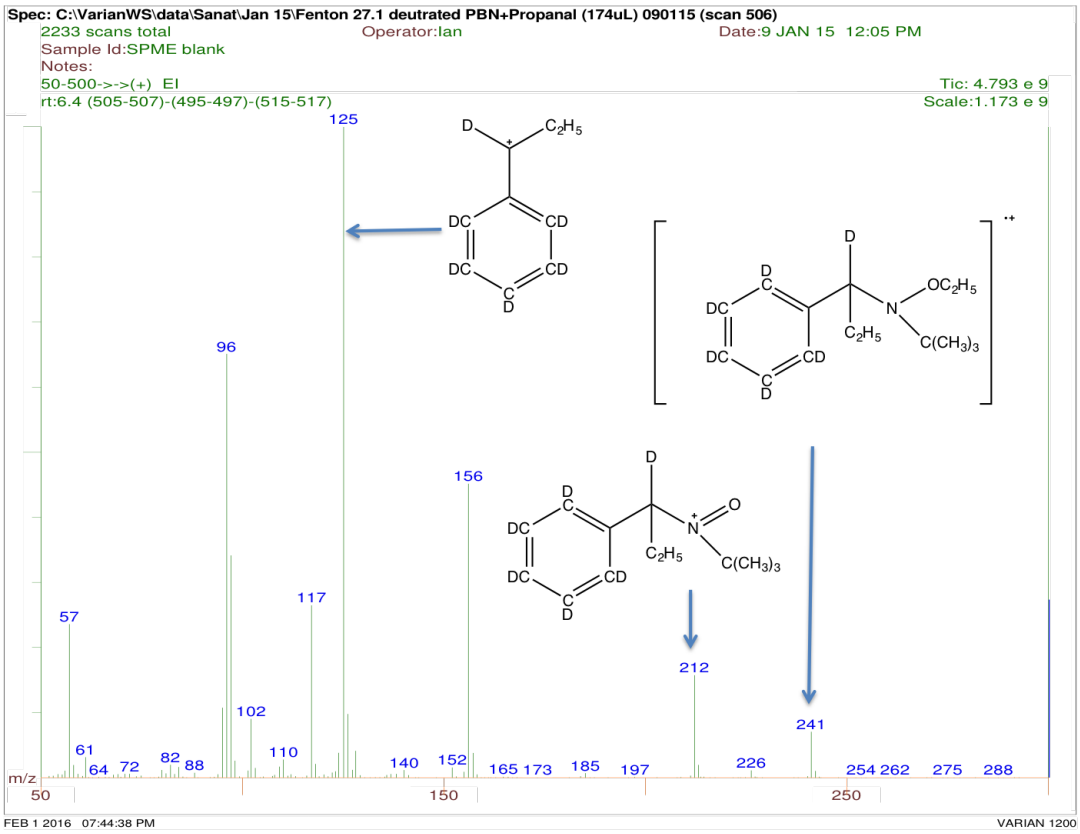

Figure 5.7: Mass spectrum obtained for PBN-d_6 diethyl adduct at 6.4 minutes (from the chromatogram in Figure 5.2) with a molecular ion at m/z 241.

The TIC chromatogram (shown in Figure 5.2) shows an intense peak at 6.4 minutes and its corresponding mass spectrum (Figure 5.7) shows a molecular ion at m/z 241 corresponding to PBN-$d_6(C_2H_5)_2{}^{\bullet+}$ adduct (MW=241). The fragmentation pattern is similar to the PBN$(C_2H_5)_2$ fragment with expected mass difference depending on the substituent, shown in Figure 5.6. The fragmentation shows a loss of a methyl radical from the molecular ion giving an ion at m/z 226, and loss of an ethyl radical from the molecular ion generating an ion at m/z 212. Fragments at m/z 185 and m/z 156 are due to loss of 2-methyl-1-propene (56 Da) from the molecular ion and ion at m/z 212, respectively. The base peak at m/z 125 is due to the presence of cation shown in Figure 5.7, and is derived from the molecular ion. The fragment at m/z 96 corresponds to the partially deuterated tropylium ion ($C_7D_5H_2{}^+$) and that at m/z 57 is to the *tert*-butyl cation.

5.2.2.3 4-FPBN$(C_2H_5)_2$ adduct

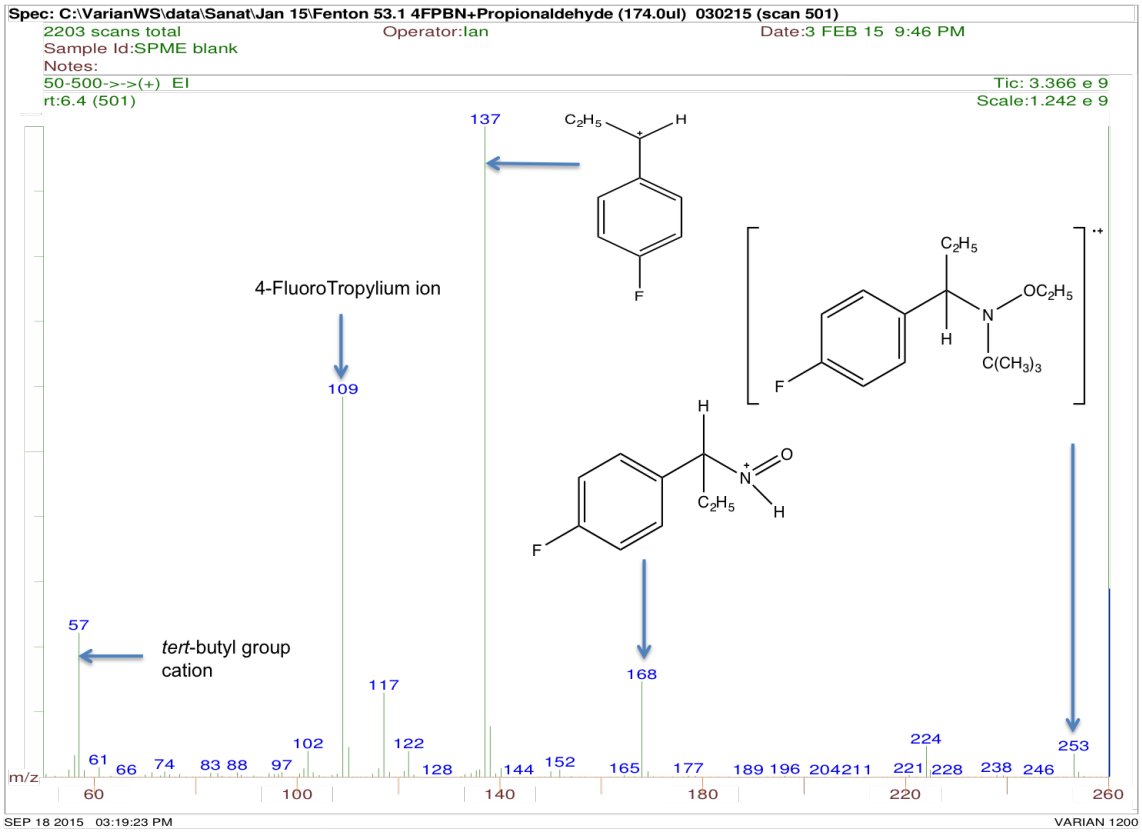

Figure 5.8: Mass spectrum obtained for 4-FPBN-diethyl adduct at 6.4 minutes (from the chromatogram in Figure 5.3) with a molecular ion at m/z 253.

The TIC chromatogram (shown in Figure 5.3) shows a 4-FPBN diethyl adduct peak with retention time 6.4 minutes and its corresponding mass spectrum shown in Figure 5.8. The mass spectrum shows a peak at m/z 253 which corresponds to the molecular ion of a 4-FPBN diethyl adduct $[4\text{-FPBN}(C_2H_5)_2]^{+\bullet}$. Loss of an methyl radical from the molecular ion results in a peak at m/z 238 (M-15). The peak at m/z 224 (M-29) corresponds to loss of an ethyl radical from the molecular ion. Loss of 2-methyl-1-propene $[(CH_3)_2C{=}CH_2]$ from the ion at m/z 224 give rise to the fragment at m/z 168 shown in Figure 5.8. The base peak at m/z 137 is due to the presence of ion shown in Figure 5.8, and is derived directly from the molecular ion. The peak at m/z 109 indicates a 4-fluoro tropylium ion $(C_7H_6F^+)$ and that at m/z 57 correspond to the *tert*-butyl group cation.

5.2.2.4 4-ClPBN$(C_2H_5)_2$ adduct

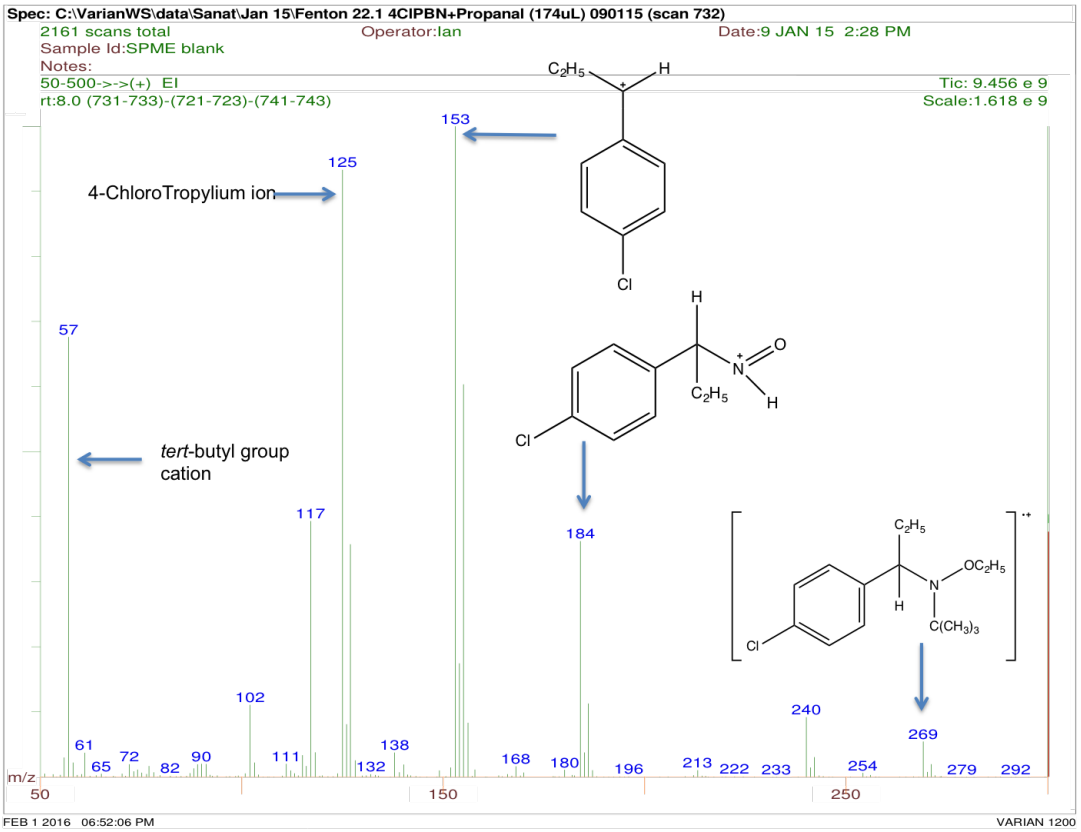

Figure 5.9: Mass spectrum obtained for 4-ClPBN-diethyl adduct at 8.0 minutes (from the chromatogram in Figure 5.4) with a molecular ion at m/z 269.

The total ion chromatogram (shown in Figure 5.4) shows 4-ClPBN diethyl adduct peak at 8.0 minutes and its mass spectrum (shown in Figure 5.9). The mass spectrum shows a peak at m/z 269 (^{35}Cl) and corresponding isotope peak at 271 (^{37}Cl) which may be assigned to the molecular ion 4-ClPBN diethyl adduct [4-ClPBN$(C_2H_5)_2]^{+\bullet}$. The fragment at m/z 254 is due to loss of a methyl radical from the molecular ion; loss of an ethyl radical from the molecular ion results in the peak at m/z 240/242 (M-29). Loss of 2-methyl-1-propene [$(CH_3)_2C{=}CH_2$] from m/z 240/242 gives rise to the fragment at 184/186 m/z shown in Figure 5.9. The base peak at m/z 153 is due to the presence of ion shown in Figure 5.9, and is derived from the molecular ion. The peak at m/z 125/127 belongs to the 4-chloro tropylium ion ($C_7H_6{}^{35}Cl^+/C_7H_6{}^{37}Cl^+$) and that at m/z 57 corresponds to the *tert*-butyl group cation.

5.2.3 Analysis and interpretation of a PBN monoethyl adduct

5.2.3.1 PBN-C_2H_5 adduct at 8.1 minutes

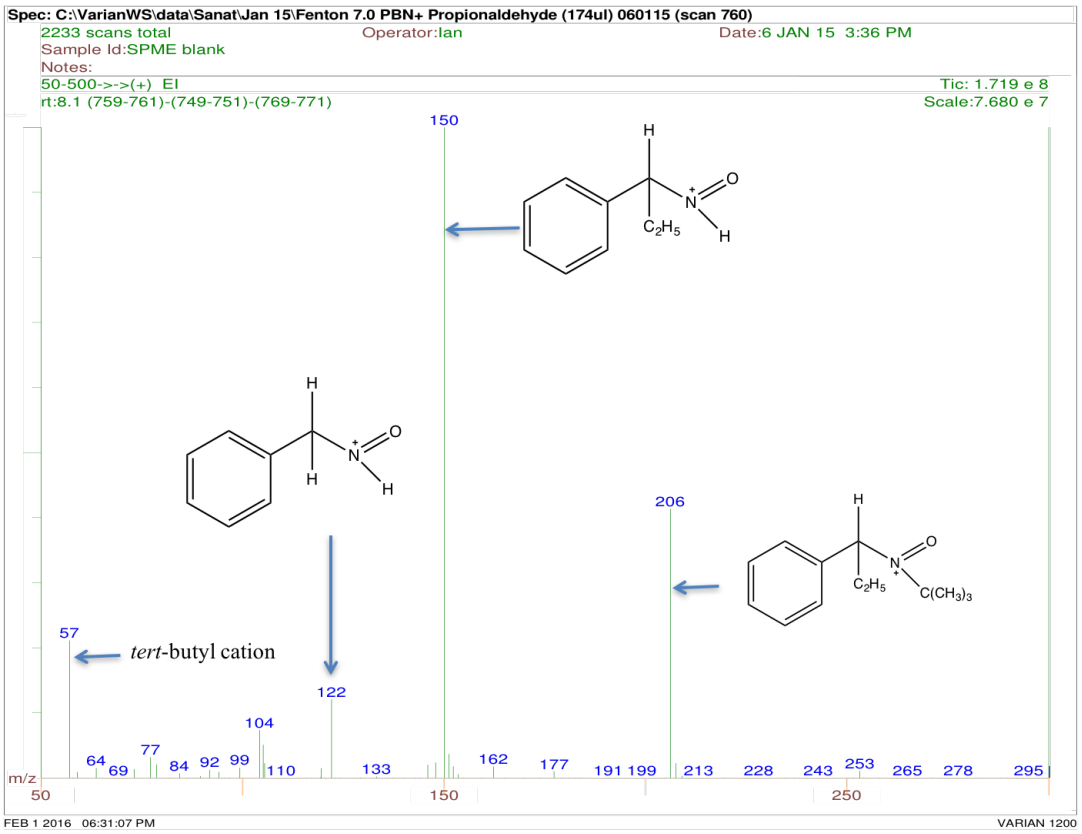

Figure 5.10: Mass spectrum corresponding to a peak at 8.1 minutes (from the chromatogram in Figure 5.1) assigned to a PBN monoethyl adduct (PBN-C_2H_5).

The mass spectrum in Figure 5.10 corresponds to the peak retained at 8.1 minutes (Figure 5.1). The mass spectrum shows a "molecular ion" at m/z 206 suggesting formation of PBN-C_2H_5 adduct. As with the monomethyl adduct of PBN (formed from the dissociation of acetaldehyde and subsequent methyl radical addition to PBN) an ethyl radical is trapped by PBN to form a nitroxide. Since the nitroxide has an unpaired electron, the molecular ion formed in the ion source of the mass spectrometer is a cation (not the usual radical cation). The fragment at m/z 191 is due to loss of a methyl radical, probably from the *tert*-butyl group on the molecular ion. The peak at m/z 177 is due to loss of an ethyl radical from the molecular ion (M-29), and that at m/z 162 is loss of 15, a methyl from m/z 177. The base peak at m/z 150 is due to loss of 2-methyl-1-propene from the molecular ion (structure shown in Figure 5.10). The fragment at m/z 122 is possible due to loss of

ethene from base peak, whereas the fragment at m/z 77 corresponds to the phenyl cation and that at m/z 57 to the *tert* butyl cation. The ion at m/z 104 is a radical cation, probably formed by dissociation of the "molecular ion" at the C-N bond. The monoethyl adducts for the various PBN derivatives follows the same general fragmentation pattern as shown in Figure 5.11.

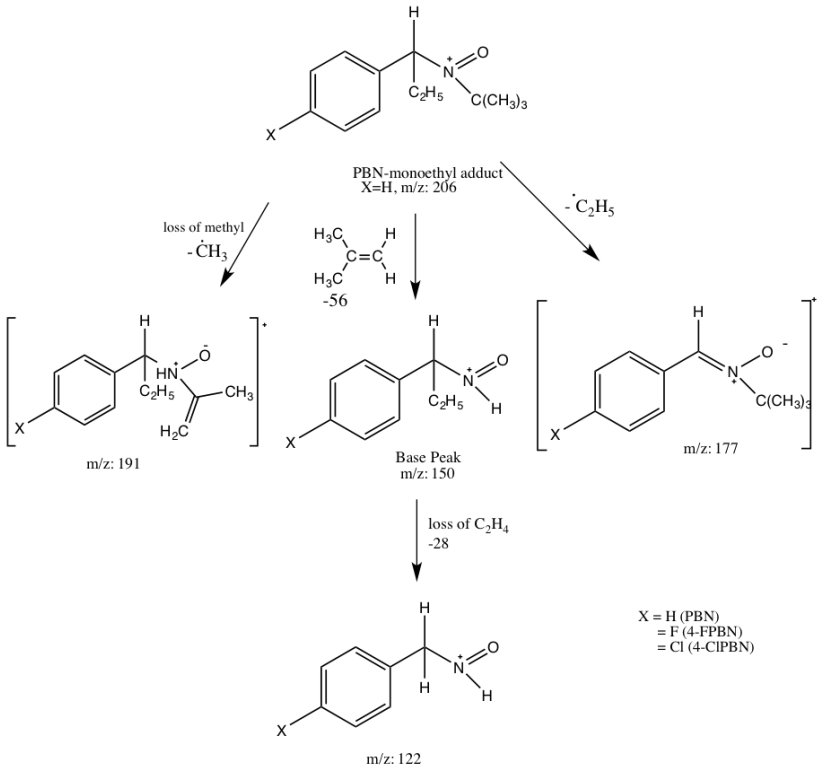

Figure 5.11: The Fragmentation scheme for the PBN monoethyl adduct.

5.2.3.2 Deuterated PBN-d_6 C_2H_5 adduct at 8.1 minutes

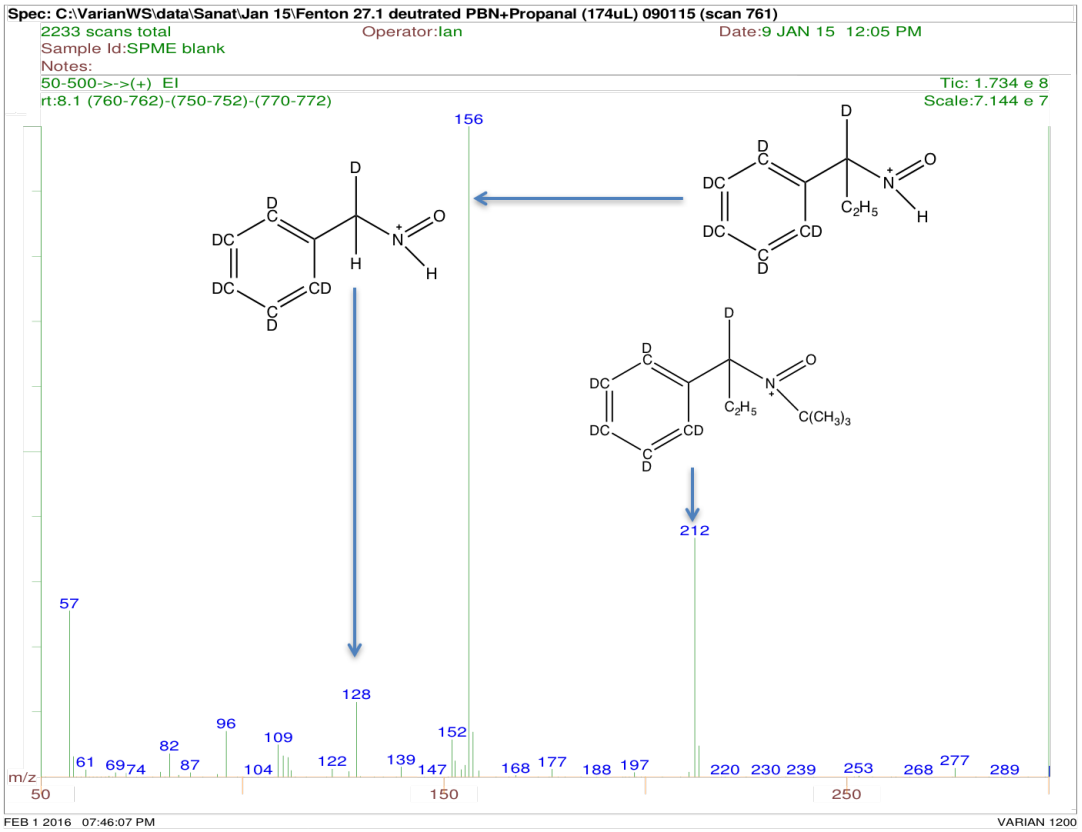

Figure 5.12: Mass spectrum corresponding to a peak at 8.1 minutes (from the chromatogram in Figure 5.2) assigned to a PBN-d_6 monoethyl adduct (PBN-d_6 C_2H_5).

The mass spectrum in Figure 5.12 corresponds to the peak retained at 8.1 minutes (Figure 5.2). The mass spectrum shows a "molecular ion" at m/z 212 suggesting formation of PBN-d_6 C_2H_5 adduct. The fragment at m/z 197 is due to loss of a methyl radical, probably from the *tert*-butyl group on the "molecular ion". The base peak at 156 m/z is due to the loss of 2-methyl-1-propene from the "molecular ion" (M-56). Fragment at m/z 128 is due to the $C_7H_2D_6NO^+$ (Figure 5.12), m/z 96 corresponding to $C_7D_5H_2^+$, m/z 82 is for deuterated phenyl cation ($C_6D_5^+$) and m/z 57 corresponds to the *tert*-butyl cation.

5.2.3.3 4-FPBN-C_2H_5 adduct at 7.9 minutes

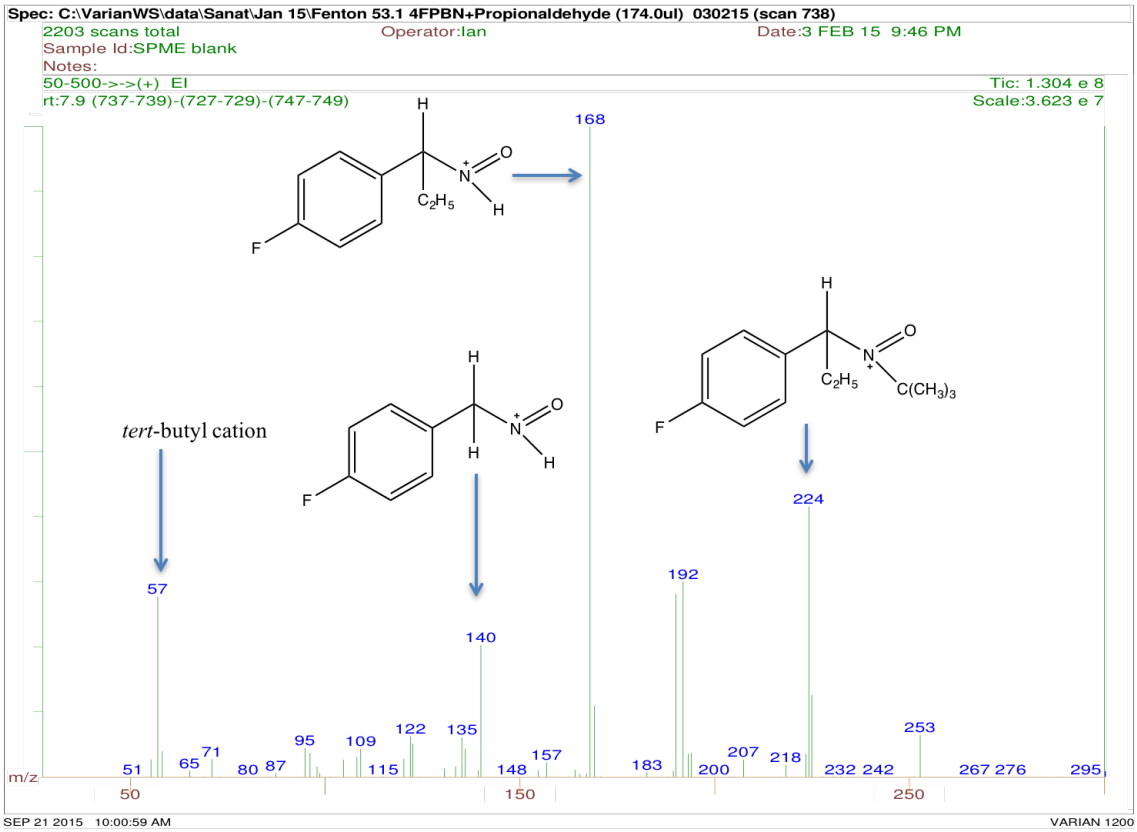

Figure 5.13: Mass spectrum corresponding to a peak at 7.9 minutes (from the chromatogram in Figure 5.3) assigned to a 4-FPBN monoethyl adduct (4-FPBN-C_2H_5).

The mass spectrum in Figure 5.14 corresponds to the peak with a retention time 7.9 minutes (Figure 5.3); showing a "molecular ion" peak at m/z 224 which suggests the formation of a (4-FPBN-C_2H_5) adduct. Loss of 2-methyl-1-propene [$(CH_3)_2C{=}CH_2$] from the "molecular ion" give rise to base peak at m/z 168 (M-56). Other fragements are: m/z 140 (loss of ethene from m/z 168), m/z 109 is for the 4-fluorotropylium ion (4-$FC_7H_7^+$), m/z 95 is for 4-$FC_6H_4^+$ and peak at 57 m/z is the characteristic peak for *tert*-butyl cation.

5.2.3.4 4-ClPBN-C_2H_5 adduct at 9.5 minutes

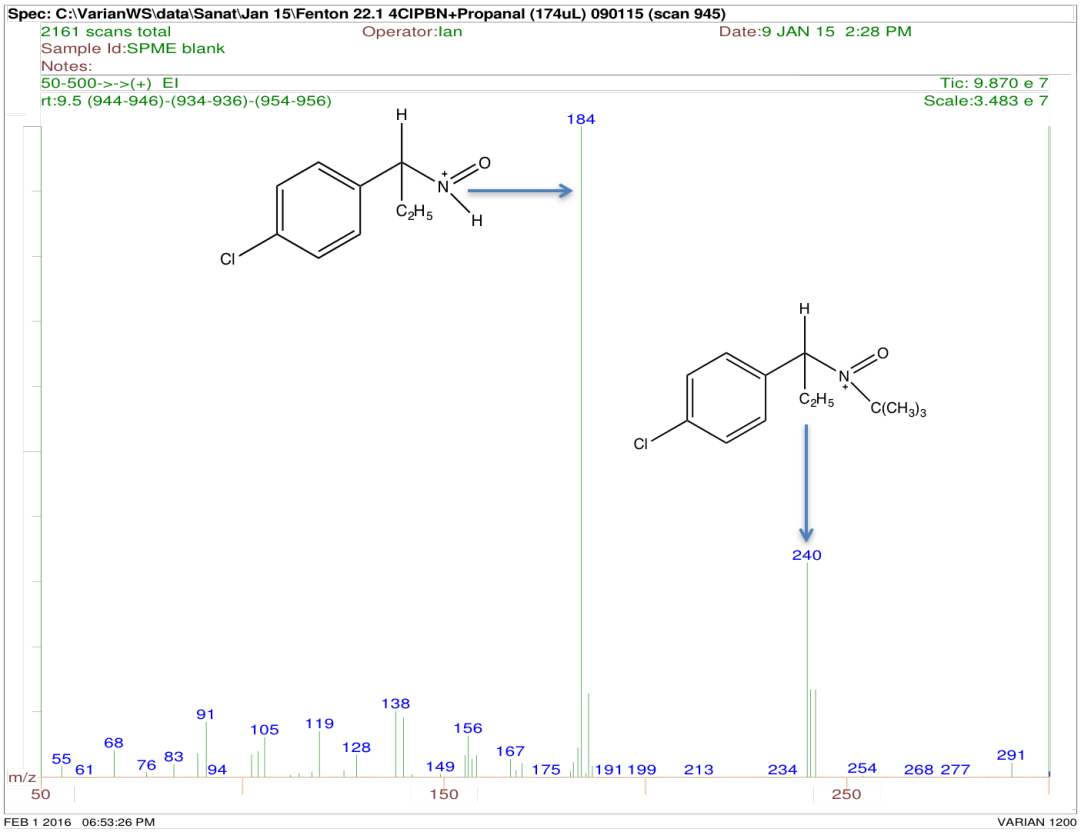

Figure 5.14: Mass spectrum corresponding to a peak at 9.5 minutes (from the chromatogram in Figure 5.4) assigned to a 4-ClPBN monoethyl adduct (4-ClPBN-C_2H_5).

The mass spectrum in Figure 5.14 corresponds to the peak with a retention time of 7.9 minutes (Figure 5.4). It shows a "molecular ion" at m/z 240/242 which correspond to the 4-ClPBN monoethyl adduct (4-ClPBN-C_2H_5). The peak at m/z 184/186 is due to loss of 2-methyl-1-propene from the "molecular ion" (M-56).

5.2.4 Anlaysis and interpretation of other C_2H_5 adduct

5.2.4.1 PBN(C_2H_5)(H) adduct at 8.6 minutes

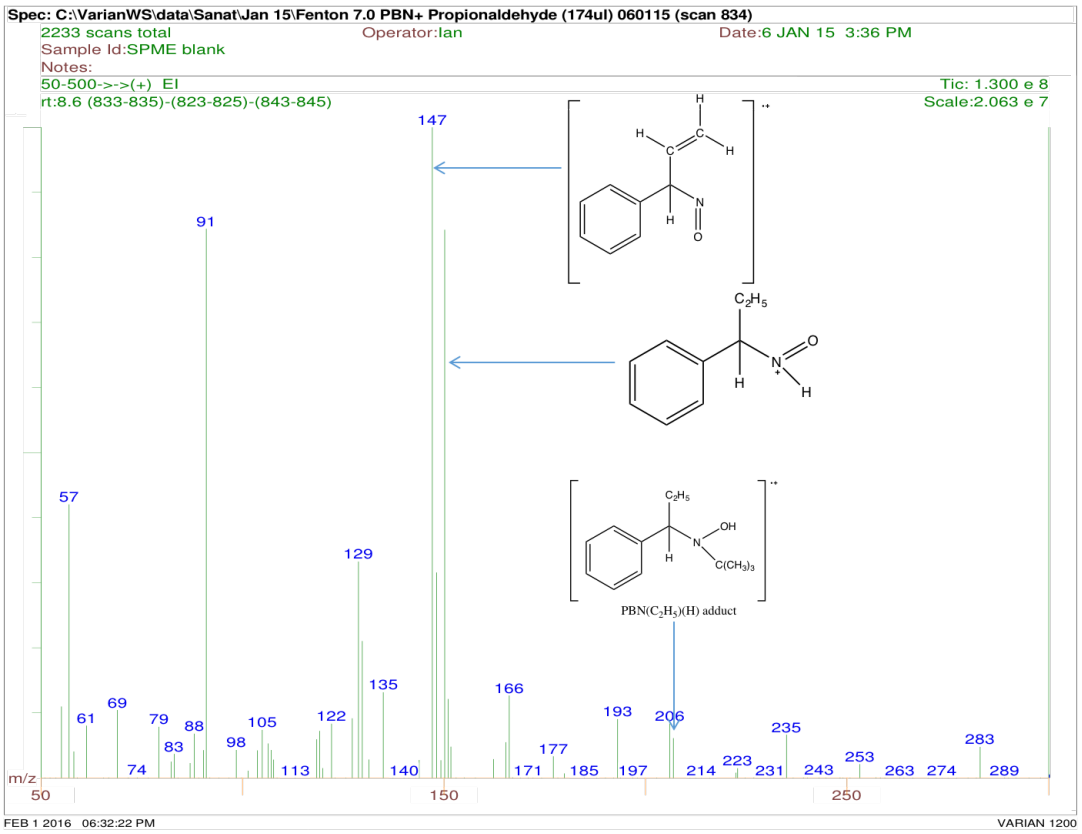

Figure 5.15: Mass Spectrum obtained for PBN(C_2H_5)(H) adduct at 8.6 minutes (from the chromatogram in Figure 5.1).

The mass spectrum shown in Figure 5.15 corresponds to the peak retained at 8.6 minutes in GC chromatogram (Figure 5.1). The mass spectrum shows a "molecular ion" peak at m/z 207. The fragment at m/z 206 is due to loss of hydrogen from the "molecular ion". The mass spectrum analysis shows a fragment at m/z 150 (M-56) (loss of 2-methyl-1-propene from m/z 206), m/z 91 and m/z 57 are for the tropylium cation and *tert*-butyl cation respectively. The base peak at m/z 147 is for the radical cation shown in (Figure 5.15) which may formed due to loss of hydrogen atom ($H^{\bullet}$, probably from HNO) and H_2 (probably from C_2H_5) from m/z 150.

5.2.4.2 Deuterated PBN-d_6 (C_2H_5)(H) adduct 8.6 minutes

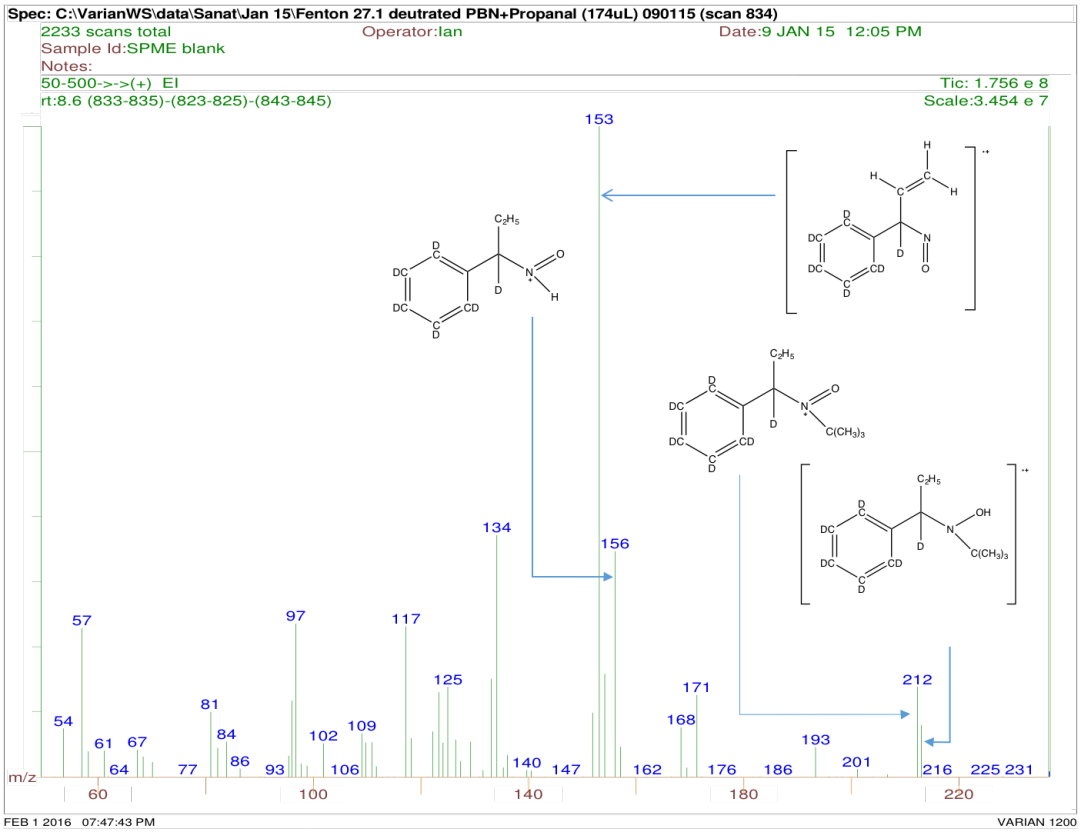

Figure 5.16: Mass Spectrum obtained for PBN-d_6(C_2H_5)(H) adduct at 8.6 minutes (from the chromatogram in Figure 5.2).

The mass spectrum shown in Figure 5.16 corresponds to the peak retained at 8.6 minutes in GC chromatogram (Figure 5.2). The mass spectrum shows a "molecular ion" at m/z 213. The fragment at m/z 212 (structure shown in Figure 5.16) is due to loss of hydrogen from molecular ion and fragment at m/z 156 (M-56) (is loss of 2-methyl-1-propene from the m/z 212). The base peak at m/z 153 could be loss of hydrogen atom ($H^{\bullet}$, probably from HNO) and H_2 (probably from C_2H_5) from m/z 156. Other fragments at m/z 97 is for the $C_7D_6H^+$ and m/z 57 is for *tert*-butyl cation.

5.2.4.3 4-FPBN(C_2H_5)(H) adduct 8.5 minutes

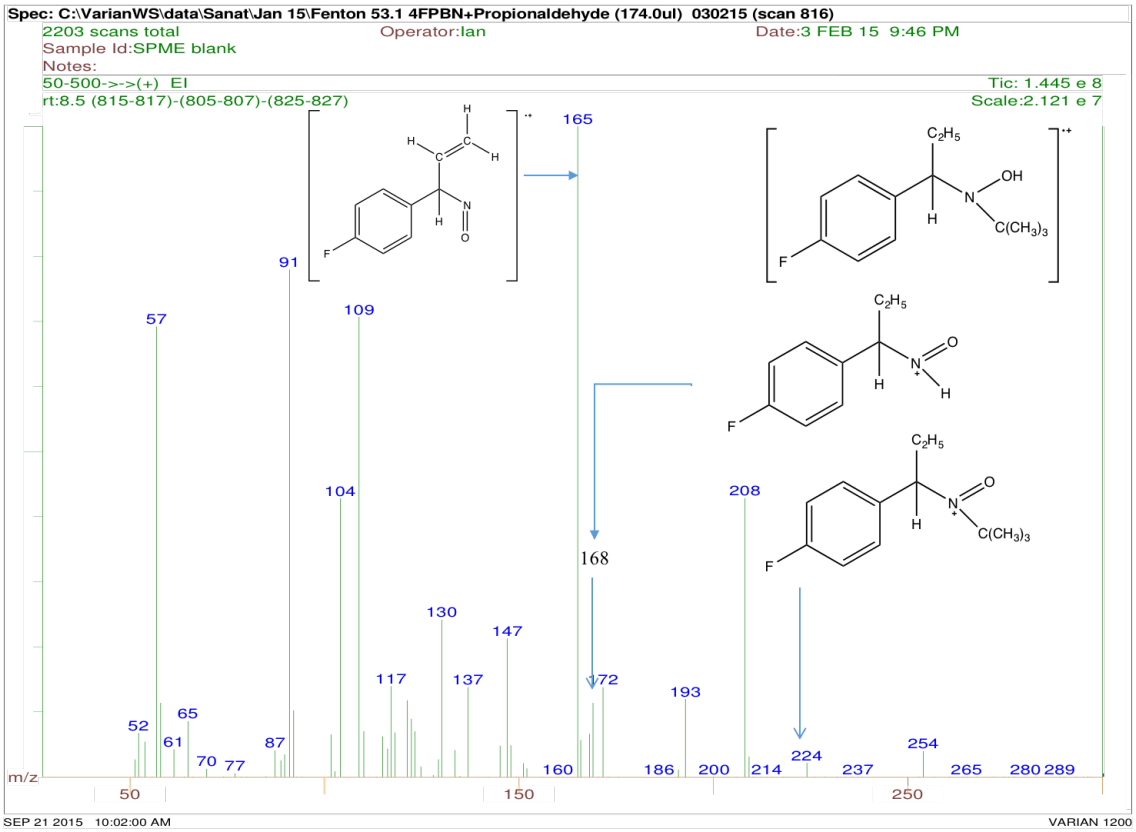

Figure 5.17: Mass Spectrum obtained for 4-FPBN(C_2H_5)(H) adduct at 8.5 minutes (structure shown in top right) from the chromatogram in Figure 5.3.

The mass spectrum shown in Figure 5.17 corresponds to the peak retained at 8.5 minutes in GC chromatogram (Figure 5.3), doesn't shows a molecular ion at m/z 225 (structure shown in top right in Figure 5.17). The mass spectrum shows a fragment at m/z 224 which could be due to the loss of hydrogen from the oxygen site. The fragment at m/z 168 (M-56) (loss of 2-methyl-1-propene), base peak at m/z 166 is loss of hydrogen atom ($H^{\bullet}$, from probably from HNO) and H_2 (probably from C_2H_5) from m/z 168. Other fragments are: m/z 109 is for the 4-fluoro tropylium cation ($C_7H_6F^+$) and m/z 57 is for *tert*-butyl cation.

5.2.4.4 4-ClPBN(C_2H_5)(H) adduct 10.0 minutes

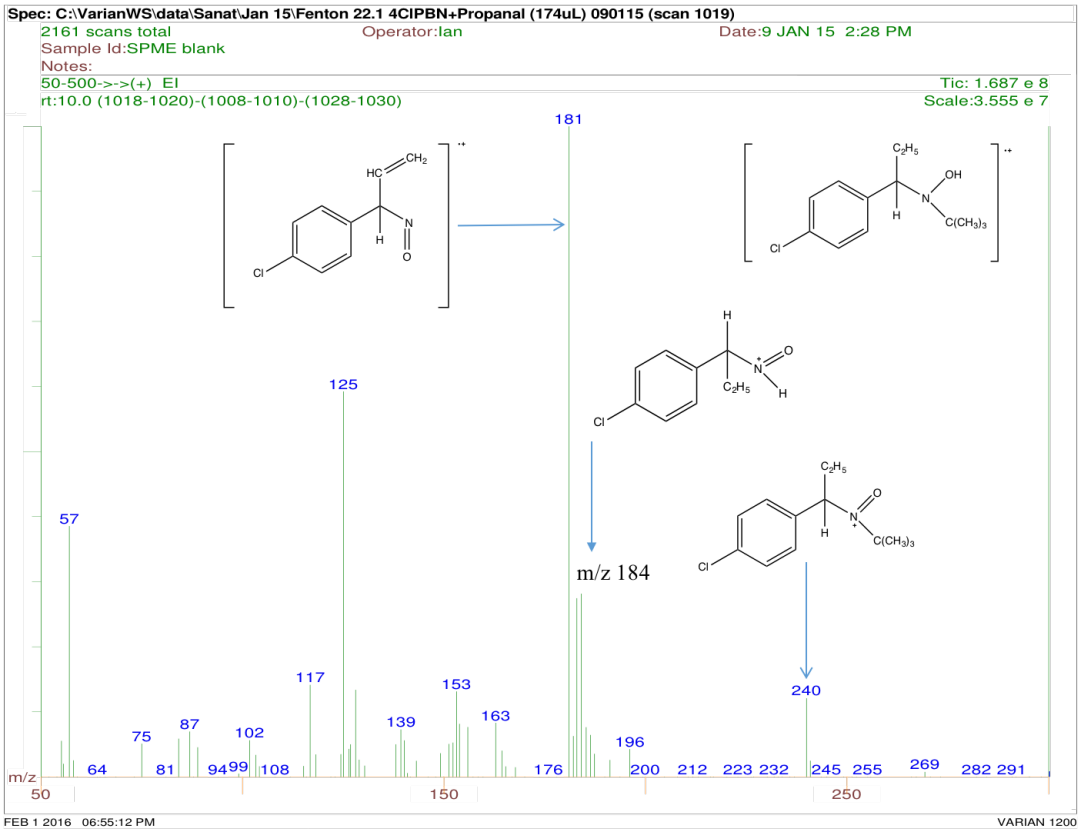

Figure 5.18: Mass Spectrum obtained for 4-ClPBN(C_2H_5)(H) adduct at 10.0 minutes (structure shown in top right) from the chromatogram in Figure 5.4.

The mass spectrum shown in Figure 5.18 corresponds to the peak retained at 10.0 minutes in GC chromatogram (Figure 5.4), doesn't shows a molecular ion at m/z 241/243. The mass spectrum shows fragment at m/z 240 is due to loss of hydrogen from the oxygen site, fragment at m/z 184/186 (M-56) (loss of 2-methyl-1-propene from m/z 240), base peak at m/z 181/183 is loss of hydrogen atom ($H^{\bullet}$, from probably from HNO) and H_2 (probably from C_2H_5) from m/z 184. Other fragments are: m/z 125/127 is for the $C_7H_6Cl^+$ and m/z 57 is for *tert*-butyl cation.

5.2.5 Analysis of other peaks

A cluster of peaks eluting before the diethyl adduct was detected in all the chromatograms as shown in section 5.2.1. With respect to PBN chromatogram (Figure 5.1), there is a

cluster of peaks containing two major compounds, of which one is benzaldehyde oxime. The mass spectrum (Figure 5.19) for the peak retained at 4.1 minutes shows a molecular ion at m/z 121 for benzaldehyde oxime. The fragment at m/z 77 corresponds to the phenyl cation and is formed due to loss of 43 m/z from the molecular ion. Depending on the PBN derivative the corresponding benzaldehyde oxime is formed with the expected change in m/z.

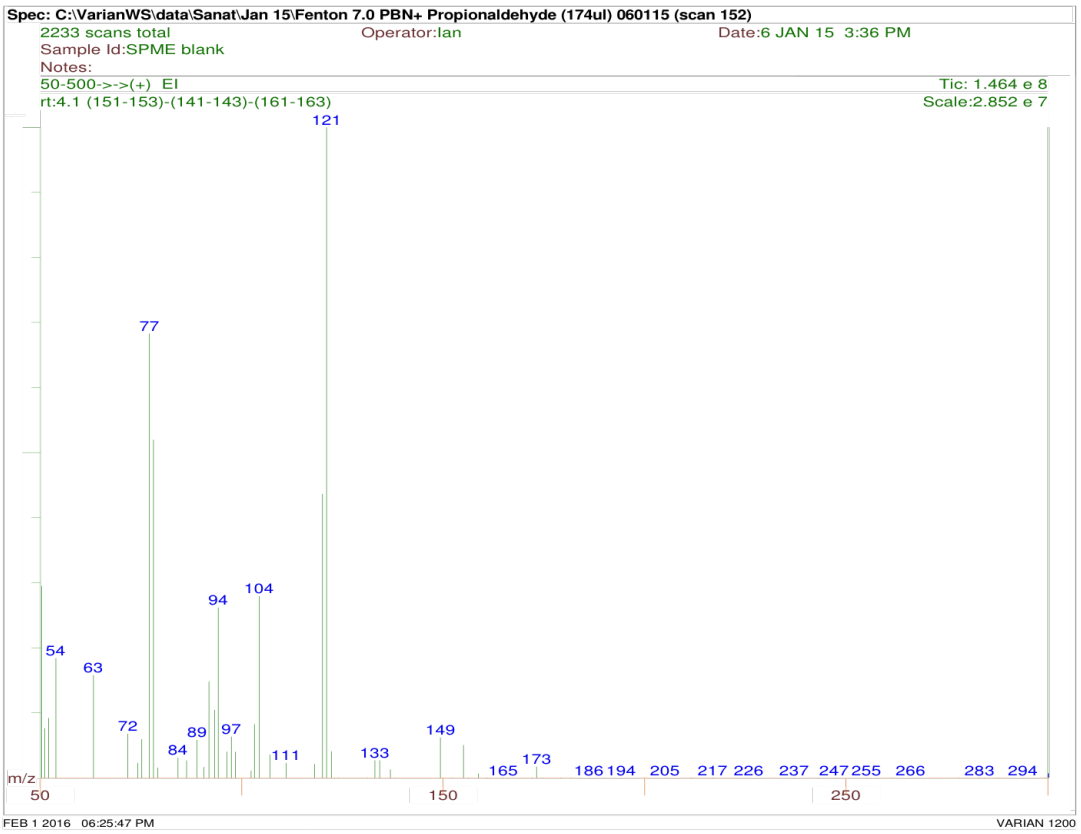

Figure 5.19: Mass Spectrum obtained for benzaldehyde oxime (peak at 4.1 minutes in the chromatogram shown in figure 5.1).

The second compound reatined at peak 4.2 minutes have been detected in all the Fenton reaction with no change in the mass spectrum fragment. Hence, it might be contamination from the the propanal (as this peak is only present in the propanal experiment).

5.3 Head Space Single Droplet Microextraction (HS-SDME)

5.3.1 Chromatogram

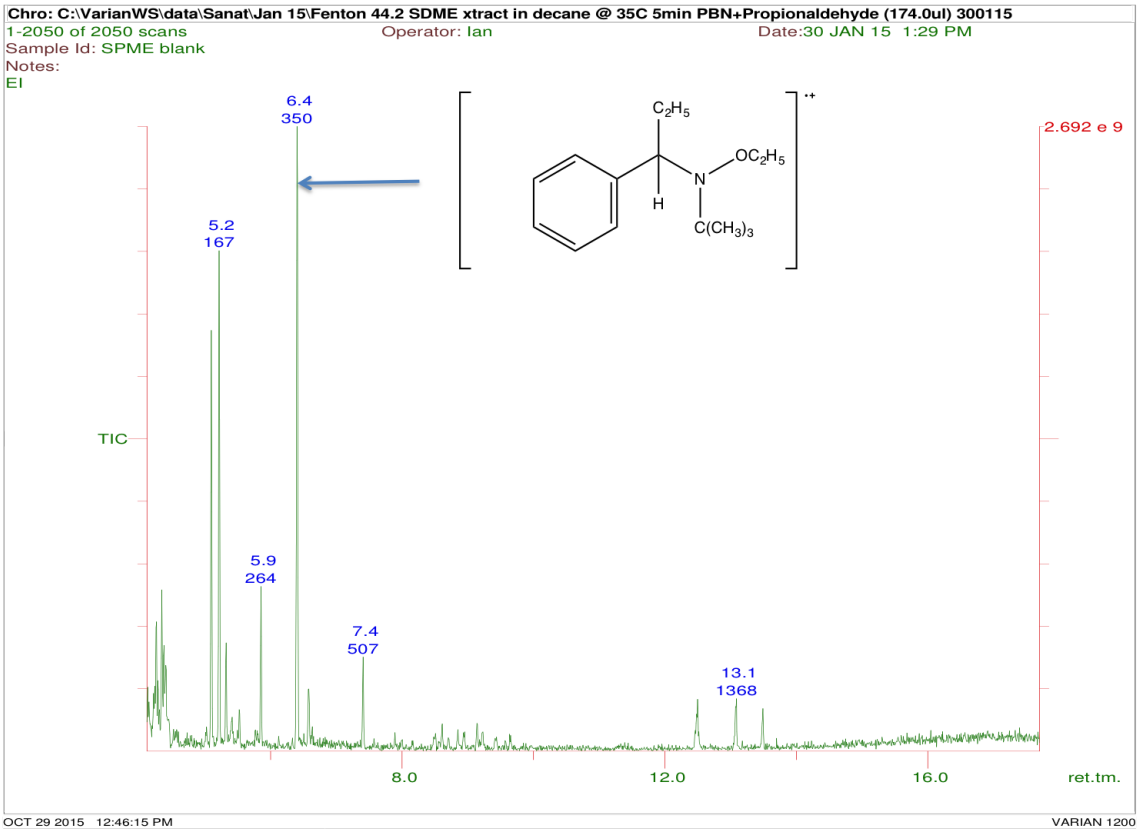

Figure 5.20: Total ion chromatogram (TIC) obtained from the GC/MS analysis of the Fenton reaction mixture containing PBN and propanal and extracted by HS-SDME.

The total ion chromatogram (TIC) obtained from HS-SDME sampling followed by GC/MS analysis of the Fenton reaction mixture containing propanal and PBN is shown in Figure 5.20. The chromatogram shows various peaks which may be assigned to alkanes (probably present in the decane solvent).

5.3.2 PBN$(C_2H_5)_2$ adduct

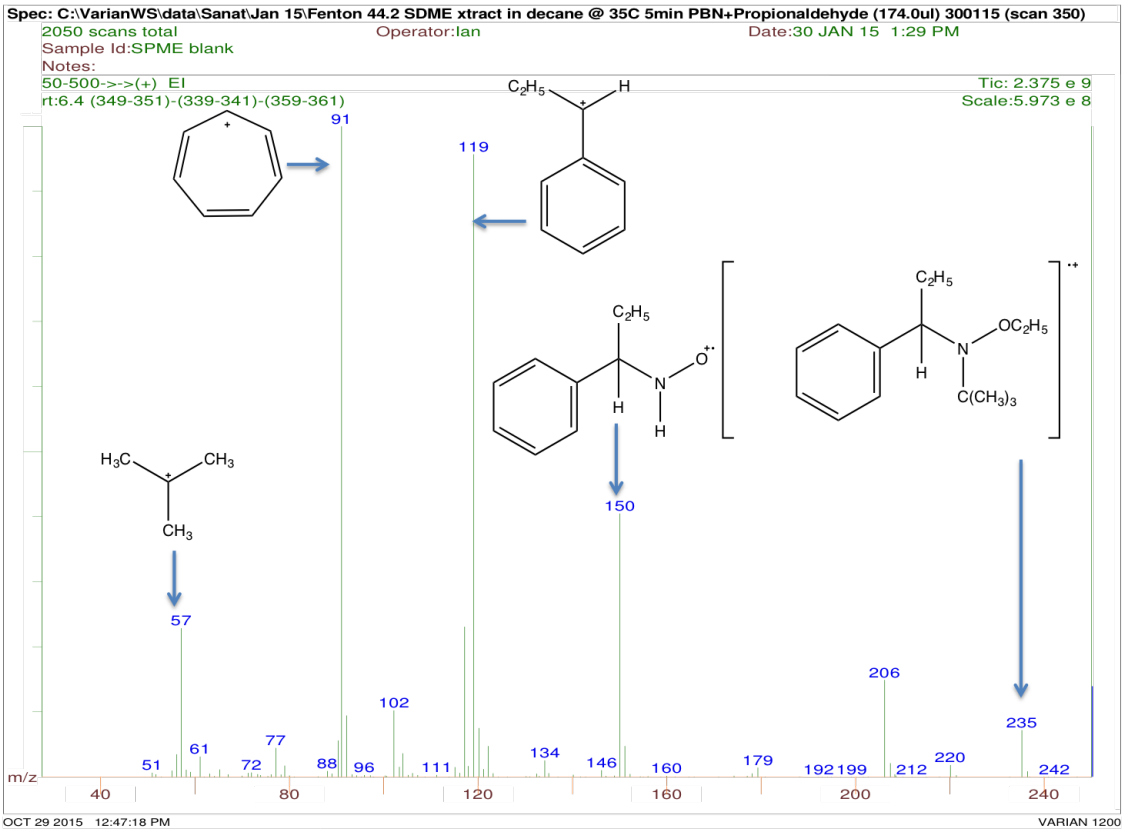

Figure 5.21: Mass spectrum obtained for PBN-diethyl adduct at 6.4 minutes (from the chromatogram in Figure 5.20) with a molecular ion at m/z 235.

The TIC chromatogram (shown in Figure 5.1) shows an intense peak at 6.4 minutes and its corresponding mass spectrum Figure 5.21 shows a a molecular ion for PBN diethyl adduct $[PBN(C_2H_5)_2]^{+\bullet}$ at m/z 235 and a base peak at m/z 91. The interpretation of the PBN$(C_2H_5)_2$ mass spectrum is shown in section 5.2.2.1.

5.3.3 Alkanes

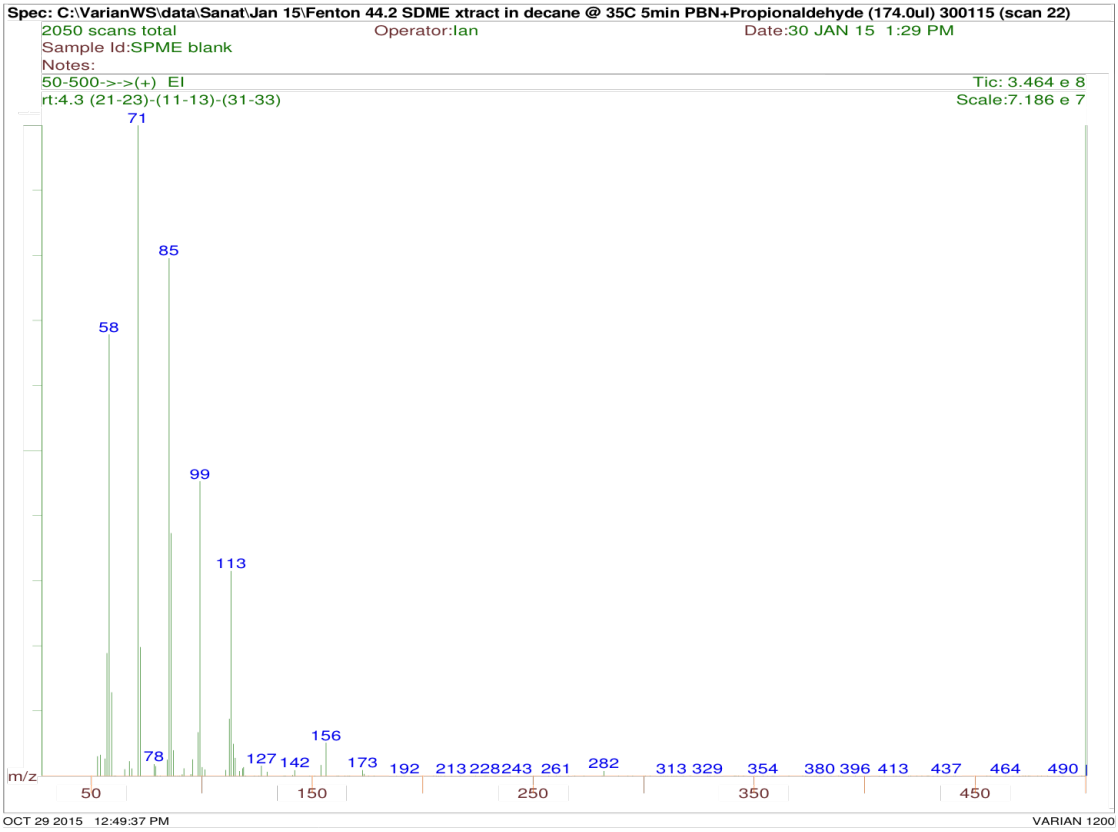

Figure 5.22: Mass spectrum for undecane at 4.3 minutes from the chromatogram in Figure 5.20.

The mass spectrum shown in Figure 5.22 shows a mixture of decane and undecane. The characteristic pattern of alkane can be seen from fragments m/z 142 to m/z 71, difference in 14 m/z between the fragments. The mass fragment shows a molecular ion at m/z 142 which corresponds to decane. Loss of methyl radical from $M^{+\bullet}$ ion to form m/z 127 followed by successive loss of ethene (a neutral olefin molecule) results in ion with m/z 99, which lose 28 to form m/z 71. Along with this loss of ethyl radical from molecular ion m/z 142 forms m/z 113 and successive loss of ethene result in fragment at m/z 85.

Further to confirm the interpretation and molecular ion (m/z 156), massbank data was used which suggested presence of undecane with $M^{+\bullet}$ at 156. With m/z 156 as molecular ion the fragmentation pattern shows loss of ethyl radical from molecular ion to form fragment at m/z 127, loss of ethene (28 amu) from m/z 127 result in fragment at m/z 99, loss of ethene from m/z 99 result in fragment at m/z 71. Hence, it can be concluded peak at 4.3 minutes contains decane and undecane.

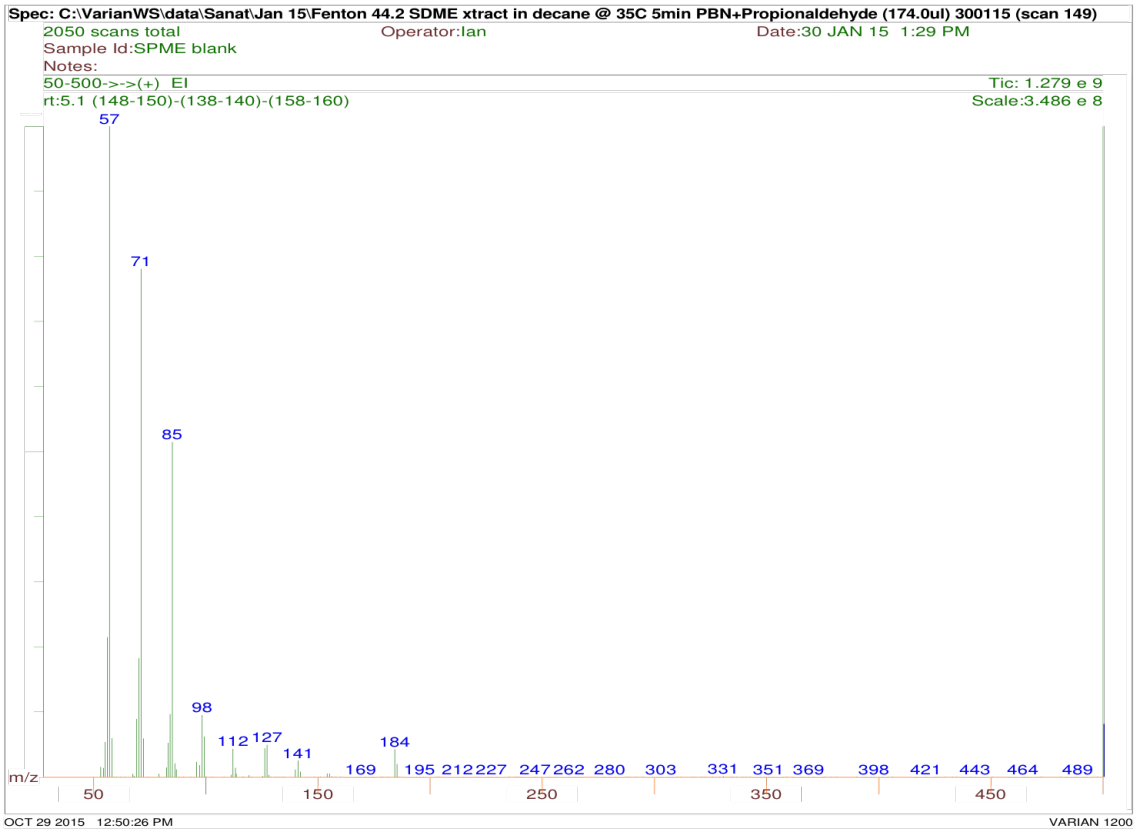

Figure 5.23: Mass spectrum for Tridecane peak at 5.1 minutes from the chromatogram in Figure 5.20.

The mass spectrum for peak at 5.1 minutes indicated this peak as a tridecane ($C_{13}H_{28}$). The spectrum shows molecular fragments at m/z 184, loss of methyl radical followed by successive loss of ethene (a neutral olefin molecule) result in ion with m/z 141. The loss of an ethyl radical and successive loss of ethene results in a fragment at m/z 127. Fragment at m/z 98 is due to loss of ethene from fragment m/z 126, fragment at m/z 85, 71 and base peak m/z 57 shows a typical pattern of alkanes: clusters of fragments separated by 14 m/z units. The mass spectrum was compared to standard tridecane mass spectrum obtained from NIST library with molecular ion at m/z 184 with fragment ions at 155, 141, 127, 113, 98, 85, 71, 57 and 43 as found the mass spectrum Figure 5.23.

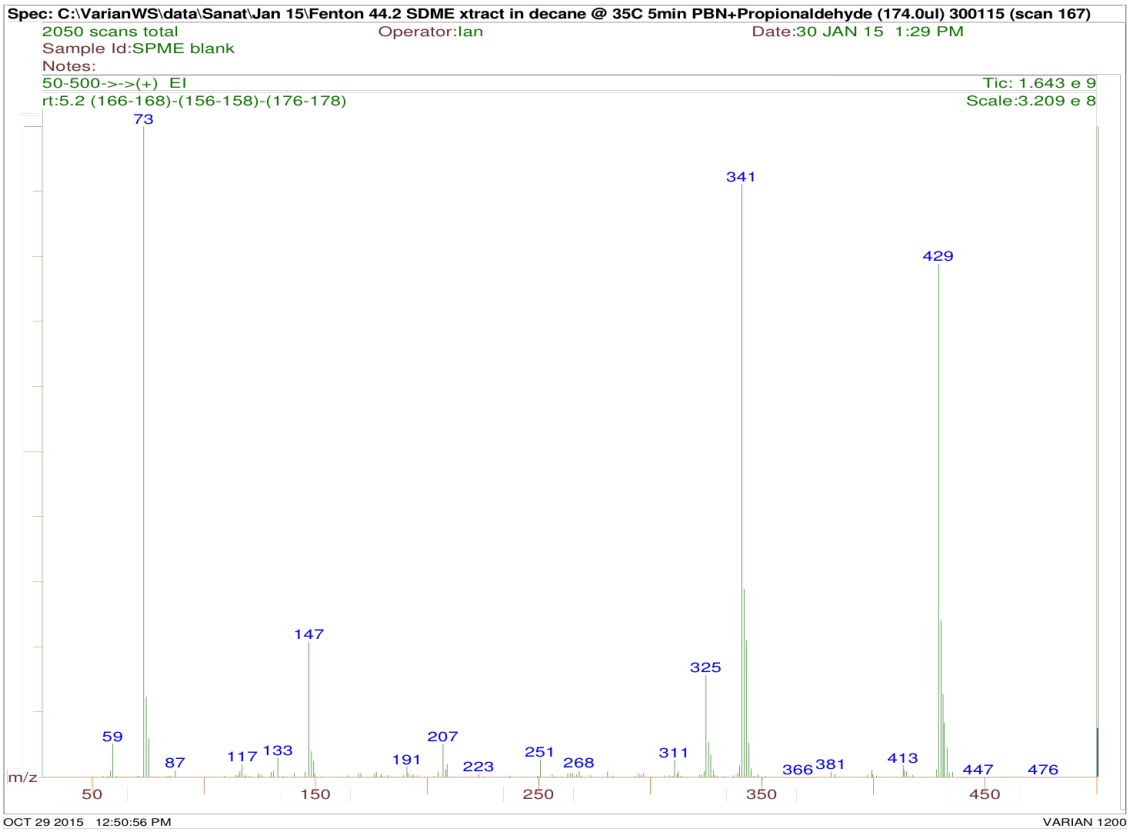

Figure 5.24: Mass spectrum obtained for Dimethylpolysiloxane peak at 5.2 minutes from the chromatogram in Figure 5.20.

The mass spectrum in Figure 5.24 for peak at 5.2 minutes indicated this peak as dimethylpolysiloxane as it show a characteristic ion which include m/z 73, 147, 207 and 429. This could commonly occur as syringe is pierced through the septum for the SDME extraction. The other source could be the column as PDMS column is used. This mass spectrum was compared to the literature mass spectrum of dimethyl polysiloxane and was found to be similar (Rood 2007).

5. Analysis of spin trapped ethyl radical from propionaldehyde (propanal)

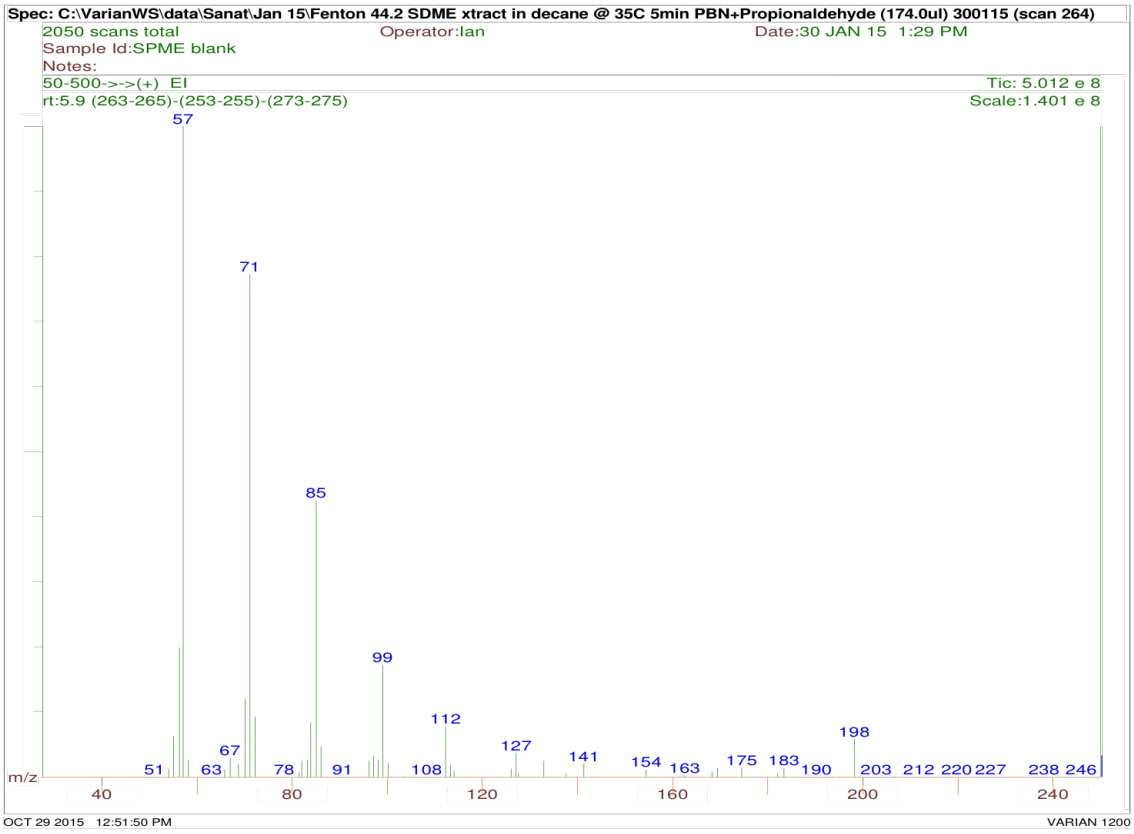

Figure 5.25: Mass spectrum for Tetradecane peak at 5.9 minutes from the chromatogram in Figure 5.20.

The mass spectrum for peak at 5.9 minutes in Figure 5.25 indicated this peak as a tetradecane ($C_{14}H_{30}$). The spectrum shows molecular fragments at m/z 198, loss of methyl radical result in fragment at m/z 183 followed by successive loss of ethene (a neutral olefin molecule) results in ion with m/z 155 (not shown in figure). This fragment along with other fragment ions can lose ethene which give m/z 155 losing 28 to form m/z 127, which loses 28 to form m/z 99, which loses 28 to form m/z 71. The loss of an ethyl radical and successive loss of ethene results in the fragment at m/z 141. Fragment at m/z 85, 71 and base peak m/z 57 shows a typical pattern of alkanes: clusters of fragments separated by 14 amu. This mass spectrum was compared to standard tetradecane mass spectrum obtained from NIST database (http://webbook.nist.gov/cgi/cbook.cgi?ID=C629594&Mask=2FF) which shows similar fragments shown in Figure 5.25.

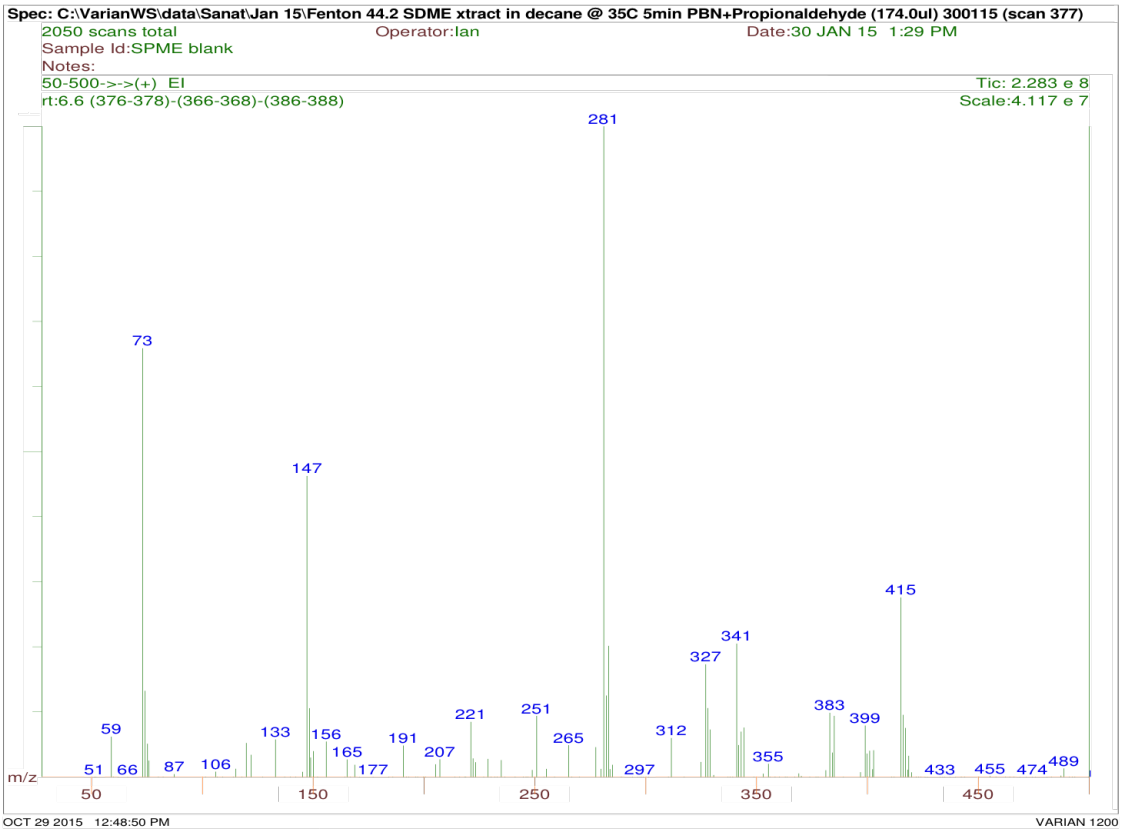

Figure 5.26: Mass spectrum obtained for Dimethylpolysiloxane peak at 6.6 minutes from the chromatogram in Figure 5.20.

The mass spectrum for Figure 5.26 shows a similar mass spectrum compared to Figure 5.24 which correspond to the dimethylpolysiloxane.

Figure 5.27: Mass spectrum obtained for Hexadecane peak at 7.4 minutes from the chromatogram in Figure 5.20.

The mass spectrum for peak at 7.4 minutes in Figure 5.27 indicated this peak as a hexadecane ($C_{16}H_{34}$). The spectrum shows molecular fragments at m/z 226, loss of methyl radical followed by successive loss of ethene (a neutral olefin molecule) results in ion with m/z 183. This fragment along with other fragment ions can lose ethene which give m/z 155 losing 28 to form m/z 127, which loses 28 to form m/z 99, which loses 28 to form m/z 71. The loss of an ethyl radical and successive loss of ethene results in the fragment at m/z 169. Fragment at m/z 113, 99, 85, 71 and base peak m/z 57 shows a typical pattern of alkanes: clusters of fragments separated by 14 amu. This mass spectrum was compared to standard hexadecane mass spectrum obtained from NIST database (http://webbook.nist.gov/cgi/cbook.cgi?ID=C544763&Mask=200) which shows similar fragments shown in Figure 5.27.

5.3.4 Confirmation of PBN diethyl adduct formation

To show diethyl PBN adducts were formed from propanal and PBN different control experiments were performed.

5.3.4.1 Fenton reaction without Iron(II)

Iron(II) is required for the production of hydroxyl radical from hydrogen peroxide in the Fenton system. The hydroxyl radicals then react with propanal to form ethyl radicals which are trapped by PBN to form diethyl PBN adduct. To confirm the diethyl PBN adduct is formed as a result of Fenton chemistry the experiment was carried out in absence of iron (II). The Fenton reaction mixture (without iron (II)) was extracted into decane by the SDME technique, and then analysed by GC/MS (total ion chromatogram is shown in Figure 5.28).

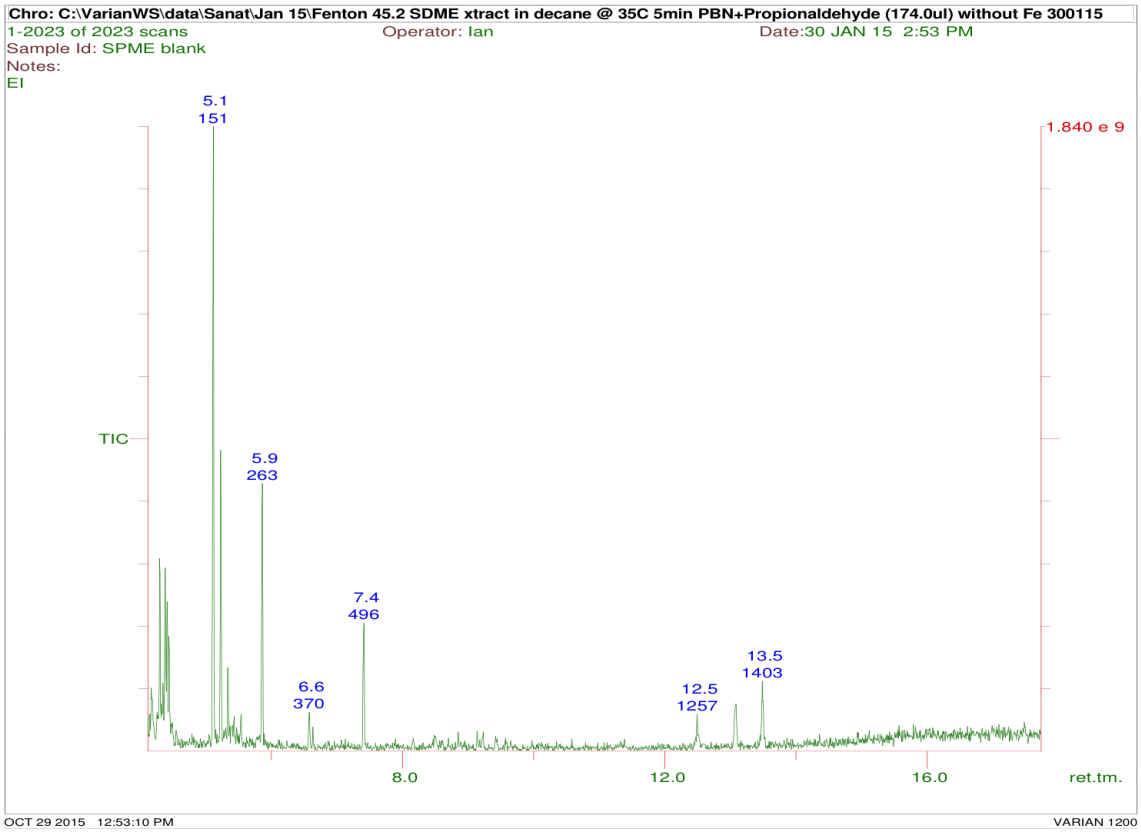

Figure 5.28: Total ion chromatogram (TIC) obtained from the analysis of the Fenton reaction mixture containing PBN and propanal but without Iron (II).

The Fenton system containing PBN and propanal but without Fe^{2+} gave the expected

chromatogram showing no presence of a peak for the diethyl PBN adduct. The peaks present in the chromatogram are for the hydrocarbons which have been identified previous section 5.3.3. These peaks in chromatogram have been identified as decane (peak around 4.1 minutes), tridecane (5.1 minutes), tetradecane (5.9 minutes) and hexadecane (7.4 minutes). Hence, from this experiment it can be concluded that diethyl PBN adduct peak is formed due to the standard Fenton involving PBN and propanal.

5.3.4.2 Fenton reaction without Propanal

To confirm propanal is the only source for ethyl radicals for the diethyl PBN adduct, The Fenton reaction was carried out without the presence of propanal. The TIC (Figure 5.29) does not show any peak at 6.4 minutes for PBN diethyl adduct.

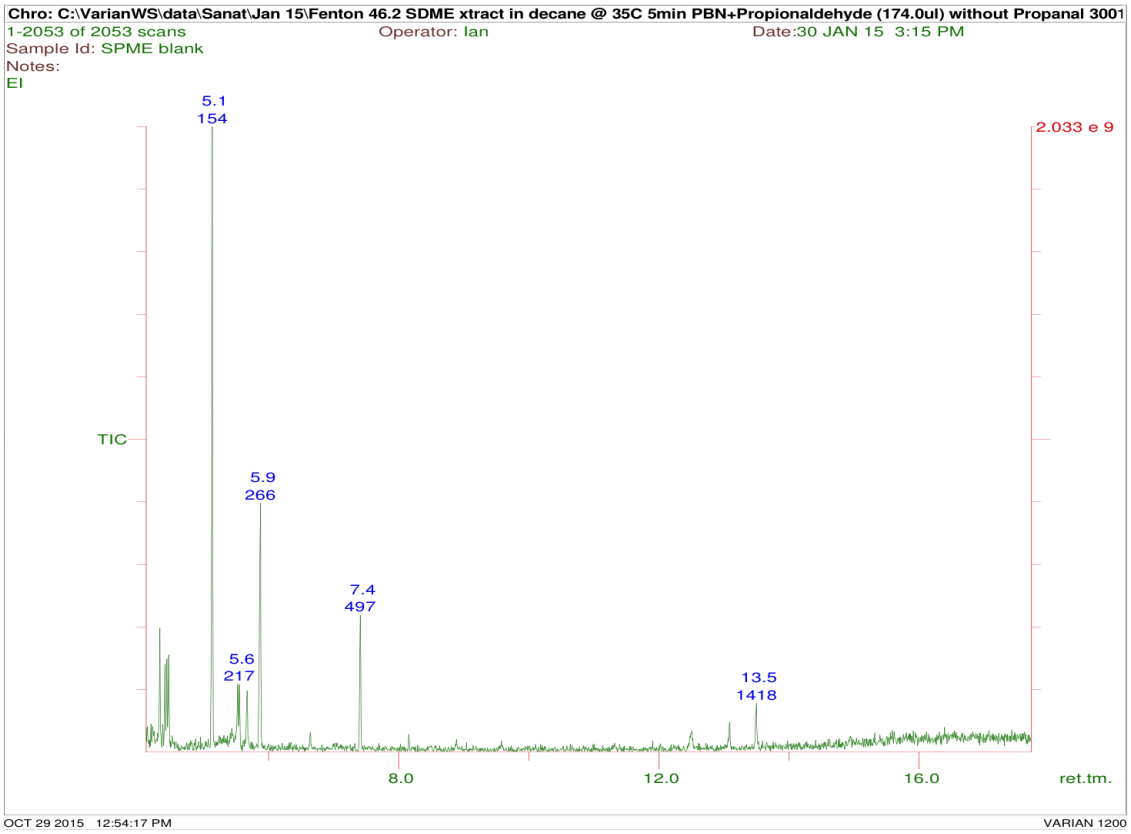

Figure 5.29: Total ion chromatogram (TIC) obtained from the analysis of the Fenton reaction mixture containing PBN and the Fenton chemicals but without propanal.

5.3.5 PBN diethyl adduct with PBN derivatives

Different PBN derivatives have been used in Fenton type chemistry to help identify the presence of a PBN diethyl adduct. In each case, the TIC shows an intense peak corresponding to the PBN diethyl adduct (summarized in Table 5.5). Along with the diethyl adduct other alkanes peak were detected in the chromatogram as mention in section 5.3.3.

Identity	Retention time (minutes)	Molecular ion (m/z)	Base Peak (m/z)	Characteristic ions
$PBN(C_2H_5)_2$	6.4	235	91	57, 77, 119, 150, 206, 220
$d_6PBN(C_2H_5)_2$	6.3	241	125	57, 97, 156, 212, 226,
4-$FPBN(C_2H_5)_2$	6.4	253	137	57, 95, 109, 168, 224
4-$ClPBN(C_2H_5)_2$	7.9	269	153	57, 11, 125, 184, 240

Table 5.5: Retention times, molecular ion values (m/z), base peaks values (m/z) and characteristic ions (m/z) for PBN diethyl adducts obtained from the SDME sampling and GC/MS analysis of the Fenton reaction involving PBN and propanal. .

5.4 Head Space Solid Phase Micro Extraction (HS-SPME)

To check the suitability of the HS-SPME technique for extraction of the diethyl PBN adduct from the Fenton reaction mixture, different SPME fibres were used. A peak was observed for $PBN(C_2H_5)_2$ at retention time 11.1 minutes (Figure 5.30) and the intensity of the peaks has been tabulated (Table 5.6).

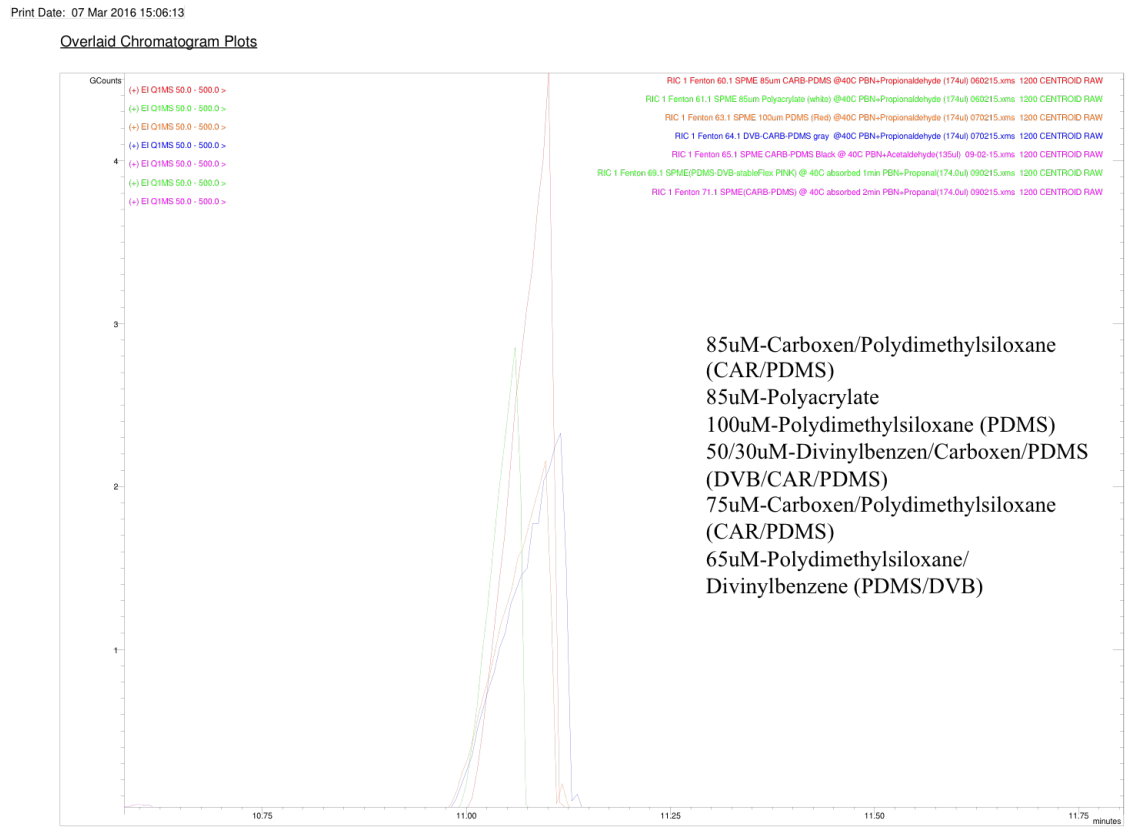

Figure 5.30: Overlaid comparision of TIC chromatogram obtained from the GC/MS analysis of the Fenton reaction mixture containing PBN and propanal and extracted by HS-SPME by different fibres. .

Different SPME fibres have different absorption and desorption towards the diethyl PBN adduct. Among the various fibres used it can be visually concluded from the chromtogram (Figure 5.30) and from the peak intensity Table (5.6) it can be concluded that 85 μm Carboxen/Polydimethylsiloxane (CAR/PDMS, needle size 24 ga) is the best fibre for extracting diethyl PBN adduct and 65 μm PDMS/DVB StableFlex as less senstive fibre. Hence, 85 μm CARB/PDMS was used for further analysis.

fibre	Retention time (minutes)	Peak area
85 μm CARB/PDMS (light blue)	11.09	1.37E+10
85 μm polyacrylate (white)	11.06	6.72E+09
100 μm PDMS (red)	11.10	8.37E+09
50/30 μm DVB/Carboxen/PDMS (gray)	11.11	4.55E+09
75 μm Carboxen/polydimethylsiloxane (needle size 24 ga, black)	10.59	7.64E+07
65 μm PDMS/DVB StableFlex (pink)	11.06	3.94E+07
75 μm Carboxen/Polydimethylsiloxane (needle size 23 ga, black)	11.07	7.00E+07

Table 5.6: PBN diethyl adduct peak area intensity extracted by different SPME fibres.

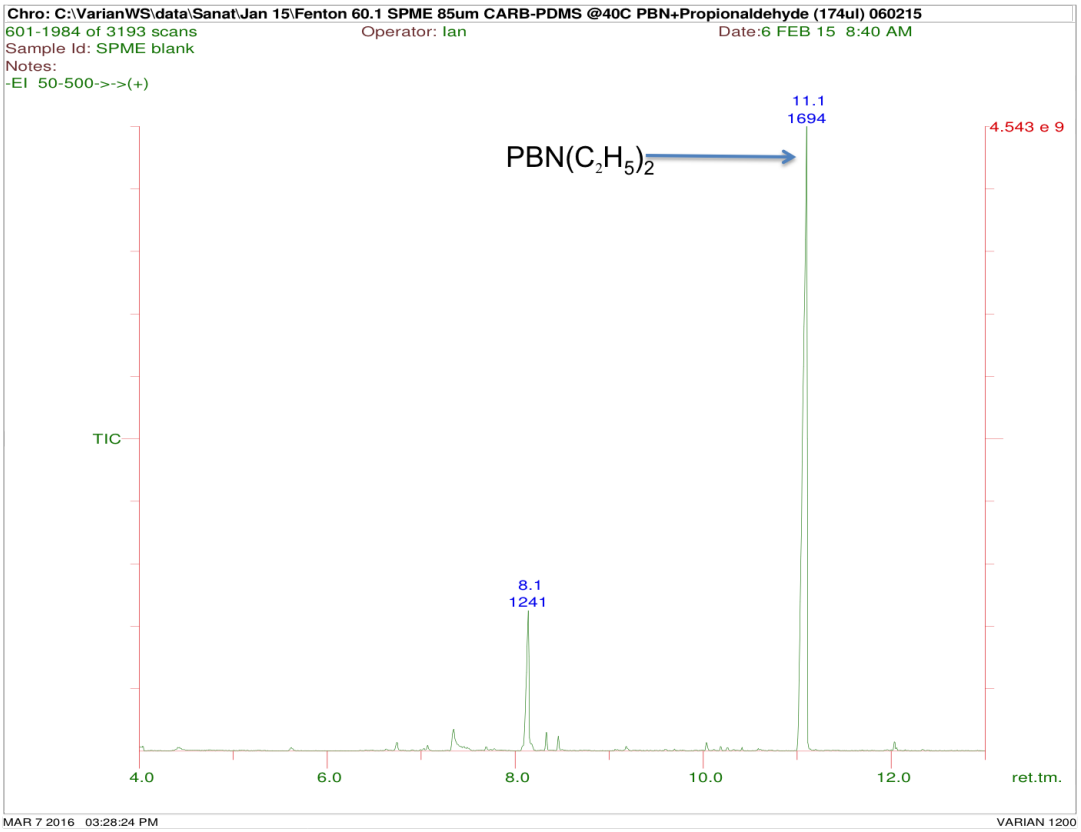

Figure 5.31: Total ion chromatogram (TIC) obtained from the HS-SPME-GC/MS analysis of the reaction mixture between PBN, methanol and DMSO in Fenton reaction

The chromatogram (Figure 5.31) obtained for the extraction of diethyl PBN adduct from the Fenton system containing PBN and propanal by 85 μm Carboxen/Polydimethylsiloxane (CAR/PDMS) fibre is shown in Figure 5.31. The chromatogram shows an intense peak at 11.1 minutes for the PBN diethyl adduct.

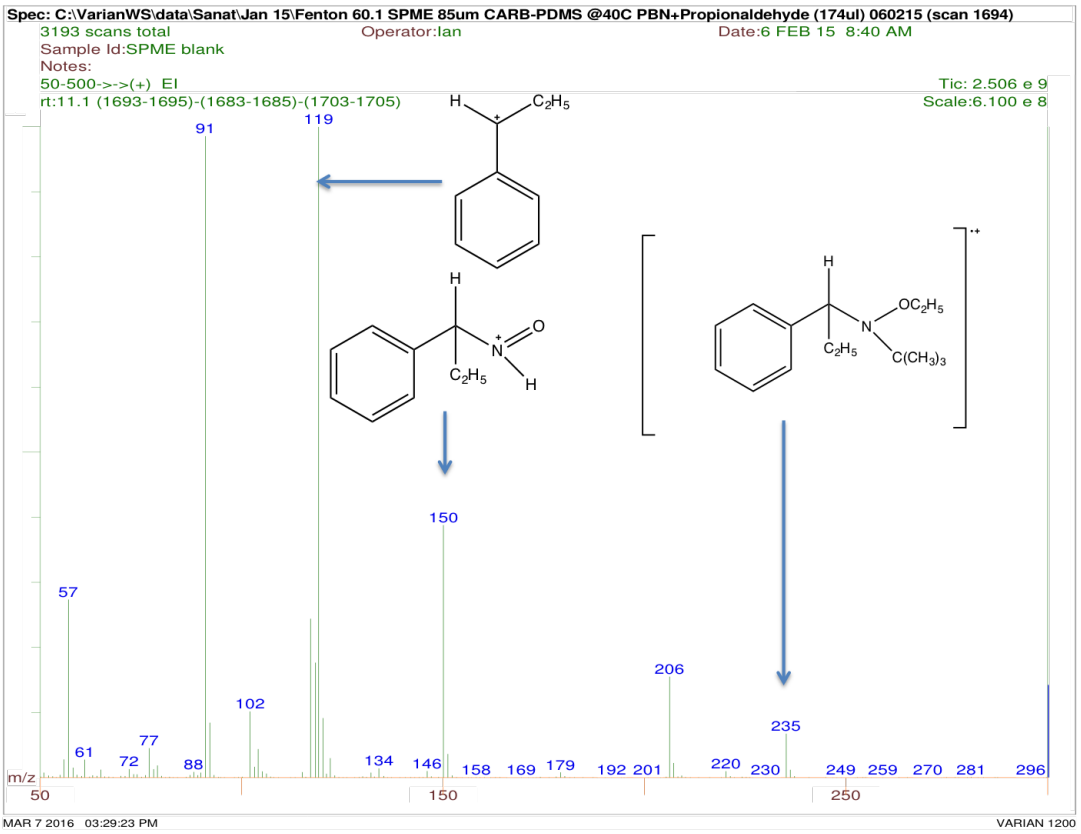

Figure 5.32: Mass spectrum obtained for PBN-diethyl adduct at 11.1 minutes (from the chromatogram in Figure 5.31) with a molecular ion at m/z 235.

The mass spectrum (Figure 5.32) shows molecular ion at m/z 235 for the PBN$(C_2H_5)_2$ adduct retained at 11.1 minutes. The fragmentation pattern is the same as when extracted by chloroform and has been described in subsection 5.2.2.1.

5.5 Discussion

The Fenton reaction was carried out in the presence of a phosphate buffer (pH=7.0), EDTA, PBN (and its derivatives), hydrogen peroxide, ascorbate, DMSO and Fe(II) to generate a PBN$(C_2H_5)_2$ adduct which was extracted by liquid liquid extraction (solvent chloroform), HS-SPME and HS-SDME (solvent decane) techniques. In the Fenton reaction, Fe(II) reacts with H_2O_2 to form hydroxyl radicals, hydroxyl ions and Fe(III) (Figure 5.33). The hydroxyl radicals generated react with propanal to form ethyl radicals or formyl radical (Figure 5.33). Fe(III) is then reduced back to Fe(II) by another molecule of hydrogen peroxide to form a hydroperoxyl radical and a proton.

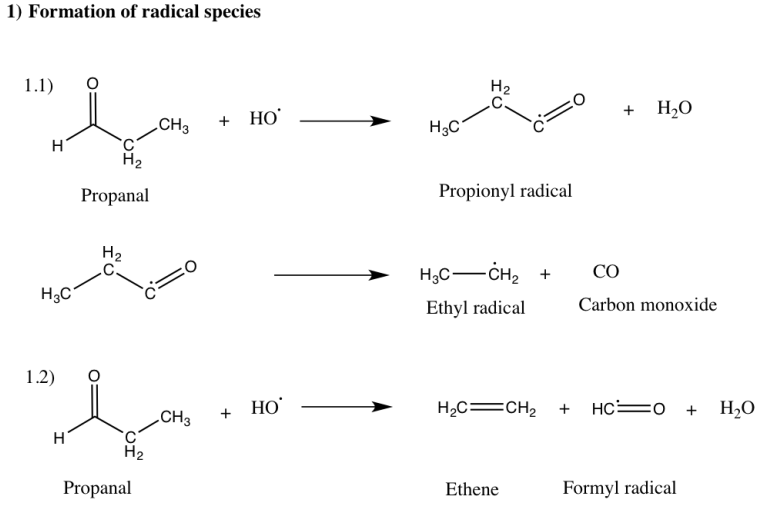

Figure 5.33: Schematic representation for formation of (1.1) ethyl radicals from propanal, (1.2) formyl radical from propanal through the Fenton mechanism.

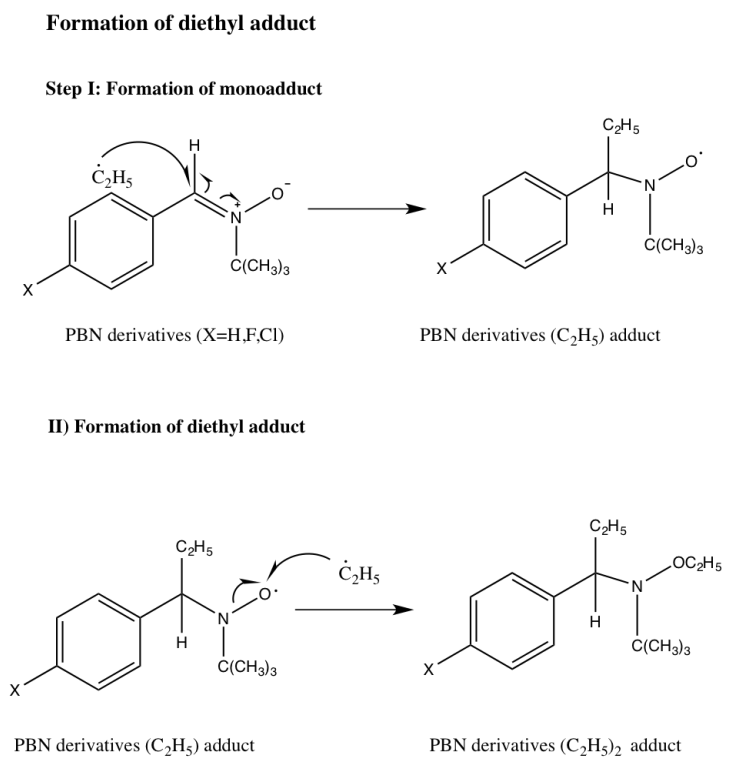

Figure 5.34: Schematic representation for formation of (I) the ethyl radical is trapped by PBN (derivatives) at the carbon site to form a monoethyl PBN adducts, (II) a second ethyl radical is added to the oxygen site of the monoethyl PBN adducts to form a PBN diethyl adducts.

5. Analysis of spin trapped ethyl radical from propionaldehyde (propanal)

The generated ethyl radical is trapped by PBN and its derivative in a two-step mechanism (Figure 5.34). In first step, the ethyl radical is added to the carbon site of PBN to form a mono-ethyl adduct and, in the second step, another ethyl radical is added to the oxygen site of PBN to form a diethyl adduct. The two-step mechanism was confirmed in chapter 3 when propanal was replaced by methanol and DMSO in the Fenton reaction and the GC/MS result showed the formation of PBN(CH_2OH)(CH_3) adducts (2.8). The formation of a diethyl PBN adduct was confirmed by using different synthesised PBN derivatives such as 4-FPBN and 4-ClPBN. These PBN derivatives, along with PBN-d_6 confirmed the diethyl adduct formation and the fragmentation pattern of diethyl adducts in the mass spectrum. The diethyl PBN derivatives adducts showed molecular ions with an addition of 58 m/z units for the two trapped ethyl radicals (Table 5.5) in the mass spectrum. The diethyl PBN derivatives adduct showed an exact fragmentation pattern.

The chromatogram of the Fenton system containing PBN and propanal extracted by chloroform shows less intense peaks and the corresponding mass spectrum shows a fragment at m/z 206 (an addition of 29 m/z units to PBN) at 8.1 minutes and 8.6 minutes (Figure 5.1). This addition of 29 Da to PBN can be either from the formyl radical or the ethyl radical as both radicals can be generated from propanal (Figure 5.33). Hence, it can be either PBN(C_2H_5)$^+$ or PBN(CHO)$^+$ or PBN(C_2H_5)(H) or isomers. These peaks are not isomers because the mass spectrum for the peak retained at 8.1 minutes and 8.6 minutes shows a different fragmentation pattern. The results obtained and presented in chapter 4 and the Fenton experiments on various aldehydes by research colleagues at the University of Salford helped to rule out PBN(CHO) adducts, as they were not detected in any of the experiments. From this information and from the mass spectrum which shows a very similar fragmentation pattern, it can be concluded that these peaks (at 8.1 and 8.6 minutes) are PBN(C_2H_5) and PBN(C_2H_5)(H) adduct. The mass spectrum doesn't show a molecular ion for PBN(C_2H_5)(H) adduct because it could rapidly fragment to form PBN(C_2H_5)$^+$. Similar results were found with other PBN derivatives supporting the presence of PBN monoethyl adducts.

The total ion chromatogram also shows a peak at 8.2 minutes and the corresponding mass spectrum shows peaks at m/z 172, 174 and 176 and in a ratio of 9:6:1 which shows the presence of two chlorine atoms in the compound. The suggested structure is 1,1-dichloro-2-phenylethene. However, the presence of fragment at m/z 57 (if assigned to *tert*-butyl cation) and EI-MS evidence from other PBN derivatives suggests it is a PBN derived compound with two ^{35}Cl atoms and hence, 1,1-dichloro-2-phenylethene could not be a molecular ion. The presence of chlorine can only be derived from the chloroform or from the impurities present in the aldehyde (as this peak was also seen in the Fenton system involving acetaldehyde as shown in chapter 4). This dichloro compound was also found with other PBN derivatives as well.

5. Analysis of spin trapped ethyl radical from propionaldehyde (propanal)

The head space single droplet microextraction (HS-SDME) technique was also applied to check its affinity and feasibility for the PBN$(C_2H_5)_2$ adduct detection. With decane as the solvent, the diethyl PBN adduct was extracted and analysed by GC/MS. The chromatogram showed the presence of diethyl PBN adducts as the most intense peak along with various alkane (decane, undecane, tridecane, tetradecane) peaks. These alkanes could be the impurities present in the decane. To confirm this, control experiments were performed. In control 1 (section 5.3.4.1), Fe^{2+} , a vital component for generating the hydroxyl radical, was removed from the reaction. The TIC showed the presence of alkanes in the chromatogram (Figure 5.28), however, no diethyl PBN adduct peak was observed, suggesting that the various alkanes present does not interfere with the Fenton reaction. The second control (section 5.3.4.2) was performed by eliminating the source of the ethyl radical (propanal). Again, no diethyl PBN adduct peak was observed in the chromatogram (Figure 5.29). These controls supported the conclusion that the diethyl PBN adducts were from the Fenton chemistry and that propanal only was the source for the ethyl radical.

A headspace solid phase microextraction (HS-SPME) was also used to extract the diethyl PBN adduct from the Fenton system. To check the affinity of diethyl PBN adduct for the SPME fibre, different SPME fibres were used. All the fibres used were able to adsorb the diethyl PBN adduct from the headspace, however, 85 μm Carboxen/ Polydimethylsiloxane (CAR/PDMS) was found to be the most suitable to extract the diethyl PBN adduct when the peak intensity from different fibres was compared. From comparison of peak intensities (Table 5.6) it can be seen that the presence of PDMS significantly improves the extraction efficiency of the fibre. The chromatogram (Figure 5.31) shows a very intense peak for the diethyl PBN adduct and the corresponding mass spectrum shows molecular ion at m/z 235.

Aldehydes (such as propanal) and acetaldehydes are important biomarkers for lipid peroxidation. For the detection of aldehydes the most common method is the derivatization method. In this method the derivatization compound such as 2, 4-dinitrophenylhydrazine or thiobarbituric acid reacts with the carbonyls. The products formed can be detected and quantified by high performance liquid chromatography (HPLC) separation and ultraviolet (UV) or by GC/MS (Uchiyama et al. 2011, Cordis et al. 1994). However, the determination of the derivatised products can be complex in some cases. Other techniques used to detect and identify VOCs such as propanal are gas chromatography coupled with different direct mass spectrometric techniques such as ion-molecule reaction mass spectrometry (IMR-MS) (Wang et al. 2012), proton transfer reaction mass spectrometry (PTR-MS) (Blake et al. 2009) and selected ion-flow tube mass spectrometry (SIFT-MS) (Pysanenko et al. 2009). These analytical techniques are very sensitive in the detection of VOCs, however, they are expensive instruments which are not readily available in many laboratories.

5. Analysis of spin trapped ethyl radical from propionaldehyde (propanal)

As alternatives to the above methods, simple, quick and efficient methods have been developed for the detection of aldehydes such as propanal by using a spin trapping compound followed by GC/MS, and extraction techniques HS-SDME and HS-SPME, followed by GC/MS. They are simple and solvent free extraction techniques, with a strong affinity for PBN diethyl adducts and can be used as an indirect approach for the detection of hydroxyl radicals.

Chapter 6

Summary, conclusion and future work

6.1 Summary and conclusion

The detection and identification of free radicals is vital due to their role in various diseases such cardiovascular disorders, cancer, neurological disorders and diabetes, to name a few. The combination of EPR spectroscopy with a spin trap is the preferred method for the detection of free radicals, however EPR is not very effective when it comes to the identification of free radicals as the EPR signal is similar for all free radicals. However, with the advancements in technology there are different instruments (such as mass spectrometry) available which can be coupled with EPR and which can be used to detect and identify free radicals. However, EPR coupling with MS is costly and also EPR are not readily available in many laboratories. Hence, alternatives to EPR such as LC/MS/MS (Qian et al. 2005), ST-NMR (Khramtsov & Clanton 2011), GC/MS (Mistry et al. 2008) and MALDI-TOF/MS (Podmore et al. 2013) may be used to detect free radicals.

In this research work GC/MS was used to detect and identify the free radicals generated using Fenton chemistry. It was demonstrated that a hydroxyl radical formed in the Fenton reaction reacts with a secondary source of free radicals (such as methanol, DMSO, acetaldehyde and propionaldehyde) which were then trapped by PBN and its derivatives to form PBN adducts. Three different extraction techniques were used to extract the PBN radical adduct from the Fenton reaction for analysis on GC/MS: direct extraction, HS-SPME GC/MS and HS-SDME GC/MS. To detect and identify the radicals generated from methanol in the Fenton reaction, the reaction mixture was extracted into chloroform and the extracted chloroform was injected onto the gas chromatograph for analysis. The chromatograms obtained showed peaks generated from the Fenton reaction when compared to the control experiments, however, the mass spectrum for the peaks was not easily interpretable due to the absence of a molecular ion. This is likely to be due to the adducts being highly unstable in the ion source and therefore heavily fragmenting. To overcome

this difficulty, methyl radicals were generated from DMSO along with methanol radicals in the Fenton reaction. The adducts were extracted with chloroform for analysis on GC/MS. The chromatograms obtained were very clear and also the mass spectrum was easily interpretable. The GC/MS analysis showed the presence of a PBN dimethyl adduct (molecular ion at m/z 213), PBN(CH_2OH)(CH_3) adduct (molecular ion at m/z 223) and a PBN hydroxyl adduct. Formation of a PBN(CH_2OH)(CH_3) adduct also helped in understanding the mechanism of formation of the adducts which involves two steps. In the first step the hydroxymethyl radical is added to the carbon site of PBN and, in the second step, the methyl radical is added to the oxygen site of the resulting nitroxide. The formation of these adducts was confirmed by using deuterated DMSO and deuterated methanol. The results showed the formation PBN(CD_3)$_2$ adduct and PBN(CD_2OH)(CD_3) adduct with an expected mass difference due to the presence of deuterium, with no change in the PBN-OH adduct. Furthermore, to understand the fragmentation pattern and the formation of the adduct, different 4-substituted PBN derivatives and PBN-d_6 were used and the results showed that the adduct had the expected mass difference depending on the PBN. Using the 4-substituted PBN derivatives also helped in identifying the position of the hydroxyl radical which attached to the benzene ring during the Fenton reaction and which could be either an ortho or meta on the aromatic ring of the PBN. The chromatogram obtained from the chloroform extraction showed the presence of a few more peaks such as unreacted PBN, benzaldehyde oxime and other peaks which might have derived from the column.

The Fenton reaction contains chemicals which, if not extracted carefully, can easily damage the column. Hence, solvent free HS-SPME was used to avoid direct contact with the Fenton reaction mixture. Different SPME fibres (CAR/PDMS, PEG and PDMS/DVB) were tested to extract the PBN adduct from the Fenton reaction mixture. All the SPME fibres were able to extract the PBN(CH_2OH)(CH_3) adduct from the headspace. However, on comparing the peak area for the PBN(CH_2OH)(CH_3) adduct under standard conditions, CARB/PDMS appeared to be the best extraction phase. The use of different PBN derivatives along with deuterated DMSO and deuterated methanol and also using the HS-SPME-GC/MS analysis showed the formation and extraction of the PBN(CH_2OH)(CH_3) adduct with the expected mass difference. The HS-SPME GC/MS chromatogram also showed the presence of other peaks (such as benzaldehyde) and siloxane related peaks (from the column or septum). However, these peaks were very small compared to the PBN dimethyl adduct or the PBN(CH_2OH)(CH_3) adduct. Hence, from this set of experiments, it can be concluded that using methyl radicals may be very useful in the detection of methanol radicals by PBN, as the presence of methyl makes the PBN adduct more volatile which can then be easily extracted by using HS-SPME for the analysis on GC/MS.

In chapter 4, radicals generated from acetaldehyde were trapped by PBN and its derivatives. Hydroxyl radicals in the Fenton system react with acetaldehyde to form $^{\bullet}CH_3$ and $^{\bullet}CH_3CO$ radicals which were trapped by PBN. The Fenton reaction mixture was extracted in chloroform for analysis on GC/MS. The GC/MS results showed presence of PBN$(CH_3)_2$ adduct [molecular ion at m/z 207], PBN(CH_3) adduct ["molecular ion" at m/z 192], PBN(CH_3)(H) adduct ["molecular ion" at m/z 193 is absent] along with unreacted PBN, benzaldehyde oxime and some other minor peaks. To confirm that these adducts were from the reaction mixture the chromatogram was compared to a control experiment (without acetaldehyde) and the only peaks observed corresponded to the unreacted PBN and benzaldehyde oxime. Further confirmation for the formation of these adduct was obtained by the use of deuterated acetaldehyde, and the chromatogram showed the formation of PBN$(CD_3)_2$ and a PBN(CD_3) adduct (as the mass spectrum showed an increase of 6 m/z and 3 m/z, respectively due to the presence of deuterium). Different PBN derivatives were used to confirm the presence of the dimethyl adducts. All PBN derivatives formed a dimethyl adduct and the EI-MS showed similar fragment patterns with the expected mass difference.

The presence of monomethyl adducts with acetaldehyde but not with the methanol/ DMSO system may be due, in part, to the difference in rate constant of methyl radical generation. The rate constant of methyl from acetaldehyde is k $=10^{-2}$ $M^{-1}sec^{-1}$ (Nakao et al. 2000*a*) and for DMSO is k=7x10^9 $M^{-1}sec^{-1}$ (Qian et al. 2005). This relatively slow production of methyl may allow a steady state build-up of PBN-(CH_3) to occur, making it detectable, for the acetaldehyde system. This also confirms the dimethyl adduct is two step mechanism.

The chromatogram for the PBN and acetaldehyde experiment shows a peak at 9.6 minutes and 10.1 minutes with similar EI mass spectra suggesting they are stereoisomers. The EI-MS studied showed presence of acetyl group in the structure which was confirmed with the deuterated acetaldehyde. A similar mass spectrum was found with other PBN derivatives and the suggested structure (Figure 4.22) contain two units of X-C_6H_4-CH- and a CH_3-C=O. This result suggests that acetyl radicals may have been trapped by PBN to form a PBN-CH_3-C=O adduct, may then react to give the suggested structure. The results can be supported from the Nakao et al. studies on metabolism of acetaldehyde (Nakao et al. 2000). They showed that acetaldehyde may be metabolised to methyl radical and acetyl radical. POBN and DMPO were used for trapping of these radicals. The EPR studies identified POBN-CH_3 and POBN-$COCH_3$ adducts. However, they found the POBN-$COCH_3$ adduct to be unstable.

The GC chromatogram of PBN and acetaldehyde also showed the presence of a peak at 6.0 minutes and the EI-MS were similar to that of the unreacted PBN (Rt=7.4 minutes). However, no firm identification of the molecular ion could be made. Based upon retention

time, which is close to that of PBN$(CH_3)_2$, the compound appears to be more volatile than the unreacted spin trap.

Different solvent free extraction techniques like HS-SDME and HS-SPME were used to avoid direct contact with the reaction mixture. When HS-SDME with decane as the solvent was used to extract the PBN adduct from the reaction mixture for analysis, the chromatogram showed a strong peak for the PBN$(CH_3)_2$ adduct. The chromatogram also showed peaks for the PBN(CH_3) and PBN(CH_3)(H) adduct. In addition, there were several peaks for the hydrocarbons which could assigned as impurities in the decane. This was confirmed when HS-SDME was performed on the decane and the chromatogram showed the same peaks for the hydrocarbons. The formation of PBN$(CH_3)_2$ and PBN(CH_3) adducts were confirmed by using deuterated acetaldehyde. The chromatogram showed formation of both adducts with the corresponding mass spectra showing an increase of 6 m/z and 3 m/z respectively due to the presence of deuterium. Hence, these studies show that HS-SDME may be used as an excellent alternative to analysis by chloroform extraction.

Hence, from the results obtained in chapter 4, it can be concluded that methyl radicals are generated from acetaldehyde in the Fenton system which can be trapped by PBN to form PBN adducts. These PBN adducts are volatile and may be extracted by HS-SDME and analysed by GC/MS. The detection of methyl radicals may be used as indirect approach for detection of hydroxyl radicals. Also, the HS-SDME GC/MS is a very simple, sensitive and cost effective technique.

A similar approach was used for the detection and identification of radicals generated from propanal. In this experiment hydroxyl radicals generated in the Fenton reaction reacted with propionaldehyde to form $^{\bullet}C_2H_5$ radicals which were trapped by PBN and its derivatives. The Fenton reaction mixture was extracted with chloroform for GC/MS analysis. The chromatogram showed the presence of a PBN$(C_2H_5)_2$ adduct ($M^{+\bullet}$ at 235 m/z) and PBN(C_2H_5) adduct ("molecular ion" at 206 m/z), PBN(C_2H_5)(H) adduct ("molecular ion" at 207 m/z) along with a chlorinated compound (exact structure unknown), unreacted PBN and benzaldehyde oxime. The mass spectrum showed a strong molecular ion for the adduct and the fragmentation was very clear and easily interpretable. To confirm the formation of the diethyl adduct, different 4-substituted PBN derivatives and PBN-d_6 were used. All the derivatives formed the diethyl adduct and their mass spectra showed exactly the same fragmentation pattern.

Other extraction techniques, namely HS-SDME (decane as solvent) and HS-SPME (CARB/PDMS fibre) were also used to extract the PBN adducts from the Fenton reaction containing propanal. The HS-SDME GC/MS analysis showed a strong peak for the PBN$(C_2H_5)_2$ adduct retained at 6.4 minutes. The chromatogram also showed various hydrocarbon peaks such as hexadecane etc. which were seen in other HS-SDME experi-

ments suggesting they could be the impurities present in the decane solvent.

HS-SPME was also used to check the sensitivity of the diethyl adduct towards the SPME fibre. Different fibres were used and CARB/PDMS proved to be the most effective for extracting the PBN(C_2H_5)$_2$ adduct from the headspace of the reaction mixture. The chromatogram obtained for the CARB/PDMS showed a very strong peak for the PBN(C_2H_5)$_2$ adduct. The chromatogram also showed weak peaks containing fragment ions for siloxanes (probably coming from the GC column, fibre or the septum).

From all these sets of experiments it can be concluded that the radicals generated from methanol, DMSO, acetaldehyde and propanal during the Fenton reaction may be easily trapped by PBN and its derivatives to form PBN adducts which can be analysed on GC/MS. These adducts are novel and may prove to be useful biomarkers of hydroxyl radical production, particularly *in vitro*. Among the three different extracting techniques (liquid liquid, HS-SDME and HS-SPME), HS-SPME offers a very easy, solvent free and single step extraction for the PBN adduct. The only disadvantages for the HS-SPME fibre are the cost of the fibre and the durability of the fibre as it can degrade over time

6.2 Future work

According to the findings of this study it is clear that further work needs to be carried out and a suggested list of future work is given below:

(i) The molecular ion for the PBN(CH_2OH)(CH_3) adduct was very weak and absent within some PBN derivatives. Potentially, using chemical ionisation (CI) mass spectrometry would give the molecular weight of the compound (as the molecular species) and help identify the adduct.

(ii) To confirm the position of the hydroxyl radicals attached to PBN, further experiments may be carried out involving 2 and 3 substituted PBN. In these cases, one should be able to see PBN-OH adduct with either 2-substituted PBN or 3-substituted PBN and if one sees the PBN-OH adduct with both then it might be worth looking into them in more detail.

(iii) For the confirmation of the PBN mono (PBN-C_2H_5) adduct in the propanal experiments, deuterated propanal (C_2D_5CHO) could be used which will show an increase of 5 m/z units for the PBN-C_2H_5 adduct due to the presence of five deuterium atoms in the adduct. Additionally, using deuterated propanal will confirm the formation of the PBN(C_2H_5)$_2$ adduct as well.

(iv) The presence of acetyl radicals can also be confirmed by using ^{13}C labelled acetaldehyde ($CH_3{}^{13}CHO$) which would show a molecular ion one mass unit higher for PBN-$^{13}COCH_3$ adduct.

References

Abe, K., Suezawa, H., Hirota, M. & Ishii, T. (1984), 'Mass spectrometric determination of spin adducts of hydroxyl and aryl free radicals', *J. CHEM. SOC. PERKIN TRANS. II* pp. 29–34.

Agadjanyan, Z., Dmitriev, L. & Dugin, S. (2005), 'A new role of phosphoglucose isomerase. involvement of the glycolytic enzyme in aldehyde metabolism', *Biochemistry (Moscow)* **70**, 1251–1255.

Agarwal, D. & Srivastava, L. (2001), 'Does moderate alcohol intake protect against coronary heart disease?', *Indian Heart J.* **53**, 224–230.

Aikens, J. & Dix, T. (1991), 'Perhydroxyl radical (hoo.) initiated lipid peroxidation. the role of fatty acid hydroperoxides.', *J. Biol. Chem.* **266**(23), 15091–8.

Aikens, J. & Dix, T. (1993), 'Hydrodioxyl (perhydroxyl), peroxyl, and hydroxyl radical-initiated lipid peroxidation of large unilamellar vesicles (liposomes): comparative and mechanistic studies.', *Arch. Biochem. Biophys.* **305**(2), 516–525.

Al-Abed, Y., Mitsuhashi, T., Li, H., Lawson, J., FitzGerald, G., Founds, H., Donnelly, T., Cerami, A., Ulrich, P. & Bucala, R. (1999), 'Inhibition of advanced glycation endproduct formation by acetaldehyde: role in the cardioprotective effect of ethanol.', *Proc. Nat. Acad. Sci. USA* **96**, 2385–2390.

Albano, E., Clot, P., Comoglio, A., Dianzani, M. & Tomasi, A. (1994), 'Free radical activation of acetaldehyde and its role in protein alkylation', *FEBS Lett.* **348**, 65–69.

Albano, E. & Parola, M., eds (2015), *Studies on Hepatic Disorders*, Humana Press.

Albano, E., Tomasi, A., Goria-Gatti, L. & Dianzani, M. (1988), 'Spin trapping of free radical species produced during the microsomal metabolism of ethanol', *Chem. Biol. Interact.* **65**, 223–234.

References

Amir, S., Hartvigsen, K., Gonen, A., Leibundgut, G., Que, X., Jensen-Jarolim, E., Wagner, O., Tsimikas, S., Witztum, J. & Binder, C. (2012), 'Peptide mimotopes of malondialdehyde epitopes for clinical applications in cardiovascular disease', *J. Lipid Res.* **53**, 1316–1326.

Antoniak, D. T., Duryee, M. J., Mikuls, T. R., Thiele, G. M. & Anderson, D. (2015), 'Aldehyde-modified proteins as mediators of early inflammation in atherosclerotic disease', *Free Radic. Biol. Med.* **89**, 409–418.

Argyropoulos, D. S., Li, H., Gaspar, A. R., Smith, K., Lucia, L. A. & Rojas, O. J. (2006), 'Quantitative 31p nmr detection of oxygen-centered and carbon-centered radical speciesa', *Bioorganic Medicinal Chemistry* **14**(12), 4017–4028.

Awasthi, D., Churg, D., Torbati, D., Carey, M. & Pryor, W. (1997), 'Oxidative stress following traumatic brain injury in rats', *Surg. Neurol.* **47**(6), 575–581.

Aytacoglu, B., Calikoglu, M., Tamer, L. & Coskun, B. e. a. (2006), 'Alcohol induced lung damage and increased oxidative stress', *Respiration* **73**, 100–104.

Babior, B. M., Curnutte, J. T. & Kipnes, R. S. (1975), 'Biological defense mechanisms. evidence for the participation of superoxide in bacterial killing by xanthine oxidase.', *J. Lab. Clin. Med.* **85**(2), 235–44.

Babior, B. M., Kipnes, R. S. & Curnutte, J. T. (1973), 'Biological defense mechanisms. the production by leukocytes of superoxide, a potential bactericidal agent.', *J. Clin. Invest.* **52**(3), 741–744.

Bacic, G., Spasojevic, I., Secerov, B. & Mojovic, M. (2008), 'Spin-trapping of oxygen free radicals in chemical and biological systems: New traps, radicals and possibilities', *Spectrochimica Acta Part A: Molecular and Biomolecular Spectroscopy* **69**(5), 1354–1366.

Badger, T. M., Ronis, M. J. J., Seitz, H. K., Albano, E., Ingelman-Sundberg, M. & Lieber, C. S. (2003), 'Alcohol metabolism: role in toxicity and carcinogenesis.', *Alcohol. Clin. Exp. Res.* **27**, 336–347.

Balaban, R., Nemoto, S. & Finkel, T. (2005), 'Mitochondria, oxidants, and aging', *Cell* **120**(4), 483–495.

Balasubramanian, K., Nalini, S. & Manohar, M. (1992), 'Nonesterified fatty acids and lipid peroxidation', *Mol. Cell. Biochem.* **111**, 131–135.

References

Bannister, J. & Bannister, W. (1985), 'Production of oxygen-centered radicals by neutrophils and macrophages as studied by electron spin resonance (esr).', *Environ. Health Perspect.* **64**, 37–43.

Bartosz, G. (2003), Total antioxidant capacity, Vol. 37 of *Advances in Clinical Chemistry*, Elsevier, pp. 219 – 292.

Bartsch, H. & Nair, J. (2004), 'Oxidative stress and lipid peroxidation-derived dna-lesions in inflammation driven carcinogenesis', *Cancer Detect. Prev.* **28**, 385–391.

Baskin, S. & Salem, H. (1997), *Oxidants, antioxidants and free Radicals*, Taylor and Francis. U.K.

Batlle, R. & Neri, C. (2004), 'Application of single-drop microextraction to the determination of dialkyl phthalate esters in food simulants', *J. Chromatogr. A* **1045**(1-2), 29–35.

Blake, R., Monks, P. & Ellis, A. (2009), 'Proton transfer reaction mass spectrometry', *Chem. Rev.* **109**(3), 861–896.

Boh, E., Baricos, W., Bernofsky, C. & Steele, R. (1982), 'Mitochondrial chemiluminescence elicited by acetaldehyde', *J. Bioenerg. Biomembr.* **14**(2), 115133.

Boiteux, S., Gajewski, E., Laval, J. & Dizdaroglu, M. (1992), 'Substrate specificity of the escherichia coli fpg protein (formamidopyrimidine-dna glycosylase): excision of purine lesions in dna produced by ionizing radiation or photosensitization.', *Biochemistry* **31**(1), 106–110.

Borges, F. & Fernandes, E.and Roleira, F. (2002), 'Progress towards the discovery of xanthine oxidase inhibitors.', *Curr. Med. Chem.* **9**, 195–217.

Brand, M. (2010), 'The sites and topology of mitochondrial superoxide production', *Experimental Gerontology* **45**(7-8), 466–472. Special Issue: Mitochondria in aging and age-related disease.

Brien, J. F. & Loomis, C. W. (1983), 'Pharmacology of acetaldehyde', *Can. J. Physiol. Pharmacol.* **61**, 1–22.

Britigan, B., Cohen, M. & Rosen, G. (1987), 'Detection of the production of oxygen-centered free radicals by human neutrophils using spin trapping techniques: A critical perspective', *J. Leukoc. Biol.* **41**(4), 349–362.

Brocardo, P. S., Gil-Mohapel, J. & Christie, B. R. (2011), 'The role of oxidative stress in fetal alcohol spectrum disorders', *Brain Research Reviews* **67**(1-2), 209–225.

References

Brooks, P. J. & Theruvathu, J. (2005), 'Dna adducts from acetaldehyde: implications for alcohol-related carcinogenesis', *Alcohol* **35**(3), 187–193.

Brown, R. A. & Savage, A. O. (1996), 'Effects of acute acetaldehyde, chronic ethanol, and pargyline treatment on agonist responses of the rat aorta.', *Toxicol. Appl. Pharmacol.* **136**, 170–178.

Buettner, G. (1993), 'The pecking order of free radicals and antioxidants: lipid peroxidation, alpha-tocopherol, and ascorbate', *Arch. Biochem. Biophys.* **300**, 535–543.

Cadenas, E. (1997), 'Basic mechanisms of antioxidant activity', *Biofactors* **6**, 391–397.

Carr, A., McCall, M. R. & Frei, B. (2000), 'Oxidation of ldl by myeloperoxidase and reactive nitrogen species-reaction pathways and antioxidant protection.', *Arterioscl. Thromb. Vasc. Biol.* **20**, 1716–1723.

Carruthers, V., Moreno, S. & Sibley, L. (1999), 'Ethanol and acetaldehyde elevate intracellular [ca2+] and stimulate microneme discharge in toxoplasma gondii.', *Biochem. J.* **342**, 379–386.

Castro, G., Costantini, M., Delgado de Layno, A. & Castro, J. (2002), 'Rat liver microsomal and nuclear activation of methanol to hydroxymethyl free radicals', *Toxicol. Lett.* **129**(3), 227–236.

Castro, G., Delgado De Layno, A. & Castro, J. (1997), 'Hydroxyl and 1-hydroxyethyl free radical detection using spin traps followed by derivatization and gas chromatography-mass spectrometry', *Redox Report* **3**(5-6), 343–347. Ethanol free radical.

Catala, A. (2006), 'An overview of lipid peroxidation with emphasis in outer segments of photoreceptors and the chemiluminescence assay', *Int. J. Biochem. Cell Biol.* **38**, 1482–1495.

Catala, A. (2009), 'Lipid peroxidation of membrane phospholipids generates hydroxy-alkenals and oxidized phospholipids active in physiological and/or pathological conditions', *Chem. Phys. Lipids* **157**(1), 1–11.

Chamulitrat, W., Hughes, M., Eling, T. & Mason, R. (1991), 'Superoxide and peroxyl radical generation from the reduction of polyunsaturated fatty acid hydroperoxides by soybean lipoxygenase', *Arch. Biochem. Biophys.* **290**, 153–159.

Chen, B., Keshive, M. & Deen, W. (1998), 'Diffusion and reaction of nitric oxide in suspension cell cultures', *Biophys. J.* **75**, 745–754.

References

Chen, C., Pan, C., Chen, C. & Huang, M. (2011), 'Increased oxidative dna damage in patients with alcohol dependence and its correlation with alcohol withdrawal severity', *Alc Clin Exp Res.* **35**, 338–344.

Chiueh, C. C. (1999), 'Neuroprotective properties of nitric oxide.', *Ann. N.Y. Acad. Sci.* **890**, 301–311.

Cline, S., Lodeiro, M., Marnett, L., Cameron, C. & Arnold, J. (2010), 'Arrest of human mitochondrial rna polymerase transcription by the biological aldehyde adduct of dna, m1dg', *Nucleic Acids Res.* **38**, 7546–7557.

Colombini, V., Bancon-Montigny, C., Yang, L., Maxwell, P., Sturgeon, R. E. & Mester, Z. (2004), 'Headspace single drop microextration for the detection of organotin compounds', *Talanta* **63**(3), 555–560.

Colombrita, C., Calabrese, V., Stella, A., Mattei, F., Alkon, D. & Scapagnini, G. (2003), 'Regional rat brain distribution of heme oxygenase-1 and manganese superoxide dismutase mrna: Relevance of redox homeostasis in the aging processes', *Exp. Biol. Med.* **228**(5), 517–524.

Comber, M., Girling, A., den Haan, K. & Whale, G. (2015), 'Oil refinery experience with the assessment of refinery effluents and receiving waters using biologically-based methods', *Integr. Environ. Assess. Manag.* **9999**, 1–13.

Commoner, B., Townsend, J. & Pake, G. E. (1954), 'Free radicals in biological materials', *Nature* **174**, 689–691.

Cordis, G. A., Bagchi, D., Maulik, N. & Das, D. K. (1994), 'High-performance liquid chromatographic method for the simultaneous detection of malonaldehyde, acetaldehyde, formaldehyde, acetone and propionaldehyde to monitor the oxidative stress in heart', *J. Chromatogr. A* **661**(1), 181–191.

Crestini, C., Marsh, J., Bianchetti, G. & Lange, H. (2015), 'Identification and quantification of radical species by 31p nmr-based spin trapping-a case study nh4oh/h2o2-based hair bleaching', *Microchem. J.* **121**, 112 – 121.

Csordas, G. & Hajnoczky, G. (2009), 'Sr/er-mitochondrial local communication: Calcium and ros', *Biochimica et Biophysica Acta (BBA) - Bioenergetics* **1787**(11), 1352–1362. Mitochondrial Calcium in Health and Disease.

Dalle-Donne, I., Scaloni, A. & Allan Butterfield, D., eds (2006), *REDOX PROTEOMICS-from Protein Modification to Cellular Dysfunction and Diseases*, John Wiley and Sons, Inc.

Das, S. K. & Vasudevan, D. (2007), 'Alcohol-induced oxidative stress', *Life Sci.* **81**(3), 177–187.

Dasgupta, A. & Klein, K. (2014), Chapter 4 - oxidative stress caused by cigarette smoking, alcohol abuse, and drug abuse, *in* A. D. Klein, ed., 'Antioxidants in Food, Vitamins and Supplements', Elsevier, San Diego, pp. 59–75.

Davies, M. (1988), 'Detection of peroxyl and alkoxyl radicals produced by reaction of hydroperoxides with heme-proteins by electron spin resonance spectroscopy', *Biochim. Biophys. Acta.* **964**, 28–35.

Davis, R. & Frearson, M. (1987), *Mass Spectrometry Analytical Chemistry by Open Learning*, John Wiley and Sons, Ltd, London.

De Grey, A. D. N. J. (2002), 'Ho2*: the forgotten radical.', *DNA Cell Biol.* **21**(4), 251–257.

De Gruijl, F. (1999), 'Skin cancer and solar uv radiation', *Eur. J. Cancer* **35**(14), 2003–2009.

De Jager, L. & Anthony, A. (2000), 'Development of a rapid screening technique for organochlorine pesticides using solvent microextraction (sme) and fast gas chromatography (gc)', *Analyst* **125**, 1943–1948.

De Jager, L. & Anthony, A. (2001), 'Development of a screening method for cocaine and cocaine metabolites in urine using solvent microextraction in conjunction with gas chromatography', *J. Chromatogr. A* **911**(1), 97–105.

Deans, A. & West, S. (2011), 'Dna interstrand crosslink repair and cancer', *Nat. Rev. Cancer* **11**, 467–280.

DeBalsi, K., Hoff, K. & Copeland, W. (2016), 'Role of the mitochondrial dna replication machinery in mitochondrial dna mutagenesis, aging and age related diseases', *Ageing Res. Rev.* pp. –.

Dedon, P. & Tannenbaum, S. (2004), 'Reactive nitrogen species in the chemical biology of inflammation', *Arch. Biochem. Biophys.* **423**, 12–22.

Del, R., Stewart, A. & Pellegrini, N. (2005), 'A review of recent studies on malondialdehyde as toxic molecule and biological marker of oxidative stress', *Nutr. Metab Cardiovasc. Dis.* **15**, 316–328.

References

Deng, C., Yao, N., Li, N. & Zhang, X. (2005), 'Headspace single-drop microextraction within-drop derivatization for aldehyde analysis', *Journal of Seperation Science* **28**, 2301–2305.

Denninger, J. & Marletta, M. (1999), 'Guanylate cyclase and the no radical cgmp signaling pathway', *Biochimica et Biophysica Acta (BBA) - Bioenergetics* **1411**(2-3), 334–350.

Diaz Gomez, M., Castro, G., Delgado de Layo, A., Costantini, M. & Castro, J. (2000), 'Cytochrome p450 reductase mediated anaerobic biotransformation of ethanol to 1-hydroxyethyl-free radicals and acetaldehyde', *Toxicology* **154**(1-3), 113–122. cited By 18.

Dmitriev, L. & Dugin, S. (2007), 'Aldehydes and disturbance of carbohydrate metabolism: some consequences and possible approaches to its normalization', *Arch. Physiol. Biochem.* **113**, 87–95.

Dmitriev, L. & Titov, V. (2010), 'Lipid peroxidation in relation to ageing and the role of endogenous aldehydes in diabetes and other age-related diseases, ageing', *Res. Rev.* **9**, 200–210.

Dolch, M., Chouker, A., Hornuss, C., Frey, L., Irlbeck, M., Praun, S., Leidlmair, C., Villinger, J. & Schelling, G. (2015), 'Quantification of propionaldehyde in breath of patients after lung transplantation', *Free Radic. Biol. Med.* **85**, 157–164.

Doser, T., Turdi, S., Thomas, D., Epstein, P., Li, S. & Ren, J. (2009), 'Transgenic overexpression of aldehyde dehydrogenase 2 rescues chronic alcohol intake induced myocardial hypertrophy and contractile dysfunction', *Circulation* **119**(14), 1941–1949.

Droge, W. (2002), 'Free radicals in the physiological control of cell function', *Physiol. Rev.* **82**, 47–95.

Eriksson, C. (2001), 'The role of acetaldehyde in the actions of alcohol (update 2000)', *Alcohol. Clin. Exp. Res.* **25**(5 Suppl ISBRA), 15S–32S.

Esterbauer, H., Schaur, R. & Zollner, H. (1991), 'Chemistry and biochemistry of 4-hydroxynonenal, malonaldehyde and related aldehydes', *Free Radic. Biol. Med.* **11**, 81–128.

Esterbauer, H. & Zollern, H. (1989), 'Methods for determination of aldehydic lipid peroxidation products', *Free Radic. Biol. Med.* **7**(2), 197 – 203.

References

Ferger, B., Teismann, P., Earl, C., kuschinosky, K. W. & Oertel, H. (2000), 'The protective effects of pbn against mptp toxicity are independent of hydroxyl radical trapping.', *Pharmacology Biochemistry and Behavior* **65**(3), 425–431.

Finkel, T. & Holbrook, N. (2000), 'Oxidants, oxidative stress and the biology of ageing', *Nature* **408**(6809), 239–247.

Floyd, R. (1990), ''role of oxygen free radicals in carcinogenesis and brain ischemia', *FASEB J.* **4**, 2587–97.

Floyd, R. A., Kopke, R. D., Choi, C., Foster, S., Doblas, S. & Towner, R. A. (2008), 'Nitrones as therapeutics', *Free Radic. Biol. Med.* **45**(10), 1361–1374.

Floyd, R. & Carney, J. (1992), 'Free radical damage to protein and dna: mechanisms involved and relevant observations on brain undergoing oxidative stress', *Ann. Neurol.* **32**, S22–S27.

Floyd, R., Hensley, K., Foster, M., Kelleher-Andersson, J. & Wood, P. (2002), 'Nitrones, their value as therapeutics and probes to understand aging.', *Mech. Ageing Dev.* **123**(8), 1021–1031.

Forman, H. (2016), 'Glutathione-from antioxidant to post-translational modifier', *Archives of Biochemistry and Biophysics* **595**, 64–67. Special Issue: Tribute Issue: Helmut Sies and Oxidative Stress: venit, vidit, vicit.

Freeman, C., javille, B. A., Karoui, H., Tuccio, B., Le Moigne, F., Culcasi, M., Pietri, S., Lauricella, R. & Tordo, P. (1995), '5-(diethoxyphosphoryl)-5-methyl-1-pyrroline n-oxide: a new efficient phosphorylated nitrone for the in vitro and in vivo spin trapping of oxygen-centered radicals', *J. Med. Chem.* **38**, 258–265.

Furchgott, R. & Vanhoutte, P. (1989), 'Endothelium-derived relaxing and contracting factors.', *The FASEB Journal* **3**(9), 2007–2018.

Gerschman, R., Gilbert, D., Nye, S., Dwyer, P. & Fenn, W. (1954), 'Oxygen poisoning and x-irradiation: a mechanism in common', *Science* **119**, 62362–62366.

Ghafourifar, P. & Cadenas, E. (2005), 'Mitochondrial nitric oxide synthase', *Trends Pharmacol. Sci.* **26**(4), 190–5.

Gitto, S., Golfieri, L., Caputo, F., Grandi, S. & Andreone, P. (2016), 'Multidisciplinary view of alcohol use disorder: From a psychiatric illness to a major liver disease', *Biomolecules* **6**(1), 11.

Gomberg, M. (1900), 'An instance of trivalent carbon: triphenylmethyl', *J. Am. Chem. Soc.* **22**, 751–771.

Gonthier, B., Jeunet, A. & Barret, L. (1991), 'Electron spin resonance study of free radicals produced from ethanol and acetaldehyde after exposure to a fenton system or to brain and liver microsomes', *Alcohol* **8**(5), 369–375.

Gray, C. & O'Connell, J. (2003), 'Stroke: beyond thrombolysis and back to basics', *Q. J. Med.* **96**, 179–181.

Green, A., Ashwood, T., Odergren, T. & Jackson, D. (2003), 'Nitrones as neuroprotective agents in cerebral ischemia, with particular reference to nxy-059', *Pharmacol. Ther.* **100**(3), 195–214.

Guo, R. & Ren, J. (2010), 'Alcohol and acetaldehyde in public health: From marvel to menace', *Int. J. Environ. Res. Public. Health* **7**, 1285–1301.

Halliwell, B. & Gutteridge, J. (2007), *Free radicals in biology and medicine*, fourth edn, Oxford University Press Inc.

Halpern, A. (1984), 'Spin trapping of radicals in tritiated methanol', *Chem. Phys. Lett.* **103**(6), 523–525.

Han, D., Canali, R., Garcia, J., Aguilera, R., Gallaher, T. K. & Cadenas, E. (2005), 'Sites and mechanisms of aconitase inactivation by peroxynitrite: Modulation by citrate and glutathione.', *Biochemistry* **44**(11986-11996.).

Harbour, J. & Bolton, J. (1975), 'Superoxide formation in spinach chloroplasts: electron spin resonance detection by spin trapping', *Biochem. Biophys. Res. Commun.* **64**, 803–807.

Harman, D. (1956), 'Aging: a theory based on free radical and radiation chemistry', *J. Gerontol.* **11**, 298–300.

Higinbotham, K., Rice, J., Diwan, B., Kasprzak, K., Reed, C. & Perantoni, A. (1992), 'Ggt to gtt transversions in codon 12 of the k-ras oncogene in rat renal sarcomas induced with nickel subsulfide or nickel subsulfide/iron are consistent with oxidative damage to dna', *Cancer Res.* **52**(17), 4747–4751.

Hill, H. & Thornalley, P. (1983), 'The effect of spin traps on phenylhydrazine-induced haemolysis', *BBA - Molecular Cell Research* **762**(1), 44–51.

Hinton, R. & Janzen, E. (1992), 'Synthesis and characterization of phenyl-substituted c-phenyl-n-tert-butylnitrones and some of their radical adducts', *J. Org. Chem.* **57**(9), 2646–2651.

Hoffmann, E. & Stroobant, V. (2007), *Mass Spectrometry principles and applications*, third edn, John Wiley and Sons, Ltd.

Hou, L. & Lee, H. K. (2002), 'Application of static and dynamic liquid-phase microextraction in the determination of polycyclic aromatic hydrocarbons', *J. Chromatogr. A* **976**(1-2), 377–385. 7th International Symposium on Hyphenated Techniques in Chromatography and Hyphenated Chromatographic Analyzers.

Huang, H., Kozekov, I., Kozekova, A., Wang, H., Lloyd, R., Rizzo, C. & Stone, M. (2010), 'Dna cross-link induced by trans-4-hydroxynonenal', *Environ. Mol. Mutagen* **51**, 625–634.

Inoue, M., Sato, E., Nishikawa, M., Park, A., Kira, Y., Imada, I. & Utsumi, K. (2003), 'Mitochondrial generation of reactive oxygen species and its role in aerobic life', *Curr. Med. Chem.* **10**, 2495–2505.

Janzen, E. (1970), 'Spin trapping', *Acct. Chem. Res.* **4**(1), 31–40.

Janzen, E. & Dubose, C. M. (1993), 'Electron impact mass spectra of some substituted c-phenyl n-tert-butyl nitrones (pbns)', *Anal. Lett.* **26**(12), 2661–2666.

Janzen, E., Hinton, R. & Kotake, Y. (1992), 'Substituent effect on the stability of the hydroxyl radical adduct of alpha-phenyl n-tert-butyl nitrone (pbn)', *Tetrahedron Lett.* **33**(10), 1257–1260.

Janzen, E., Weber, J., Haire, D. & Fung, D. (1985), 'Gas chromatography-mass spectroscopy (gc/ms) of single and double spin adducts of pbn and the hydroxylamines of corresponding structure', *Anal. Lett.* **18**(14), 1749–1757.

Jeannot, M. & Cantwell, F. (1997), 'Mass transfer characteristics of solvent extraction into a single drop at the tip of a syringe needle', *Anal. Chem.* **69**, 2935–2940.

Jiang, R., Cudjoe, E., Bojko, B., Abaffy, T. & Pawliszyn, J. (2013), 'A non-invasive method for in vivo skin volatile compounds sampling', *Analytica Chimica Acta* **804**, 111–119.

Jimenez, E., Gilles, M. & Ravishankara, A. (2003), 'Kinetics of the reactions of the hydroxyl radical with ch3oh and c2h5oh between 235 and 360 k', *Journal of Photochemistry and Photobiology A: Chemistry* **157**(2-3), 237–245. Atmospheric Photochemistry.

References

Jomova, K., Vondrakova, D., Lawson, M. & Valko, M. (2010), 'Metals, oxidative stress and neurodegenerative disorders', *Mol. Cell. Biochem.* **345**, 91–104.

Kadiiska, M. & Mason, R. (2000), 'Acute methanol intoxication generates free radicals in rats: an esr spin trapping investigation', *Free Radic. Biol. Med.* **28**(7), 1106–1114.

Kalyanaraman, B., Joseph, J. & Parthasarathy, S. (1991), 'The spin trap, alpha-phenyl n-tert-butylnitrone, inhibits the oxidative modification of low density lipoprotein', *FEBS letters* **280**(1), 17–20.

Kasazaki, K., Yasukawa, K., Sano, H. & Utsumi, H. (2003), 'Non-invasive analysis of reactive oxygen species generated in nh4oh-induced gastric lesions of rats using a 300 mhz in vivo esr technique', *Free Radic. Res.* **37**(7), 757–766.

Khramtsov, V., Berliner, L. J. & Clanton, T. L. (1999), 'Nmr spin trapping: detection of free radical reactions using a phosphorus-containing nitrone spin trap', *Magn. Reson. Med.* **42**(2), 228–234.

Khramtsov, V. & Clanton, T. (2011), 'Nmr spin trapping: insight into the hidden life of free radical adducts', *Appl. Magn. Reson.* **41**(2-4), 305–323.

Khramtsov, V., Reznikov, V., Berliner, L., Litkin, A.K. andGrigorev, I. & Clanton, T. (2001), 'Nmrspin trapping: detection of free radical reactions with a new fluorinated dmpo analog', *Free Radic. Biol. Med.* **30**(10), 1099–1107.

Kikugawa, K. & Beppu, M. (1987), 'Involvement of lipid oxidation products in the formation of fluorescent and cross-linked proteins', *Chem. Phys. Lipids* **44**, 277–296.

Kim, S., Vilela, G., Bouajila, J., Dias, A. G., Cyrino, F. Z., Bouskela, E., Costa, P. R. & Nepveu, F. (2007), 'alpha-phenyl-n-tert-butyl nitrone (pbn) derivatives: Synthesis and protective action against microvascular damages induced by ischemia/reperfusion', *Bioorg. Med. Chem.* **15**(10), 3572–3578.

Kishimoto, Y., Saito, N., Kurita, K., Shimokado, K., Maruyama, K. & Ishigami, A. (2013), 'Ascorbic acid enhances the expression of type 1 and type 4 collagen and svct2 in cultured human skin fibroblasts', *Biochem. Biophys. Res. Commun.* **430**(2), 579–584.

Klaunig, J., Xu, Y., Bachowski, S. & Jiang, J. (1997), *Free Radical Toxicology*, K.B. Wallace, London: Taylor and Francis.

Kopani, M., Celec, P., Danisovic, L., Michalka, P. & Biro, C. (2006), 'Oxidative stress and electron spin resonance', *Clin. Chim. Acta* **364**(1-2), 61–66.

Koshlan, D. J. (1992), 'The molecule of the year.', *Science* **258**, 1861.

Kotake, Y. & Janzen, E. (1991), 'Decay and fate of the hydroxyl radical adduct of alpha-phenyl-n-tert-butylnitrone in aqueous media', *J. Am. Chem. Soc.* **113**(25), 9503–9506.

Kotamraju, S., Tampo, Y., Kalivendi, S. V., Joseph, J., Chitambar, C. R. & Kalyanaraman, B. (2004), 'Nitric oxide mitigates peroxide-induced iron-signaling, oxidative damage, and apoptosis in endothelial cells: role of proteasomal function?', *Arch. Biochem. Biophys.* **423**(1), 74 – 80.

Kramer, R., Sauer-Heilborn, A., Welte, T., Guzman, C., Hofle, M. & Abraham, W. (2015), 'A rapid method for breath analysis in cystic fibrosis patients.', *Eur. J. Clin. Microbiol. Infect. Dis.* **34**(4), 745–751.

Lange, L. & Sobel, B. (1983*a*), 'Mitochondrial dysfunction induced by fatty acid ethyl esters, myocardial metabolites of ethanol.', *J. Clin. Invest.* **72**, 724–731.

Lange, L. & Sobel, B. (1983*b*), 'Myocardial metabolites of ethanol.', *Circ. Res.* **52**, 479–482.

Lee, J., Son, Y., Pratheeshkumar, P. & Shi, X. (2012), 'Oxidative stress and metal carcinogenesis', *Free Radic. Biol. Med.* **53**(4), 742–757.

Lee, Y., Aroor, A. & Shukla, S. (2002), 'Temporal activation of p42/44 mitogen-activated protein kinase and c-jun n-terminal kinase by acetaldehyde in rat hepatocytes and its loss after chronic ethanol exposure.', *J. Pharmacol. Exp. Ther.* **301**, 908–914.

Leonard, S. S., Harris, G. K., & Shi, X. (2004), 'Metal-induced oxida- tive stress and signal transduction.', *Free Radic. Biol. Med.* **37**, 1921–1942.

Li, X. H., Xu, X. B., Wang, X. T. & Ma, L. L. (2004), 'Headspace single drop microextraction with gas chromatography for determination of volatile halocarbons in water samples', *Int. J. Environ. Anal. Chem.* **84**, 633–645.

Liang, Q., Carlson, E. C., Borgerding, A. J. & Epstein, P. N. (1999), 'A transgenic model of acetaldehyde overproduction accelerates alcohol cardiomyopathy.', *J. Pharmacol. Exp. Ther.* **291**, 766–772.

Ligor, T. & Buszewski, B. (2000), 'Extraction of trace organic pollutants from aqueous samples by a single drop method', *Chromatographia* **51**(1), S279–S282.

Lin, H., Wang, B., Zeng, L., Li, G., Sha, Y., Wu, D. & Liu, B. (2013), 'Development of solvent micro-extraction combined with derivatization', *J. Chromatogr. A* **1296**, 235–242. Microreactions in Separation Science: Reagents and Techniques.

References

Liochev, S. I. & Fridovich, I. (1994), 'The role of o2 in the production of ho: In vitro and in vivo.', *Free Radic. Biol. Med.* **16**, 29–33.

Liu, H. & Dasgupta, P. (1996), 'Analytical chemistry in a drop. solvent extraction in a microdrop', *Anal. Chem.* **68**, 1817–1821.

Lobo, V., Patil, A., Phatak, A. & Chandra, N. (2010), 'Free radicals, antioxidants and functional foods: Impact on human health.', *Pharmacognosy Reviews* **4**(8), 118–126. **URL:** *http://www.ncbi.nlm.nih.gov/pmc/articles/PMC3249911/*

Lord, H. & Pawliszyn, J. (2000), 'Evolution of solid-phase microextraction technology', *J. Chromatogr. A* **885**, 153–193.

Lord, H., Zhang, X., Musteata, F., Vuckovic, D. & Pawliszyn, J. (2011), 'In vivo solid-phase microextraction for monitoring intravenous concentrations of drugs and metabolites.', *Nat. Protoc.* **6**, 896–924.

Lourenco, C. & Turner, C. (2014), 'Breath analysis in disease diagnosis: Methodological considerations and applications', *Metabolites* **4**, 465–498.

Lu, S. (2009), 'Regulation of glutathione synthesis', *Mol. Aspects Med.* **30**, 42–59.

Lushchak, V. (2014), 'Free radicals, reactive oxygen species, oxidative stress and its classification', *Chem. Biol. Interact.* **224**, 164–175.

Maddukuri, L., Eoff, R., Choi, J., Rizzo, C., Guengerich, F. & Marnett, L. (2010), 'In vitro bypass of the major malondialdehyde-and base propenal-derived dna adduct by human y-family dna polymerases kappa, iota, and rev1.', *Biochemistry* **49**, 8415–8424.

Makrigiorgos, G., Bump, E., Huang, C., Baranowska-Kortylewicz, J. & Kassis, A. (1995), 'A fluorimetric method for the detection of copper-mediated hydroxyl free radicals in the immediate proximity of dna', *Free Radic. Biol. Med.* **18**(4), 669–678.

Malhotra, J. & Kaufman, R. (2007), 'Endoplasmic reticulum stress and oxidative stress: A vicious cycle or a double-edged sword?', *Antioxidants and Redox Signaling* **9**(12), 2277–2293.

Malins, D., Polissar, N. L. & Gunselman, S. (1996), 'Progression of human breast cancers to the metastatic state is linked to hydroxyl radical induced dna damage', *Proc Natl Acad Sci USA* **93**(6), 2557–2563.

Mallikarjuna, K., Sahitya, P. C., Reddy, K. S. & Rajendra, W. . F. (2008), 'Ethanol toxicity: rehabilitation of hepatic antioxidant defense system with dietary ginger', *Fitoterapia* **79**, 174–178.

Mandavilli, B., Santos, J. & Houten, B. (2002), 'Mitochondrial dnarepair and aging', *Mutation Research Fundamental and Molecular Mechanisms of Mutagenesis* **509**(1-2), 127–151.

Mantle, D. & Preedy, V. (1999), 'Free radicals as mediators of alcohol toxicity', *Adverse Drug React. Toxicol. Rev.* **18**(4), 235–252.

Marchitti, S., Brocker, C., Stagos, D. & Vasiliou, V. (2008), 'Non-p450 aldehyde oxidizing enzymes: the aldehyde dehydrogenase superfamily', *Expert Opin. Drug Metab. Toxicol.* **4**(6), 697–720.

Marnett, L. (1999), 'Lipid peroxidation-dna damage by malondialdehyde', *Mutat. Res.* **424**, 83–95.

Marnett, L. (2002), 'Oxy radicals, lipid peroxidation and dna damage', *Toxicology* **181-182**, 219–222.

McCord, J. & Fridovich, I. (1969), 'Superoxide dismutase: an enzymic function for erythrocuprein (hemocuprein)', *J. Biol. Chem.* **244**, 6049–6055.

McCormick, M., Buettner, G. & Britigan, B. (1995), 'The spin trap 4-pobn stimulates peroxidase-mediated oxidation of deferoxamine: Implications for pharmacological use of spin-trapping agents', *J. Biol. Chem.* **270**(49), 29265–29269.

McMaster, C. & McMaster, M. (1998), *GCMS A practical users guide*, Wiley-VCH.

Mena, N., Bulteau, A., Salazar, J., Hirsch, E. & Nunez, M. (2011), 'Effect of mitochondrial complex i inhibition on fe-s cluster protein activity', *Biochem. Biophys. Res. Commun.* **409**(2), 241–246.
URL: *http://www.sciencedirect.com/science/article/pii/S0006291X11007443*

Michaelis, L. (1939), 'Free radicals as intermediate steps of oxidation-reduction', *Cold Spring Harb. Symp. Quant. Biol.* **7**, 33–49.

Miller, D., Buettner, G. & Aust, S. (1990), 'Transition metals as catalysts of autoxidation reactions.', *Free Radic. Biol. Med.* **8**, 95–108.

Min, D. B. & Boff, J. M. (2002), 'Chemistry and reaction of singlet oxygen in foods', *Comprehensive Reviews in Food Science and Food Safety* **1**(2), 58–72.
URL: *http://dx.doi.org/10.1111/j.1541-4337.2002.tb00007.x*

Minko, I., Kozekov, I., Harris, T., Rizzo, C., Lloyd, R. & Stone, M. (2009), 'Chemistry and biology of dna containing 1,n(2)-deoxyguanosine adducts of the alpha,beta-unsaturated aldehydes acrolein, crotonaldehyde, and 4-hydroxynonenal', *Chem. Res. Toxicol.* **22**, 759–778.

Mistry, P., , Nigar, N., Purdie, A. & Podmore, I. (2008), 'Indirect detection of hydroxyl radicals using spin trapping and gas chromatography-mass spectrometry', *J. Chem. Res.* **7**, 395–397.

Mittal, C. & Murad, F. (1977), 'Activation of guanylate cyclase by superoxide dismutase and hydroxyl radical: a physiological regulator of guanosine 3,5 -monophosphate formation', *Proc Natl Acad Sci.* **74**, 4360–4364.

Moeskops, B., Steeghs, M., Swam, K., Cristescu, S., Scheepers, P. & Harren, F. (2006), 'Real-time trace gas sensing of ethylene, propanal and acetaldehyde from human skin in vivo', *Physiol. Meas.* **27**(11), 1187–1196.

Muller, F. L., Liu, Y. & Van Remmen, H. (2004), 'Complex iii releases superoxide to both sides of the inner mitochondrial membrane.', *J. Biol. Chem.* **279**, 49064–49073.

Munnia, A., Bonassi, S., Verna, A., Quaglia, R., Pelucco, D., Ceppi, M., Neri, M., Buratti, M., Taioli, E., Garte, S. & Peluso, M. (2006), 'Bronchial malondialdehyde dna adducts, tobacco smoking, and lung cancer.', *Free Radic. Biol. Med.* **41**, 1499–1505.

Murphy, M. (2009), 'How mitochondria produce reactive oxygen species', *Biochem. J.* **417**, 1–13.

Nackerdien, Z., Olinski, R. & Dizdaroglu, M. (1992), 'Dna base damage in chromatin of gamma-irradiated cultured human cells.', *Free Radic. Res. Commun.* **16**(4), 259–273.

Nair, J., De, F., Izzotti, A. & Bartsch, H. (2007), 'Lipid peroxidation-derived etheno-dna adducts in human atherosclerotic lesions', *Mutat. Res.* **621**, 95–105.

Nair, J., Srivatanakul, P., Haas, C., Jedpiyawongse, A., Khuhaprema, T., Seitz, H. & Bartsch, H. (2010), 'High urinary excretion of lipid peroxidation-derived dna damage in patients with cancer-prone liver diseases', *Mutat. Res.* **683**, 23–28.

Nair, U., Bartsch, H. & Nair, J. (2007), 'Lipid peroxidation-induced dna damage in cancer-prone inflammatory diseases: a review of published adduct types and levels in humans', *Free Radic. Biol. Med.* **43**, 1109–1120.

Nakae, D., Kotake, Y., Kishida, H., Hensley, K., Denda, A., Kobayashi, Y., Kitayama, W., Tsujiuchi, T., Sang, H., Stewart, C., Tabatabaie, T., Floyd, R. & Konishi, Y. (1998),

'Inhibition by phenyl n-tert-butyl nitrone of early phase carcinogenesis in the livers of rats fed a choline-deficient, l-amino acid-defined diet', *Cancer Res.* **58**(20), 4548–4551.

Nakagawa, S. (2016), 'Relative yields of radicals produced in deuterated methanol by irradiation', *Radiat. Phys. Chem.* **122**, 73–76.

Nakamura, K., Iwahashi, K., Furukawa, A., Ameno, K., Kinoshita, H., Ijiri, I., Sekine, Y., Suzuki, K., Iwata, Y., Minabe, Y. & Mori, N. (2003), 'Acetaldehyde adducts in the brain of alcoholics', *Arch. Toxicol.* **77**, 591–593.

Nakao, L., Kadiiska, M., Mason, R., Grijalba, M. & Augusto, O. (2000*a*), 'Metabolism of acetaldehyde to methyl and acetyl radicals: in vitro and in vivo electron paramagnetic resonance spin-trapping studies', *Free Radic. Biol. Med.* **29**(8), 721–729.

Nakao, L., Kadiiska, M., Mason, R., Grijalba, M. & Augusto, O. (2000*b*), 'Metabolism of acetaldehyde to methyl and acetyl radicals: in vitro and in vivo electron paramagnetic resonance spin-trapping studies', *Free Radic. Biol. Med.* **29**(8), 721–729.

Nigam, S. & Schewe, T. (2000), 'Phospholipase a2s and lipid peroxidation', *Biochim. Biophys. Acta.* **1488**, 167–181.

Nishimura, F. T., Fukunaga, T., Kajiura, H., Umeno, K., Takakura, H., Ono, T. & Nishijo, H. (2002), 'Effects of aldehyde dehydrogenase-2 genotype on cardiovascular and endocrine responses to alcohol in young japanese subjects.', *Auton. Neurosci.* **102**, 60–70.

Noor, R., Mittal, S. & Iqbal, J. (2002), 'Superoxide dismutase applications and relevance to human diseases', *Med. Sci. Monit.* **8**(9), 210–215.

Novelli, G., Angiolini, P., Tani, R., Consales, G. & Bordi, L. (1986), 'Phenyl-t-butyl-nitrone is active against traumatic shock in rats.', *Free Radic. Res. Commun.* **1**(5), 321–327.

Oba, T., Maeno, Y., Nagao, M., Sakuma, N. & Murayama, T. (2008), 'Cellular redox state protects acetaldehyde-induced alteration in cardiomyocyte function by modifying ca2+ release from sarcoplasmic reticulum.', *Am. J. Physiol Heart Circ. Physiol.* **294**, H121–H133.

O'Brien, P., Siraki, A. & N., S. (2005), 'Aldehyde sources, metabolism, molecular toxicity mechanisms, and possible effects on human health.', *Crit. Rev. Toxicol.* **35**, 609–62.

Ortiz de montellano, P., Augusto, O., Viola, F. & Kunze, K. (1983), 'Carbon radicals in the metabolism of alkyl hydrazines', *J. Biol. Chem.* **258**, 8623–8629.

References

Ott, M., Gogvadze, V., Orrenius, S. & Zhivotovsky, B. (2007), 'Mitochondria, oxidative stress and cell death', *Apoptosis* **12**, 913–922.

Palmer, R., Rees, D., Ashton, D. & Moncada, S. (1988), 'L-arginine is the physiological precursor for the formation of nitric oxide in endothelium-dependent relaxation', *Biochem. Biophys. Res. Commun.* **153**(3), 1251 – 1256.

Paracchini, L., Jotti, A., Bottiroli, G., Prosperi, E., Supino, R. & Piccinini, F. (1993), 'The spin trap alpha-phenyl-tert-butyl nitrone protects against myelotoxicity and cardiotoxicity of adriamycin while preserving the cytotoxic activity', *Anticancer Res.* **13**(5 A), 1607–1612.

Paulette, C. & Archibald, F. (1987), 'Manganese complexes and the generation and scavenging of hydroxyl free radicals', *Free Radic. Biol. Med.* **5**, 325–333.

Pawliszyn, J. (2003), 'Sample preparation quo vadis ?', *Anal. Chem.* **75**(11), 2543–2558.

Peng, F., Tang, S., Huang, M. & Chen, C. e. a. (2005), 'Oxidative status in patients with alcohol dependence: a clinical study in taiwan', *J. Toxicol. Environ. Health A* **68**, 1497–1509.

Petersen, D. & Doorn, J. (2004), 'Reactions of 4-hydroxynonenal with proteins and cellular targets', *Free Radic. Biol. Med.* **37**, 937–945.

Pizzimenti, S., Ciamporcero, E., Daga, M., Pettazzoni, P., Arcaro, A., Cetrangolo, G., Minelli, R., Dianzani, C., Lepore, A., Gentile, F. & Barrera, G. (2013), 'Interaction of aldehydes derived from lipid peroxidation and membrane proteins', *Frontiers in physiology* **4**, 242.

Podmore, I., Cunliffe, L. & Heshmati, M. (2013), 'Rapid detection of free radicals using spin trapping and maldi-tof mass spectrometry', *J. Chem. Res.* **37**(1), 45–47.

Poli, G., Leonarduzzi, G., Biasi, F. & Chiarpotto, E. (2004), 'Oxidative stress and cell signalling', *Curr. Med. Chem.* **11**(9), 1163–1182.

Psillakis, E. & Kalogerakis, N. (2001), 'Solid-phase microextraction versus single-drop microextraction for the analysis of nitroaromatic explosives in water samples', *J. Chromatogr. A* **938**(1-2), 113–120. 10th Symposium on Handling of Environmental and Biological Samples in Chromatography.

Puntarulo, S. & Cederbaum, A. (1989), 'Chemiluminescence from acetaldehyde oxidation by xanthine oxidase involves generation of and interactions with hydroxyl radicals', *Alcoholism: Clinical and Experimental Research* **13**(1), 84–90.

References

Pwaliszyn, J. (2009), *Handbook of solid phase microextraction.*, Chemical Industry Press, Beijing.

Pysanenko, A., Spanel, P. & Smith, D. (2009), 'Analysis of the isobaric compounds propanol, acetic acid and methyl formate in humid air and breath by selected ion flow tube mass spectrometry, sift-ms', *Int. J. Mass Spectrom.* **285**(1-2), 42–48.
URL: *http://www.sciencedirect.com/science/article/pii/S1387380609001286*

Qian, S., Kadiiska, M., Guo, Q. & Mason, R. (2005), 'A novel protocol to identify and quantify all spin trapped free radicals from in vitro/in vivo interaction of ho and dmso: Lc/esr, lc/ms and dual spin trapping combinations', *Free Radic. Biol. Med.* **38**(1), 125–135.

Qian, S. Q., Wang, H., Schafer, F. Q. & Buettner, G. (2000), 'Epr detection of lipid-derived free radicals from pufa, ldl, and cell oxidations', *Free Radic. Biol. Med.* **29**(6), 568–579.

Qian, S., Yue, G., Tomer, K. & Mason, R. (2003), 'Identification of all classes of spin-trapped carbon-centered radicals in soybean lipoxygenase-dependent lipid peroxidations of omega-6 polyunsaturated fatty acids via lc/esr, lc/ms, and tandem ms', *Free Radic. Biol. Med.* **34**(8), 1017–1028.

Quertemont, E. & Didone, V. (2006), 'Role of acetaldehyde in mediating the pharmacological and behavioral effects of alcohol.', *Alcohol Res. Health* **29**, 258–265.

Rajasinghe, H., Jayatilleke, E. & Shaw, S. (1990), 'Dna cleavage during ethanol metabolism: Role of superoxide radicals and catalytic iron', *Life Sci.* **47**(9), 807–814.

Reinke, L. (2002), 'Spin trapping evidence for alcohol-associated oxidative stress', *Free Radic. Biol. Med.* **32**(10), 953–957.

Reinke, L., Moore, D., Sang, H., Janzen, E. & Kotake, Y. (2000), 'Aromatic hydroxylation in pbn spin trapping by hydroxyl radicals and cytochrome p-450', *Free Radic. Biol. Med.* **28**(3), 345–350.

Ren, J., Davidoff, A. J. & Brown, R. A. (1997), 'Acetaldehyde depresses shortening and intracellular ca2+ transients in adult rat ventricular myocytes', *Cell. Mol. Biol.* **43**, 825–834.

Ren, J. & Wold, L. (2008), 'Mechanisms of alcoholic heart disease', *Therapeutic Advances in Cardiovascular Disease* **2**(6), 497–506.

References

Riley, P. (1994), 'Free radicals in biology: oxidative stress and the effects of ionizing radiation', *Int. J. Radiat. Biol.* **65**, 27–33.

Rood, D. (2007), *The Troubleshooting and Maintenance Guide for Gas Chromatographers*, fourth edn, WILEYVCH Verlag GmbH and Co. KGaA.

Rossi, F., Della Bianca, V. & Togni, P. d. (1985), 'Mechanisms and functions of the oxygen radicals producing respiration of phagocytes', *Comp. Immunol. Microbiol. Infect. Dis.* **8**(2), 187–204.

Ryu, D., Yang, H., Lee, S., Park, C., Jin, Y. & Park, Y. (2013), 'Crotonaldehyde induces heat shock protein 72 expression that mediates anti apoptotic effects in human endothelial cells', *Toxicol. Lett.* **223**(2), 116–123.

Sainz, R., Lombo, F. & Mayo, J. (2012), 'Radical decisions in cancer redox control of cell growth and death', *Cancers (Basel)* **4**(2), 442–473.

Samuni, A., Chevion, M. & Czapski, G. (1984), 'Roles of copper and o(2) in the radiation-induced inactivation of t7 bacteriophage', *Radiat. Res.* **99**, 562–572.

Samuni, A., Samuni, A. & Swartz, H. (1989), 'The cellular-induced decay of dmpo spin adducts of radical oh and radical o2.', *Free Radic. Biol. Med.* **6**, 179–183.

Savvidou, S., Karatzidou, K., Tsakiri, K., Gagalis, A., Hytiroglou, P. & Goulis, J. (2016), 'Circulating adiponectin levels in type 2 diabetes mellitus patients with or without non alcoholic fatty liver disease: Results of a small, open-label, randomized controlled intervention trial in a subgroup receiving short-term exenatide', *Diabetes Res. Clin. Pract.* **113**, 125–134.

Sayre, L., Lin, D., Yuan, Q., Zhu, X. & X., T. (2006), 'Protein adducts generated from products of lipid oxidation: focus on hne and one.', *Drug Metab. Rev.* **38**(4), 651–675.

Schoppet, M. & Maisch, B. (2001), 'Alcohol and the heart.', *Herz* **26**, 345–352.

Shaikhali, J., Heiber, I., Seidel, T., Stroher, E., Hiltscher, H., Birkmann, S., Dietz, K. & Baier, M. (2008), 'The redox-sensitive transcription factor rap2.4a controls nuclear expression of 2-cys peroxiredoxin a and other chloroplast antioxidant enzymes', *BMC Plant Biology* **8**(1), 1–14.

Siddiq, T., Richardson, P. J., Mitchell, W. D., Teare, J. & Preedy, V. R. (1993), 'Ethanol-induced inhibition of ventricular protein synthesis in vivo and the possible role of acetaldehyde.', *Cell Biochem. Funct.* **11**, 45–54.

References

Sies, H. & Cadenas, E. (1985), 'Oxidative stress: damage to intact cells and organs', *Philos. Trans. R. Soc. Lond. B: Biol. Sci.* **311**, 617–631.

Sies, H., Stahl, W. & Sevanian, A. (2005), 'Nutritional, dietary and postprandial oxidative stress', *J. Nutr.* **135**, 969–972.

Simm, A. & Bromme, H. (2005), 'Reactive oxygen species (ros) and aging: Do we need them can we measure them should we block them ?', *Signal Transduction* **5**, 115–125.

Skrzydlewska, M., Elas, M., Farbiszawski, R. & Roszkowska, A. (2000), 'Effect of methanol intoxication on free radical induced protein oxidation', *J. Appl. Toxicol.* **20**, 239–243.

Slater, T. (1984), 'Free radical mechanism in tissue injury.', *Journal of Biochem.* **222**, 1–15.

Soffritti, M., Belpoggi, F., Lambertin, L., Lauriola, M., Padovani, M. & Maltoni, C. (2002), 'Results of long term experimental studies on the carcinogenicity of formaldehyde and acetaldehyde in rats', *Ann. N. Y. Acad. Sci.* **982**, 87–105.

Soliman, A., Lo, A., Banerjee, M., El Ghawalby, N., Khaled, H., Bayoumi, S., Seifeldin, I., Abdel Aziz, A., Abbruzzese, J., Greenson, J. & Hamilton, S. (2007), 'Differences in k-ras and p53 gene mutations among pancreatic adenocarcinomas associated with regional environmental pollution', *Carcinogenesis* **28**(8), 1794–17949.

Spagnoli, A., Spadoni, G., Sesti, G., Principe, D., Germani, D. & Boscherini, B. (1995), 'Effect of insulin on hydrogen peroxide production by human polymorphonuclear leukocytes.', *Hormone Research in Paediatrics* **43**, 286–293.

Spiteller, D. & Spiteller, G. (2000), 'Identification of toxic 2,4-decadienal in oxidized, low-density lipoprotein by solid-phase microextraction', *Angewandte Chemie - International Edition* **39**(3), 583–585.

Sramkova, I., Horstkotte, B., Solich, P. & Sklenarova, H. (2014), 'Automated in-syringe single-drop head-space micro-extraction applied to the determination of ethanol in wine samples', *Anal. Chim. Acta* **828**, 53–60.

Stamler, J., Single, D. & Loscalzo, J. (1992), 'Biochemistry of nitric oxide and its redox-activated forms', *Science* **258**, 1898–1902.

Steeghs, M., Moeskops, B., Swam, K., Cristescu, S., Scheepers, P. & Harren, F. (2006), 'On-line monitoring of uv-induced lipid peroxidation products from human skin in vivo using proton-transfer reaction mass spectrometry', *Int. J. Mass Spectrom.* **253**(1-2), 58–64.

Theis, A., Waldack, A. J., Hansen, S. M. & Jeannot, M. A. (2001), 'Headspace solvent microextraction', *Anal. Chem.* **73**(23), 5651–5654. PMID: 11774903.

Thiele, G. M., Worrall, S., Tuma, D., Klassen, L., Wyatt, T. & Nagata, N. (2001), 'The chemistry and biological effects of malondialdehyde-acetaldehyde adducts', *Alcohol. Clin. Exp. Res.* **25**, 218S–224S.

Toh, Y., Oki, E., Ohgaki, K., Sakamoto, Y., Ito, S., Egashira, A., Saeki, H., Kakeji, Y., Morita, M., Sakaguchi, Y., Okamura, T. & Maehara, Y. (2010), 'Alcohol drinking, cigarette smoking, and the development of squamous cell carcinoma of the esophagus: molecular mechanisms of carcinogenesis.', *Int. J. Clin. Oncol.* **15**, 135–144.

Townsend, D., Tew, K. & Tapiero, H. (2003), 'The importance of glutathione in human disease', *Biomed. Pharmacother.* **57**(3-4), 145–155.

Tu, B., Ho-Schleyer, S., Travers, K. & Weissman, J. (2000), 'Biochemical basis of oxidative protein folding in the endoplasmic reticulum', *Science* **290**, 1571–1574.

Tuma, D., Thiele, G., Xu, D., Klassen, L. & Sorrell, M. (1996), 'Acetaldehyde and malondialdehyde react together to generate distinct protein adducts in the liver during long-term ethanol administration', *Hepatology* **23**, 872–880.

Turrens, J. F. (2003), 'Mitochondrial formation of reactive oxygen species', *The Journal of physiology* **552**(2), 335–344.

Uchida, K. (1999), 'Current status of acrolein as a lipid peroxidation product', *Trends Cardiovasc. Med.* **9**, 109–113.

Uchiyama, S., Inaba, Y. & Kunugita (2011), 'Derivatization of carbonyl compounds with 2,4-dinitrophenylhydrazine and their subsequent determination by high-performance liquid chromatography', *Journal of Chromatography B* **879**(17-18), 1282–1289.

Valavanidis, A., Vlachogianni, T. & Fiotakis, C. (2009), '8-hydroxy-2-deoxyguanosine (8-ohdg): A critical biomarker of oxidative stress and carcinogenesis', *J Environ Sci Health C Environ Carcinog Ecotoxicol Rev* **27**, 120–139.

Valko, M., Izakovic, M., Mazur, M., Rhodes, C. J. & Telser, J. (2004), 'Role of oxygen radicals in dna damage and cancer incidence.', *Mol. Cell. Biochem.* **26**, 37–56.

Valko, M., Leibfritz, D., Moncol, J., Cronin, M., Mazur, M. & Telser, J. (2007), 'Free radicals and antioxidants in normal physiological functions and human disease', *The International Journal of Biochemistry and Cell Biology* **39**(1), 44–84.

Valko, M., Morris, H. & Cronin, M. T. D. (2005), 'Metals, toxicity and oxidative stress.', *Curr. Med. Chem.* **12**, 1161–1208.

Valko, M., Rhodes, C., Moncol, J., Izakovic, M. & Mazur, M. (2006), 'Free radicals, metals and antioxidants in oxidative stress-induced cancer', *Chem. Biol. Interact.* **160**(1), 1–40.

Van Lancker, F., Adams, A., Delmulle, B., De Saeger, S., Moretti, A., Van Peteghem, C. & De Kimpe, N. (2008), 'Use of headspace spme-gc-ms for the analysis of the volatiles produced by indoor molds grown on different substrates.', *J. Environ. Monit.* **10**(10), 1127–1133.

Vas, G., & Vekey, K. (2004), 'Solid-phase microextraction: a powerful sample preparation tool prior to mass spectrometric analysis', *J. Mass Spectrom.* **39**(3), 233–254.

Vasiliou, V., Thompson, D. C., Smith, C., Fujita, M. & Chen, Y. (2013), 'Aldehyde dehydrogenases: From eye crystallins to metabolic disease and cancer stem cells', *Chem. Biol. Interact.* **202**(1-3), 2–10. Enzymology and Molecular Biology of Carbonyl Metabolism 16.

Vorbach, C., Harrison, R. & Capecchi, M. R. (2003), 'Xanthine oxi- doreductase is central to the evolution and function of the innate immune system.', *Trends Immunol.* **24**, 512–517.

Voss, P. & Siems, W. (2006), 'Clinical oxidation parameters of aging.', *Free Radic. Res.* **40**, 1339–1349.

Voulgaridou, G., Anestopoulos, I., Franco, R., Panayiotidis, M. & Pappa, A. (2011), 'Dna damage induced by endogenous aldehydes: Current state of knowledge', *Mutat. Res.* **711**, 13–27.

Wagner, B., Buettner, G. & Burns, C. (1994), 'Free radical-mediated lipid peroxidation in cells: oxidizability is a function of cell lipid bis-allylic hydrogen content.', *Biochemistry* **33**, 4449–4453.

Wagner, B., Buettner, G., Oberley, L. & Burns, C. (1998), 'Sensitivity of k-562 and hl60 cells to edelfosin, an ether lipid drug, correlates with production of active oxygen species', *Cancer Res.* **58**, 2809–2816.

Wang, C., Turunen, S., Kummu, O., Veneskoski, M., Lehtimaki, J. andNissinen, A. & Horkko, S. (2013), 'Natural antibodies of newborns recognize oxidative stress-related malondialdehyde acetaldehyde adducts on apoptotic cells and atherosclerotic plaques', *Int. Immunol.* **25**, 575–687.

Wang, H., Kozekov, I., Harris, T. & Rizzo, C. (2003), 'Site-specific synthesis and reactivity of oligonucleotides containing stereochemically defined 1,n2-deoxyguanosine adducts of the lipid peroxidation product trans-4-hydroxynonenal', *J. Am. Chem. Soc.* **125**, 5687–5700.

Wang, H., Xie, W., Chen, M. & Guo, L. (2012), 'Determination of hazardous volatile organic compounds in the hoffmann list by ion molecule reaction mass spectrometry', *Rapid Commun. Mass Spectrom.* **26**(16), 1841–1848.

Wang, T., Pysanenko, A., Dryahina, K. & Spanel, P. (2008), 'Analysis of breath, exhaled via the mouth and nose, and the air in the oral cavity', *J. Breath Res.* **2**, 1–12.

Waris, G. & Ahsan, H. (2006), 'Reactive oxygen species: role in the development of cancer and various chronic conditions', *Journal of Carcinogenesis* **5**(1), 14.

White, A., Crawford, K., Patt, C. & Lad, P. (1976), 'Activation of soluble guanylate cyclase from rat lung by incubation or by hydrogen peroxide', *J. Biol. Chem.* **251**, 7304–7312.

Willis, M., Klassen, L., Carlson, D., Brouse, C. & Thiele, G. (2004), 'Malondialdehyde-acetaldehyde haptenated protein binds macrophage scavenger receptor(s) and induces lysosomal damage', *Int. Immunopharmacol.* **4**, 885–899.

Winterbourn, C. (2008), 'Reconciling the chemistry and biology of reactive oxygen species', *Nat. Chem. Biol.* **4**, 278–286.

Wyatt, T., Kharbanda, K., Tuma, D., Sisson, J. & Spurzem, J. (2005), 'Malondialdehyde-acetaldehyde adducts decrease bronchial epithelial wound repair', *Alcohol* **36**, 31–40.

Wyre, H. & Thrasher, J. (2016), Chapter 21 effects of smoking, alcohol, and exercise on prostate cancer, *in* J. H. Mydlo & C. J. Godec, eds, 'Prostate Cancer (Second Edition)', second edition edn, Academic Press, San Diego, pp. 183–189.

Yang, Y., Liu, D., Wang, Q., Long, Q., Zhao, S., Zhang, Z., Ma, Y., Wang, Z., Chen, L. & Wang, L. (2016), 'Alcohol consumption and risk of coronary artery disease: A dose response meta analysis of prospective studies', *Nutrition* **32**(6), 637–644.

Ye, Z., Zhang, J., Townsend, D. & Tew, K. (2015), 'Oxidative stress, redox regulation and diseases of cellular differentiation', *Biochimica et Biophysica Acta (BBA) - General Subjects* **1850**(8), 1607–1621.

Yoerger, D., Best, C., McQuillan, B., Supple, G., Guererro, J.L. ans Cluette Brown, J., Hasaba, A., Picard, M., Stone, J. & Laposata, M. (2006), 'Rapid fatty acid ethyl ester

synthesis by porcine myocardium upon ethanol infusion into the left anterior descending coronary artery', *Am. J. Pathol.* **168**(5), 1435–1442.

Yokoyama, A., Muramatsu, T., Omori, T., Yokoyama, T., Matsushita, S., Higuchi, S., Maruyama, K. & Ishii, H. (2001), 'Alcohol and aldehyde dehydrogenase gene polymorphisms and oropharyngolaryngeal, esophageal and stomach cancers in japanese alcoholics', *Carcinogenesis* **22**(3).

Yu, Y., Sun, X., Liu, Y., Pan, Y. & Zhao, Y. (2014), 'Odor fingerprinting of listeria monocytogenes recognized by spme-gc-ms and e-nose.', *Can. J. Microbiol.* **61**(5), 367–372.

Zakhari, S. (2006), 'Overview: how is alcohol metabolized by the body?', *Alcohol Res. Health* **29**, 245–254.

Zhang, X., Li, S., Brown, R. A. & Ren, J. (2004), 'Ethanol and acetaldehyde in alcoholic cardiomyopathy: from bad to ugly en route to oxidative stress.', *Alcohol* **32**, 175–186.

Zima, T., Fialova, L., Mestek, O., Janebova, M., Crkovska, J., Malbohan, I., Stipek, S., Mikulikova, L. & Popov, P. (2001), 'Oxidative stress, metabolism of ethanol and alcohol-related diseases', *J. Biomed. Sci.* **8**(1), 59–70.

Zoia, L. & Argyropoulos, D. (2009), 'Phenoxy radical detection using 31p nmr spin trapping', *J. Phys. Org. Chem.* **22**(11), 1070–1077.

Zoia, L., Perazzini, R., Crestini, C. & Argyropoulos, D. (2011), 'Understanding the radical mechanism of lipoxygenases using 31p-nmr spin trapping', *Bioorg. Med. Chem.* **19**(9), 3022–3028.